Report No. 170 / UILU ENG-95-4005

A Fatigue Model for Thermite Rail Welds

by

G. T. Fry and F. V. Lawrence

A report of
MATERIALS ENGINEERING — MECHANICAL BEHAVIOR
College of Engineering, University of Illinois at Urbana-Champaign
April 1995

A FATIGUE MODEL FOR THERMITE RAIL WELDS

BY

GARY THOMAS FRY

B.S., University of Illinois at Urbana-Champaign, 1990
M.S., University of Illinois at Urbana-Champaign, 1992

THESIS

Submitted in partial fulfillment of the requirements
for the degree of Doctor of Philosophy in Civil Engineering
in the Graduate College of the
University of Illinois at Urbana-Champaign, 1995

Urbana, Illinois

ACKNOWLEDGMENTS

A special debt of thanks is owed to Professor Frederick V. Lawrence, Jr. for providing inspiration, encouragement, and guidance.

For invaluable technical assistance, Professor Arthur Robinson and Professor Roger Steele are gratefully acknowledged.

Other people have been supportive of this project and deserve special mention: Mrs. Erin Fry, Professor David Pecknold, Professor Huseyin Sehitoglu, Professor German Gurfinkel, Dr. Lev Khazanovich, Professor John Wetzel, Professor Tarek Shawki, and members of *The Fatigue Group*.

This project was conducted under the auspices of The Association of American Railroads which provided technical and financial support.

TABLE OF CONTENTS

LIST OF SYMBOLS

$2a$	Total length of the Hertzian contact zone in the rail-head stress analysis
d	Depth of the rail strip in the rail-head stress analysis
f	Value of Findley's Critical-Plane Fatigue Damage Parameter
G_r	Shear modulus of the rail layer in the rail-head stress analysis
G_s	Shear modulus of the support layer in the rail-head stress analysis
i	Imaginary unit, $\sqrt{-1}$
κ	Material constant used in Findley's Parameter
λ	Transform variable used in the Fourier integral
λ_X	Ellipsoidal discontinuity's longitudinal-semiaxis length in the local-stress analysis
λ_Y	Ellipsoidal discontinuity's vertical-semiaxis length in the local-stress analysis
λ_Z	Ellipsoidal discontinuity's transverse-semiaxis length in the local-stress analysis
N	Normal component of the wheel load in the rail-head stress analysis
n_0	Peak value of applied Hertzian normal traction in the rail-head stress analysis
N_n	Fatigue defect nucleation life
ν_r	Poisson's ratio of the rail strip in the rail-head stress analysis
π	An arbitrary plane in space
P	An arbitrary point in space
T	Tangential component of the wheel load in the rail-head stress analysis
t	Thickness of the rail layer in the rail-head stress analysis
t_0	Peak value of the applied Hertzian tangential traction in the rail-head stress analysis
X	Global coordinate directed along the rail's longitudinal axis
Y	Global coordinate directed perpendicular to the rail's running surface
Z	Global coordinate directed transverse to the rail's cross-section

1 INTRODUCTION

1.1 OBJECTIVE AND SCOPE

The objective of this project is to examine the fatigue behavior of thermite-welded railroad rail and in particular the occurrence of fatigue defects in the rail head. A rail-head local-stress fatigue model (RAHELS) is developed to predict the type of rail-head defect that forms under a given set of operating conditions and to predict the nucleation life of the defect.

Thermite rail welds usually contain pores and alumina inclusions. Using the RAHELS model, the effects of these discontinuities are examined for different discontinuity locations, shapes, and orientations. In addition, the effects of residual stresses in the rail head, seasonal temperature variations, vertical wheel loads, tangential wheel loads, and track-foundation stiffness are explored. Predictions are compared with experimental observations to examine the validity of the RAHELS model. Suggestions for improving the fatigue performance of thermite rail welds are presented.

1.2 THERMITE RAIL WELDS

The process of thermite rail welding began in 1906 (Gibert 1988). Thermite rail welds are used currently to join and repair continuous welded rail in the field (Steele 1985). Beginning with Tinnon (1938), descriptions contained in the *Welding Handbook* reveal an interesting history of the evolution of the process.

Figure 1 is a schematic drawing of a typical modern thermite rail welding process. A one-inch gap between the ends of abutting rails is enclosed by a split sand mold. The thermite reaction produces molten steel in a crucible which is suspended above the mold. After a dwell time of 25 to 35 seconds, the steel is released into the mold and solidifies. Jha (1989) presents a detailed study of the thermite rail welding process.

Production of thermite rail welds is convenient, but the process is increasingly viewed with disfavor because thermite welds display inferior fatigue performance in revenue service (Hauser 1978). An experimental evaluation of thermite rail welds was performed as part of a full-scale testing program known as the Heavy Axle Load program or HAL (Brave 1990). Observations from the HAL program indicate that thermite rail welds are preferential sites for the formation of rail-head fatigue defects when compared to rail base metal or electric flash butt rail welds.

The HAL program, which began in 1988 and is currently active, is conducted jointly by the Federal Railroad Administration and the Association of American Railroads (Reiff 1990). The HAL tests are performed on the grounds of the Transportation Technology Center located near Pueblo, Colorado. A unit train (a train consisting of cars with identical axle loads) travels around a full-scale loop of track until a component fails. Several systems are monitored including the locomotives, the cars, and the track structure. Similar programs have been ongoing since 1976 (Reiff 1990).

The HAL unit train usually consists of 75 cars with each axle loaded to 0.3470 MN (39 tons). The train is operated at 64 km/hr (40 mph) around a 4.38 km (2.72 mi.) loop of track. During its circuit, the train negotiates four curves. Each curve is designed so that the outer rail receives more vertical wheel load than the inner rail when the train runs at the design speed. The loop is joined with electric flash butt rail welds, thermite rail welds, and bolted connections.

Some of the observations from the HAL program will be compared with the predictions of the RAHELS model. Brave (1990) presents observations of thermite rail welds from the start of the HAL program to the passage of approximately 3,846,000 axles. Nineteen thermite rail welds were removed from the HAL loop after rail-head fatigue defects were detected in them. Data from these welds are contained in Tables 2A - 4.

1.3 RAIL-HEAD DEFECTS

In this study, the term *metallurgical discontinuity* refers to a nonmetallic particle or pore that has a diameter of the order of a few metal-grain diameters; the term *fatigue defect* refers to a crack that is roughly the size of a dime (20 mm). Figure 2 is an optical photomicrograph of metallurgical discontinuities in the head region of a thermite rail weld. Figure 3 is a photograph of a fatigue crack in the head region of a thermite rail weld.

The *Rail Defect Manual* describes eight rail-head fatigue defects (Sperry Rail Service 1989). Defects are classified into three categories depending on the propagation plane of the defect: surface, transverse, and longitudinal defects (see Fig. 4). Table 1 lists each rail-head defect with its classification. Some defects propagate in multiple planes and have names indicative of this behavior: for example, detail fracture from shelling and compound fissure.[1] Note that although Table 1 lists shelling as a surface defect, it is commonly observed below the surface, and in this study, it is regarded as a subsurface defect.

The RAHELS model considers the nucleation and early growth aspects of rail-head fatigue defect formation. Propagation of an incipient crack is not considered by the RAHELS model; hence, the model cannot determine which of the defects listed in Table 1 as transverse defects is most likely to form under a given set of operating conditions. In this study, any defect that is predicted with a transverse orientation is nominally classified as detail fracture.

1.4 METALLURGICAL DISCONTINUITIES AND FATIGUE

Oderio (1992), Fry (1992), and Liu (1994) provide results of porosity and inclusion measurements taken in thermite rail welds. It is not clear what type of discontinuity is more damaging, but the available evidence seems to point to porosity. As

[1]The *Rail Defect Manual* contains photographs of most of these defects.

stated previously, thermite rail welds perform worse than the rail base metal itself and electric flash butt rail welds. Rail base metal contains inclusions, but the rolling process in rail manufacture should eradicate the type of porosity found in unforged steel castings such as standard thermite rail welds (Carpenter et al. 1993). The forging operation in electric flash butt rail welding should also eradicate such porosity. Fry (1992) presents a technique that incorporates a forging operation with the standard thermite rail welding process. Thermite welds thus modified contain less porosity, have smaller inclusion contents, and exhibit monotonic and fatigue properties similar to electric flash butt rail welds (Fry 1992; Liu 1994). Brooksbank and Andrews (1972) conclude "...that the presence of certain types of inclusion ... will be beneficial to fatigue properties. Consequently, the assessment of the properties of a steel should not be made on the total inclusion content ... but on a detailed knowledge of the size and composition of the predominant inclusions."

The fatigue literature presents many investigations that assess the damaging role of metallurgical discontinuities such as porosity and inclusions. Both experimental and analytical studies have been published (Puskar and Golovin 1985; Suresh 1991). Experimental results show evidence that fatigue cracks tend to nucleate at discontinuities (Lankford and Kusenberger 1973; Bowles and Schijve 1973; Fowler and Tetelman 1978; McEvily and Minakawa 1981; Hyzak and Bernstein 1982a; Hyzak and Bernstein 1982b; Carpenter et al. 1993). Crack nucleation is an important consideration for a rail-head fatigue model; the nucleation process is observed to consume 90% of the total fatigue life for many rail-head defects (Steele 1994).

Murakami (1989) presents a literature review and discussion assaying discontinuity characteristics that are important in terms of fatigue. He concludes that discontinuity *size,* and *location,* are critical fatigue parameters. Hyzak and Bernstein (1982b) conclude that for low strain ranges (implying high-cycle fatigue) discontinuity *shape* is critical. Discontinuity *composition* is identified as important by Carpenter et al. (1993). Discontinuity *orientation* is also considered important (Puskar and Golovin 1985).

Several studies present calculations of stress fields associated with discontinuities: e.g., Eshelby (1957), Brooksbank and Andrews (1972), Andrews and Brooksbank (1972), Miller and Keer (1983), and O'Toole and Santare (1990). Fatigue analyses, however, commonly regard microscopic discontinuities as cracks: e. g., Chiu et al. (1971), Tallian and McCool (1971), Tallian (1971), Chipperfield and Blicblau (1984), and Murakami (1989). Another approach regards discontinuities as sites for unusually harmful dislocation mechanisms: e.g., Tanaka and Mura (1982). RAHELS uses the solution presented in Eshelby (1957) to compute local stresses at the periphery of metallurgical discontinuities.

1.5 RAIL-HEAD STRESSES

The stresses that develop from wheel-rail contact cause plastic deformation on the running surface of the rail (Martin and Hay 1970). If the peak contact stress falls below a critical value known as the "shakedown limit", cumulative residual stresses eventually assume a configuration that prevents further plastic deformation in the contact patch: a process termed "elastic shakedown." If the peak contact stress rises above the "shakedown limit", one of two inelastic behaviors will result: "plastic shakedown" or "ratchetting". Yu (1992) presents a detailed study of cyclic rolling contact. Jiang (1993) presents a detailed study of cyclic plasticity.

Although plastic deformation is confined to a shallow region near the running surface, fatigue defects commonly nucleate at a greater depth in the rail head where material behavior is elastic (Martin and Hay 1970; Jiang and Sehitoglu 1992; Steele and Joerms 1993). The rail-head stress analysis in RAHELS is used to approximate elastic behavior below the running surface of the rail. A solution for the elastic fields in a two-layered half-plane subjected to Hertzian contact is derived for the RAHELS model in this study. Similar evaluations are presented in Smith and Liu (1953) for a single-layered half-plane and Kannel and Tevaarwerk (1984) for a single-layered half-space. The two-layered solution is

used as a means of capturing the effects of the relatively compliant support system below the rail.

1.6 MULTI-AXIAL FATIGUE PARAMETER CONCEPTS

The most important aspect of a fatigue model is the method used for computing fatigue damage. In many models, these computations take the form of evaluating one or more multi-axial fatigue parameters. Multi-axial fatigue parameters are functions constructed to isolate those tensor-field characteristics that contribute most to fatigue damage in a material. Some multi-axial fatigue parameters depend on the stress-tensor history; others use the strain-tensor history. Often the parameters are empirically based.

Two types of multi-axial fatigue parameters are common: critical-plane fatigue parameters and bulk fatigue parameters. The development of critical-plane parameters is motivated by experimental observations indicating that fatigue cracks nucleate as planar defects. The use of critical-plane fatigue parameters requires that a tensor history be resolved into components acting on a selection of material planes through the evaluation point. The plane corresponding to the largest value of the parameter through time is the critical plane (i.e., the plane upon which a fatigue defect is most likely to form).

Bulk fatigue parameters are scalar-valued functions of a tensor history. That is, they take as input the components of a tensor history and generate a single number as output. In both parameter types, the parameter value is regarded as a numerical index of fatigue damage, and these values are often correlated with experimental data so that fatigue-life estimates can be made. The RAHELS model uses a critical-plane multi-axial fatigue parameter called Findley's Parameter (Findley 1959) which is discussed more fully in the next chapter.

1.7 PREVIOUS RAIL-HEAD FATIGUE MODELS

Rail fatigue models help answer two fundamental questions which control the economics of railway track systems: By how much will the formation of fatigue defects

accelerate or decelerate if certain operating conditions are changed? When will a detectable fatigue defect propagate and cause a catastrophic rail break?

Previous rail-fatigue models have been developed. Although each of the models provides different types of information to address the fundamental questions, the concepts contained in the models have similarities. It is possible to group the models in a way that will simplify comparing the concepts used in the RAHELS model with the concepts used in previous models.

Most rail fatigue models fall into one of two groups: nucleation models or propagation models. The aim of nucleation models is to determine the number of axles of a certain weight that can pass before a fatigue defect will form in the rail, assuming that there is no pre-existing defect. Propagation models assume the pre-existence of a well-defined fatigue defect and aim at finding the propagation characteristics of the defect in terms of the number of passing axles. Some models incorporate both capabilities, but even these tend to put more emphasis on either the nucleation approach or the propagation approach.

Specific examples of nucleation models include Martin and Hay (1970), Abbott and Zarembski (1980), Jiang and Sehitoglu (1992), and Steele and Joerms (1993). Propagation models include Sampath et al. (1978), Chipperfield and Blicblau (1984), Farris et al. (1987), Yu and Keer (1989), Farris, et al. (1990).

The RAHELS model is a nucleation model and uses Findley's Critical-Plane Fatigue Parameter to compute fatigue damage. Abbott and Zarembski (1980) presents a one-dimensional model, which then does not use multi-axial fatigue parameter concepts. All of the other nucleation models quantify rail fatigue damage using bulk fatigue parameters.

Eshelby's solution for a 3-D local-stress analysis of an ellipsoidal discontinuity is used in the RAHELS model to evaluate the peripheral stresses of metallurgical discontinuities such as pores and inclusions. The tensors used in the previous nucleation

models are rail-head stress histories that are computed assuming a discontinuity- and defect-free material.

Foundation effects are an integral part of the rail-head stress analysis in the RAHELS model. Foundation effects are incorporated in previous models by using results from simple beam-on-elastic-foundation analyses superposed on computed rail-head stresses.

1.8 OVERVIEW OF THE RAHELS FATIGUE MODEL

Figure 5 is a schematic drawing of a longitudinal-section of a railroad rail. A location below the running surface of the rail is indicated in Fig. 5 with a small square. As a wheel approaches, passes over and departs from a location such as indicated in Figure 5, the material is subjected to a time-history of stress, $\Sigma(t)$. In the RAHELS model, the "histories" for a given depth below the running surface are computed using a static analysis. Stresses are computed "ahead" of the wheel-rail contact patch, beneath the contact patch, and "behind" the contact patch. These approximate global-stress histories, $\Sigma(t)$, are applied as external tractions on the extended volume surrounding an ellipsoidal discontinuity (Fig. 6). Local-stress histories, p(t), are computed at points on the periphery of the discontinuity (Fig. 6). The local stress histories are resolved into normal and shearing components on a selection of material planes (Fig. 7). The maximum range of shear stress is determined for each plane (Fig. 8), and Findley's Parameter is computed. The plane that results in the largest value of Findley's Parameter is the "critical plane" or the plane upon which a fatigue defect is predicted to nucleate.

2 PROCEDURES

2.1 THE RAIL-HEAD STRESS ANALYSIS

Figure 9 is a schematic drawing of the idealized wheel-rail-support system used in the RAHELS model. The contact zone between the wheel and the rail is modeled using Hertzian contact approximations on both the vertical wheel load and the tangential wheel load (see also Smith and Liu 1953). The rail is modeled as an infinitely long elastic strip of depth, d, and thickness, t. The supporting elements beneath the rail are combined and modeled as an elastic half-plane. The rail strip and the support layer are bonded together.

In this idealized system, exact expressions can be obtained for the rail-strip stresses. A solution technique presented in Uflyand (1965, 36-39) is adapted to solve the problem. Details of the solution method are provided in Appendix A. Appendix B is a print-out of the *Mathematica* document (called a notebook) that contains the normal load solution (Wolfram Research, Inc. 1993).[2] Appendix C is a print-out of the *Mathematica* notebook for the tangential load solution. The solutions can be combined, but having them separated facilitates constructing combinations of normal and tangential loading.

The support layer is constructed from an imaginary material that has the same Poisson's ratio as the rail strip. Young's modulus for the support layer is calibrated using a range of "reasonable" track modulus values.[3] The calibration proceeds as follows. The vertical displacement under a concentrated unit load is calculated using beam-on-elastic-foundation assumptions. Using a trial-and-error procedure, Young's modulus in the support layer of the model is determined that causes a mid-depth displacement in the rail

---

[2]*Mathematica* is a proprietary symbolic computer mathematics software package. *Mathematica* was used herein to construct solutions and perform computations. The package consists of two programs: a front-end program, or user interface, and a kernel program which "does the math". The front-end and kernel can be run on separate machines and linked through a network as was the case for this study. The front-end was run on an Apple Macintosh IIci personal computer and the kernel on a Hewlett-Packard 700 series workstation.

[3]For a discussion of track modulus, see Hay (1982).

strip under a concentrated unit load to be the same as the beam-on-elastic-foundation displacement. This analysis is performed for ten values of track modulus between 6.89 MPa (1000 psi) and 68.9 MPa (10,000 psi) and is included in the notebook in Appendix B.

A 3-D rail cannot be modeled properly using a 2-D analysis. Therefore, two variables characteristic of the actual rail are used to define the rail-strip cross-section in the RAHELS model: depth and moment of inertia. The depth of the rail strip (d) is the same as the depth of the actual rail; the thickness (t) is computed so that the moment of inertia of the rail strip in the RAHELS model is the same as the moment of inertia of the actual rail. The computed thickness is used only to scale the applied contact tractions so that the integrals of the tractions over the contact patch are equal to the specified values of vertical and tangential wheel load.

A rail section used commonly in the HAL track loop is considered in this study and has the A.R.E.A. designation 136RE. The values used to define the 136RE rail section for the RAHELS model are as follows: depth, 185.7 mm (7.3125 in.) and moment of inertia, 39.5 x 10^6 mm^4 (94.9 $in.^4$). The calculated value for the RAHELS model's rail-strip thickness is 74.0 mm (2.91 in.). The elastic constants for the rail strip in the RAHELS model, Young's modulus and Poisson's ratio, are 206,850 MPa (30,000,000 psi) and 0.33 respectively. The monotonic proportional limit value given in Fry (1992) for the standard thermite rail weld is used to define the yield point for the thermite weld metal used in the RAHELS model: σ_y = 586 MPa (85 ksi).

The RAHELS model regards the railroad wheel as a circular disk with the same thickness as the rail strip. The radius of the disk is a variable which is defined by the radius of the actual wheel. The same size wheel as used in the HAL program is used in this study; the HAL wheel has a radius of 482.6 mm (19 in.). The elastic properties of the disk are the same as the rail strip. For a given wheel load (normal or tangential), Hertzian contact approximations are used to compute a traction boundary condition for the running

surface of the rail strip (Fig. 4). The governing expressions are contained in Appendices A, B, and C (see also Smith and Liu 1953).

2.2 THE METALLURGICAL DISCONTINUITY ANALYSIS

The RAHELS model regards metallurgical discontinuities as stress concentrators. The elastic solution presented in Eshelby (1957) is used to compute the three dimensional stress fields in the rail-steel at the periphery of the discontinuities. Appendix D is a printout of the *Mathematica* notebook that contains the solution.

If the von Mises yield function value at any point at the periphery of a discontinuity exceeds 586 MPa (85 ksi), then the local-stress analysis of that discontinuity is considered ***invalid*** because the solution depends on elastic-material-behavior assumptions. In addition, the solution considers the discontinuities to be remote from one another and also remote from bounding surfaces.

Only two types of metallurgical discontinuities are considered in this study: pores and alumina inclusions; these two are the predominant metallurgical discontinuities observed in thermite rail welds. The elastic properties for the alumina inclusion are 413,700 MPa (60,000 ksi) for Young's Modulus and 0.25 for Poisson's Ratio. The porosity is defined using zero as the value for Young's modulus; Poisson's Ratio can be any number.

2.3 THE FATIGUE DAMAGE ANALYSIS

The RAHELS model uses Findley's Parameter to compute fatigue damage (Findley 1959). Findley's Parameter is a critical-plane multi-axial fatigue parameter which requires that a *stress*-tensor history be resolved into components acting on a selection of material planes through each evaluation point (Fig. 7).

For each candidate plane, the maximum range of shear stress is determined (Fig. 8) as well as the maximum normal stress. These two quantities are combined according to Findley's criterion for fatigue damage:

$$f = \frac{\Delta\tau_{max}}{2} + \kappa\sigma_{max}; \tag{1}$$

where "f" is Findley's parameter, and "κ" is an empirical material constant - approximately 0.3 for steel (Findley 1959). The plane that results in the most damaging parameter value through time is the critical plane (i.e., the plane upon which a fatigue defect is predicted to nucleate).

The logarithm of fatigue life is commonly regarded as being inversely proportional to the logarithm of Findley's Parameter. A fatigue-life correlation is constructed using high-cycle rotating-beam fatigue data on thermite rail welds (Liu 1994). The fatigue evaluation computations are organized at the end of the *Mathematica* notebook in Appendix D.

2.4 APPLICATION OF THE RAHELS MODEL

A *Standard Set* of variable definitions is presented in Table 5 that is intended to be a reasonable representation of conditions in the HAL testing program. Analytical results from the *Standard Set* are used as the basis of comparison throughout this study. Ten additional variable sets are defined in Table 6 and are used in a study of how rail-head fatigue damage varies with depth below the running surface for different operating conditions. Table 7 provides an outline for an examination of discontinuity shape and orientation effects. Table 8 lists the variable definitions for three analyses that are used to investigate the effects of a very soft foundation, winter or depressed temperature conditions (net axial tension in the rail), and summer or elevated temperature conditions (net axial compression in the rail).

3 RESULTS

3.1 DAMAGE VS. DEPTH

Tables 9-19 present the results for the damage versus depth analyses defined in Table 6. The unit normal vector to the discontinuity at the point of evaluation is denoted by "P." Results from three points on the surface of each discontinuity are presented: P = (1,0,0) - intersection with the X-axis, P = (0,1,0) - intersection with the Y-axis, and P = (0,0,1) - intersection with the Z-axis. The largest value of Findley's Parameter occurs at one of these points in each analysis.

The results for the *Standard Set* (see Table 5) are contained in Table 9. Local yielding occurs on at least one point down to a depth of 7 mm (0.28 in.). Below 7 mm the analyses for the *Standard Set* are considered valid. The point on the surface of the discontinuity surface where the Y-axis intersects it, P = (0,1,0), is the critical point when the discontinuity is examined at a location 15 mm (0.59 in.) below the running surface. The critical value of Findley's Parameter for the *Standard Set* is 168.2 MPa (24.4 ksi). The direction cosines for the critical plane are (0.26, 0.00, 0.97). Figure 10 is a plot of the global stress history for the *Standard Set* at the critical depth. Figure 11 is a plot of the standard-set residual stresses as they vary with depth below the running surface. Figure 12 is a plot of the local stress history for the *Standard Set* at the critical depth and point.

The results for *Set 1* (no residual stresses - see Table 6) are contained in Table 10. Local yielding occurs to a depth of 4 mm (0.16 in.). Below 4 mm the analyses for *Set 1* are considered valid. The point on the surface of the discontinuity where the z-axis intersects it, P = (0,0,1), is the critical point when the discontinuity is examined at a location 4 mm (0.16 in.) below the running surface. The critical value of Findley's Parameter for *Set 1* is 166.2 MPa (24.1 ksi). The direction cosines for the critical plane are (1.00, 0.00, 0.00).

The results for *Set 2* (added tangential wheel load - see Table 6) are contained in Table 11. Local yielding occurs to a depth of 7 mm (0.28 in.). Below 7 mm the analyses for *Set 2* are considered valid. The point on the surface of the discontinuity where the Y-axis intersects it, P = (0,1,0), is the critical point when the discontinuity is examined at a location 15 mm (0.59 in.) below the running surface. The critical value of Findley's Parameter for *Set 2* is 170.3 MPa (24.7 ksi). The direction cosines for the critical plane are (0.26, 0.00, 0.97).

The results for *Set 3* (smaller vertical wheel load - see Table 6) are contained in Table 12. Local yielding occurs to a depth of 7 mm (0.28 in.). Below 7 mm the analyses for *Set 3* are considered valid. The point on the surface of the discontinuity where the Y-axis intersects it, P = (0,1,0), is the critical point when the discontinuity is examined at a location 15 mm (0.59 in.) below the running surface. The critical value of Findley's Parameter for *Set 3* is 163.4 MPa (23.7 ksi). The direction cosines for the critical plane are (0.26, 0.00, 0.97).

The results for *Set 4* (stiffer foundation - see Table 6) are contained in Table 13. Local yielding occurs to a depth of 7 mm (0.28 in.). Below 7 mm the analyses for *Set 4* are considered valid. The point on the surface of the discontinuity where the Y-axis intersects it, P = (0,1,0), is the critical point when the discontinuity is examined at a location 15 mm (0.59 in.) below the running surface. The critical value of Findley's Parameter for *Set 4* is 167.5 MPa (24.3 ksi). The direction cosines for the critical plane are (0.26, 0.00, 0.97).

The results for *Set 5* (stiffer foundation with tangential wheel load - see Table 6) are contained in Table 14. Local yielding occurs to a depth of 7 mm (0.28 in.). Below 7 mm the analyses for *Set 5* are considered valid. The point on the surface of the discontinuity where the Y-axis intersects it, P = (0,1,0), is the critical point when the discontinuity is examined at a location 15 mm (0.59 in.) below the running surface. The critical value of

Findley's Parameter for *Set 5* is 169.6 MPa (24.6 ksi). The direction cosines for the critical plane are (0.26, 0.00, 0.97).

The results for *Set 6* (oxide discontinuity - see Table 6) are contained in Table 15. No local yielding occurs. The analyses for *Set 6* are considered valid for all depths except Y = 0. The point on the surface of the discontinuity where the Y-axis intersects it, P = (0,1,0), is the critical point when the discontinuity is examined at a location 2 mm (0.08 in.) below the running surface. The critical value of Findley's Parameter for *Set 6* is 105.5 MPa (15.3 ksi). The direction cosines for the critical plane are (1.00, 0.00, 0.00).

The results for *Set 7* (oxide discontinuity with tangential wheel load - see Table 6) are contained in Table 16. The analyses for *Set 7* are considered valid for all depths except Y = 0. The point on the surface of the discontinuity where the Y-axis intersects it, P = (0,1,0), is the critical point when the discontinuity is examined at a location 2 mm (0.08 in.) below the running surface. The critical value of Findley's Parameter for *Set 7* is 105.5 MPa (15.3 ksi). The direction cosines for the critical plane are (1.00, 0.00, 0.00).

The results for *Set 8* (football-shaped oxide discontinuity - see Table 6) are contained in Table 17. No local yielding occurs. The analyses for *Set 8* are considered valid for all depths except Y = 0. The point on the surface of the discontinuity where the Y-axis intersects it, P = (0,1,0), is the critical point when the discontinuity is examined at a location 2 mm (0.08 in.) below the running surface. The critical value of Findley's Parameter for *Set 8* is 106.9 MPa (15.5 ksi). The direction cosines for the critical plane are (1.00, 0.00, 0.00).

The results for *Set 9* (football-shaped oxide discontinuity with tangential wheel load - see Table 6) are contained in Table 18. Local yielding occurs to a depth of nearly 1 mm (0.04 in.). The analyses for *Set 9* are considered valid for depths below 1 mm (0.04 in.). The point on the surface of the discontinuity where the X-axis intersects it, P = (1,0,0), is the critical point when the discontinuity is examined at a location 1 mm (0.04 in.) below the

running surface. The critical value of Findley's Parameter for *Set 9* is 108.2 MPa (15.7 ksi). The direction cosines for the critical plane are (0.17, 0.98, 0.00).

The results for *Set 10* (no discontinuity - see Table 6) are contained in Table 19. No local yielding occurs. The analyses for *Set 10* are considered valid for all depths. The critical value of Findley's Parameter for *Set 10* is 82.0 MPa (11.9 ksi) and occurs at the running surface. The direction cosines for the critical plane are (0.00, 0.77, 0.64).

Figures 13-23 are plots of the data from Tables 9 through 19 respectively. Findley's Parameter is represented on the horizontal axis, and depth below the running surface is represented on the vertical axis. Data from the zone where local plasticity occurs falls in the shaded region. The discontinuity is shown schematically with the three analysis points indicated. Arrows are drawn from each analysis point to its corresponding data plot(s). Figures 13-23 also display data from the *Standard Set*. The dashed line in these figures at 7 mm (0.28 in.) below the running surface denotes the local plasticity cessation depth for the *Standard Set*. Figures 24-34 are schematic drawings of the critical planes from each of the analyses defined in Table 6. Note that the X-Y plane is a plane of symmetry for these analyses so that there are actually two planes predicted as equally critical: one for $Z > 0$ and one for $Z < 0$. The plane on the $Z > 0$ side is shown.

3.2 IMPURITY SHAPE AND ORIENTATION

Tables 20-25 contain the results of the pore shape and orientation analyses.

3.3 SEASONAL TEMPERATURE: WINTER VS. SUMMER

Table 26 contains the results of the temperature analyses. Winter conditions have a critical point at the Y-axis intersection, P = (0,1,0). The critical value of Findley's Parameter is 179.3 MPa (26.0 ksi). The direction cosines for the critical plane are (0.42, 0.00, 0.91). Summer conditions have a critical point at the X-axis intersection, P = (1,0,0). The critical value of Findley's Parameter is 168.9 MPa (24.5 ksi). The direction cosines for the critical plane are (0.00, 0.34, 0.94).

Figure 35 is a schematic drawing of the critical plane for winter conditions. Figure 36 is a schematic drawing of the critical plane for summer conditions.

3.4 FOUNDATION STIFFNESS

The results for the standard foundation are described above with the *Standard Set*: Findley's Parameter, 168.2 MPa (24.4 ksi), and critical plane, (0.26, 0.00, 0.97). The results for the stiff foundation are described above with *Set 4*: Findley's Parameter, 167.5 MPa (24.3 ksi), and critical plane, (0.26, 0.00, 0.97). The results for the weak foundation are contained in Table 26. The critical point is at the Y-axis intersection, P = (0,1,0). The critical value of Findley's Parameter is 173.1 MPa (25. ksi). The direction cosines for the critical plane are (0.34, 0.00, 0.94).

Figure 24 is a schematic drawing of the critical plane for the standard foundation. Figure 28 is a schematic drawing of the critical plane for the stiff foundation. Figure 37 is a schematic drawing of the critical plane for the weak foundation.

3.5 NUCLEATION LIVES

The logarithm of nucleation life, N_n, is commonly regarded as being inversely proportional to the logarithm of Findley's Parameter, f:

$$N_n = A f^c; c < 0. \tag{3.1}$$

Using the data from Liu (1994) and a least-squares-fit algorithm (see Appendix D), the following parameter-life correlation expression is obtained:

$$N_n = 10^{17.318} (0.145\ f)^{-7.452}. \tag{3.2}$$

The units are cycles or number of axles. Findley's Parameter, f, is measured in MPa.

4 DISCUSSION

4.1 LIMITATIONS OF THE RAHELS FATIGUE MODEL

The RAHELS fatigue model was developed to examine the high-cycle fatigue behavior of thermite-welded railroad rails. Since the deformation of rail steel in a high-cycle fatigue environment is nominally elastic, the analyses used in the RAHELS model consider only elastic conditions.

The RAHELS model predicts the nucleation life of incipient cracks which emanate from metallurgical discontinuities such as pores. The model does not consider interaction among discontinuities or discontinuity-size effects. Additionally, the model gives no indication as to whether the incipient cracks will propagate to form a dominant crack.

The RAHELS model regards inclusions as perfectly bonded to the metal matrix; inclusions are commonly not bonded to the metal matrix. In a fatigue environment, hard brittle inclusions sometimes break into several pieces.

The RAHELS model uses experimentally-measured rail-head residual stresses. Both vertical and tangential wheel loads effect the state of residual stresses in the rail head. Since the model does not calculate the residual stresses, the predicted effects of vertical and tangential wheel loads on fatigue damage are uncoupled from the effects that they have on residual stresses.

4.2 PREDICTIONS OF THE RAHELS FATIGUE MODEL

4.2.1 The Effects of Pores and Inclusions

Thermite rail welds usually contain pores and alumina inclusions. Which of these discontinuities is more damaging apparently is not known. Referring to Figs. 19-22, the RAHELS model predicts that under *Standard-Set* conditions, pores are much more damaging. These figures also show that the model predicts pores to be most damaging

when they are located 15 mm (0.59 in.) below the running surface, the depth at which the tensile residual stresses reach a maximum.

The type of rail-head defect that is predicted to form under *Standard Set* conditions is similar to a vertical split head (see Fig. 24). Three of the defects predicted for the alumina inclusion analyses (*Sets 6-8*) are similar to detail fractures (see Figs. 30-32). The analysis of the elongated alumina inclusion in *Set 9* indicates that a vertical split head will form (Fig. 33).

Since both of these metallurgical discontinuities are usually present in thermite rail welds, the prediction of the RAHELS model suggests that rail-head fatigue defects which form in thermite rail welds preferentially nucleate at pores and not at inclusions.

4.2.2 The Effects of Pore Shape

Three axes must be specified to define the shape of a pore: a major axis, a minor axis, and a median axis. Using ratios of the lengths of the axes lengths (e. g., λ_y / λ_Z), it is possible to display the predictions from the pore shape and orientation analyses (Tables 20 through 25) in a single diagram. Figure 38 shows that the RAHELS model predicts that the type of defect that will form and the nucleation life of the defect are strongly influenced by pore shape and orientation. In order to construct Figure 38, two of the pore axes must be defined relative to the third, and each of the pore axes must be aligned with one of the coordinate axes. The coordinate system of the rail defines a longitudinal axis, X, a vertical axis, Y, and a transverse axis, Z (see Fig. 2). The pore shape and orientation analyses (Table 7) satisfy these conditions since discontinuity size effects are not considered in the model, and all of the pores considered in these analyses are aligned with the coordinate axes of the rail.

The horizontal coordinate in Figure 38 represents the ratio of the longitudinal axis to the transverse axis of the pore. The vertical coordinate represents the ratio of the vertical axis to the transverse axis of the pore. Therefore, each point on the diagram represents not

just one pore but all pores having the same axis ratios. For example, the point (1,1) in Figure 38 represents all spherical pores.

The three lines (horizontal, inclined, and vertical) on the diagram in Figure 38 indicate transition from poker-chip shaped pores to football-shaped pores. Specifically, the data points which lie on the vertical line represent the transition from PCH-shaped pores through spherical-shaped pores to FBY-shaped pores. The data points which lie on the horizontal line represent the transition from PCT-shaped pores through spherical-shaped pores to FBX-shaped pores. The data points which lie on the diagonal line represent the transition from PCV-shaped pores through spherical-shaped pores to FBZ-shaped pores. To provide a visual guide for these transitions, schematic drawings of the six limiting pore shapes and the sphere are inset at the perimeter of the diagram.

The shapes at the endpoints of each of the three lines in Figure 38 are important because these extreme shapes cause local plasticity under the *Standard Set* conditions. Lines which connect these points around the perimeter of the diagram delineate the limit of the applicability of the RAHELS model for the *Standard Set.* Shapes outside the perimeter cannot be considered using the model since local plastic deformation violates the assumptions of elastic-material-behavior in the model. All of the shapes within the perimeter of the diagram can be considered using the model.

Three different types of defects were predicted in the pore-shape and orientation analyses and are indicated by the shaded regions in Figure 38: shelling, vertical split head, and detail fracture. Classification of the defects was accomplished by comparing the predicted critical fatigue plane with defect descriptions contained in the *Rail Defect Manual* (Sperry Rail Service 1989). The distinct boundaries between defect zones are misleading and result from the classification procedure. For example, with reference to the three middle columns of Table 24, the first four rows list the critical data for four of the shapes in the PCT analyses. The first critical plane is shown schematically in Figure 24. This plane seems to be in reasonable agreement with descriptions for a vertical split head. Refer again

to the three middle columns of Table 24 and notice how the orientation of the critical plane changes as the pore shape changes. As the pore shape becomes more like a poker chip, the orientation of the critical plane becomes similar to the orientation observed for detail fractures. Clearly, there is some judgment required to classify the defects; the boundaries in Figure 38 were drawn at what appeared to be the most appropriate locations. It is interesting to note that even experts in defect detection will sometimes disagree over the classification of an observed rail defect.

Contour lines drawn on Figure 38 indicate fatigue-crack nucleation lives in millions of axle passages. The PCT analyses provide the worst case: 176,000 axles. The FBZ analyses provide the best case: 72,361,000 axles.

The three different rail-head defects predicted are caused by different pore shapes (Fig. 38). In rough terms, shelling nucleates at PCH-shaped pores, and detail fractures nucleate at PCT-shaped pores. These pores have a similar *shape*, but are *oriented* 90° apart. The orientations of the pores are similar to the orientations of the defects that they cause. The vertical split head defect is predicted for a relatively large range of pore shapes and orientations.

The least damaging pore shape and the most damaging pore shape both cause detail fracture. Two orders of magnitude span the ratio between the life predicted for the detail fracture at the least damaging pore and the life predicted for the detail fracture at the most damaging pore.

The RAHELS model predicts that both the type of defect that forms under a given set of operating conditions and the nucleation life of the defect can be vastly different for different pore shapes and orientations.

4.2.3 The Possible Effects of Pore Size

Incipient cracks emanating from large pores will have a higher propensity to propagate and form a dominant crack. As the size and number of pores decreases, the

number of cycles required to form a dominant crack increases. There are analytical predictions which suggest that there is a critical pore size from which incipient fatigue cracks cease to be effective in forming a dominant crack (Ting 1991). This evidence has important implications for the RAHELS model which will be discussed below.

There is a zone from the running surface to a depth of 7 mm below the running surface where local plastic deformation is predicted at the periphery of the discontinuities for several of the analyses in this study. The material behavior in this zone is associated with low-cycle fatigue response and thus rapid formation of fatigue cracks. However, in light of the concepts presented by Ting (1991), incipient cracks in this zone might not propagate to form a dominant crack. In this zone, there are measured large compressive residual stresses superposed on large compressive wheel-rail contact stresses. On the contrary, below 7 mm, in the region where material behavior is always predicted to be elastic, the residual stresses are tensile and would provide a better environment for the propagation of incipient fatigue cracks.

4.2.4 The Effects of Residual Stresses

Figure 13 shows the predictions of the RAHELS model in the absence of residual stresses. The location of maximum damage moves upward from 15 mm below the running surface, as found for the *Standard Set,* to 4 mm (0.16 in.) below the running surface. However, the amount of fatigue damage (i.e., the value of Findley's Parameter) remains roughly the same. The type of defect predicted in the absence of residual stresses is similar to a detail fracture (Fig. 24).

4.2.5 The Effects of Seasonal Temperatures

Winter weather produces cold rail temperatures causing the rail to decrease in length. This effect can cause axial tensile stresses in continuous welded rail which in turn cause "pull-aparts" - large gaps between the ends of adjacent rails. Summer weather has the opposite effect. The compressive stresses in continuous-welded-rail that are associated

with summer temperatures are dangerous because these stresses can cause track buckling and subsequent derailments of trains. To minimize the occurrences of pull-aparts and track buckling, continuous-welded-rail is installed at an empirically established "neutral temperature." The value of the neutral temperature changes with geographic location.

As seen in Table 26, a net axial tension in the rail is more damaging in terms of fatigue than a net axial compression. The RAHELS model predicts that the two different temperature regimes favor the formation of two different defects. The defect associated with winter conditions is predicted to be a vertical split head. However for summer conditions, shelling is predicted.

4.2.6 The Effects of Wheel Loads

As seen in Fig. 15, by adding a tangential wheel load of 0.052 MN (11,700 lbf) to the *Standard Set* conditions, fatigue damage increases only slightly. Figure 16 shows that a 15% decrease in vertical wheel load produces a 3% decrease in fatigue damage (value of Findley's Parameter).

Vertical wheel load is predicted to be more influential on fatigue damage than tangential wheel load. Increases in either vertical or tangential wheel loads are predicted to cause decreases in fatigue life.

4.2.7 The Effects of Foundation Stiffness

A 60% increase in foundation stiffness from the *Standard Set* produced a 3% increase in fatigue life. An 80% decrease in foundation stiffness produced a 19% decrease in fatigue life. The effects of foundation stiffness are predicted to be modest when compared to the effects of other variables.

4.3 COMPARISON OF PREDICTIONS WITH HAL OBSERVATIONS

There are only limited experimental data available to examine the validity of the predictions of the RAHELS fatigue model. The most useful data available are the HAL program's observations of thermite rail welds that were removed from the track loop

because the welds developed subsurface rail-head fatigue defects. Tables 2A through 3B list a nominal classification for each of the observed defects (shell, detail fracture, etc.) and an estimate of the number of axles that passed before a defect was detected. The *Standard-Set* definitions in Table 5 are intended to be a reasonable representation of the HAL testing conditions.

Unfortunately, the observations from the HAL program do not include enough information to define the fatigue-initiating discontinuity in the RAHELS model. The model requires that the type, shape, location, and orientation of the critical discontinuity are known. Therefore, it will only be possible to show that the predictions made by the RAHELS model are in reasonable agreement with the HAL observations.

The HAL data from Table 4 is indicated in Figure 39 in zones having the observed lives of each defect. Without information on the discontinuity which initiates the observed defect, little more can be said about the agreement between the predictions of the RAHELS model and the observations of the HAL testing program. However, it is encouraging to note that even using essentially arbitrary assumptions as to the characteristics of the critical metallurgical discontinuity, the RAHELS model predicts lives and defects which are in agreement with the HAL program observations.

4.4 Suggestions for Improving Fatigue Performance

Changing the shape of thermite rail weld pores to the optimum shape indicated in Fig. 38 or eradicating porosity altogether would substantially improve the fatigue performance of thermite rail welds. Modified thermite rail welding (Fry 1992) is a process currently being developed which has the potential to eradicate porosity that is usually observed in thermite rail welds.

Residual stresses were predicted to have a strong influence on rail-head defect formation in thermite rail welds. Removing the surface layer of compressive residual stresses by grinding should also remove the subsurface zone of equilibrated tensile

stresses. Referring to Figure 13, the critical depth will jump from a pre-grind level of 15 mm (0.59 in.) to a post-grind level of 4 mm (0.16 in.). This effect is only temporary since the compressive surface residual stresses will return in service. During the accumulation of compressive stresses, the critical depth will move downward until residual stresses reach a steady state. Although current rail grinding practices are established to control the effects of rail wear, it might be possible to optimize rail grinding practices with respect to rail wear and residual stress management. Another method of managing residual stresses might be to use a bank of lasers, or other heat sources, to perform a controlled *in situ* heat treatment and thermal stress relief of the rail head.

Changes to the other variables that were examined do not offer the potential for improvement that is possible through the elimination of porosity and reduction of residual stresses.

4.5 FUTURE WORK

To provide data to test the RAHELS model definitively, measurements of the discontinuity that initiates fatigue damage should be made.

This study concentrated on unit train operations to facilitate comparison with published data. A study of revenue-service load histories would be possible by incorporating a variable amplitude fatigue evaluation in the model.

The effects of defect size and defect propagation were not considered in this model since it was assumed that nucleation life constitutes the dominant portion of total defect life.

Studies in which the model is applied to rail in general or other non-rail fatigue-prone components that contain metallurgical discontinuities might be attempted.

5 CONCLUSIONS

Six conclusions follow from the analyses using the RAHELS model:

1) The RAHELS model predicts that pores in thermite rail welds are much more damaging than the alumina inclusions that are also present.
2) The RAHELS model predicts that the shape and the orientation of pores in thermite rail welds have a strong influence on the type of rail-head fatigue defect that forms under a given set of operating conditions. Pore shape and orientation also have a strong influence on the nucleation life of the defect.
3) The RAHELS model predicts that porosity is most damaging at a depth of 15 mm below the running surface of the rail, the depth at which the rail-head tensile residual stresses are maximum.
4) The RAHELS model predicts that axial tensile stresses resulting from cold winter temperatures are more damaging in terms of rail-head defect formation than axial compressive stresses resulting from summer temperatures. In addition, the model predicts that the two different seasons favor the formation of two different rail-head fatigue defects: vertical split head in the winter and shelling in the summer.
5) The RAHELS model predicts that increases in either vertical or tangential wheel loads cause increases in fatigue damage. The vertical wheel load is predicted to have a stronger influence.
6) The RAHELS model predicts that track-foundation stiffness has a negligible influence on rail-head fatigue defect formation. This result implies that the stresses directly associated with wheel-rail contact contribute most to the formation of fatigue defects in the rail-head.

These conclusions suggest the following two means that give some promise for improving the fatigue performance of thermite rail welds:

1) Eradicating porosity in thermite rail welds would significantly improve the fatigue performance of the welds. A "Squeeze" thermite rail welding procedure is currently being developed and has the potential to eliminate the porosity that is usually present in thermite rail welds.
2) Controlled grinding of the rail head could remove the surface layer of compressive rail-head residual stresses and would necessarily decrease or remove altogether the equilibrated subsurface tensile residual stresses. It should be possible to optimize a rail-grinding schedule that would significantly improve the fatigue performance of thermite rail welds.

TABLES

Table 1

Rail-Head Fatigue Defects

Name	Type
Shelling†	Surface Defect
Transverse Fissure	Transverse Defect
Compound Fissure	Transverse Defect
Detail Fracture from Shelling	Transverse Defect
Detail Fracture from Head Check	Transverse Defect
Detail Fracture from Welded Bond Connection	Transverse Defect
Horizontal Split Head	Longitudinal Defect
Vertical Split Head	Longitudinal Defect

Source: Sperry Rail Service (1989)

†Shelling is regarded as a subsurface fatigue defect in this study.

Table 2A

FAST/HAL Thermite Rail Weld Data (shelling, outer rail)†

Weld Identification	Life to Weld Removal (millions of axles)
03-0743	3.69
03-1674	0.93
25-0046	1.83
25-0070	1.83
25-0093	1.64
25-0182	0.75
25-0726	1.28
25-1225	1.51
25-1249	1.51
25-1618	1.42
Average	1.64 ± 0.76

†Source: Brave (1990)

Table 2B

FAST/HAL Thermite Rail Weld Data
(detail fractures, outer rail)†

Weld Identification	Life to Weld Removal (millions of axles)
03-0269	2.09
31-0251	1.44
Average	1.77 ± 0.33

†Source: Brave (1990)

Table 3A

FAST/HAL Thermite Rail Weld Data
(shelling, inner rail)†

Weld Identification	Life to Weld Removal (millions of axles)
03-0268	3.69
03-0363††	3.69
25-0343	3.69
25-1364	3.69
31-0265	1.44
Average	3.24 ± 0.90

†Source: Brave (1990)
††Also listed as Vertical Split Head

Table 3B

FAST/HAL Thermite Rail Weld Data (detail fractures, inner rail)†

Weld Identification	Life to Weld Removal (millions of axles)
03-0079	3.69
25-1161	3.69
Average	3.69

†Source: Brave (1990)

Table 4

Summary of FAST/HAL Thermite Rail Weld Data

	Average Life to Weld Removal (millions of axles)
All Shells	2.17 ± 1.11
All Detail Fractures	2.73 ± 0.99

Table 5

Variables Defining the *Standard Set*

Variable	Value
Rail Type	A.R.E.A. 136 RE
Wheel Radius	0.4826 m (19 in.)
Track Modulus	34.5 MPa (5,000 psi)
Vertical Wheel Load	N = 0.1735 MN (39,000 lbf)
Tangential Wheel Load	0 MN
Residual Stresses	Steele and Joerms (1993, 4-6, 44)
Discontinuity Type	Pore
Discontinuity Shape: $\frac{X^2}{\lambda_X^2}+\frac{Y^2}{\lambda_Y^2}+\frac{Z^2}{\lambda_Z^2}=1$	$\frac{\lambda_X}{\lambda_Z}=\frac{\lambda_Y}{\lambda_Z}=1$ (spherical)

Table 6
Variable-Set Definitions for Damage vs. Depth Analyses

Analysis	Variables that Differ from the *Standard Set*
Standard Set	None
Set 1	Residual Stresses: 0 MPa
Set 2	Tangential Wheel Load: T = 0.052 MN (11,700 lbf)
Set 3	Vertical Wheel Load: N = 0.1468 MN (33,000 lbf)
Set 4	Track Modulus: 55.2 MPa (8,000 psi)
Set 5	Track Modulus: 55.2 MPa, Tangential Wheel Load: T = 0.052 MN
Set 6	Discontinuity Type: Oxide
Set 7	Discontinuity Type: Oxide, Tangential Wheel Load: T = 0.052 MN
Set 8	Discontinuity Type: Oxide, Discontinuity Shape: $\frac{\lambda_X}{\lambda_Z} = 4; \frac{\lambda_Y}{\lambda_Z} = 1$
Set 9	Discontinuity Type: Oxide, Discontinuity Shape: $\frac{\lambda_X}{\lambda_Z} = 4; \frac{\lambda_Y}{\lambda_Z} = 1$, Tangential Wheel Load: T = 0.052 MN
Set 10	Discontinuity Type: None

Table 7

Variable-Set Definitions for Pore-Shape and Orientation Analyses†

Analysis††	Pore Shape		Pore Orientation (Fig. 2)
STD	$\frac{\lambda_X}{\lambda_Z} = 1; \frac{\lambda_Y}{\lambda_Z} = 1$	(basketball)	N/A
FBX	$\frac{\lambda_X}{\lambda_Z} > 1; \frac{\lambda_Y}{\lambda_Z} = 1$	(football)	Along X-Axis
FBY	$\frac{\lambda_X}{\lambda_Z} = 1; \frac{\lambda_Y}{\lambda_Z} > 1$	(football)	Along Y-Axis
FBZ	$\frac{\lambda_X}{\lambda_Z} = \frac{\lambda_Y}{\lambda_Z} < 1$	(football)	Along Z-Axis
PCH	$\frac{\lambda_X}{\lambda_Z} = 1; \frac{\lambda_Y}{\lambda_Z} < 1$	(poker chip)	Parallel to Horizontal Plane
PCV	$\frac{\lambda_X}{\lambda_Z} = \frac{\lambda_Y}{\lambda_Z} > 1$	(poker chip)	Parallel to Vertical Plane
PCT	$\frac{\lambda_X}{\lambda_Z} < 1; \frac{\lambda_Y}{\lambda_Z} = 1$	(poker chip)	Parallel to Transverse Plane

† All other variables are taken from the *Standard Set.*
†† Analyses performed at Y = -15 mm

Table 8

Variable-Set Definitions for Weak Foundation and Temperature Analyses

Analysis†	Variables that Differ from the *Standard Set*
STD	None
WKF	Track Modulus: 6.89 MPa (1000 psi)
WTR	Axial Residual Stress: Added Tension 103.4 MPa (15, 000 psi)
SMR	Axial Residual Stress: Added Compression 68.9 MPa (10, 000 psi)

† Analyses performed at Y = -15 mm

Table 9

Analysis Results for the *Standard Set*

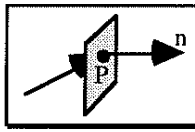

A plane with normal vector, n, passes through a point, P, at the discontinuity's surface. †

	P = (1, 0, 0)			P = (0, 1, 0)			P = (0, 0, 1)		
Depth (mm)	Yield Function (MPa)	Findley's Parameter (MPa)	Unit Normal to Nucleation Plane, n	Yield Function (MPa)	Findley's Parameter (MPa)	Unit Normal to Nucleation Plane, n	Yield Function (MPa)	Findley's Parameter (MPa)	Unit Normal to Nucleation Plane, n
0	470.9	188.9	(.00, .77, .64)	922.5	122.0	(.62, .74, .26)	1058.3	247.5	(.00, .71, .71)
1	786.0	157.9	(.77, .64, .00)	478.5	69.6	(.50, .29, .82)	943.8	193.1	(.00, .64, .77)
2	901.1	133.1	(.77, .64, .00)	348.2	66.9	(.00, .64, .77)	945.3	151.7	(.00, .64, .77)
3	894.2	115.1	(.82, .57, .00)	278.5	71.0	(.57, .00, .82)	908.7	137.2	(1.0, .00, .00)
4	826.0	99.3	(.82, .57, .00)	231.0	75.8	(.57, .00, .82)	830.8	122.7	(1.0, .00, .00)
5	733.6	88.9	(.82, .57, .00)	205.4	77.2	(.57, .00, .82)	732.9	108.2	(1.0, .00, .00)
6	638.4	82.0	(.82, .57, .00)	203.4	80.0	(.50, .00, .87)	630.2	97.2	(1.0, .00, .00)
8	490.2	99.3	(.00, .57, .82)	238.6	94.4	(.42, .00, .91)	449.5	83.4	(1.0, .00, .00)
10	433.0	120.6	(.00, .50, .87)	307.5	115.1	(.34, .00, .94)	328.2	74.5	(.97, -.26, .00)
15	508.8	155.1	(.00, .34, .94)	*468.8*	*168.2*	*(.26, .00, .97)*	247.5	76.5	(1.0, .00, .00)
20	486.1	144.1	(.00, .26, .97)	461.9	166.2	(.26, .00, .97)	231.0	73.8	(1.0, -.09, .00)
25	255.1	74.5	(.00, .34, .94)	228.2	88.3	(.42, .00, .91)	155.8	61.4	(1.0, .00, .00)

1 ksi = 6.895 MPa, 1 in. = 25.4 mm

† The vector (1, 0, 0) is directed along the rail axis; (0, 1, 0) points to the running surface; (0, 0, 1) completes the right-handed system.

Table 10

Analysis Results for *Set 1* (no residual stresses)

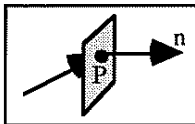

A plane with normal vector, n, passes through a point, P, at the discontinuity's surface. †

	P = (1, 0, 0)			P = (0, 1, 0)			P = (0, 0, 1)		
Depth (mm)	Yield Function (MPa)	Findley's Parameter (MPa)	Unit Normal to Nucleation Plane, n	Yield Function (MPa)	Findley's Parameter (MPa)	Unit Normal to Nucleation Plane, n	Yield Function (MPa)	Findley's Parameter (MPa)	Unit Normal to Nucleation Plane, n
0	715.7	210.3	(.00, .71, .71)	795.7	220.6	(.71, .00, .71)	969.4	251.0	(.71, .00, .71)
1	721.9	216.5	(.00, .71, .71)	449.5	145.5	(.50, .00, .87)	774.3	217.9	(.00, .71, .71)
2	675.0	192.4	(.00, .71, .71)	279.9	113.1	(.50, .00, .87)	672.2	201.3	(1.0, .00, .00)
3	601.9	168.2	(.00, .71, .71)	239.9	102.0	(.50, .00, .87)	588.8	186.2	(1.0, -.09, .00)
4	527.4	148.2	(.00, .71, .71)	207.5	92.4	(.57, .00, .82)	*514.3*	*166.2*	*(1.0, .00, .00)*
5	461.3	129.6	(.00, .71, .71)	176.5	82.0	(.57, .00, .82)	449.5	146.9	(1.0, .00, .00)
6	406.1	114.5	(.60, .72, .34)	161.3	71.7	(.57, .00, .82)	395.8	130.3	(1.0, .00, .00)
8	322.7	92.4	(.60, .72, .34)	146.2	60.7	(.57, .00, .82)	314.4	104.8	(1.0, .00, .00)
10	264.8	77.2	(.62, .74, .26)	128.2	51.7	(.57, .00, .82)	258.6	84.8	(.26, .97, .00)
15	180.0	54.5	(.12, .70, .71)	105.5	37.9	(.57, .00, .82)	176.5	60.0	(1.0, .00, .00)
20	134.4	42.7	(.00, .71, .71)	91.7	29.6	(.57, .00, .82)	133.8	45.5	(.09, 1.0, .00)
25	106.9	35.2	(.00, .71, .71)	81.4	24.8	(.57, .00, .82)	107.6	37.2	(1.0, .00, .00)

1 ksi = 6.895 MPa, 1 in. = 25.4 mm

† The vector (1, 0, 0) is directed along the rail axis; (0, 1, 0) points to the running surface; (0, 0, 1) completes the right-handed system.

Table 11

Analysis Results for *Set 2* (added tangential wheel load)

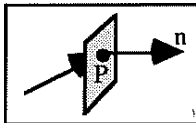

A plane with normal vector, n, passes through a point, P, at the discontinuity's surface. †

	P = (1, 0, 0)			P = (0, 1, 0)			P = (0, 0, 1)		
Depth (mm)	Yield Function (MPa)	Findley's Parameter (MPa)	Unit Normal to Nucleation Plane, n	Yield Function (MPa)	Findley's Parameter (MPa)	Unit Normal to Nucleation Plane, n	Yield Function (MPa)	Findley's Parameter (MPa)	Unit Normal to Nucleation Plane, n
0	476.4	230.3	(.13, .75, .64)	1091.4	311.0	(-.71,.71, .00)	1213.5	397.1	(.70, .12, .71)
1	786.0	175.1	(.71, .71, .00)	617.8	92.4	(.57, .00, .82)	1006.6	217.2	(.32, .56, .77)
2	901.1	142.0	(.77, .64, .00)	455.7	86.2	(.57, .00, .82)	975.6	168.2	(.36, .53, .77)
3	896.3	121.3	(.82, .57, .00)	353.0	88.9	(.57, .00, .82)	926.7	140.7	(1.0, -.09, .00)
4	829.4	104.1	(.82, .57, .00)	281.3	88.9	(.57, .00, .82)	843.2	123.4	(1.0, -.09, .00)
5	737.0	93.1	(.82, .57, .00)	248.9	86.9	(.57, .00, .82)	742.6	109.6	(1.0, -.09, .00)
6	641.9	86.2	(.77, .64, .00)	246.8	88.3	(.50, .00, .87)	638.5	98.6	(1.0, -.09, .00)
8	493.0	102.7	(.00, .57, .82)	265.4	100.7	(.50, .00, .87)	457.1	83.4	(1.0, .00, .00)
10	435.1	123.4	(.00, .50, .87)	311.0	118.6	(.42, .00, .91)	335.1	77.9	(-.98, .17, .00)
15	510.2	156.5	(.00, .34, .94)	*469.5*	*170.3*	*(.26, .00, .97)*	250.3	75.8	(1.0, .00, .00)
20	486.8	145.5	(.00, .26, .97)	462.6	167.5	(.26, .00, .97)	233.0	75.2	(1.0, -.09, .00)
25	255.8	75.8	(.00, .42, .91)	228.9	90.3	(.42, .00, .91)	157.2	61.4	(1.0, -.09, .00)

1 ksi = 6.895 MPa, 1 in. = 25.4 mm

† The vector (1, 0, 0) is directed along the rail axis; (0, 1, 0) points to the running surface; (0, 0, 1) completes the right-handed system.

Table 12

Analysis Results for *Set 3* (smaller vertical wheel load)

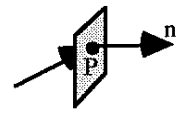

A plane with normal vector, n, passes through a point, P, at the discontinuity's surface. †

	P = (1, 0, 0)			P = (0, 1, 0)			P = (0, 0, 1)		
Depth (mm)	Yield Function (MPa)	Findley's Parameter (MPa)	Unit Normal to Nucleation Plane, n	Yield Function (MPa)	Findley's Parameter (MPa)	Unit Normal to Nucleation Plane, n	Yield Function (MPa)	Findley's Parameter (MPa)	Unit Normal to Nucleation Plane, n
0	417.8	171.7	(.00, .82, .57)	858.4	107.6	(.57, .82, .00)	979.1	228.9	(.00, .71, .71)
1	732.2	143.4	(.77, .64, .00)	420.6	55.2	(.41, .49, .77)	868.7	174.4	(.00, .64, .77)
2	841.1	116.5	(.82, .57, .00)	317.2	57.9	(.00, .71, .71)	877.0	132.4	(.00, .57, .82)
3	830.8	98.6	(.82, .57, .00)	248.2	60.0	(.57, .00, .82)	843.2	118.6	(1.0, .00, .00)
4	763.9	82.7	(.82, .57, .00)	204.1	64.1	(.57, .00, .82)	768.8	102.0	(1.0, .00, .00)
5	675.0	73.1	(.82, .57, .00)	180.6	66.9	(.57, .00, .82)	674.3	88.9	(1.0, .00, .00)
6	584.0	67.6	(.82, .57, .00)	178.6	70.3	(.50, .00, .87)	576.4	80.0	(1.0, .00, .00)
8	444.7	86.9	(.00, .50, .87)	219.9	86.2	(.42, .00, .91)	404.7	68.9	(1.0, .00, .00)
10	398.5	110.3	(.00, .50, .87)	295.1	108.2	(.34, .00, .94)	290.3	62.7	(1.0, .00, .00)
15	490.2	148.9	(.00, .26, .97)	*460.6*	*163.4*	*(.26, .00, .97)*	222.7	67.6	(1.0, .00, .00)
20	471.6	140.0	(.00, .26, .97)	455.7	162.0	(.26, .00, .97)	215.1	66.9	(1.0, -.09, .00)
25	242.0	70.3	(.00, .34, .94)	224.1	84.8	(.34, .00, .94)	143.4	55.8	(1.0, .00, .00)

1 ksi = 6.895 MPa, 1 in. = 25.4 mm

† The vector (1, 0, 0) is directed along the rail axis; (0, 1, 0) points to the running surface; (0, 0, 1) completes the right-handed system.

Table 13

Analysis Results for *Set 4* (stiffer foundation)

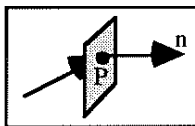

A plane with normal vector, n, passes through a point, P, at the discontinuity's surface. †

	P = (1, 0, 0)			P = (0, 1, 0)			P = (0, 0, 1)		
Depth (mm)	Yield Function (MPa)	Findley's Parameter (MPa)	Unit Normal to Nucleation Plane, n	Yield Function (MPa)	Findley's Parameter (MPa)	Unit Normal to Nucleation Plane, n	Yield Function (MPa)	Findley's Parameter (MPa)	Unit Normal to Nucleation Plane, n
0	473.0	187.5	(.00, .77, .64)	909.4	118.6	(.62, .74, .26)	1048.7	247.5	(.00, .71, .71)
1	788.8	157.2	(.77, .64, .00)	465.4	68.3	(.50, .29, .82)	939.8	193.1	(.00, .64, .77)
2	903.9	132.4	(.77, .64, .00)	335.8	66.9	(.00, .64, .77)	944.6	151.7	(.00, .64, .77)
3	896.3	114.4	(.82, .57, .00)	266.1	68.9	(.00, .64, .77)	909.4	137.2	(1.0, .00, .00)
4	828.7	98.6	(.82, .57, .00)	218.6	74.5	(.57, .00, .82)	832.2	122.7	(1.0, .00, .00)
5	736.4	88.3	(.82, .57, .00)	193.1	75.8	(.57, .00, .82)	734.3	108.2	(1.0, .00, .00)
6	640.5	82.0	(.82, .57, .00)	191.0	78.6	(.50, .00, .87)	631.6	97.2	(1.0, .00, .00)
8	491.6	97.9	(.00, .57, .82)	231.0	93.1	(.42, .00, .91)	450.9	83.4	(1.0, .00, .00)
10	433.0	119.3	(.00, .50, .87)	304.7	113.8	(.34, .00, .94)	329.6	74.4	(.97, -.26, .00)
15	507.5	153.8	(.00, .34, .94)	*468.2*	*167.5*	*(.26, .00, .97)*	251.7	76.5	(1.0, .00, .00)
20	484.7	143.4	(.00, .26, .97)	462.6	164.8	(.26, .00, .97)	237.2	73.8	(.99, -.07, .00)
25	255.4	73.1	(.00, .34, .94)	229.6	86.9	(.42, .00, .91)	161.3	61.4	(1.0, .00, .00)

1 ksi = 6.895 MPa, 1 in. = 25.4 mm

† The vector (1, 0, 0) is directed along the rail axis; (0, 1, 0) points to the running surface; (0, 0, 1) completes the right-handed system.

Table 14

Analysis Results for *Set 5* (stiffer foundation with tangential wheel load)

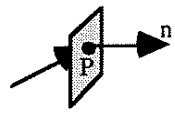

A plane with normal vector, n, passes through a point, P, at the discontinuity's surface. †

	P = (1, 0, 0)			P = (0, 1, 0)			P = (0, 0, 1)		
Depth (mm)	Yield Function (MPa)	Findley's Parameter (MPa)	Unit Normal to Nucleation Plane, n	Yield Function (MPa)	Findley's Parameter (MPa)	Unit Normal to Nucleation Plane, n	Yield Function (MPa)	Findley's Parameter (MPa)	Unit Normal to Nucleation Plane, n
0	479.2	228.9	(.13, .75, .64)	1078.3	313.0	(.71, .71, .00)	1202.4	399.2	(.70, .12, .71)
1	788.8	174.4	(.71, .71, .00)	605.4	91.7	(.64, .00, .77)	1001.8	216.5	(.32, .56, .77)
2	903.9	141.3	(.77, .64, .00)	443.3	84.8	(.57, .00, .82)	974.2	167.5	(.37, .53, .77)
3	899.1	120.7	(.82, .57, .00)	339.9	88.3	(.57, .00, .82)	926.7	139.3	(.99, -.09, .00)
4	832.2	103.4	(.82, .57, .00)	268.9	87.6	(.57, .00, .82)	844.6	124.1	(.99, -.09, .00)
5	739.8	93.1	(.82, .57, .00)	236.5	85.5	(.57, .00, .82)	743.9	109.6	(.99, -.09, .00)
6	644.7	85.5	(.82, .57, .00)	234.4	86.9	(.57, .00, .82)	639.8	98.6	(.99, -.09, .00)
8	494.4	101.4	(.00, .57, .82)	255.1	99.3	(.50, .00, .87)	458.5	84.1	(1.0, .00, .00)
10	435.7	122.0	(.00, .50, .87)	306.1	117.9	(.34, .00, .94)	335.8	77.9	(-.98, .17, .00)
15	508.8	155.8	(.00, .34, .94)	*468.8*	*169.6*	*(.26, .00, .97)*	254.4	76.5	(1.0, .00, .00)
20	485.4	144.8	(.00, .26, .97)	463.3	166.9	(.26, .00, .97)	238.6	75.2	(.99, -.09, .00)
25	255.1	74.5	(.00, .42, .91)	229.6	88.9	(.42, .00, .91)	162.7	61.4	(.99, -.09, .00)

1 ksi = 6.895 MPa, 1 in. = 25.4 mm

† The vector (1, 0, 0) is directed along the rail axis; (0, 1, 0) points to the running surface; (0, 0, 1) completes the right-handed system.

Table 15

Analysis Results for *Set 6* (oxide discontinuity)

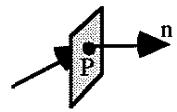

A plane with normal vector, n, passes through a point, P, at the discontinuity's surface. †

	P = (1, 0, 0)			P = (0, 1, 0)			P = (0, 0, 1)		
Depth (mm)	Yield Function (MPa)	Findley's Parameter (MPa)	Unit Normal to Nucleation Plane, n	Yield Function (MPa)	Findley's Parameter (MPa)	Unit Normal to Nucleation Plane, n	Yield Function (MPa)	Findley's Parameter (MPa)	Unit Normal to Nucleation Plane, n
0	417.8	60.7	(.71, .00, .71)	279.9	91.0	(.00, .77, .64)	242.0	45.5	(.00, .82, .57)
1	288.9	98.6	(.00, 1.0, .00)	355.1	97.9	(1.0, .00, .00)	208.2	29.0	(.07, .76, .64)
2	296.5	104.1	(1.0, .00, .00)	*415.1*	*105.5*	*(1.0, .00, .00)*	238.6	34.5	(1.0, .00, .00)
3	284.1	99.3	(1.0, .00, .00)	420.6	95.8	(1.0, .00, .00)	248.2	34.5	(1.0, .00, .00)
4	262.7	91.7	(1.0, .00, .00)	394.4	85.5	(1.0, .00, .00)	239.9	33.8	(1.0, .00, .00)
5	239.2	83.4	(1.0, .00, .00)	354.4	77.2	(1.0, .00, .00)	224.1	33.1	(1.0, .00, .00)
6	216.5	76.5	(1.0, .00, .00)	311.6	71.7	(1.0, .00, .00)	207.5	33.8	(1.0, .00, .00)
8	183.4	70.3	(1.0, .00, .00)	239.2	67.6	(1.0, .00, .00)	189.6	42.7	(.09, .49, .87)
10	166.9	67.6	(1.0, .00, .00)	199.9	64.1	(1.0, .00, .00)	195.8	60.7	(.07, .42, .91)
15	169.6	77.9	(1.0, .00, .00)	197.2	66.9	(.82, .00, .57)	247.5	97.2	(.15, .21, .97)
20	158.6	75.2	(1.0, .00, .00)	183.4	61.4	(.70, -.06, .71)	235.1	96.5	(.10, .14, .98)
25	88.9	53.8	(1.0, .00, .00)	106.9	42.7	(1.0, .00, .00)	122.0	47.6	(.26, .22, .94)

1 ksi = 6.895 MPa, 1 in. = 25.4 mm

† The vector (1, 0, 0) is directed along the rail axis; (0, 1, 0) points to the running surface; (0, 0, 1) completes the right-handed system.

Table 16

Analysis Results for *Set 7* (oxide discontinuity with tangential wheel load)

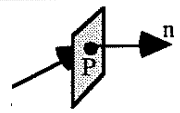

A plane with normal vector, n, passes through a point, P, at the discontinuity's surface. †

	P = (1, 0, 0)			P = (0, 1, 0)			P = (0, 0, 1)		
Depth (mm)	Yield Function (MPa)	Findley's Parameter (MPa)	Unit Normal to Nucleation Plane, n	Yield Function (MPa)	Findley's Parameter (MPa)	Unit Normal to Nucleation Plane, n	Yield Function (MPa)	Findley's Parameter (MPa)	Unit Normal to Nucleation Plane, n
0	562.6	168.9	(-.77, .00, .64)	416.4	125.5	(.38, .66, .64)	313.0	93.1	(.75, .13, .64)
1	427.5	103.4	(.17, .98, .00)	417.1	99.3	(.99, -.09, .00)	236.5	36.5	(.38, .66, .64)
2	388.9	104.8	(.99, -.09, .00)	*453.7*	*105.5*	*(1.0, .00, .00)*	251.0	35.9	(.98, -.17, .00)
3	348.2	101.4	(.99, -.09, .00)	444.7	97.2	(1.0, .00, .00)	255.1	35.9	(.99, -.09, .00)
4	309.6	91.7	(.99, -.09, .00)	410.9	85.5	(1.0, .00, .00)	244.1	34.5	(.99, -.09, .00)
5	275.8	83.4	(1.0, .00, .00)	367.5	77.9	(1.0, .00, .00)	227.5	33.8	(.99, -.09, .00)
6	247.5	77.2	(1.0, .00, .00)	322.7	73.1	(1.0, .00, .00)	211.0	34.5	(.99, -.09, .00)
8	206.2	70.3	(1.0, .00, .00)	249.6	67.6	(1.0, .00, .00)	192.4	43.4	(.21, .45, .87)
10	182.7	67.6	(1.0, .00, .00)	209.6	64.1	(1.0, .00, .00)	197.9	61.4	(.18, .38, .91)
15	175.1	77.9	(1.0, .00, .00)	200.6	66.9	(.76, .07, .64)	248.2	97.9	(.15, .21, .97)
20	161.3	76.5	(1.0, .00, .00)	184.8	61.4	(.71, .00, .71)	235.8	96.5	(.13, .11, .98)
25	93.1	53.8	(1.0, .00, .00)	108.9	42.7	(1.0, .00, .00)	122.0	48.3	(.30, .17, .94)

1 ksi = 6.895 MPa, 1 in. = 25.4 mm

† The vector (1, 0, 0) is directed along the rail axis; (0, 1, 0) points to the running surface; (0, 0, 1) completes the right-handed system.

Table 17

Analysis Results for *Set 8* (football-shaped oxide discontinuity)

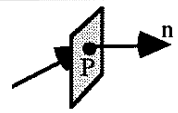

A plane with normal vector, n, passes through a point, P, at the discontinuity's surface. †

	P = (1, 0, 0)			P = (0, 1, 0)			P = (0, 0, 1)		
Depth (mm)	Yield Function (MPa)	Findley's Parameter (MPa)	Unit Normal to Nucleation Plane, n	Yield Function (MPa)	Findley's Parameter (MPa)	Unit Normal to Nucleation Plane, n	Yield Function (MPa)	Findley's Parameter (MPa)	Unit Normal to Nucleation Plane, n
0	535.7	75.8	(.71, .00, .71)	320.6	80.0	(.00, .77, .64)	307.5	43.4	(.71, .00, -.71)
1	317.8	99.3	(.00, 1.0, .00)	324.1	97.2	(1.0, .00, .00)	197.9	27.6	(.00, 1.0, .00)
2	304.1	105.5	(1.0, .00, .00)	*378.5*	*106.9*	*(1.0, .00, .00)*	212.4	35.9	(1.0, .00, .00)
3	281.3	102.0	(1.0, .00, .00)	388.2	98.6	(1.0, .00, .00)	224.8	36.5	(.99, -.09, .00)
4	256.5	93.8	(1.0, .00, .00)	365.4	88.9	(1.0, .00, .00)	218.6	35.2	(1.0, .00, .00)
5	231.7	84.8	(1.0, .00, .00)	328.2	80.0	(1.0, .00, .00)	204.1	34.5	(1.0, .00, .00)
6	210.3	77.9	(1.0, .00, .00)	287.5	73.8	(1.0, .00, .00)	188.9	34.5	(1.0, .00, .00)
8	180.6	69.6	(1.0, .00, .00)	219.3	67.6	(1.0, .00, .00)	172.4	37.2	(.98, .00, .17)
10	162.7	66.2	(1.0, .00, .00)	182.7	64.1	(1.0, .00, .00)	178.6	55.2	(.04, .42, .91)
15	156.5	78.6	(1.0, .00, .00)	178.6	66.9	(.91, .00, .42)	226.1	91.0	(.22, .13, .97)
20	146.2	79.3	(1.0, .00, .00)	166.9	61.4	(.86, -.08, .50)	214.4	90.3	(.24, .09, .97)
25	83.4	57.9	(1.0, .00, .00)	97.9	44.8	(1.0, .00, .00)	111.0	45.5	(.41, .11, .91)

1 ksi = 6.895 MPa, 1 in. = 25.4 mm

† The vector (1, 0, 0) is directed along the rail axis; (0, 1, 0) points to the running surface; (0, 0, 1) completes the right-handed system.

Table 18

Analysis Results for *Set 9* (football-shaped oxide discontinuity with tangential wheel load)

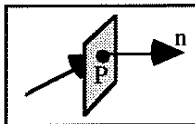

A plane with normal vector, n, passes through a point, P, at the discontinuity's surface. †

	P = (1, 0, 0)			P = (0, 1, 0)			P = (0, 0, 1)		
Depth (mm)	Yield Function (MPa)	Findley's Parameter (MPa)	Unit Normal to Nucleation Plane, n	Yield Function (MPa)	Findley's Parameter (MPa)	Unit Normal to Nucleation Plane, n	Yield Function (MPa)	Findley's Parameter (MPa)	Unit Normal to Nucleation Plane, n
0	699.1	217.9	(-.76, .07, .64)	459.9	137.2	(.75, .13, .64)	398.5	122.7	(-.77, .00, .64)
1	*474.4*	*108.2*	*(.17, .98, .00)*	407.5	100.0	(.99, -.09, .00)	240.6	38.6	(.34, .94, .00)
2	403.3	106.9	(.99, -.09, .00)	430.2	106.9	(1.0, .00, .00)	228.9	38.6	(-.98, .17, .00)
3	350.3	104.8	(.99, -.09, .00)	418.5	100.0	(1.0, .00, .00)	231.7	38.6	(.98, -.17, .00)
4	307.5	94.5	(.99, -.09, .00)	385.4	88.9	(1.0, .00, .00)	223.4	36.5	(.98, -.17, .00)
5	273.0	85.5	(.99, -.09, .00)	344.0	80.7	(1.0, .00, .00)	207.5	35.2	(.98, -.17, .00)
6	244.8	78.6	(.99, -.09, .00)	302.0	74.5	(1.0, .00, .00)	192.4	35.2	(.99, -.09, .00)
8	204.1	69.6	(1.0, .00, .00)	233.0	67.6	(1.0, .00, .00)	175.1	39.3	(.41, .41, .82)
10	180.6	66.2	(.99, -.09, .00)	196.5	64.1	(.99, -.09, .00)	181.3	56.5	(.27, .32, .91)
15	166.2	78.6	(1.0, .00, .00)	183.4	66.9	(.86, .07, .50)	227.5	91.7	(.22, .13, .97)
20	148.9	80.0	(.99, -.09, .00)	168.2	62.1	(.87, .00, .50)	215.1	91.0	(.25, .07, .97)
25	87.6	57.9	(1.0, .00, .00)	100.0	44.8	(1.0, .00, .00)	111.0	46.2	(.49, .09, .87)

1 ksi = 6.895 MPa, 1 in. = 25.4 mm

† The vector (1, 0, 0) is directed along the rail axis; (0, 1, 0) points to the running surface; (0, 0, 1) completes the right-handed system.

Table 19

Analysis Results for *Set 10* (no discontinuity)

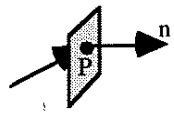

A plane with normal vector, n, passes through a point, P, at the discontinuity's surface. †

	P = (1, 0, 0)			P = (0, 1, 0)			P = (0, 0, 1)		
Depth (mm)	Yield Function (MPa)	Findley's Parameter (MPa)	Unit Normal to Nucleation Plane, n	Yield Function (MPa)	Findley's Parameter (MPa)	Unit Normal to Nucleation Plane, n	Yield Function (MPa)	Findley's Parameter (MPa)	Unit Normal to Nucleation Plane, n
0	*378.5*	*82.0*	*(.00, .77, .64)*	N/A	N/A	N/A	N/A	N/A	N/A
1	327.5	57.2	(1.0, .00, .00)	N/A	N/A	N/A	N/A	N/A	N/A
2	368.9	68.9	(1.0, .00, .00)	N/A	N/A	N/A	N/A	N/A	N/A
3	379.2	66.2	(1.0, .00, .00)	N/A	N/A	N/A	N/A	N/A	N/A
4	361.3	60.7	(1.0, .00, .00)	N/A	N/A	N/A	N/A	N/A	N/A
5	330.3	55.8	(1.0, .00, .00)	N/A	N/A	N/A	N/A	N/A	N/A
6	296.5	52.4	(1.0, .00, .00)	N/A	N/A	N/A	N/A	N/A	N/A
8	245.5	51.0	(1.0, .00, .00)	N/A	N/A	N/A	N/A	N/A	N/A
10	226.8	57.2	(.00, .50, .87)	N/A	N/A	N/A	N/A	N/A	N/A
15	254.4	80.7	(.03, .34, .94)	N/A	N/A	N/A	N/A	N/A	N/A
20	239.2	78.6	(.30, .17, .94)	N/A	N/A	N/A	N/A	N/A	N/A
25	131.0	42.7	(.87, .00, .50)	N/A	N/A	N/A	N/A	N/A	N/A

1 ksi = 6.895 MPa, 1 in. = 25.4 mm

† The vector (1, 0, 0) is directed along the rail axis; (0, 1, 0) points to the running surface; (0, 0, 1) completes the right-handed system.

Table 20

Results for PCH Analysis

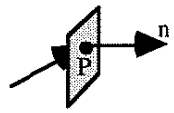

A plane with normal vector, n, passes through a point, P, at the discontinuity's surface. †

	P = (1, 0, 0)			P = (0, 1, 0)			P = (0, 0, 1)		
$(\frac{\lambda_x}{\lambda_z}, \frac{\lambda_y}{\lambda_z})$	Yield Function (MPa)	Findley's Parameter (MPa)	Unit Normal to Nucleation Plane, n	Yield Function (MPa)	Findley's Parameter (MPa)	Unit Normal to Nucleation Plane, n	Yield Function (MPa)	Findley's Parameter (MPa)	Unit Normal to Nucleation Plane, n
(1.00, 1.00)	508.8	155.1	(.00, .34, .94)	*468.8*	*168.2*	*(.26, .00, .97)*	247.5	76.5	(1.0, .00, .00)
(1.00, 0.84)	497.1	151.0	(.00, -.34, .94)	*447.5*	*160.6*	*(.26, .00, .97)*	262.7	77.2	(1.0, .00, .00)
(1.00, 0.67)	486.8	148.2	(.00, -.42, .91)	*422.0*	*151.7*	*(.26, .00, .97)*	284.1	79.3	(1.0, .00, .00)
(1.00, 0.51)	*480.6*	*150.3*	*(.00, -.50, .87)*	390.9	140.7	(.26, .00, .97)	315.8	84.8	(1.0, .00, .00)
(1.00, 0.35)	*493.0*	*164.8*	*(.00, -.57, .82)*	353.7	126.9	(.26, .00, .97)	373.7	110.3	(.06, -.71, .70)
(1.00, 0.19)	*588.8*	*231.0*	*(.35, -.71, .61)*	308.2	111.0	(.26, .00, .97)	525.4	211.0	(.00, -.77, .64)

1 ksi = 6.895 MPa, 1 in. = 25.4 mm

† The vector (1, 0, 0) is directed along the rail axis; (0, 1, 0) points to the running surface; (0, 0, 1) completes the right-handed system.

Table 21

Results for FBX Analysis

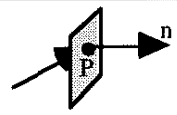

A plane with normal vector, n, passes through a point, P, at the discontinuity's surface. †

	P = (1, 0, 0)			P = (0, 1, 0)			P = (0, 0, 1)		
$(\frac{\lambda_X}{\lambda_Z}, \frac{\lambda_Y}{\lambda_Z})$	Yield Function (MPa)	Findley's Parameter (MPa)	Unit Normal to Nucleation Plane, n	Yield Function (MPa)	Findley's Parameter (MPa)	Unit Normal to Nucleation Plane, n	Yield Function (MPa)	Findley's Parameter (MPa)	Unit Normal to Nucleation Plane, n
(1.00, 1.00)	508.8	155.1	(.00, .34, .94)	*468.8*	*168.2*	*(.26, .00, .97)*	247.5	76.5	(1.0, .00, .00)
(1.17, 1.00)	533.7	162.0	(.00, .34, .94)	*490.9*	*173.7*	*(.26, .00, .97)*	255.8	70.3	(1.0, .00, .00)
(1.34, 1.00)	555.0	168.9	(.00, .34, .94)	*509.5*	*179.3*	*(.17, .00, .98)*	264.1	66.9	(1.0, .00, .00)
(1.50, 1.00)	573.0	173.7	(.00, .34, .94)	*526.1*	*184.1*	*(.17, .00, .98)*	271.7	64.1	(1.0, .00, .00)
(1.67, 1.00)	588.8	178.6	(.00, .34, .94)	*541.2*	*188.2*	*(.17, .00, .98)*	278.5	62.1	(.00, -.77, .64)

1 ksi = 6.895 MPa, 1 in. = 25.4 mm

† The vector (1, 0, 0) is directed along the rail axis; (0, 1, 0) points to the running surface; (0, 0, 1) completes the right-handed system.

Table 22

Results for PCV Analysis

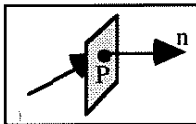

A plane with normal vector, n, passes through a point, P, at the discontinuity's surface. †

	P = (1, 0, 0)			P = (0, 1, 0)			P = (0, 0, 1)		
$(\frac{\lambda_X}{\lambda_Z}, \frac{\lambda_Y}{\lambda_Z})$	Yield Function (MPa)	Findley's Parameter (MPa)	Unit Normal to Nucleation Plane, n	Yield Function (MPa)	Findley's Parameter (MPa)	Unit Normal to Nucleation Plane, n	Yield Function (MPa)	Findley's Parameter (MPa)	Unit Normal to Nucleation Plane, n
(1.00, 1.00)	508.8	155.1	(.00, .34, .94)	*468.8*	*168.2*	*(.26, .00, .97)*	247.5	76.5	(1.0, .00, .00)
(1.11, 1.11)	534.3	162.7	(.00, .34, .94)	*497.8*	*177.2*	*(.26, .00, .97)*	244.1	71.7	(1.0, .00, .00)
(1.22, 1.22)	560.5	171.7	(.00, .26, .97)	*526.8*	*185.5*	*(.17, .00, .98)*	242.0	67.6	(1.0, .00, .00)
(1.33, 1.33)	588.1	180.6	(.00, .26, .97)	*557.1*	*195.1*	*(.17, .00, .98)*	239.2	64.1	(1.0, .00, .00)

1 ksi = 6.895 MPa, 1 in. = 25.4 mm

† The vector (1, 0, 0) is directed along the rail axis; (0, 1, 0) points to the running surface; (0, 0, 1) completes the right-handed system.

Table 23

Results for FBY Analysis

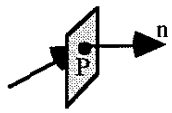

A plane with normal vector, n, passes through a point, P, at the discontinuity's surface. †

	P = (1, 0, 0)			P = (0, 1, 0)			P = (0, 0, 1)		
$(\frac{\lambda_X}{\lambda_Z}, \frac{\lambda_Y}{\lambda_Z})$	Yield Function (MPa)	Findley's Parameter (MPa)	Unit Normal to Nucleation Plane, n	Yield Function (MPa)	Findley's Parameter (MPa)	Unit Normal to Nucleation Plane, n	Yield Function (MPa)	Findley's Parameter (MPa)	Unit Normal to Nucleation Plane, n
(1.00, 1.00)	508.8	155.1	(.00, .34, .94)	*468.8*	*168.2*	*(.26, .00, .97)*	247.5	76.5	(-1.0, .00, .00)
(1.00, 1.34)	530.9	163.4	(.00, .26, .97)	*503.3*	*180.6*	*(.26, .00, .97)*	224.8	75.8	(-1.0, .00, .00)
(1.00, 1.67)	548.1	170.3	(.00, .26, .97)	*526.8*	*188.9*	*(.26, .00, .97)*	210.3	76.5	(-1.0, .00, .00)
(1.00, 2.01)	561.9	176.5	(.00, .26, .97)	*544.7*	*195.1*	*(.26, .00, .97)*	199.3	77.2	(-1.0, .00, .00)
(1.00, 2.35)	573.0	180.6	(.00, .17, .98)	*557.8*	*199.9*	*(.26, .00, .97)*	191.0	77.9	(-1.0, .00, .00)
(1.00, 2.69)	581.2	184.8	(.00, .17, .98)	*568.1*	*203.4*	*(.26, .00, .97)*	184.1	78.6	(-1.0, .00, .00)
(1.00, 3.03)	588.1	187.5	(.00, .17, .98)	*576.4*	*206.2*	*(.26, .00, .97)*	179.3	79.3	(-1.0, .00, .00)

1 ksi = 6.895 MPa, 1 in. = 25.4 mm

† The vector (1, 0, 0) is directed along the rail axis; (0, 1, 0) points to the running surface; (0, 0, 1) completes the right-handed system.

Table 24

Results for PCT Analysis

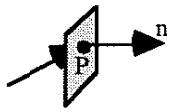

A plane with normal vector, n, passes through a point, P, at the discontinuity's surface. †

	P = (1, 0, 0)			P = (0, 1, 0)			P = (0, 0, 1)		
$(\frac{\lambda_X}{\lambda_Z}, \frac{\lambda_Y}{\lambda_Z})$	Yield Function (MPa)	Findley's Parameter (MPa)	Unit Normal to Nucleation Plane, n	Yield Function (MPa)	Findley's Parameter (MPa)	Unit Normal to Nucleation Plane, n	Yield Function (MPa)	Findley's Parameter (MPa)	Unit Normal to Nucleation Plane, n
(1.00, 1.00)	508.8	155.1	(.00, .34, .94)	*468.8*	*168.2*	*(.26, .00, .97)*	247.5	76.5	(-1.0, .00, .00)
(0.80, 1.00)	474.4	144.1	(.00, .34, .94)	*439.2*	*161.3*	*(-.34, .00, .94)*	237.2	87.6	(-1.0, .00, .00)
(0.60, 1.00)	432.3	130.3	(.00, .34, .94)	*407.5*	*156.5*	*(-.42, .00, .91)*	231.0	107.6	(-1.0, .00, .00)
(0.40, 1.00)	382.7	113.8	(.00, .34, .94)	*385.4*	*161.3*	*(-.64, .00, .77)*	246.1	150.3	(-1.0, .00, .00)
(0.20, 1.00)	323.4	93.8	(.00, .34, .94)	590.2	252.3	(-.82, .00, .57)	*526.8*	*287.5*	*(-1.0, .00, .00)*

1 ksi = 6.895 MPa, 1 in. = 25.4 mm

† The vector (1, 0, 0) is directed along the rail axis; (0, 1, 0) points to the running surface; (0, 0, 1) completes the right-handed system.

Table 25

Results for FBZ Analysis

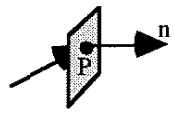

A plane with normal vector, n, passes through a point, P, at the discontinuity's surface. †

	P = (1, 0, 0)			P = (0, 1, 0)			P = (0, 0, 1)		
$(\frac{\lambda_x}{\lambda_z}, \frac{\lambda_y}{\lambda_z})$	Yield Function (MPa)	Findley's Parameter (MPa)	Unit Normal to Nucleation Plane, n	Yield Function (MPa)	Findley's Parameter (MPa)	Unit Normal to Nucleation Plane, n	Yield Function (MPa)	Findley's Parameter (MPa)	Unit Normal to Nucleation Plane, n
(1.00, 1.00)	508.8	155.1	(.00, .34, .94)	*468.8*	*168.2*	*(.26, .00, .97)*	247.5	76.5	(-1.0, .00, .00)
(0.75, 0.75)	453.7	137.2	(.00, .34, .94)	*406.1*	*149.6*	*(-.34, .00, .94)*	256.5	88.9	(-1.0, .00, .00)
(0.50, 0.50)	404.7	122.7	(.00, .42, .91)	*350.3*	*134.4*	*(-.42, .00, .91)*	269.6	106.2	(-1.0, .00, .00)
(0.25, 0.25)	365.4	113.1	(.00, .50, .87)	308.9	123.4	(-.50, .00, .87)	*288.9*	*128.2*	*(-1.0, .00, .00)*
$(\frac{1}{500}, \frac{1}{500})$	341.3	108.2	(.00, .57, .82)	291.6	119.3	(-.64, .00, .77)	304.7	145.5	*(-1.0, .00, .00)*

1 ksi = 6.895 MPa, 1 in. = 25.4 mm

† The vector (1, 0, 0) is directed along the rail axis; (0, 1, 0) points to the running surface; (0, 0, 1) completes the right-handed system.

Table 26

Results for Weak Foundation and Temperature Analyses

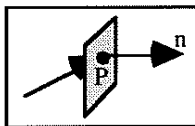

A plane with normal vector, n, passes through a point, P, at the discontinuity's surface. †

	P = (1, 0, 0)			P = (0, 1, 0)			P = (0, 0, 1)		
Analysis	Yield Function (MPa)	Findley's Parameter (MPa)	Unit Normal to Nucleation Plane, n	Yield Function (MPa)	Findley's Parameter (MPa)	Unit Normal to Nucleation Plane, n	Yield Function (MPa)	Findley's Parameter (MPa)	Unit Normal to Nucleation Plane, n
STD	508.8	155.1	(.00, .34, .94)	*468.8*	*168.2*	*(.26, .00, .97)*	247.5	76.5	(1.0, .00, .00)
WKF	515.0	160.6	(.00, .34, .94)	*475.7*	*173.1*	*(.34, .00, .94)*	233.0	76.5	(1.0, .00, .00)
WTR	491.6	133.8	(.00, .34, .94)	*499.9*	*179.3*	*(.42, .00, .91)*	373.7	140.0	(1.0, .00, .00)
SMR	*525.4*	*168.9*	*(.00, .34, .94)*	496.4	163.4	(.17, .00, .98)	235.8	41.6	(.00, .64, .77)

1 ksi = 6.895 MPa, 1 in. = 25.4 mm

† The vector (1, 0, 0) is directed along the rail axis; (0, 1, 0) points to the running surface; (0, 0, 1) completes the right-handed system.

FIGURES

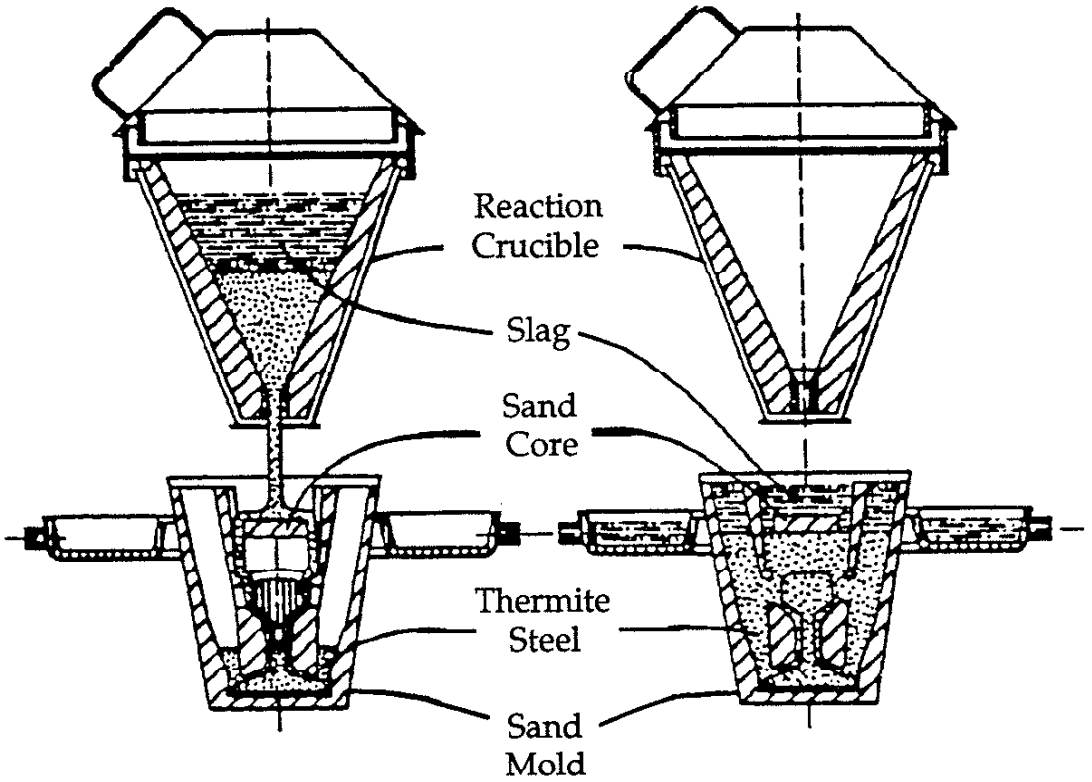

Fig. 1. Schematic drawing of a typical modern thermite rail welding process. (Adapted from Schroeder and Poirier 1980, Fig. 1)

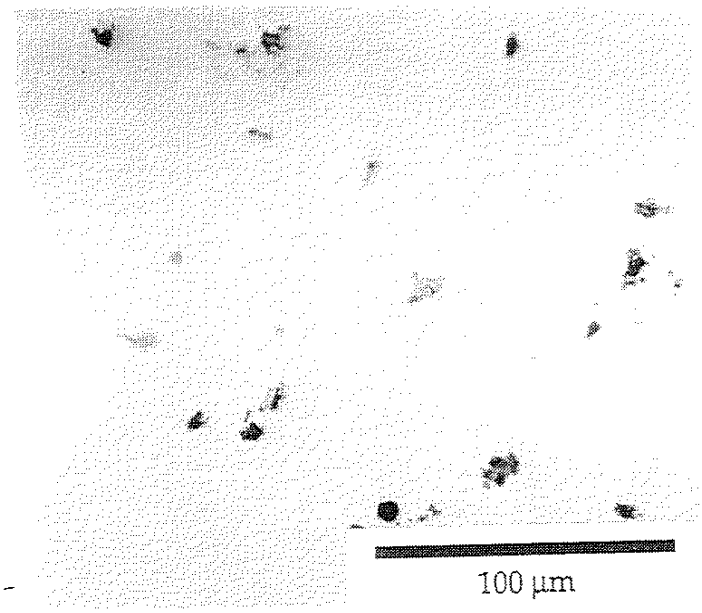

Fig. 2. Optical photomicrograph of metallurgical discontinuities in the head region of a thermite rail weld (Magnification ≈ 400x).
(Adapted from Fry 1992, Fig. 7)

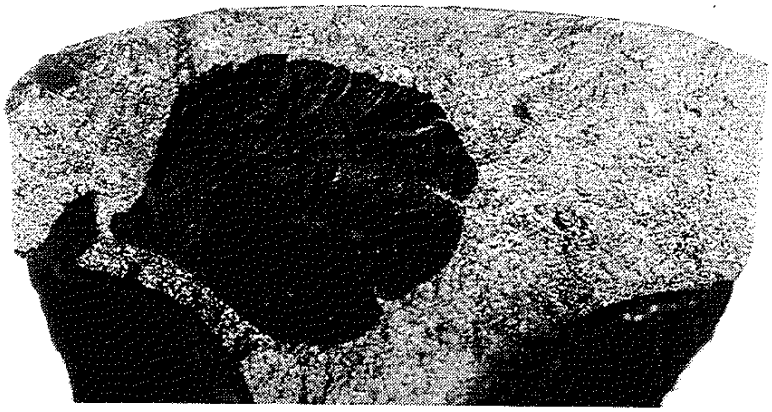

Fig. 3. Photograph of a fatigue defect in the head region of a thermite rail weld. (Adapted from Oderio 1992, Fig. 3)

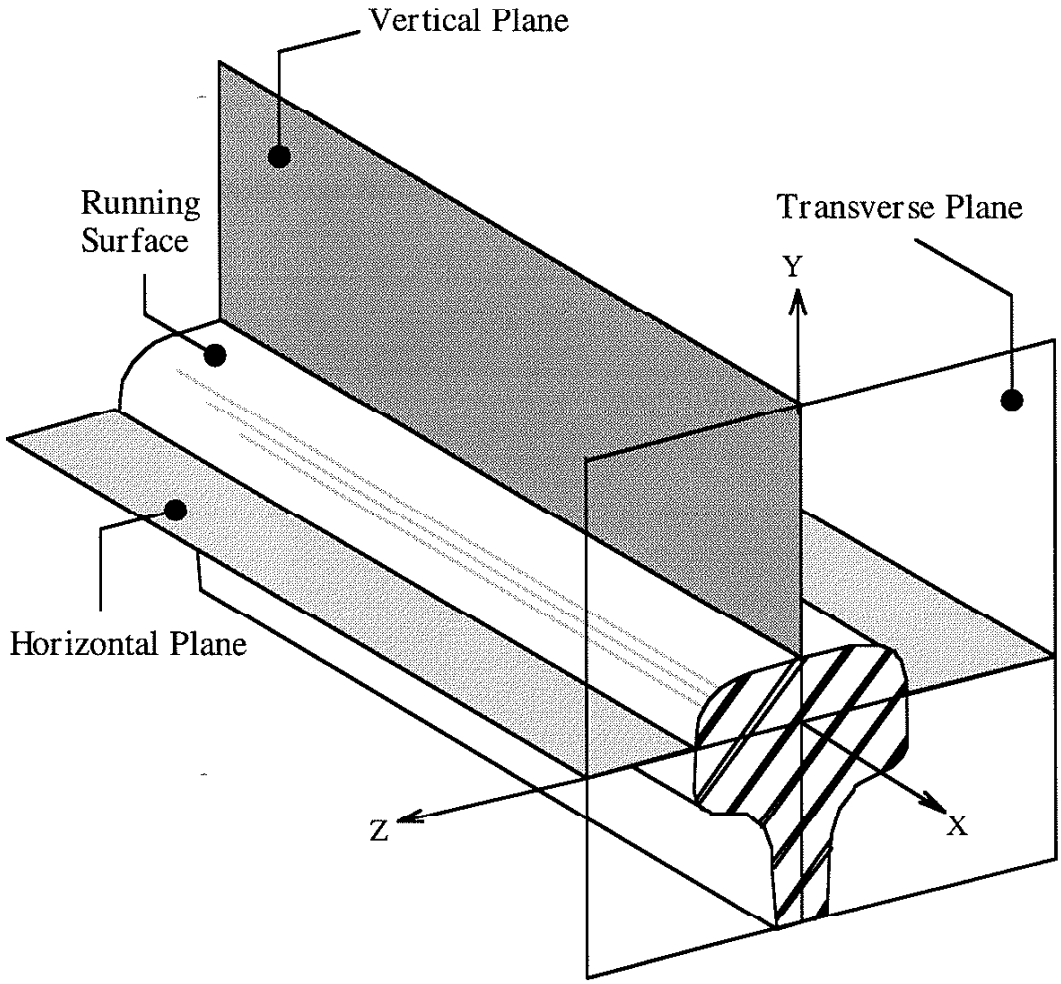

Fig. 4. Planes of propagation for rail-head defects. Surface defects occur at or near the running surface. Defects that propagate in the transverse plane are called transverse defects. Longitudinal defects propagate in either the vertical plane or the horizontal plane (see also Table 1).

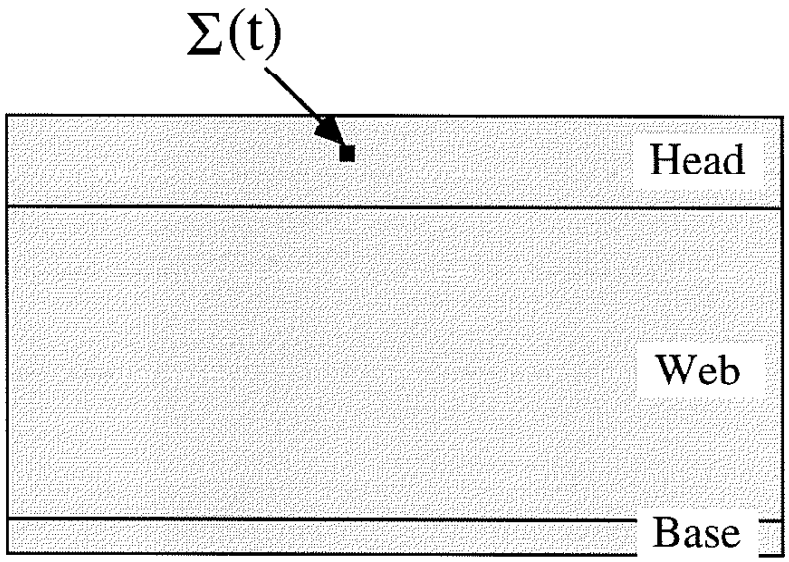

Fig. 5. Schematic drawing of a longitudinal-section of a railroad rail. Global stress histories Σ(t) are computed at points below the running surface in the rail head.

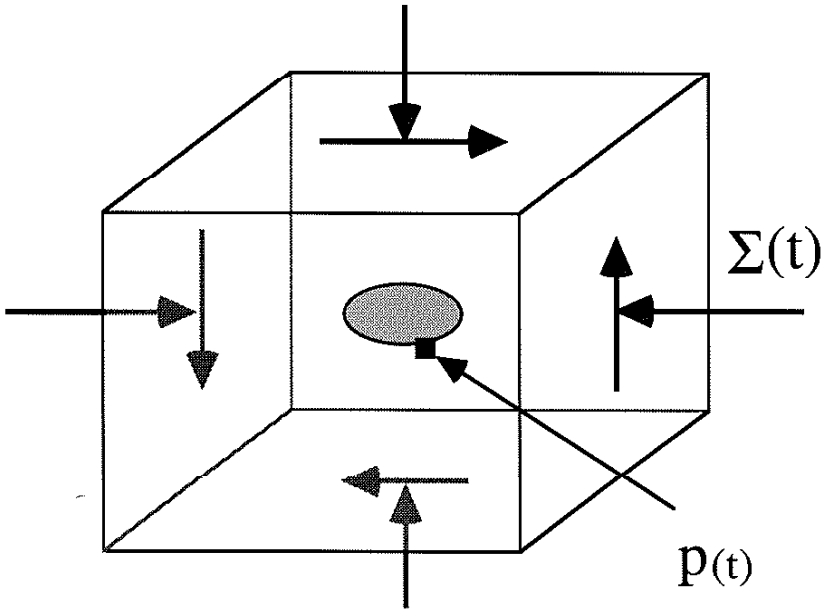

Fig. 6. The global rail-head stresses, Σ(t), are applied to the extended volume surrounding the discontinuity. The local stresses, p(t), are computed at points in the metal matrix at the periphery of the discontinuity.

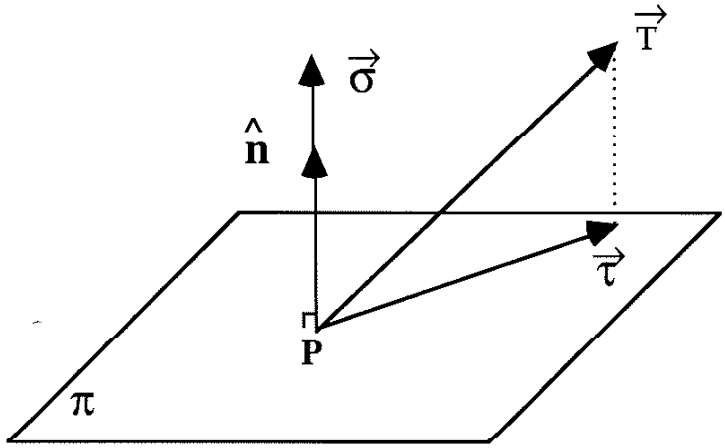

Fig. 7. Schematic drawing of a traction vector on a plane. The traction vector T, from the local stress history, p(t), is resolved into its normal component, σ, and its shearing component, τ, on plane π through point P.

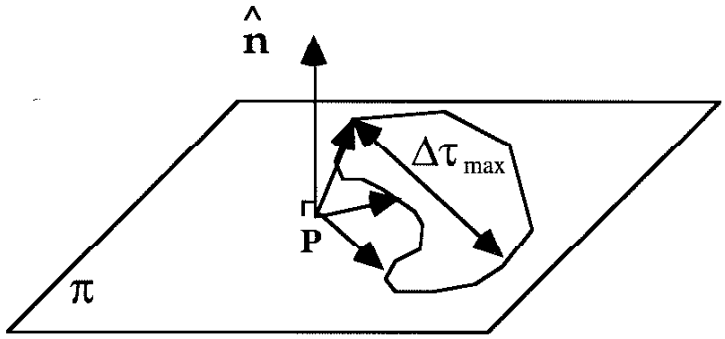

Fig. 8. Schematic drawing of maximum-range-of-shear-stress on a plane. The maximum range of local shear stress on plane π through point P is calculated as $|\Delta\tau_{max}|$. $|\Delta\tau_{max}|$ is combined with the maximum normal stress using Findley's criteria for fatigue damage (Findley 1959).

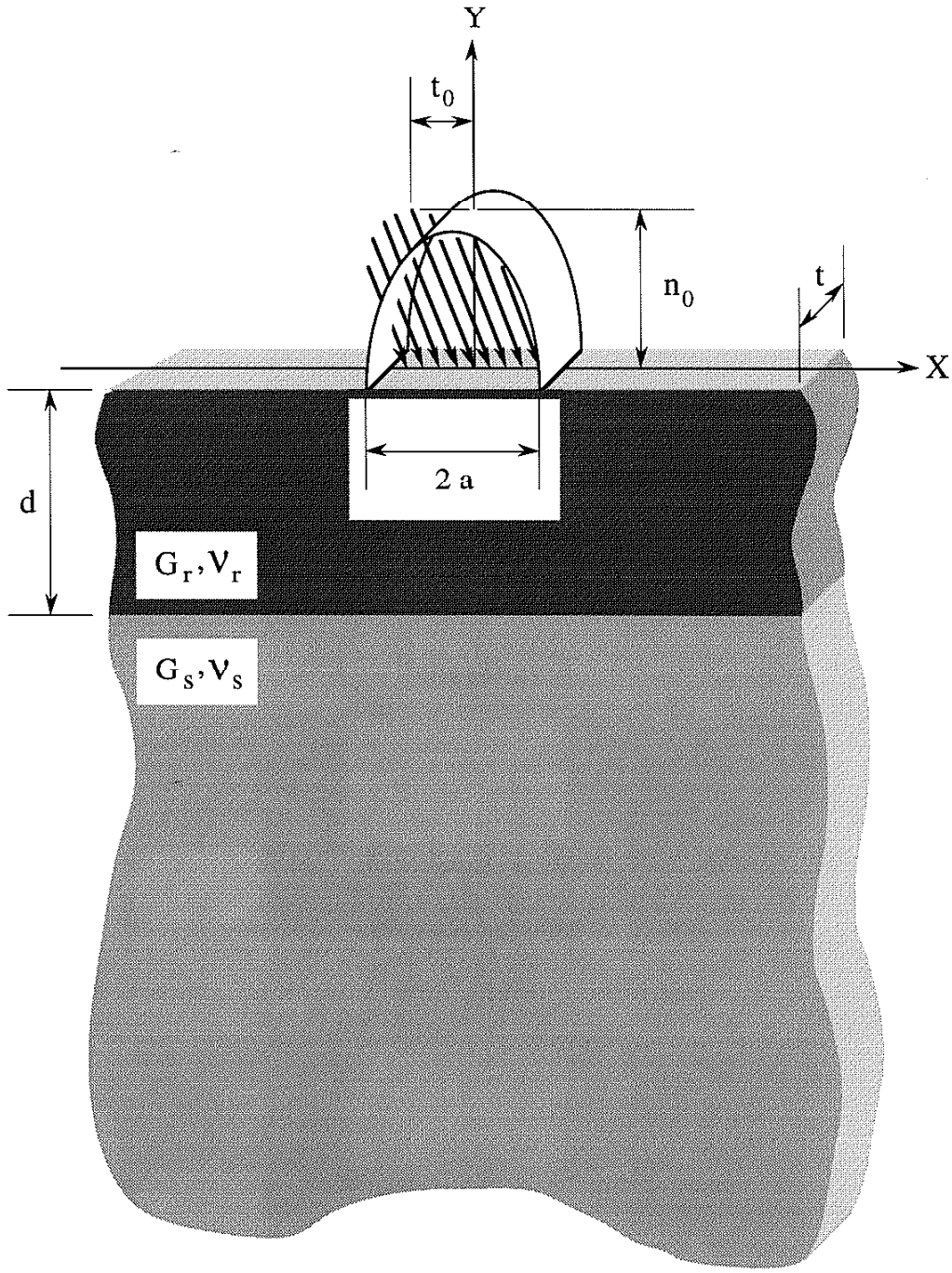

Fig. 9. Schematic drawing of track structure idealization. The rail strip (shear modulus, G_r; Poisson's ratio, ν_r; depth, d; and thickness, t) is bonded to the support layer (shear modulus, G_s; Poisson's ratio, ν_s). Wheel-rail contact is approximated by a conformal Hertzian distribution (length, 2a; peak normal stress, n_0; peak tangential stress, t_0).

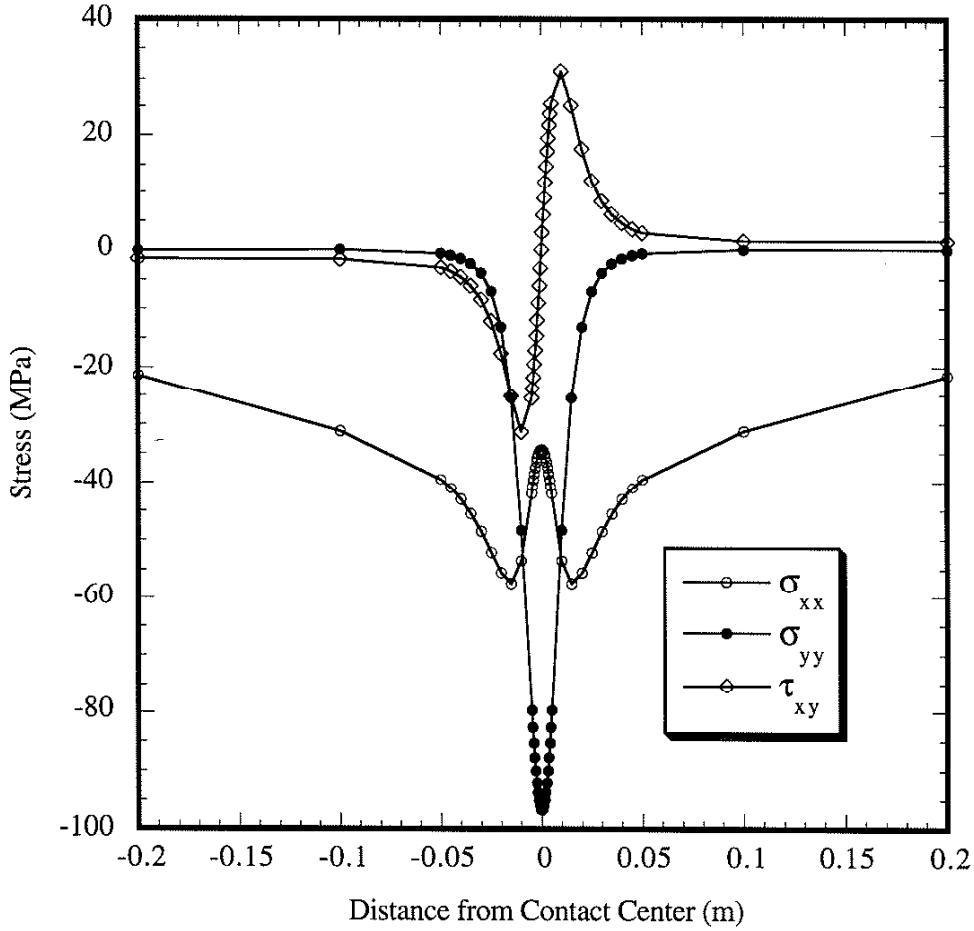

Fig. 10. Plot of a global stress history, Σ(t). This plot shows results from the *Standard Set* at the critical depth, Y = -15 mm.

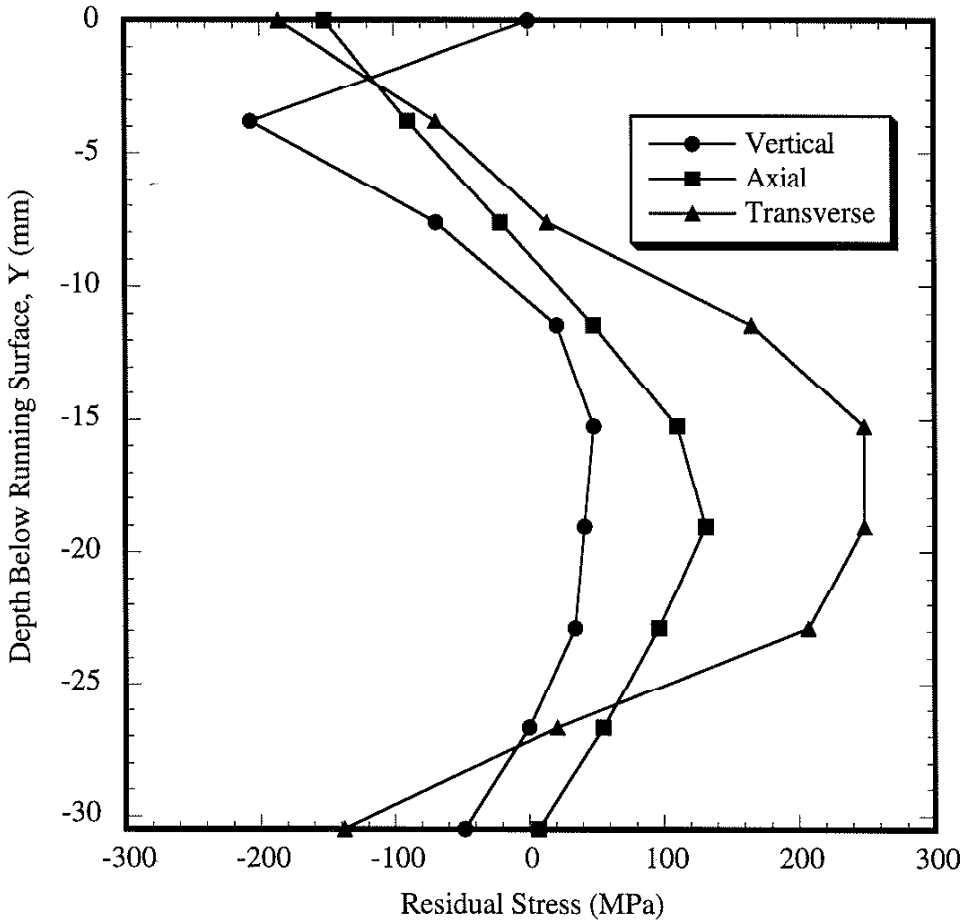

Fig. 11. Plot of residual stresses used in the *Standard Set*.
(Data from Steele and Joerms 1993)

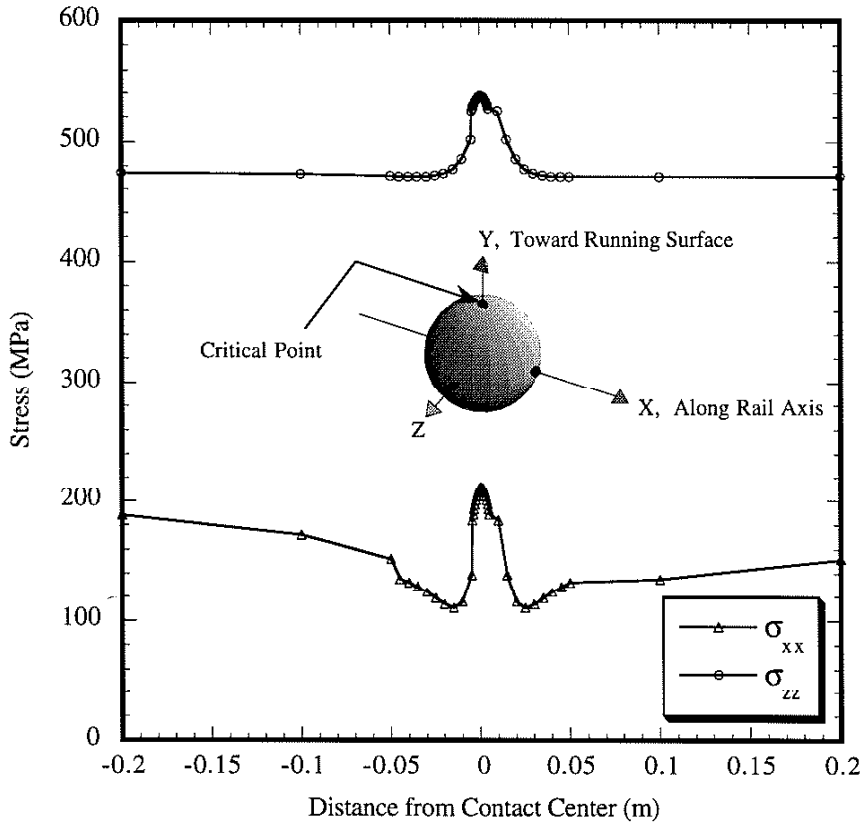

Fig. 12. Plot of a local stress history, p(t). This plot shows results from the *Standard Set* 15 mm below the rail's running surface at the critical point on the discontinuity, P = (0,1,0). σ_{xx} and σ_{zz} are shown; all other components are zero.

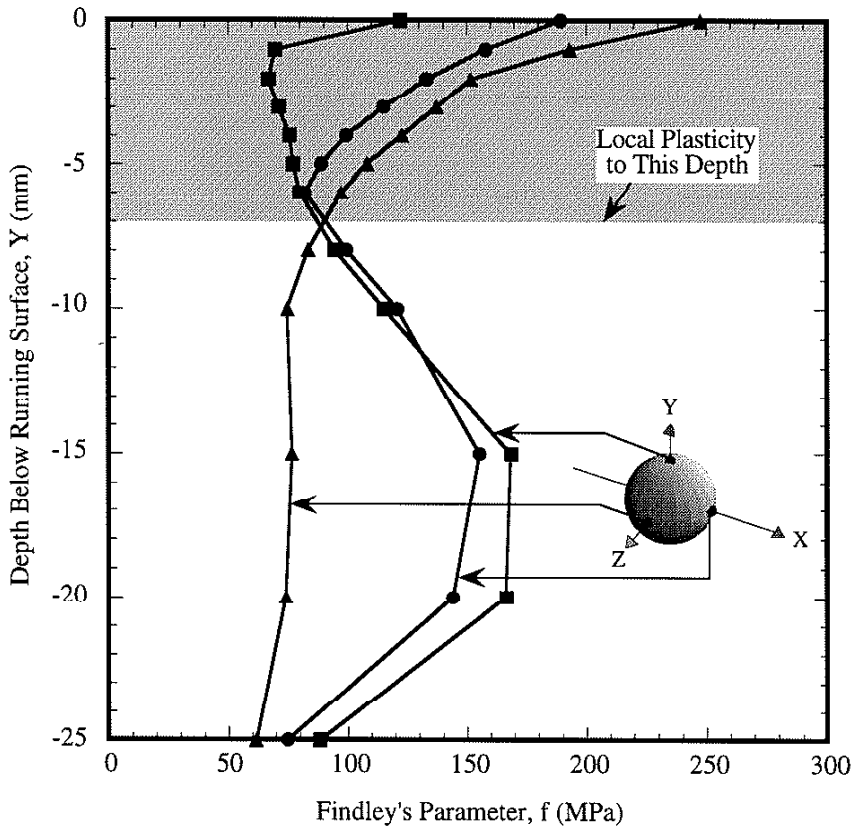

Fig. 13. Plot of Findley's Parameter as it varies with depth below the running surface of the rail for the *Standard Set*. The results from three points on the discontinuity are shown: P = (1,0,0), (0,1,0), and (0,0,1).

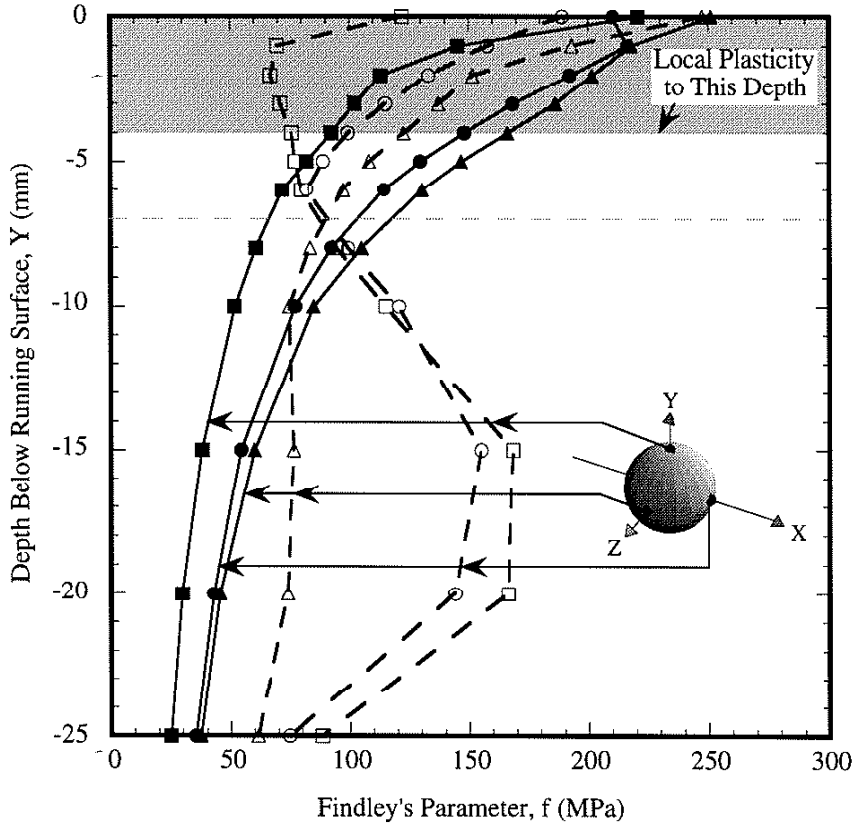

Fig. 14. Plot of Findley's Parameter as it varies with depth below the running surface of the rail for *Set 1* (no residual stresses). The results from three points on the discontinuity are shown:
P = (1,0,0), (0,1,0), and (0,0,1). The dashed lines indicate results from the *Standard Set.*

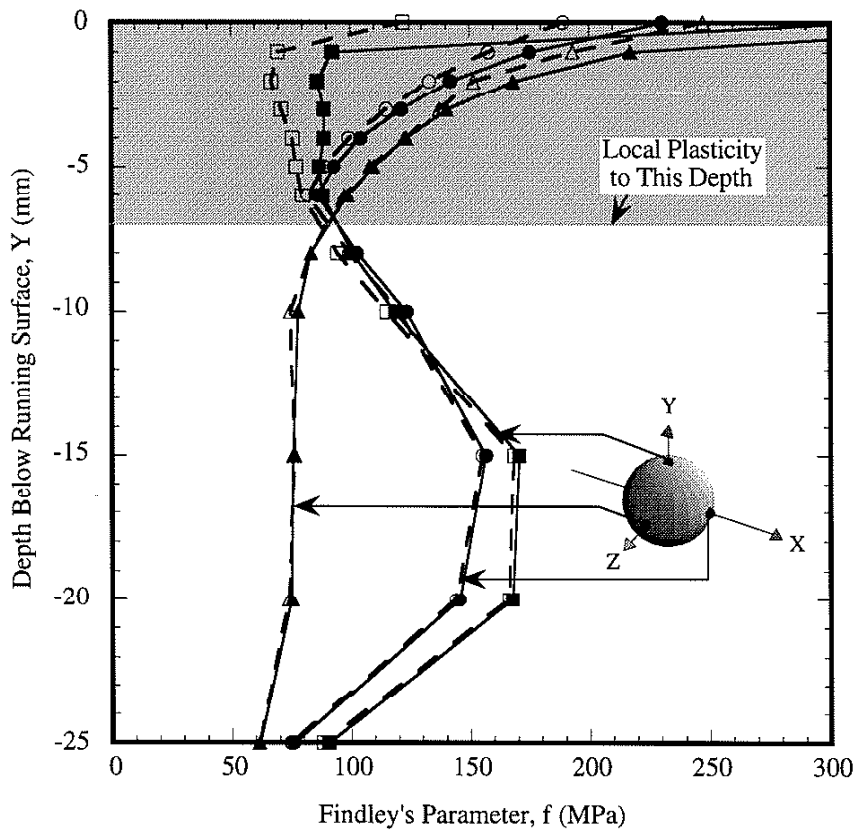

Fig. 15. Plot of Findley's Parameter as it varies with depth below the running surface of the rail for *Set 2* (added tangential wheel load). The results from three points on the discontinuity are shown:
P = (1,0,0), (0,1,0), and (0,0,1). The dashed lines indicate results from the *Standard Set.*

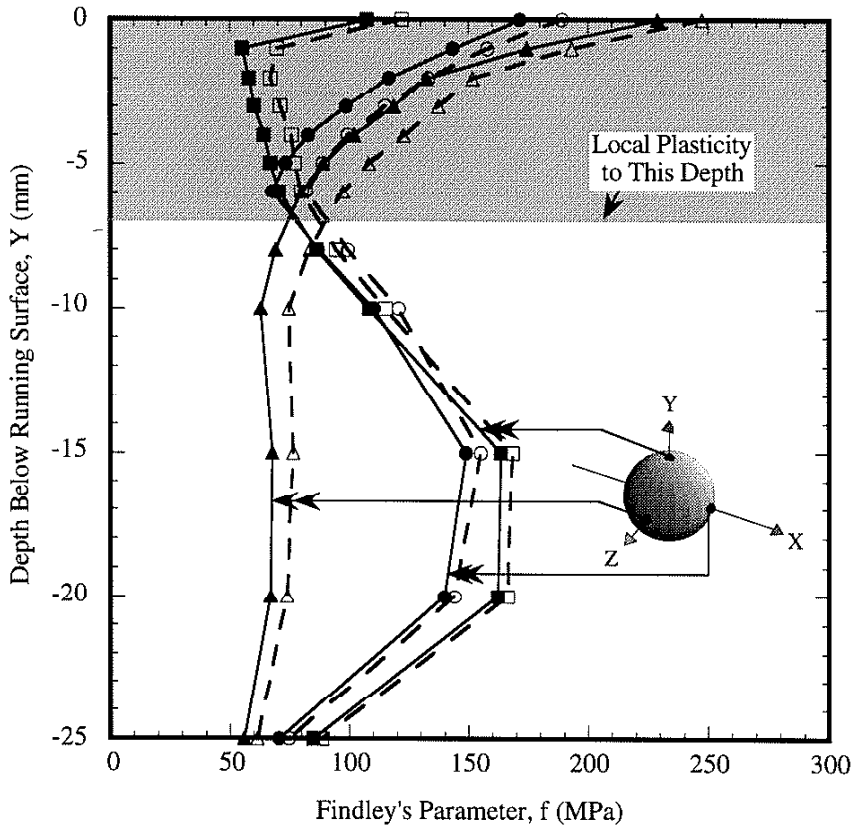

Fig. 16. Plot of Findley's Parameter as it varies with depth below the running surface of the rail for *Set 3* (smaller vertical wheel load). The results from three points on the discontinuity are shown:
P = (1,0,0), (0,1,0), and (0,0,1). The dashed lines indicate results from the *Standard Set.*

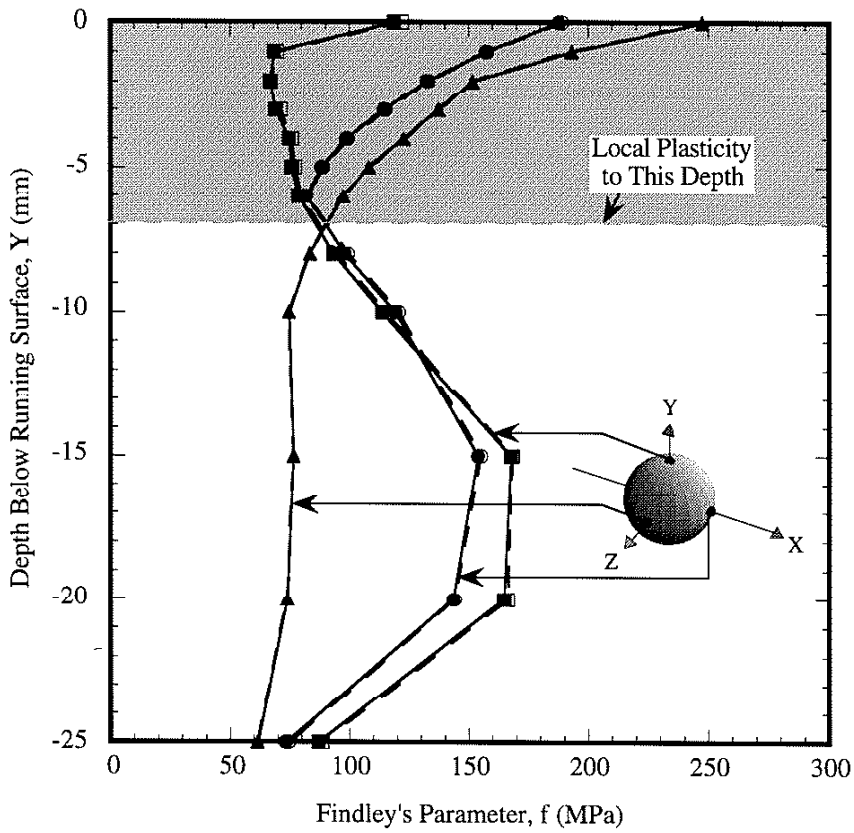

Fig. 17. Plot of Findley's Parameter as it varies with depth below the running surface of the rail for *Set 4* (stiffer foundation). The results from three points on the discontinuity are shown:
P = (1,0,0), (0,1,0), and (0,0,1). The dashed lines indicate results from the *Standard Set.*

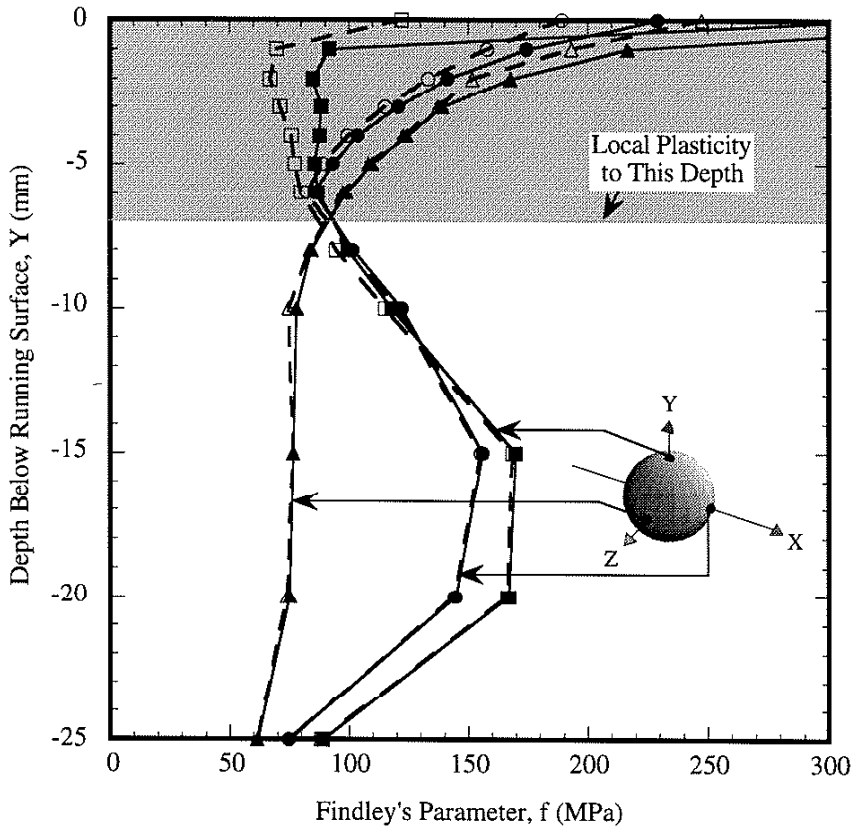

Fig. 18. Plot of Findley's Parameter as it varies with depth below the running surface of the rail for *Set 5* (stiffer foundation with tangential wheel load). The results from three points on the discontinuity are shown:
P = (1,0,0), (0,1,0), and (0,0,1). The dashed lines indicate results from the *Standard Set.*

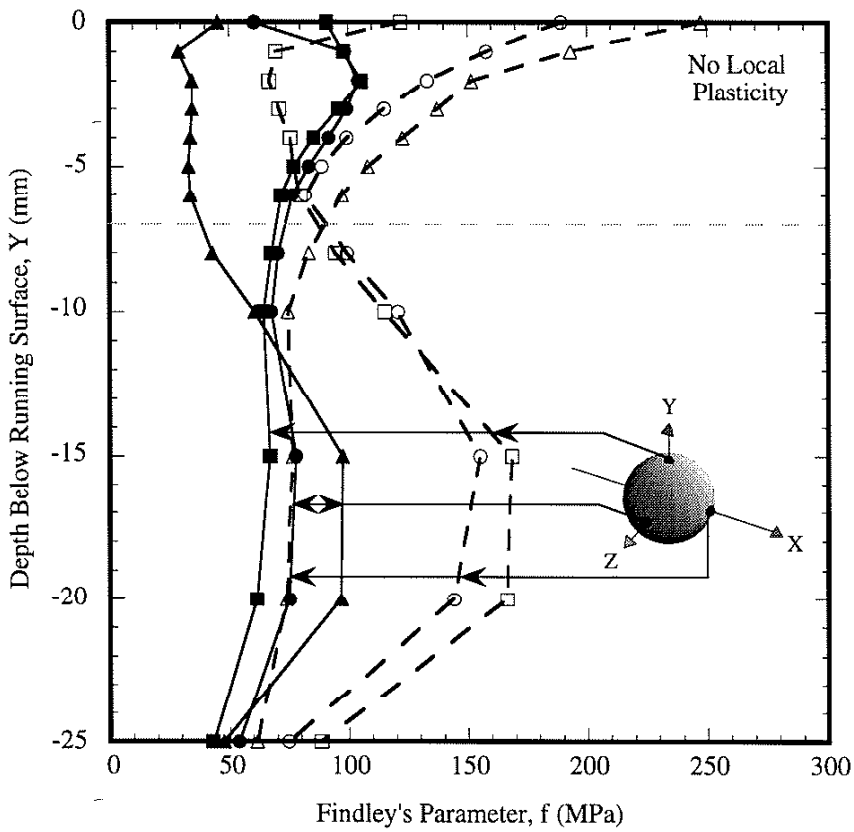

Fig. 19. Plot of Findley's Parameter as it varies with depth below the running surface of the rail for *Set 6* (oxide discontinuity). The results from three points on the discontinuity are shown:
P = (1,0,0), (0,1,0), and (0,0,1). The dashed lines indicate results from the *Standard Set.*

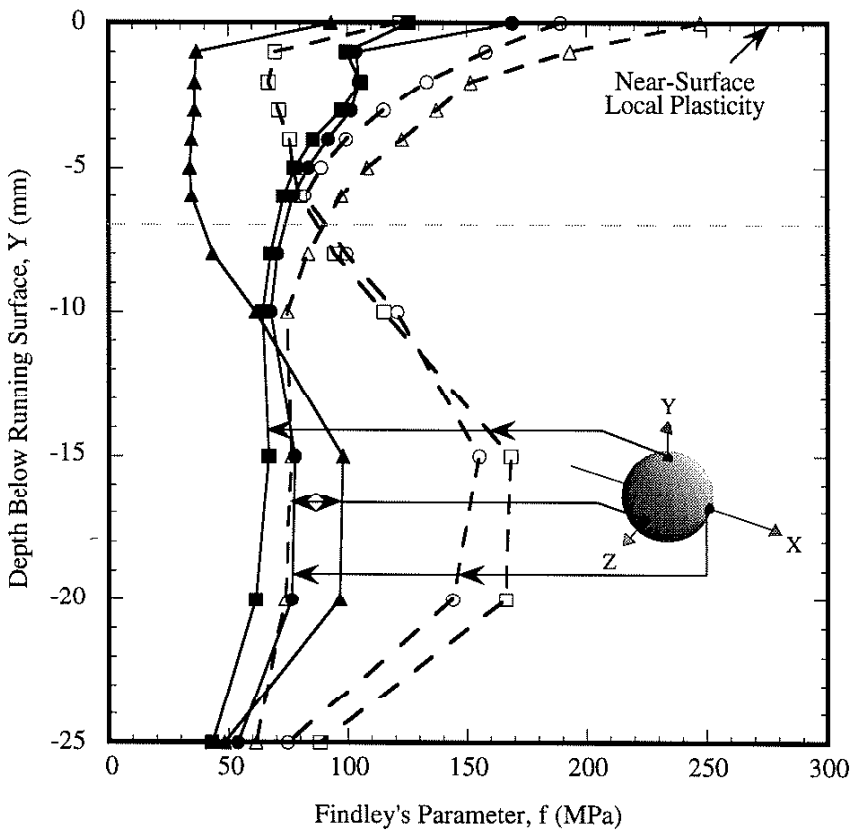

Fig. 20. Plot of Findley's Parameter as it varies with depth below the running surface of the rail for *Set 7* (oxide discontinuity with tangential wheel load). The results from three points on the discontinuity are shown:
P = (1,0,0), (0,1,0), and (0,0,1). The dashed lines indicate results from the *Standard Set.*

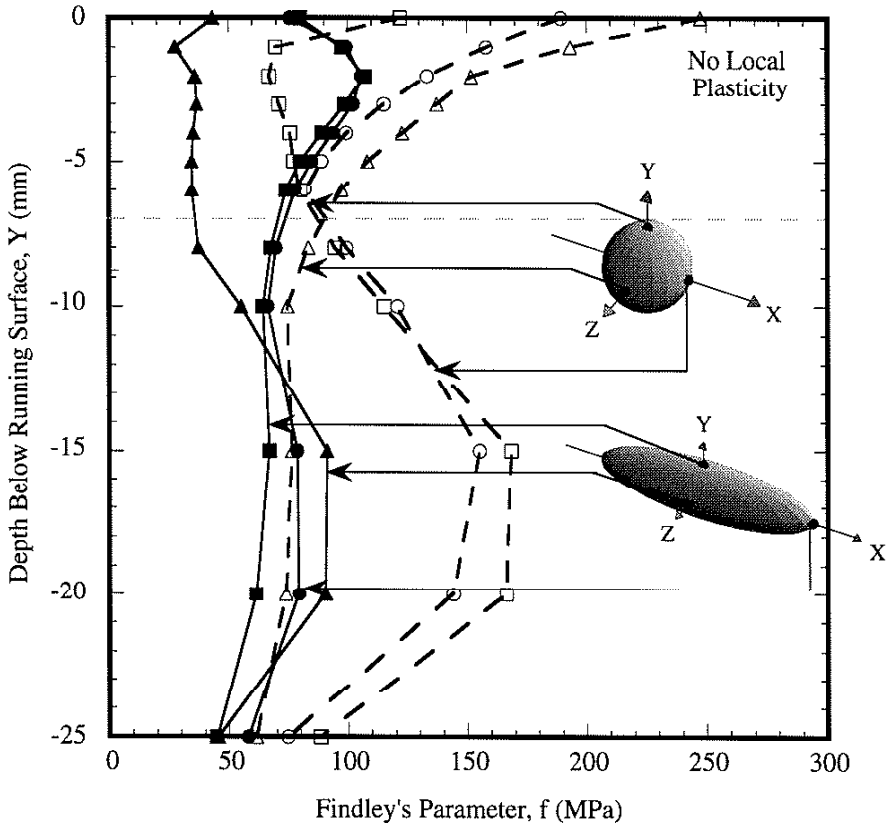

Fig. 21. Plot of Findley's Parameter as it varies with depth below the running surface of the rail for *Set 8* (football-shaped oxide discontinuity). The results from three points on the discontinuity are shown:
P = (1,0,0), (0,1,0), and (0,0,1). The dashed lines indicate results from the *Standard Set.*

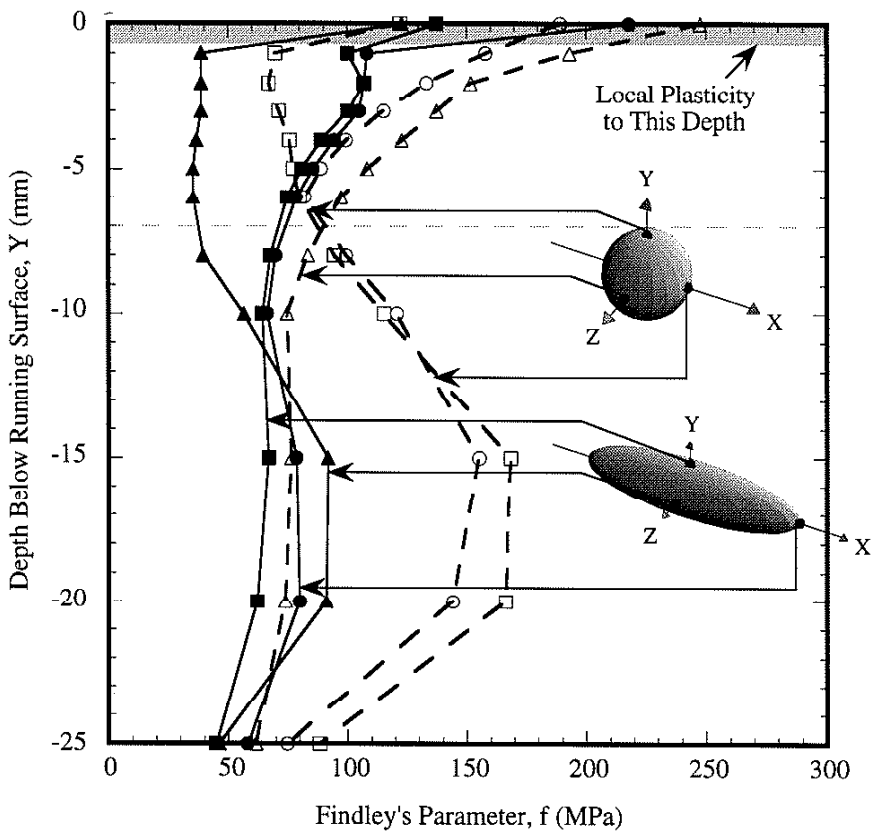

Fig. 22. Plot of Findley's Parameter as it varies with depth below the running surface of the rail for *Set 9* (football-shaped oxide discontinuity with tangential wheel load). The results from three points on the discontinuity are shown:
P = (1,0,0), (0,1,0), and (0,0,1). The dashed lines indicate results from the *Standard Set.*

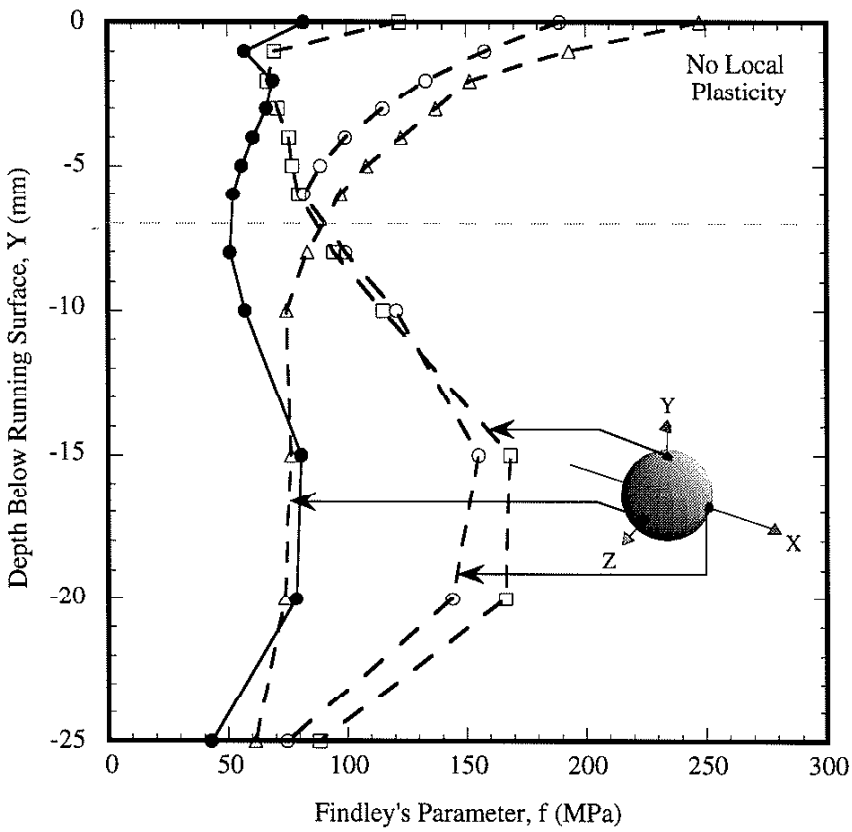

Fig. 23. Plot of Findley's Parameter as it varies with depth below the running surface of the rail for *Set 10* (no discontinuity). The dashed lines indicate results from the *Standard Set.*

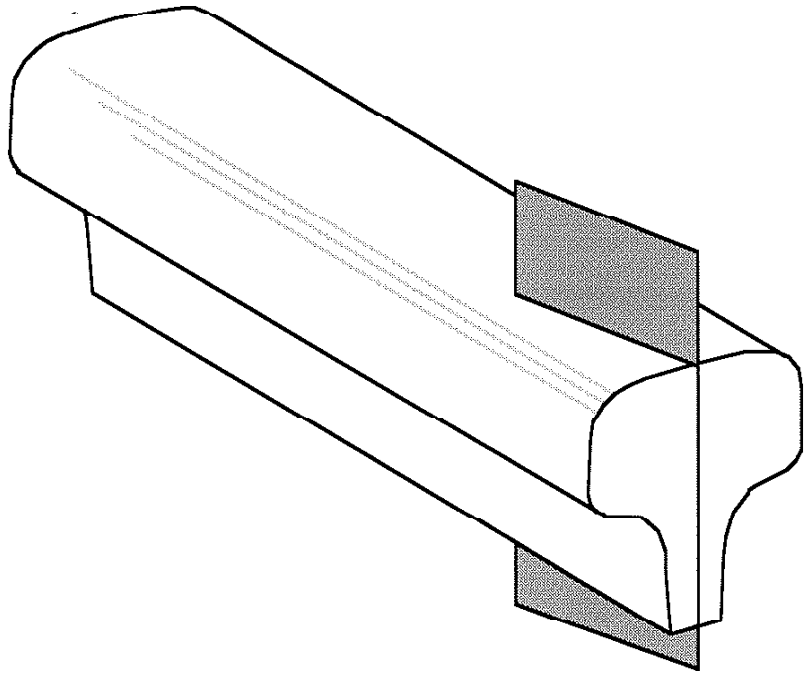

Fig. 24. Schematic drawing of the critical plane for the *Standard Set*: π = (0.26, 0.00, 0.97).

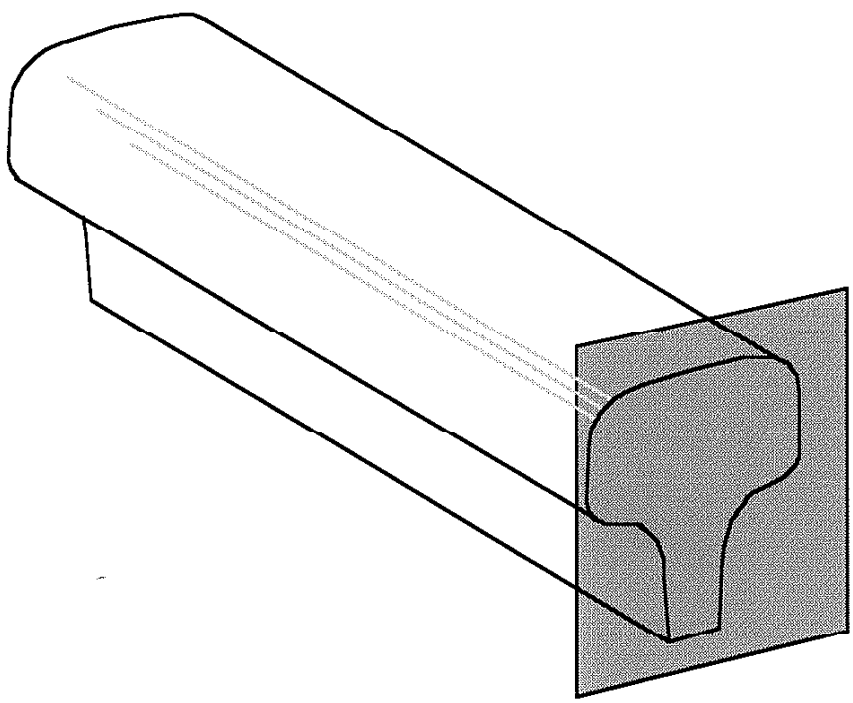

Fig. 25. Schematic drawing of the critical plane for *Set 1* (no residual stresses): π = (1.00, 0.00, 0.00).

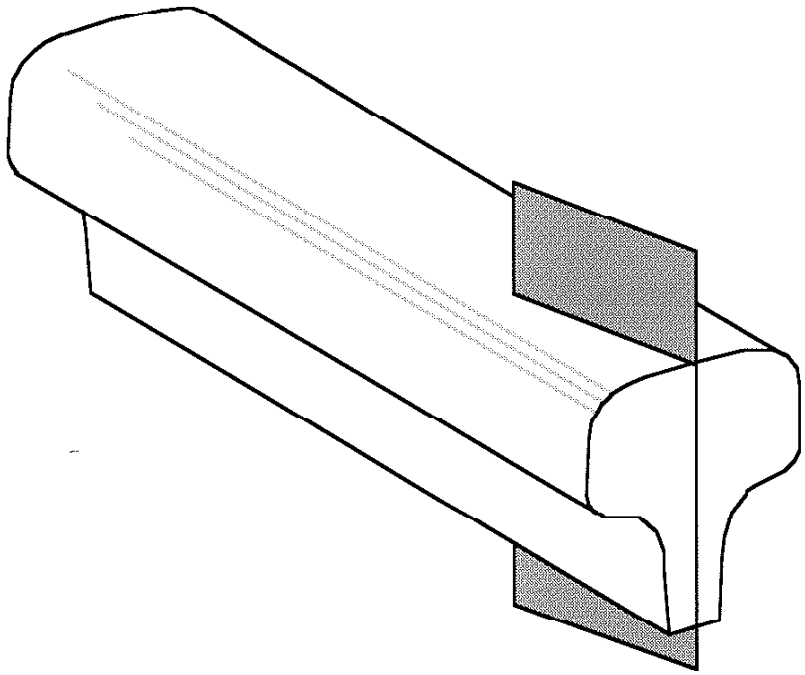

Fig. 26. Schematic drawing of the critical plane for *Set 2* (added tangential wheel load): π = (0.26, 0.00, 0.97).

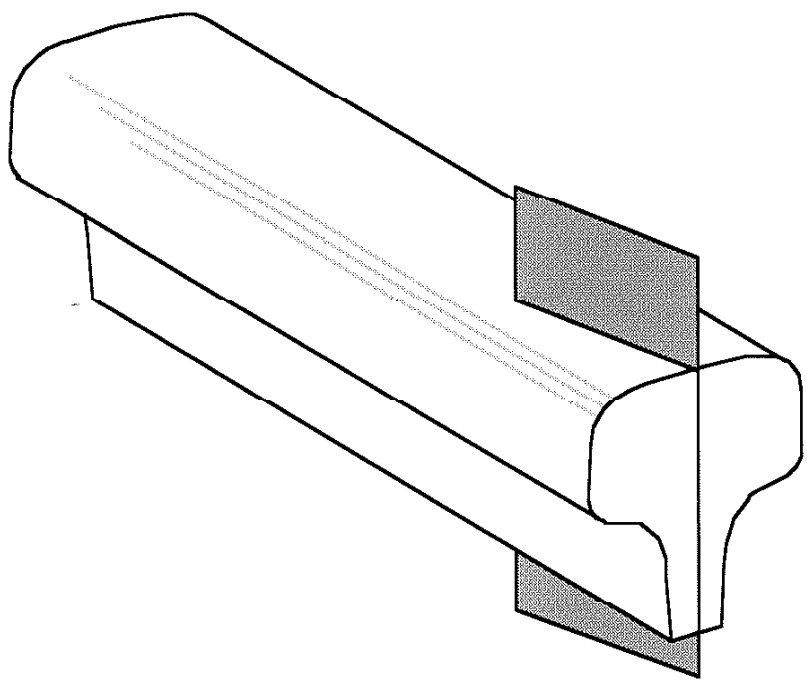

Fig. 27. Schematic drawing of the critical plane for *Set 3* (smaller vertical wheel load): π = (0.26, 0.00, 0.97).

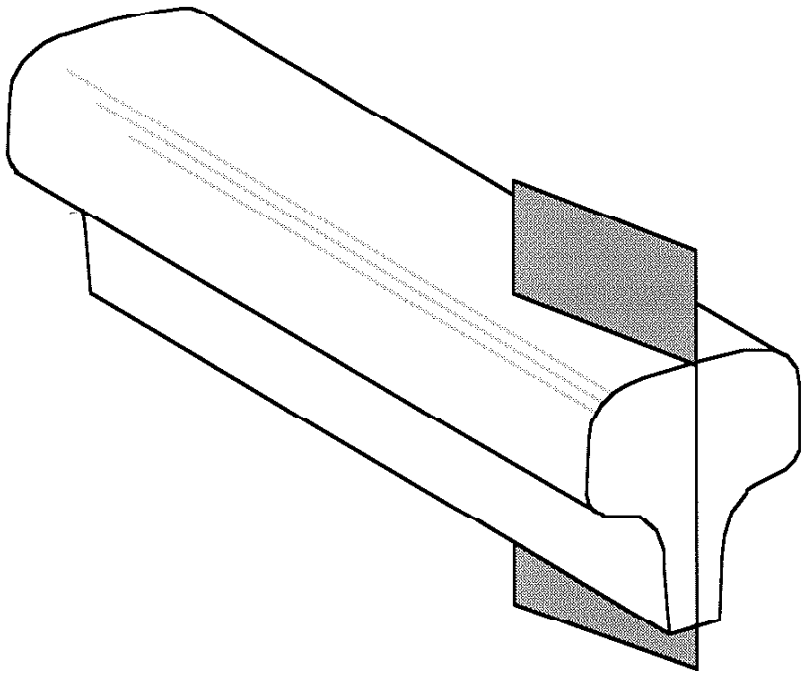

Fig. 28. Schematic drawing of the critical plane for *Set 4* (stiffer foundation): π = (0.26, 0.00, 0.97).

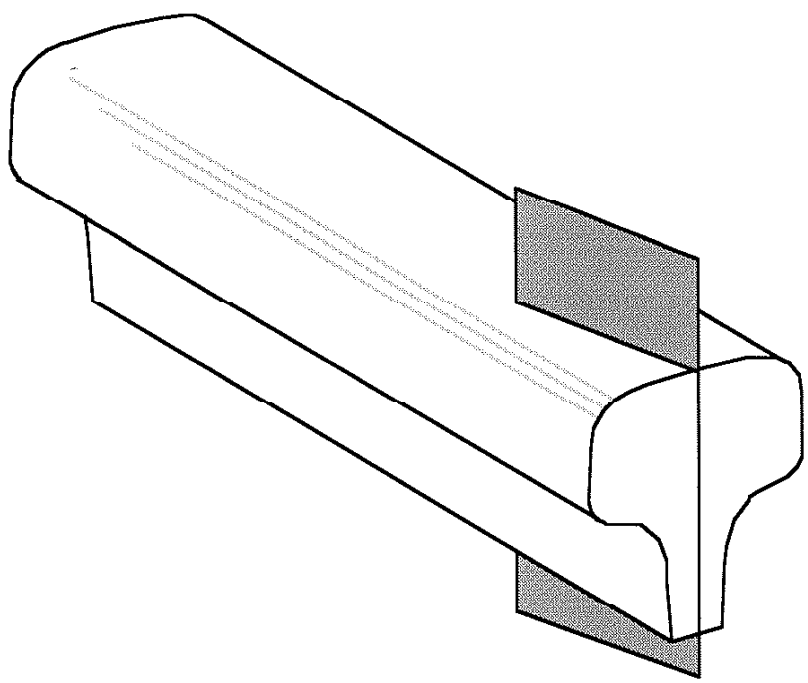

Fig. 29. Schematic drawing of the critical plane for *Set 5* (stiffer foundation with tangential wheel load): π = (0.26, 0.00, 0.97).

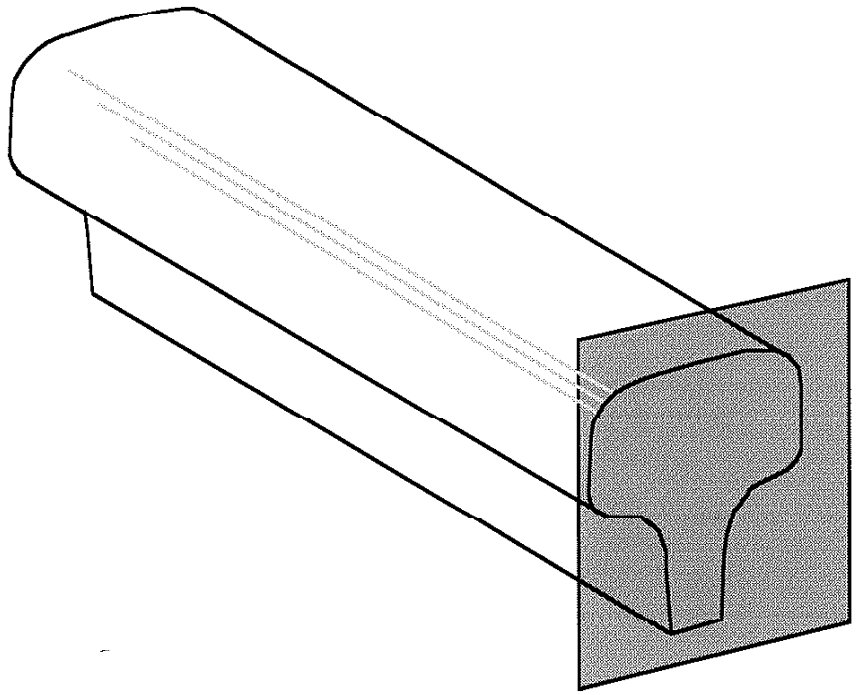

Fig. 30. Schematic drawing of the critical plane for *Set 6* (oxide discontinuity): π = (1.00, 0.00, 0.00).

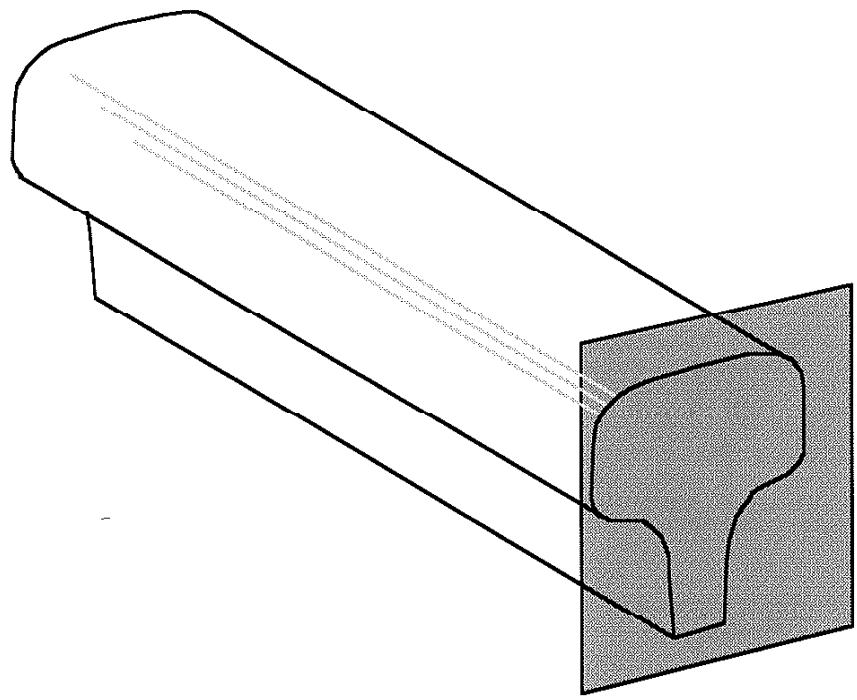

Fig. 31. Schematic drawing of the critical plane for *Set 7* (oxide discontinuity with tangential wheel load): π = (1.00, 0.00, 0.00).

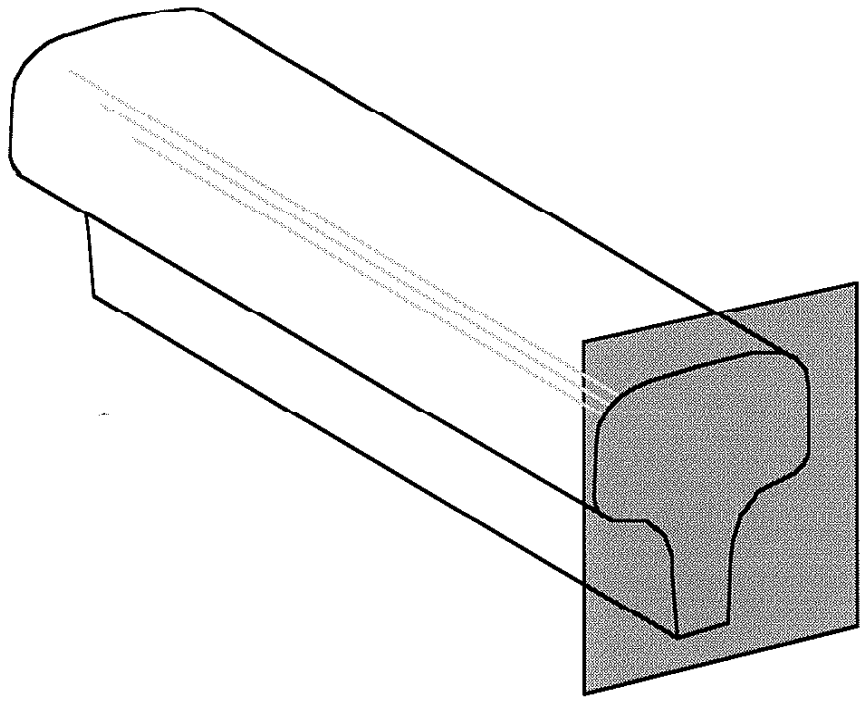

Fig. 32. Schematic drawing of the critical plane for *Set 8* (football-shaped oxide discontinuity): $\pi = (1.00, 0.00, 0.00)$.

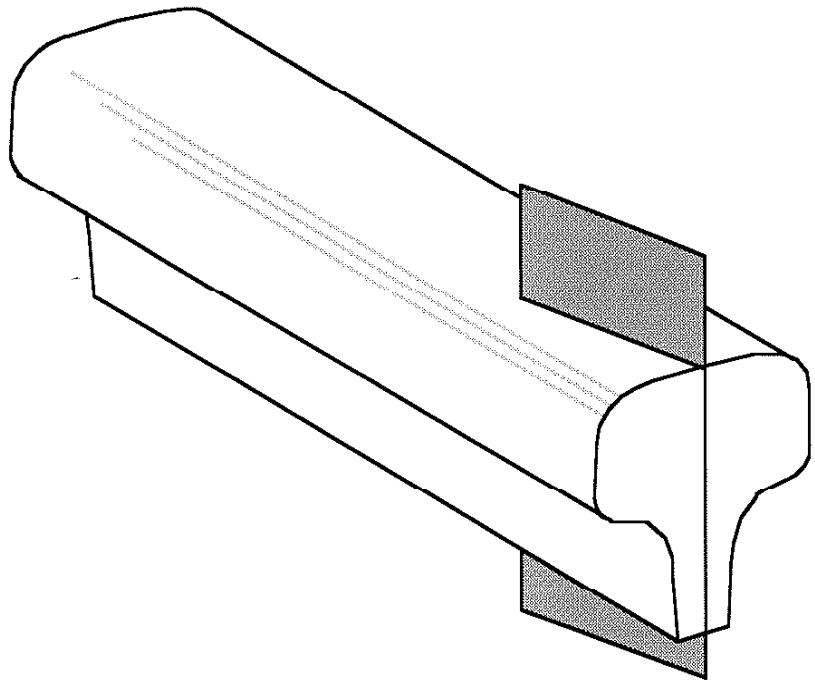

Fig. 33. Schematic drawing of the critical plane for *Set 9* (football-shaped oxide discontinuity with tangential wheel load): $\pi = (0.17, 0.98, 0.00)$.

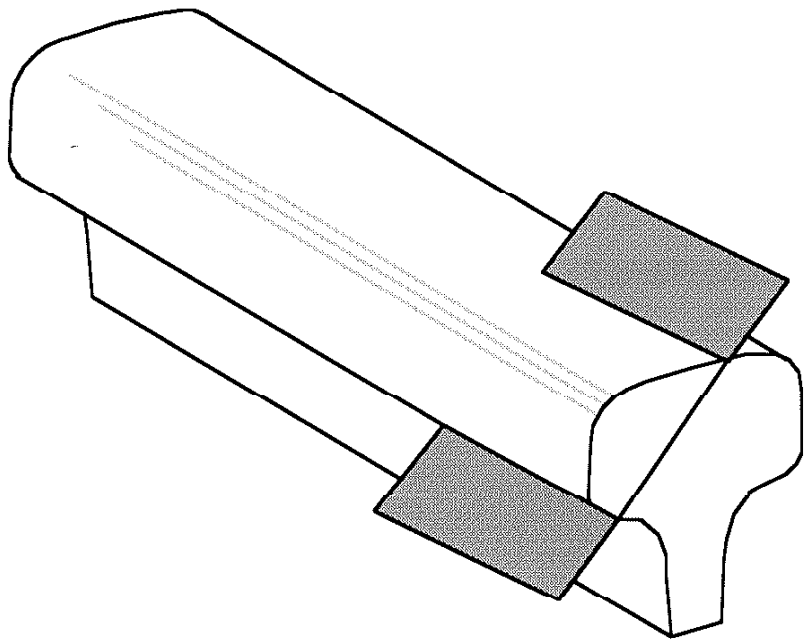

Fig. 34. Schematic drawing of the critical plane for *Set 10* (no discontinuity): π = (0.00, 0.77, 0.64).

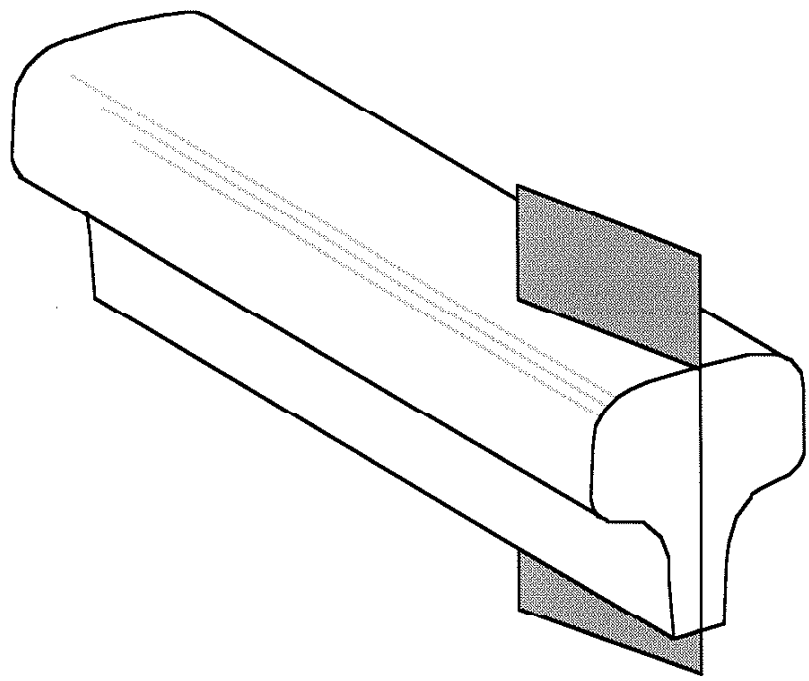

Fig. 35. Schematic drawing of the critical plane for winter conditions: π = (0.42, 0.00, 0.91).

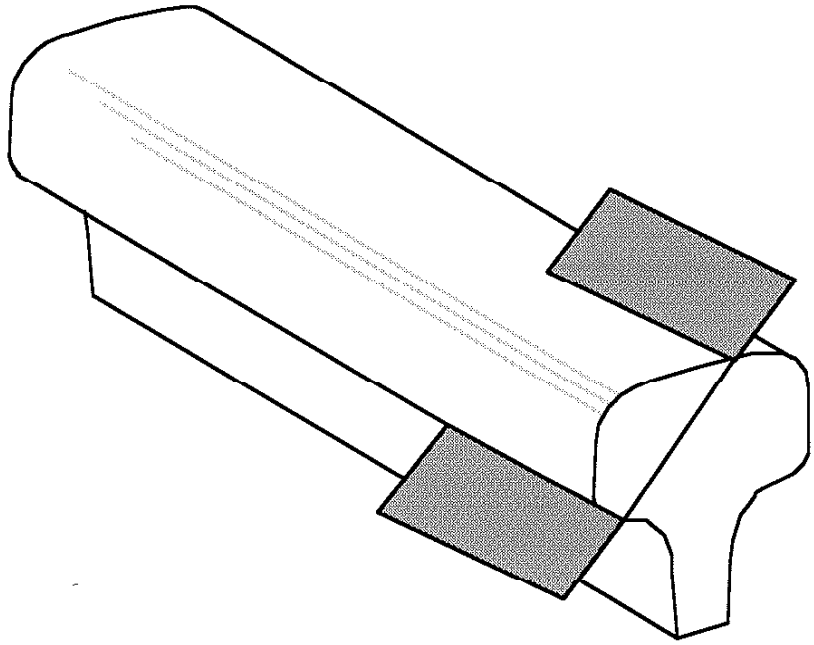

Fig. 36. Schematic drawing of the critical plane for summer conditions: π = (0.00, 0.34, 0.94).

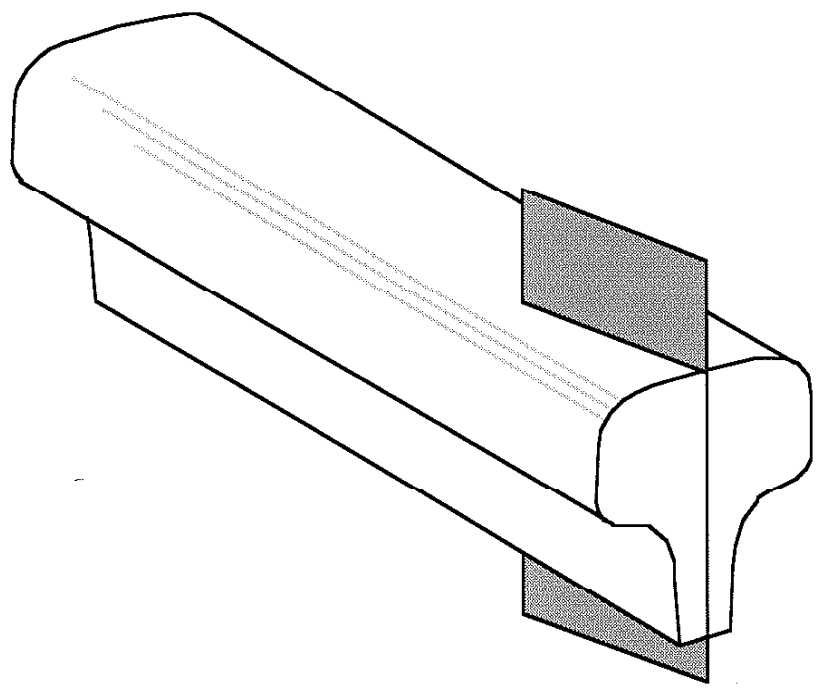

Fig. 37. Schematic drawing of the critical plane for the weak foundation; π = (0.34, 0.00, 0.94).

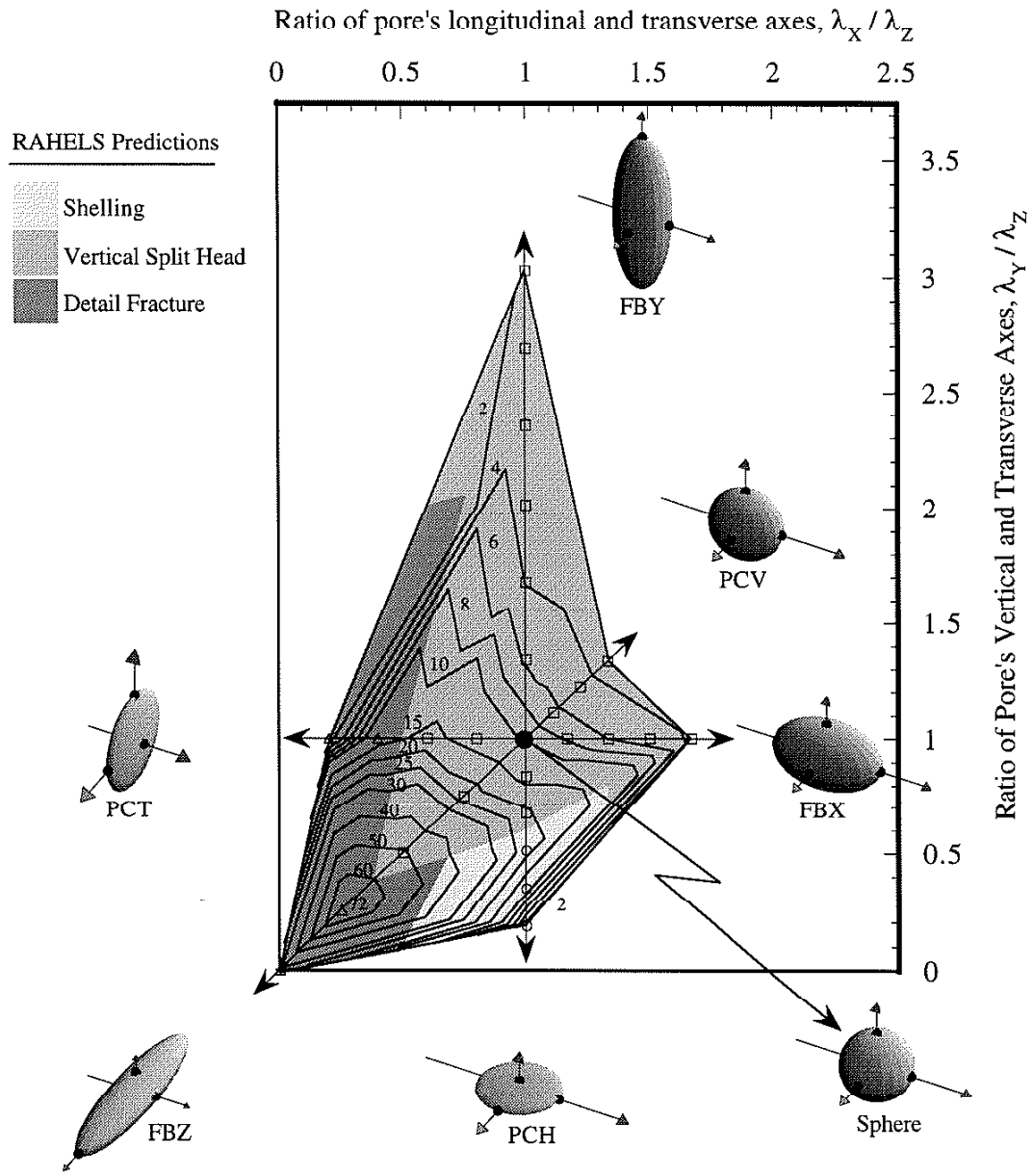

Fig. 38. The effects of pore shape. Shaded areas on the diagram indicate the different shapes which cause the same defect. Three types of defects are predicted: shelling, transverse fissure, and vertical split head. Within the shaded regions, material behavior is elastic; outside the shaded regions localized plastic deformation occurs. The lives (in millions of cycles) are indicated by contour lines; each cycle is a passage of a 0.3470 MN (39 Ton) axle.

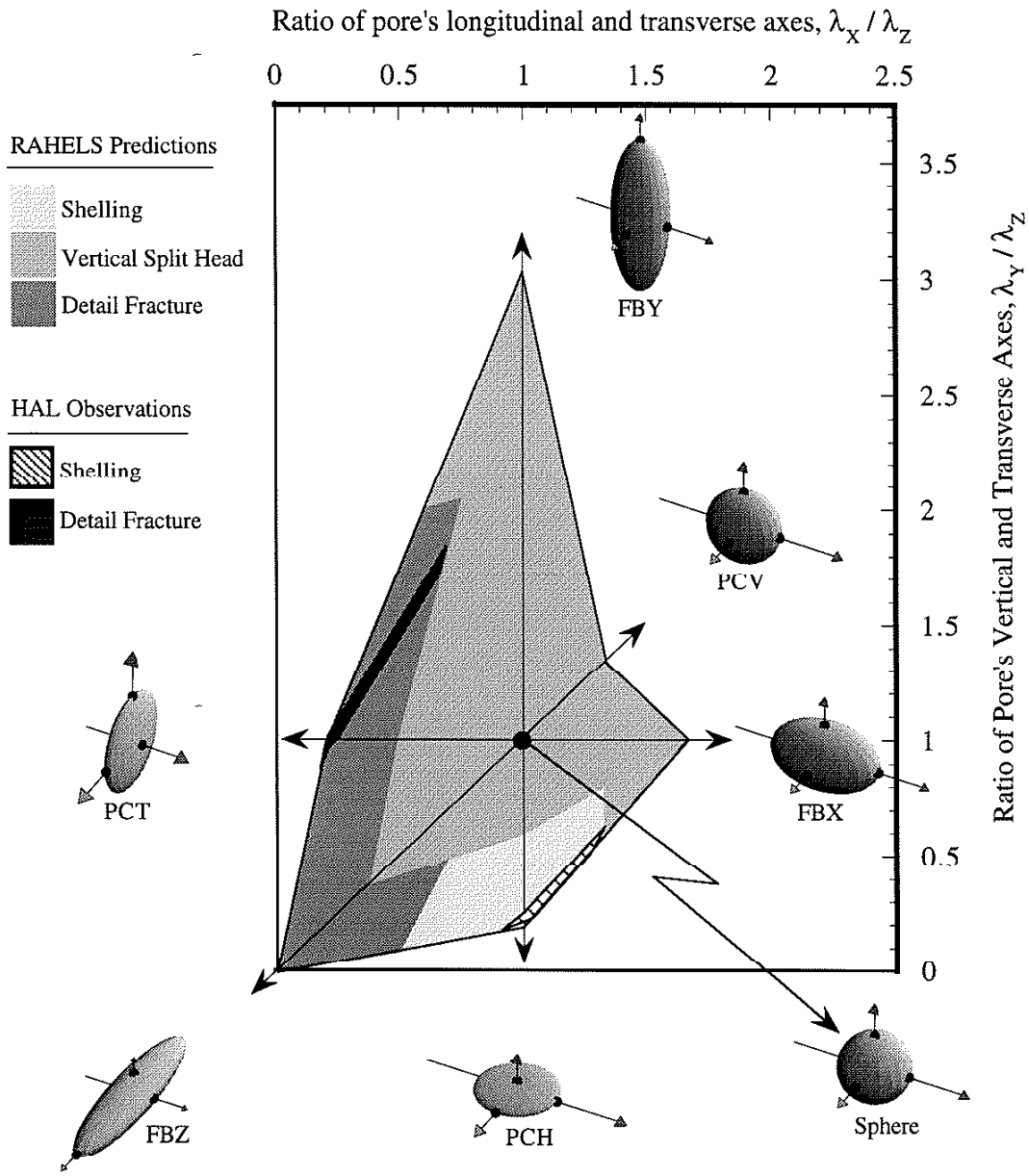

Fig. 39. Plot of experimental data and model predictions. A shaded band is plotted where the range of lives for observed defects classified as shelling crosses the region of the diagram where shelling is predicted as the dominant defect and where the predicted life contours agree with the observed lives. Another shaded zone is plotted where the range of lives for observed defects classified as detail fracture crosses the region of the diagram where detail fracture is predicted as the dominant defect and where the predicted life contours agree with the observed lives.

APPENDIX A

The rail-head stresses in the RAHELS model are computed using the elastic solution for the mixed problem of the two-layered half-plane loaded by Hertzian contact stresses as derived below (for the single-layered half-plane solution, see Smith and Liu 1953).

Figure A.1 shows a schematic drawing of the problem. The rail is modeled as an infinitely long elastic strip of depth, d. The supporting elements beneath the rail are combined and modeled as an elastic half-plane ($b \rightarrow \infty$). Normal and tangential tractions are applied to the top surface of the rail strip: f(x) and g(x) respectively. The rail strip and the support layer are bonded together. In this idealized system, exact expressions can be obtained for the rail-strip stresses. A solution technique presented in Uflyand (1965, 36-39) is adapted to solve the problem.

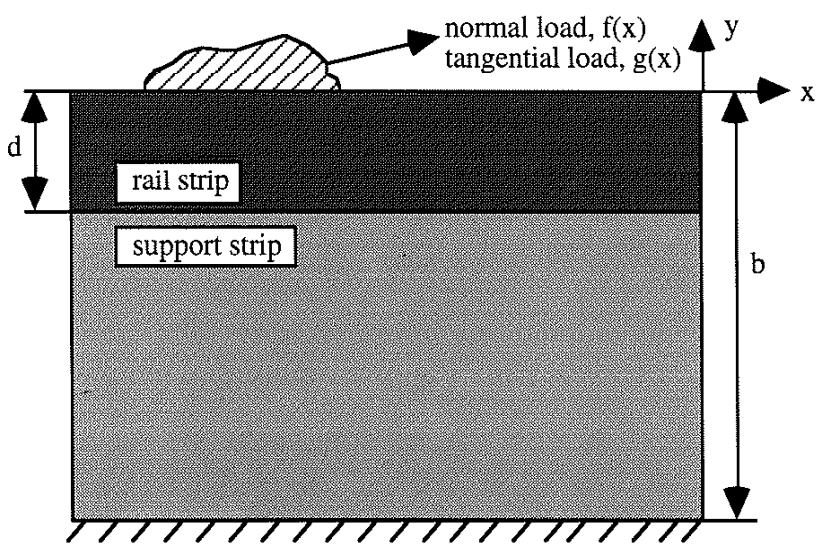

Fig. A.1. Schematic drawing of 2-D rail model.

The elastic horizontal and vertical displacements, u and v respectively, are expressed by the two Papkovich-Neuber functions, Fr and Fs, in equations A.1 to A.6 (Uflyand 1965). The subscript "r" refers to the rail strip, and the subscript "s" refers to the support strip. All functions ϕ are harmonic. The constants G and ν represent the elastic shear modulus and Poisson's ratio respectively.

$$2G_r u_r = -\frac{\partial F_r}{\partial x} + 4\left(1 - \frac{\nu_r}{1+\nu_r}\right)\phi_{1r} \tag{A.1}$$

$$2G_r v_r = -\frac{\partial F_r}{\partial y} + 4\left(1 - \frac{\nu_r}{1+\nu_r}\right)\phi_{2r} \tag{A.2}$$

$$2G_s u_s = -\frac{\partial F_s}{\partial x} + 4\left(1 - \frac{\nu_s}{1+\nu_s}\right)\phi_{1s} \tag{A.3}$$

$$2G_s v_s = -\frac{\partial F_s}{\partial y} + 4\left(1 - \frac{\nu_s}{1+\nu_s}\right)\phi_{2s} \tag{A.4}$$

$$F_r = \phi_{0r} + x\phi_{1r} + y\phi_{2r} \tag{A.5}$$

$$F_s = \phi_{0s} + x\phi_{1s} + y\phi_{2s} \tag{A.6}$$

Expressions for the stresses are obtained by applying the equations of generalized plane stress to the relations (A.1) - (A.4) with (A.5), (A.6). From the condition of the problem, ϕ_{1r} and ϕ_{1s} can be taken as zero (Uflyand 1965). The five resulting general expressions describing the elastic behavior of the plane-stress rail strip are summarized below.[4] The expressions for the support strip are similar and are found by replacing the subscript "r" by the subscript "s".

$$u_r(x,y) = \frac{1}{2G_r}\left(-\frac{\partial \phi_{0r}}{\partial x} - y\frac{\partial \phi_{2r}}{\partial x}\right) \tag{A.7}$$

---

[4]The plane-strain case can be recovered by substituting $\frac{\nu}{1-\nu}$ for ν in all expressions.

$$v_r(x,y) = \frac{1}{2G_r}\left(-\frac{\partial\phi_{0r}}{\partial y} - y\frac{\partial\phi_{2r}}{\partial y} + \frac{3-\nu_r}{1+\nu_r}\phi_{2r}\right) \tag{A.8}$$

$$\sigma_{xxr}(x,y) = -\frac{\partial^2\phi_{0r}}{\partial x^2} - y\frac{\partial^2\phi_{2r}}{\partial x^2} + \frac{2\nu_r}{1+\nu_r}\frac{\partial\phi_{2r}}{\partial y} \tag{A.9}$$

$$\sigma_{yyr}(x,y) = -\frac{\partial^2\phi_{0r}}{\partial y^2} - y\frac{\partial^2\phi_{2r}}{\partial y^2} + \frac{2}{1+\nu_r}\frac{\partial\phi_{2r}}{\partial y} \tag{A.10}$$

$$\tau_{xyr}(x,y) = -\frac{\partial^2\phi_{0r}}{\partial x\partial y} - y\frac{\partial^2\phi_{2r}}{\partial x\partial y} + \frac{1-\nu_r}{1+\nu_r}\frac{\partial\phi_{2r}}{\partial x} \tag{A.11}$$

The next step in the solution process is to derive specific ϕ functions that are consistent with the geometry and boundary conditions of the idealized system. The Fourier integral transform is used to facilitate this derivation. The Fourier transform $\bar{f}(\lambda)$ of a function f(x) is defined in equation (A.12). The inverse Fourier transform is given in equation (A.13). Hereafter, a transformed function will be denoted with an overbar. For a discussion of Fourier transforms see Carrier and Pearson (1988).

$$\bar{h}(\lambda) = \frac{1}{\sqrt{2\pi}}\int_{-\infty}^{+\infty} h(x)e^{i\lambda x}dx \tag{A.12}$$

$$h(x) = \frac{1}{\sqrt{2\pi}}\int_{-\infty}^{+\infty} \bar{h}(\lambda)e^{-i\lambda x}d\lambda \tag{A.13}$$

A useful property of the Fourier Transform is the transform of a derivative;

$$\frac{1}{\sqrt{2\pi}}\int_{-\infty}^{+\infty} h'(x)e^{i\lambda x}dx = -i\lambda\bar{h}(\lambda) \tag{A.14}$$

Since the ϕ functions are harmonic,

$$\frac{\partial^2\phi_{0r}}{\partial x^2} + \frac{\partial^2\phi_{0r}}{\partial y^2} = 0 \tag{A.15}$$

$$\frac{\partial^2\phi_{2r}}{\partial x^2}+\frac{\partial^2\phi_{2r}}{\partial y^2}=0 \tag{A.16}$$

$$\frac{\partial^2\phi_{0s}}{\partial x^2}+\frac{\partial^2\phi_{0s}}{\partial y^2}=0 \tag{A.17}$$

$$\frac{\partial^2\phi_{2s}}{\partial x^2}+\frac{\partial^2\phi_{2s}}{\partial y^2}=0. \tag{A.18}$$

Taking the transform of A.15 with respect to x results in the following ordinary differential equation:

$$-\lambda^2\bar{\phi}_{0r}+\frac{\partial^2\bar{\phi}_{0r}}{\partial y^2}=0. \tag{A.19}$$

A convenient form of the solution to A.19 is

$$\bar{\phi}_{0r}(\lambda,y)=A_{0r}e^{\lambda y}+B_{0r}e^{-\lambda y}. \tag{A.20}$$

Here A_{0r} and B_{0r} are functions of λ that are determined by the boundary conditions of the problem.

The other three transformed ϕ functions can be written down similarly;

$$\bar{\phi}_{2r}(\lambda,y)=A_{2r}e^{\lambda y}+B_{2r}e^{-\lambda y}, \tag{A.21}$$

$$\bar{\phi}_{0s}(\lambda,y)=A_{0s}e^{\lambda y}+B_{0s}e^{-\lambda y}, \tag{A.22}$$

$$\bar{\phi}_{2s}(\lambda,y)=A_{2s}e^{\lambda y}+B_{2s}e^{-\lambda y}. \tag{A.23}$$

The problem to be solved has eight boundary conditions which are shown in Figure A.1 and given in the equations below. The support strip and the rail strip extend infinitely in the plus and minus x-directions.

$$\sigma_{yyr}(x,0)=f(x) \tag{A.24}$$

$$\tau_{xyr}(x,0) = g(x) \tag{A.25}$$

$$\sigma_{yyr}(x,-d) = \sigma_{yys}(x,-d) \tag{A.26}$$

$$\tau_{xyr}(x,-d) = \tau_{xys}(x,-d) \tag{A.27}$$

$$u_r(x,-d) = u_s(x,-d) \tag{A.28}$$

$$v_r(x,-d) = v_s(x,-d) \tag{A.29}$$

$$u_s(x,-b) = 0 \tag{A.30}$$

$$v_s(x,-b) = 0 \tag{A.31}$$

Taking the transform of equations A.7 to A.11 with respect to x results in the following. (As before, the support strip equations are obtained by replacing the subscript "r" by the subscript "s".)

$$\bar{u}_r(\lambda,y) = \frac{i\lambda}{2G_r}\left(\bar{\phi}_{0r} + y\bar{\phi}_{2r}\right) \tag{A.32}$$

$$\bar{v}_r(\lambda,y) = \frac{1}{2G_r}\left(-\frac{\partial\bar{\phi}_{0r}}{\partial y} - y\frac{\partial\bar{\phi}_{2r}}{\partial y} + \frac{3-\nu_r}{1+\nu_r}\bar{\phi}_{2r}\right) \tag{A.33}$$

$$\bar{\sigma}_{xxr}(\lambda,y) = \lambda^2\bar{\phi}_{0r} + \lambda^2 y\bar{\phi}_{2r} + \frac{2\nu_r}{1+\nu_r}\frac{\partial\bar{\phi}_{2r}}{\partial y} \tag{A.34}$$

$$\bar{\sigma}_{yyr}(\lambda,y) = -\frac{\partial^2\bar{\phi}_{0r}}{\partial y^2} - y\frac{\partial^2\bar{\phi}_{2r}}{\partial y^2} + \frac{2}{1+\nu_r}\frac{\partial\bar{\phi}_{2r}}{\partial y} \tag{A.35}$$

$$\bar{\tau}_{xyr}(\lambda,y) = i\lambda\frac{\partial\bar{\phi}_{0r}}{\partial y} + i\lambda y\frac{\partial\bar{\phi}_{2r}}{\partial y} - \frac{1-\nu_r}{1+\nu_r}\,i\lambda\bar{\phi}_{2r} \tag{A.36}$$

The solution now proceeds by taking the transform with respect to x of each of the boundary condition statements (A.24-A.31) -- which will result in expressions similar to

A.32-A.36, substituting in A.20-A.23, and solving for the eight coefficients.[5] To recover the rail-head stresses, the inverse transform of equations A.34-A.36 is then evaluated. Before performing the stress calculations in this study, the limit as $b \rightarrow \infty$ was taken (see Appendices B and C).

Evaluation of the inverse Fourier transforms was facilitated by using asymptotic expressions for the integrands for values of λ larger than λ^*. The value of λ^* was determined so that the relative error of the asymptotic expression was less than 0.01% for a given integrand at the maximum depth below the running surface that was examined in this study (y = -0.0254 m). Note that for a given value of λ, the error of the asymptotic expressions increases with increasing depth below the running surface in the rail strip.

Under a concentrated load, the asymptotic integrands can be evaluated exactly over $[\lambda^*,\infty]$. This result from a concentrated unit load can be used to evaluate any distributed load by constructing an appropriate convolution.

For $[0,\lambda^*]$, the exact integrands were evaluated using the internal numerical integration function in *Mathematica*.

---

[5]The Fourier transform of the 2-dimensional Hertzian contact stress distribution given in Smith and Liu (1953), and used herein, is $\sqrt{\frac{\pi}{2}}\,\frac{n_0 J_1(|a\lambda|)}{|\lambda|}$.

APPENDIX B

Mathematica Notebook for the Normal Load Solution

1+1

2

Presentation of the Papkovich-Neuber Function

For the Rail

i) Fr = phi0r + x Phi1r + y Phi2r; phi0r, phi1r, and phi2r are harmonic
ii) 2 modr ur = -Dx(Fr) + 4(1 - 1/(1+nur)) phi1r
iii) 2 modr vr = -Dy(Fr) + 4(1 - 1/(1+nur)) phi2r
where Dx( ) and Dy( ) denote differentiation wrt x and y respectively

For the Support

iv) Fs = phi0s + x Phi1s + y Phi2s; phi0s, phi1s, and phi2s are harmonic
v) 2 mods us = -Dx(Fs) + 4(1 - 1/(1+nus)) phi1s
vi) 2 mods vs = -Dy(Fs) + 4(1 - 1/(1+nus)) phi2s
where Dx( ) and Dy( ) denote differentiation wrt x and y respectively

Description of Solution

Using the theorems of infinitesimal elasticity, and the above relationships (i - vi) expressions can be derived for displacements, strains, and stresses in terms of the phi0#, phi1#, and phi2# functions. Using the arbitrariness of one of the functions, phi1# are set to zero. The phi0# and phi2# functions are expressed in the frequency domain as linear combinations of exponential functions with coefficients determined by the boundary conditions. In the present case there are 8 coefficients -- which are functions of the frequency coordinate, w. Therefore, 8 boundary condition equations are required. Once the coefficients are determined as functions of w, the spatial domain stresses can be recovered by evaluating the Inverse Fourier Transform on the stress component expressions in the frequency domain.

Descriptions of Variables

Physical Domain -> an infinitely long elastic strip bonded to an elastic half-space

x -> Horizontal Coordinate (positive to the right) [L]
y -> Vertical Coordinate (positive upward) [L]
w -> Fourier Transform Coordinate [1/L]
wstar-> Value of "w" where Asymptotic Expressions become Admissible [1/L]
d -> Depth of Rail Strip [L]
b -> Depth of Support Strip [L]
modr -> Shear Modulus of the Rail [F/L^2]
nur -> Poisson's Ratio for the Rail
mods -> Shear Modulus of the Support [F/L^2]
nus -> Poisson's Ratio for the Support
n0 -> Peak Value of Hertzian Normal Traction [F/L^2]
a -> Half-Width of Contact Zone [L]
fbar -> Transformed Normal Traction Function [F/L]
a0r, b0r, a2r, b2r, a0s, b0s, a2s, b2s -> Harmonic Function Coefficients

Clear the Variables

```
Clear[x,y,w,wstar,d,b,modr,nur,mods,nus,n0,a,fba
r,a0r,b0r,a2r,b2r,a0s,b0s,a2s,b2s]
```

Definitions of Harmonic Functions in the Frequency Domain

```
Clear[fphi0r,fphi2r,fphi0s,fphi2s]

fphi0r[y_] = (a0r Exp[w y] + b0r Exp[-w y]);

fphi2r[y_] = (a2r Exp[w y] + b2r Exp[-w y]);

fphi0s[y_] = (a0s Exp[w y] + b0s Exp[-w y]);

fphi2s[y_] = (a2s Exp[w y] + b2s Exp[-w y]);
```

Definitions of Stresses and Displacements in the Frequency Domain

```
Clear[fsigxr,fsigyr,ftauxyr,fur,fvr,fsigxs,fsigy
s,ftauxys,fus,fvs]

fsigxr[y_] = w^2 fphi0r[y] + y w^2 fphi2r[y] +2
nur/(1+nur) D[fphi2r[y],{y,1}];

fsigyr[y_] = -D[fphi0r[y],{y,2}] - y
D[fphi2r[y],{y,2}]+2/(1+nur) D[fphi2r[y],{y,1}];

ftauxyr[y_] = I w D[fphi0r[y],{y,1}] + I w y
D[fphi2r[y],{y,1}] - I w (1-nur)/(1+nur)
fphi2r[y];

fur[y_]=1/(2 modr) (I w fphi0r[y] + y I w
fphi2r[y]);

fvr[y_]=1/(2 modr) (-D[fphi0r[y],{y,1}]-y
D[fphi2r[y],{y,1}]+(3-nur)/(1+nur) fphi2r[y]);

fsigxs[y_] = w^2 fphi0s[y] + y w^2 fphi2s[y] +2
nus/(1+nus) D[fphi2s[y],{y,1}];

fsigys[y_] = -D[fphi0s[y],{y,2}] - y
D[fphi2s[y],{y,2}]+2/(1+nus) D[fphi2s[y],{y,1}];

ftauxys[y_] = I w D[fphi0s[y],{y,1}] + I w y
D[fphi2s[y],{y,1}] - I w (1-nus)/(1+nus)
fphi2s[y];

fus[y_]=1/(2 mods) (I w fphi0s[y] + y I w
fphi2s[y]);

fvs[y_]=1/(2 mods) (-D[fphi0s[y],{y,1}]-y
D[fphi2s[y],{y,1}]+(3-nus)/(1+nus) fphi2s[y]);
```

Definitions of Inverse Fourier Transform Integrands for the Stress Components (real parts only -- the coefficients a0r, b0r, etc. are pure real)

```
Clear[intxr,intyr,inttauxyr,intvr]

intxr[a0r_,b0r_,a2r_,b2r_]=Collect[Numerator[Tog
ether[fsigxr[y]]], {a0r,a2r,b0r,b2r,Exp[w
y],Exp[-w y]}] 2/(Sqrt[2 Pi]
Denominator[Together[fsigxr[y]]]);
```

```
intyr[a0r_,b0r_,a2r_,b2r_]=Collect[Numerator[Tog
ether[fsigyr[y]]],  {a0r,a2r,b0r,b2r,Exp[w
y],Exp[-w  y]}]  2/(Sqrt[2  Pi]
Denominator[Together[fsigyr[y]]]);
```

```
inttauxyr[a0r_,b0r_,a2r_,b2r_]=Collect[Expand[Nu
merator[Together[ftauxyr[y]]]  (-2  I)],
{a0r,a2r,b0r,b2r,Exp[w  y],Exp[-w  y]}]/(Sqrt[2
Pi]  Denominator[Together[ftauxyr[y]]]);
```

```
intvr[a0r_,b0r_,a2r_,b2r_]=Collect[Numerator[Tog
ether[fvr[y]]],  {a0r,a2r,b0r,b2r,Exp[w  y],Exp[-w
y]}]  2/(Sqrt[2  Pi]
Denominator[Together[fvr[y]]]);
```

Determine the Unknown Coefficients

Boundary Condition Expansions

```
Clear[nur,nus]
```

```
nur=33/100
```

$$\frac{33}{100}$$

```
nus=33/100
```

$$\frac{33}{100}$$

```
Clear[eq1,eq2,eq3,eq4,eq5,eq6,eq7,eq8]
eq1=Expand[fsigyr[0]];
eq2=Expand[ftauxyr[0]];
eq3=Expand[fsigyr[-d]-fsigys[-d]];
eq4=Expand[ftauxyr[-d]-ftauxys[-d]];
eq5=Expand[fur[-d]-fus[-d]];
eq6=Expand[fvr[-d]-fvs[-d]];
eq7=Expand[fus[-b]];
```

```
eq8=Expand[fvs[-b]];
```

■ *Coefficient Matrix Construction and Matrix Equation Solution*

```
Clear[mat,coeflist]

mat = {
{Coefficient[eq1,a0r],Coefficient[eq1,b0r],Coeff
icient[eq1,a2r],Coefficient[eq1,b2r],Coefficient
[eq1,a0s],Coefficient[eq1,b0s],Coefficient[eq1,a
2s],Coefficient[eq1,b2s]},
{Coefficient[eq2,a0r],Coefficient[eq2,b0r],Coeff
icient[eq2,a2r],Coefficient[eq2,b2r],Coefficient
[eq2,a0s],Coefficient[eq2,b0s],Coefficient[eq2,a
2s],Coefficient[eq2,b2s]},
{Coefficient[eq3,a0r],Coefficient[eq3,b0r],Coeff
icient[eq3,a2r],Coefficient[eq3,b2r],Coefficient
[eq3,a0s],Coefficient[eq3,b0s],Coefficient[eq3,a
2s],Coefficient[eq3,b2s]},
{Coefficient[eq4,a0r],Coefficient[eq4,b0r],Coeff
icient[eq4,a2r],Coefficient[eq4,b2r],Coefficient
[eq4,a0s],Coefficient[eq4,b0s],Coefficient[eq4,a
2s],Coefficient[eq4,b2s]},
{Coefficient[eq5,a0r],Coefficient[eq5,b0r],Coeff
icient[eq5,a2r],Coefficient[eq5,b2r],Coefficient
[eq5,a0s],Coefficient[eq5,b0s],Coefficient[eq5,a
2s],Coefficient[eq5,b2s]},
{Coefficient[eq6,a0r],Coefficient[eq6,b0r],Coeff
icient[eq6,a2r],Coefficient[eq6,b2r],Coefficient
[eq6,a0s],Coefficient[eq6,b0s],Coefficient[eq6,a
2s],Coefficient[eq6,b2s]},
{Coefficient[eq7,a0r],Coefficient[eq7,b0r],Coeff
icient[eq7,a2r],Coefficient[eq7,b2r],Coefficient
[eq7,a0s],Coefficient[eq7,b0s],Coefficient[eq7,a
2s],Coefficient[eq7,b2s]},
{Coefficient[eq8,a0r],Coefficient[eq8,b0r],Coeff
icient[eq8,a2r],Coefficient[eq8,b2r],Coefficient
[eq8,a0s],Coefficient[eq8,b0s],Coefficient[eq8,a
2s],Coefficient[eq8,b2s]}};

coeflist=LinearSolve[mat,{1,0,0,0,0,0,0,0}];
```

■ *Define the Coefficients*

```
Clear[a0r,a2r,b0r,b2r]
```

```
a0r=Together[coeflist[[1]]];
b0r=Together[coeflist[[2]]];
a2r=Together[coeflist[[3]]];
b2r=Together[coeflist[[4]]];
```

Find Limit of Coefficients (b --> Infinity)

```
domexpcoeff[expr_,mant_,bigexp_,arbexp_]:=Max[Ca
ses[expr,(mant^(x2_ bigexp arbexp +
y2_)|mant^(x2_ bigexp arbexp))->x2, Infinity]]
domexp[expr_,mant_,bigexp_,arbexp_]:=Cases[expr,
(mant^(x_ bigexp arbexp + y_)|mant^(x_ bigexp
arbexp)) /; x ==
domexpcoeff[expr,mant,bigexp,arbexp], Infinity]
collectterms[expr_,formlist_]:=Sum[Coefficient[E
xpand[expr],formlist[[i]]]
formlist[[i]],{i,1,Length[formlist]}]
simpa0=Min[domexpcoeff[Numerator[a0r],E,b,w],dom
expcoeff[Denominator[a0r],E,b,w]];
simpb0=Min[domexpcoeff[Numerator[b0r],E,b,w],dom
expcoeff[Denominator[b0r],E,b,w]];
simpa2=Min[domexpcoeff[Numerator[a2r],E,b,w],dom
expcoeff[Denominator[a2r],E,b,w]];
simpb2=Min[domexpcoeff[Numerator[b2r],E,b,w],dom
expcoeff[Denominator[b2r],E,b,w]];
numlsta0=Union[domexp[Numerator[a0r],E,b,w]];
numlstb0=Union[domexp[Numerator[b0r],E,b,w]];
numlsta2=Union[domexp[Numerator[a2r],E,b,w]];
numlstb2=Union[domexp[Numerator[b2r],E,b,w]];
xpndnuma0=collectterms[Numerator[a0r],numlsta0];
xpndnumb0=collectterms[Numerator[b0r],numlstb0];
xpndnuma2=collectterms[Numerator[a2r],numlsta2];
xpndnumb2=collectterms[Numerator[b2r],numlstb2];
```

```
denlsta0=Union[domexp[Denominator[a0r],E,b,w]];
denlstb0=Union[domexp[Denominator[b0r],E,b,w]];
denlsta2=Union[domexp[Denominator[a2r],E,b,w]];
denlstb2=Union[domexp[Denominator[b2r],E,b,w]];
xpnddena0=collectterms[Denominator[a0r],denlsta0
];
xpnddenb0=collectterms[Denominator[b0r],denlstb0
];
xpnddena2=collectterms[Denominator[a2r],denlsta2
];
xpnddenb2=collectterms[Denominator[b2r],denlstb2
];
holda0=Expand[E^(-simpa0  b  w)
xpndnuma0]/Expand[(E^(-simpa0  b  w)  xpnddena0)];
holdb0=Expand[E^(-simpb0  b  w)
xpndnumb0]/Expand[(E^(-simpb0  b  w)  xpnddenb0)];
holda2=Expand[E^(-simpa2  b  w)
xpndnuma2]/Expand[(E^(-simpa2  b  w)  xpnddena2)];
holdb2=Expand[E^(-simpb2  b  w)
xpndnumb2]/Expand[(E^(-simpb2  b  w)  xpnddenb2)];
lima0r=Cancel[Limit[holda0,b->Infinity]];
limb0r=Cancel[Limit[holdb0,b->Infinity]];
lima2r=Cancel[Limit[holda2,b->Infinity]];
limb2r=Cancel[Limit[holdb2,b->Infinity]];
```

Appearance of Coefficients

Coefficients before Limit

?a0r

```
a0r = ((-635256279*E^(6*d*w)*modr^2 +
       635256279*E^(8*d*w)*modr^2 -
       635256279*E^(4*b*w + 2*d*w)*modr^2 +
       1270512558*E^(2*b*w + 4*d*w)*modr^2 +
       635256279*E^(4*b*w + 4*d*w)*modr^2 -
       1270512558*E^(2*b*w + 6*d*w)*modr^2 +
       1270512558*E^(6*d*w)*modr*mods -
       1270512558*E^(8*d*w)*modr*mods +
       1270512558*E^(4*b*w + 2*d*w)*modr*mods -
       2541025116*E^(2*b*w + 4*d*w)*modr*mods +
       1591727442*E^(4*b*w + 4*d*w)*modr*mods -
       321214884*E^(2*b*w + 6*d*w)*modr*mods -
       635256279*E^(6*d*w)*mods^2 +
635256279*E^(8*d*w)*mods^2 -
       635256279*E^(4*b*w + 2*d*w)*mods^2 -
       1591727442*E^(2*b*w + 4*d*w)*mods^2 +
       635256279*E^(4*b*w + 4*d*w)*mods^2 +
       1591727442*E^(2*b*w + 6*d*w)*mods^2 +
       1270512558*d*E^(6*d*w)*modr^2*w +
       1270512558*d*E^(4*b*w + 2*d*w)*modr^2*w -
       2541025116*d*E^(2*b*w + 4*d*w)*modr^2*w -
       637635516*d*E^(6*d*w)*modr*mods*w -
       637635516*d*E^(4*b*w + 2*d*w)*modr*mods*w -
       2851520000*b*E^(2*b*w + 4*d*w)*modr*mods*w +
       4126791032*d*E^(2*b*w + 4*d*w)*modr*mods*w -
       632877042*d*E^(6*d*w)*mods^2*w -
       632877042*d*E^(4*b*w + 2*d*w)*mods^2*w -
       1585765916*d*E^(2*b*w + 4*d*w)*mods^2*w +
       2522062242*d^2*E^(6*d*w)*modr^2*w^2 +
       2522062242*d^2*E^(4*b*w + 2*d*w)*modr^2*w^2 +
       630506716*b^2*E^(2*b*w + 4*d*w)*modr^2*w^2 -
       1261013432*b*d*E^(2*b*w + 4*d*w)*modr^2*w^2 -
       4413617768*d^2*E^(2*b*w + 4*d*w)*modr^2*w^2 -
       630506716*b^2*E^(2*b*w + 6*d*w)*modr^2*w^2 +
       1261013432*b*d*E^(2*b*w + 6*d*w)*modr^2*w^2 -
       630506716*d^2*E^(2*b*w + 6*d*w)*modr^2*w^2 -
```

```
        1265754084*d^2*E^(6*d*w)*modr*mods*w^2 -
        1265754084*d^2*E^(4*b*w + 2*d*w)*modr*mods*w^2
-
        5025232632*b^2*E^(2*b*w + 4*d*w)*modr*mods*w^2 -
        1270494736*b*d*E^(2*b*w + 4*d*w)*modr*mods*w^2 +
        8827235536*d^2*E^(2*b*w + 4*d*w)*modr*mods*w^2 -
        635247368*b^2*E^(2*b*w + 6*d*w)*modr*mods*w^2 +
        1270494736*b*d*E^(2*b*w + 6*d*w)*modr*mods*w^2 -
        635247368*d^2*E^(2*b*w + 6*d*w)*modr*mods*w^2 -
        1256308158*d^2*E^(6*d*w)*mods^2*w^2 -
        1256308158*d^2*E^(4*b*w + 2*d*w)*mods^2*w^2 -
        1265754084*b^2*E^(2*b*w + 4*d*w)*mods^2*w^2 +
        2531508168*b*d*E^(2*b*w + 4*d*w)*mods^2*w^2 -
        4413617768*d^2*E^(2*b*w + 4*d*w)*mods^2*w^2 +
        1265754084*b^2*E^(2*b*w + 6*d*w)*mods^2*w^2 -
        2531508168*b*d*E^(2*b*w + 6*d*w)*mods^2*w^2 +
        1265754084*d^2*E^(2*b*w + 6*d*w)*mods^2*w^2 -
        1261013432*b^2*d*E^(2*b*w + 4*d*w)*modr^2*w^3 +
        2522026864*b*d^2*E^(2*b*w + 4*d*w)*modr^2*w^3 -
        1261013432*d^3*E^(2*b*w + 4*d*w)*modr^2*w^3 +
        2522026864*b^2*d*E^(2*b*w + 4*d*w)*modr*mods*w^3
-
        5044053728*b*d^2*E^(2*b*w + 4*d*w)*modr*mods*w^3
+
        2522026864*d^3*E^(2*b*w + 4*d*w)*modr*mods*w^3 -
        1261013432*b^2*d*E^(2*b*w + 4*d*w)*mods^2*w^3 +
        2522026864*b*d^2*E^(2*b*w + 4*d*w)*mods^2*w^3 -
        1261013432*d^3*E^(2*b*w + 4*d*w)*mods^2*w^3 -
        2503205768*b^2*d^2*E^(2*b*w + 4*d*w)*modr^2*w^4
+
        5006411536*b*d^3*E^(2*b*w + 4*d*w)*modr^2*w^4 -
        2503205768*d^4*E^(2*b*w + 4*d*w)*modr^2*w^4 +
        5006411536*b^2*d^2*E^(2*b*w +
4*d*w)*modr*mods*w^4 -
        10012823072*b*d^3*E^(2*b*w +
4*d*w)*modr*mods*w^4 +
        5006411536*d^4*E^(2*b*w + 4*d*w)*modr*mods*w^4 -
        2503205768*b^2*d^2*E^(2*b*w + 4*d*w)*mods^2*w^4
+
        5006411536*b*d^3*E^(2*b*w + 4*d*w)*mods^2*w^4 -
        2503205768*d^4*E^(2*b*w + 4*d*w)*mods^2*w^4))/
    (w^2*(1261031121*E^(4*b*w)*modr^2 +
        1261031121*E^(4*d*w)*modr^2 -
        2522062242*E^(6*d*w)*modr^2 +
```

```
1261031121*E^(8*d*w)*modr^2 -
2522062242*E^(2*b*w + 2*d*w)*modr^2 -
2522062242*E^(4*b*w + 2*d*w)*modr^2 +
5044124484*E^(2*b*w + 4*d*w)*modr^2 +
1261031121*E^(4*b*w + 4*d*w)*modr^2 -
2522062242*E^(2*b*w + 6*d*w)*modr^2 -
2522062242*E^(4*b*w)*modr*mods +
3159697758*E^(4*d*w)*modr*mods -
637635516*E^(6*d*w)*modr*mods -
2522062242*E^(8*d*w)*modr*mods -
637635516*E^(2*b*w + 2*d*w)*modr*mods -
637635516*E^(4*b*w + 2*d*w)*modr*mods +
1275271032*E^(2*b*w + 4*d*w)*modr*mods +
3159697758*E^(4*b*w + 4*d*w)*modr*mods -
637635516*E^(2*b*w + 6*d*w)*modr*mods +
1261031121*E^(4*b*w)*mods^2 +
1261031121*E^(4*d*w)*mods^2 +
3159697758*E^(6*d*w)*mods^2 +
1261031121*E^(8*d*w)*mods^2 +
3159697758*E^(2*b*w + 2*d*w)*mods^2 +
3159697758*E^(4*b*w + 2*d*w)*mods^2 +
7917084484*E^(2*b*w + 4*d*w)*mods^2 +
1261031121*E^(4*b*w + 4*d*w)*mods^2 +
3159697758*E^(2*b*w + 6*d*w)*mods^2 -
5044124484*d^2*E^(6*d*w)*modr^2*w^2 -
1251602884*b^2*E^(2*b*w + 2*d*w)*modr^2*w^2 +
2503205768*b*d*E^(2*b*w + 2*d*w)*modr^2*w^2 -
1251602884*d^2*E^(2*b*w + 2*d*w)*modr^2*w^2 -
5044124484*d^2*E^(4*b*w + 2*d*w)*modr^2*w^2 +
2503205768*b^2*E^(2*b*w + 4*d*w)*modr^2*w^2 -
5006411536*b*d*E^(2*b*w + 4*d*w)*modr^2*w^2 +
12591454736*d^2*E^(2*b*w + 4*d*w)*modr^2*w^2 -
1251602884*b^2*E^(2*b*w + 6*d*w)*modr^2*w^2 +
2503205768*b*d*E^(2*b*w + 6*d*w)*modr^2*w^2 -
1251602884*d^2*E^(2*b*w + 6*d*w)*modr^2*w^2 +
2531508168*d^2*E^(6*d*w)*modr*mods*w^2 -
1261013432*b^2*E^(2*b*w + 2*d*w)*modr*mods*w^2 +
2522026864*b*d*E^(2*b*w + 2*d*w)*modr*mods*w^2 -
1261013432*d^2*E^(2*b*w + 2*d*w)*modr*mods*w^2 +
2531508168*d^2*E^(4*b*w + 2*d*w)*modr*mods*w^2 +
2522026864*b^2*E^(2*b*w + 4*d*w)*modr*mods*w^2 +
17597866272*b*d*E^(2*b*w + 4*d*w)*modr*mods*w^2 -
25182909472*d^2*E^(2*b*w + 4*d*w)*modr*mods*w^2
```

```
-
        1261013432*b^2*E^(2*b*w + 6*d*w)*modr*mods*w^2 +
        2522026864*b*d*E^(2*b*w + 6*d*w)*modr*mods*w^2 -
        1261013432*d^2*E^(2*b*w + 6*d*w)*modr*mods*w^2 +
        2512616316*d^2*E^(6*d*w)*mods^2*w^2 +
        2512616316*b^2*E^(2*b*w + 2*d*w)*mods^2*w^2 -
        5025232632*b*d*E^(2*b*w + 2*d*w)*mods^2*w^2 +
        2512616316*d^2*E^(2*b*w + 2*d*w)*mods^2*w^2 +
        2512616316*d^2*E^(4*b*w + 2*d*w)*mods^2*w^2 +
        6295727368*b^2*E^(2*b*w + 4*d*w)*mods^2*w^2 -
        12591454736*b*d*E^(2*b*w + 4*d*w)*mods^2*w^2 +
        12591454736*d^2*E^(2*b*w + 4*d*w)*mods^2*w^2 +
        2512616316*b^2*E^(2*b*w + 6*d*w)*mods^2*w^2 -
        5025232632*b*d*E^(2*b*w + 6*d*w)*mods^2*w^2 +
        2512616316*d^2*E^(2*b*w + 6*d*w)*mods^2*w^2 +
        5006411536*b^2*d^2*E^(2*b*w + 4*d*w)*modr^2*w^4
-
        10012823072*b*d^3*E^(2*b*w + 4*d*w)*modr^2*w^4 +
        5006411536*d^4*E^(2*b*w + 4*d*w)*modr^2*w^4 -
        10012823072*b^2*d^2*E^(2*b*w +
4*d*w)*modr*mods*w^4 +
        20025646144*b*d^3*E^(2*b*w +
4*d*w)*modr*mods*w^4 -
        10012823072*d^4*E^(2*b*w + 4*d*w)*modr*mods*w^4
+
        5006411536*b^2*d^2*E^(2*b*w + 4*d*w)*mods^2*w^4
-
        10012823072*b*d^3*E^(2*b*w + 4*d*w)*mods^2*w^4 +
        5006411536*d^4*E^(2*b*w + 4*d*w)*mods^2*w^4));
```

□ *?b0r*

```
b0r = ((635256279*E^(4*b*w)*modr^2 +
        635256279*E^(4*d*w)*modr^2 -
635256279*E^(6*d*w)*modr^2 -
        1270512558*E^(2*b*w + 2*d*w)*modr^2 -
        635256279*E^(4*b*w + 2*d*w)*modr^2 +
        1270512558*E^(2*b*w + 4*d*w)*modr^2 -
        1270512558*E^(4*b*w)*modr*mods +
        1591727442*E^(4*d*w)*modr*mods +
        1270512558*E^(6*d*w)*modr*mods -
        321214884*E^(2*b*w + 2*d*w)*modr*mods +
        1270512558*E^(4*b*w + 2*d*w)*modr*mods -
        2541025116*E^(2*b*w + 4*d*w)*modr*mods +
        635256279*E^(4*b*w)*mods^2 +
```

```
635256279*E^(4*d*w)*mods^2 -
        635256279*E^(6*d*w)*mods^2 +
        1591727442*E^(2*b*w + 2*d*w)*mods^2 -
        635256279*E^(4*b*w + 2*d*w)*mods^2 -
        1591727442*E^(2*b*w + 4*d*w)*mods^2 -
        1270512558*d*E^(6*d*w)*modr^2*w -
        1270512558*d*E^(4*b*w + 2*d*w)*modr^2*w +
        2541025116*d*E^(2*b*w + 4*d*w)*modr^2*w +
        637635516*d*E^(6*d*w)*modr*mods*w +
        637635516*d*E^(4*b*w + 2*d*w)*modr*mods*w +
        2851520000*b*E^(2*b*w + 4*d*w)*modr*mods*w -
        4126791032*d*E^(2*b*w + 4*d*w)*modr*mods*w +
        632877042*d*E^(6*d*w)*mods^2*w +
        632877042*d*E^(4*b*w + 2*d*w)*mods^2*w +
        1585765916*d*E^(2*b*w + 4*d*w)*mods^2*w +
        2522062242*d^2*E^(6*d*w)*modr^2*w^2 -
        630506716*b^2*E^(2*b*w + 2*d*w)*modr^2*w^2 +
        1261013432*b*d*E^(2*b*w + 2*d*w)*modr^2*w^2 -
        630506716*d^2*E^(2*b*w + 2*d*w)*modr^2*w^2 +
        2522062242*d^2*E^(4*b*w + 2*d*w)*modr^2*w^2 +
        630506716*b^2*E^(2*b*w + 4*d*w)*modr^2*w^2 -
        1261013432*b*d*E^(2*b*w + 4*d*w)*modr^2*w^2 -
        4413617768*d^2*E^(2*b*w + 4*d*w)*modr^2*w^2 -
        1265754084*d^2*E^(6*d*w)*modr*mods*w^2 -
        635247368*b^2*E^(2*b*w + 2*d*w)*modr*mods*w^2 +
        1270494736*b*d*E^(2*b*w + 2*d*w)*modr*mods*w^2 -
        635247368*d^2*E^(2*b*w + 2*d*w)*modr*mods*w^2 -
        1265754084*d^2*E^(4*b*w + 2*d*w)*modr*mods*w^2 -
        5025232632*b^2*E^(2*b*w + 4*d*w)*modr*mods*w^2 -
        1270494736*b*d*E^(2*b*w + 4*d*w)*modr*mods*w^2 +
        8827235536*d^2*E^(2*b*w + 4*d*w)*modr*mods*w^2 -
        1256308158*d^2*E^(6*d*w)*mods^2*w^2 +
        1265754084*b^2*E^(2*b*w + 2*d*w)*mods^2*w^2 -
        2531508168*b*d*E^(2*b*w + 2*d*w)*mods^2*w^2 +
        1265754084*d^2*E^(2*b*w + 2*d*w)*mods^2*w^2 -
        1256308158*d^2*E^(4*b*w + 2*d*w)*mods^2*w^2 -
        1265754084*b^2*E^(2*b*w + 4*d*w)*mods^2*w^2 +
        2531508168*b*d*E^(2*b*w + 4*d*w)*mods^2*w^2 -
        4413617768*d^2*E^(2*b*w + 4*d*w)*mods^2*w^2 +
        1261013432*b^2*d*E^(2*b*w + 4*d*w)*modr^2*w^3 -
        2522026864*b*d^2*E^(2*b*w + 4*d*w)*modr^2*w^3 +
        1261013432*d^3*E^(2*b*w + 4*d*w)*modr^2*w^3 -
        2522026864*b^2*d*E^(2*b*w + 4*d*w)*modr*mods*w^3
+
```

```
        5044053728*b*d^2*E^(2*b*w + 4*d*w)*modr*mods*w^3
-
        2522026864*d^3*E^(2*b*w + 4*d*w)*modr*mods*w^3 +
        1261013432*b^2*d*E^(2*b*w + 4*d*w)*mods^2*w^3 -
        2522026864*b*d^2*E^(2*b*w + 4*d*w)*mods^2*w^3 +
        1261013432*d^3*E^(2*b*w + 4*d*w)*mods^2*w^3 -
        2503205768*b^2*d^2*E^(2*b*w + 4*d*w)*modr^2*w^4
+
        5006411536*b*d^3*E^(2*b*w + 4*d*w)*modr^2*w^4 -
        2503205768*d^4*E^(2*b*w + 4*d*w)*modr^2*w^4 +
        5006411536*b^2*d^2*E^(2*b*w +
4*d*w)*modr*mods*w^4 -
        10012823072*b*d^3*E^(2*b*w +
4*d*w)*modr*mods*w^4 +
        5006411536*d^4*E^(2*b*w + 4*d*w)*modr*mods*w^4 -
        2503205768*b^2*d^2*E^(2*b*w + 4*d*w)*mods^2*w^4
+
        5006411536*b*d^3*E^(2*b*w + 4*d*w)*mods^2*w^4 -
        2503205768*d^4*E^(2*b*w + 4*d*w)*mods^2*w^4))/
    (w^2*(1261031121*E^(4*b*w)*modr^2 +
        1261031121*E^(4*d*w)*modr^2 -
        2522062242*E^(6*d*w)*modr^2 +
        1261031121*E^(8*d*w)*modr^2 -
        2522062242*E^(2*b*w + 2*d*w)*modr^2 -
        2522062242*E^(4*b*w + 2*d*w)*modr^2 +
        5044124484*E^(2*b*w + 4*d*w)*modr^2 +
        1261031121*E^(4*b*w + 4*d*w)*modr^2 -
        2522062242*E^(2*b*w + 6*d*w)*modr^2 -
        2522062242*E^(4*b*w)*modr*mods +
        3159697758*E^(4*d*w)*modr*mods -
        637635516*E^(6*d*w)*modr*mods -
        2522062242*E^(8*d*w)*modr*mods -
        637635516*E^(2*b*w + 2*d*w)*modr*mods -
        637635516*E^(4*b*w + 2*d*w)*modr*mods +
        1275271032*E^(2*b*w + 4*d*w)*modr*mods +
        3159697758*E^(4*b*w + 4*d*w)*modr*mods -
        637635516*E^(2*b*w + 6*d*w)*modr*mods +
        1261031121*E^(4*b*w)*mods^2 +
        1261031121*E^(4*d*w)*mods^2 +
        3159697758*E^(6*d*w)*mods^2 +
        1261031121*E^(8*d*w)*mods^2 +
        3159697758*E^(2*b*w + 2*d*w)*mods^2 +
        3159697758*E^(4*b*w + 2*d*w)*mods^2 +
        7917084484*E^(2*b*w + 4*d*w)*mods^2 +
```

```
1261031121*E^(4*b*w + 4*d*w)*mods^2 +
3159697758*E^(2*b*w + 6*d*w)*mods^2 -
5044124484*d^2*E^(6*d*w)*modr^2*w^2 -
1251602884*b^2*E^(2*b*w + 2*d*w)*modr^2*w^2 +
2503205768*b*d*E^(2*b*w + 2*d*w)*modr^2*w^2 -
1251602884*d^2*E^(2*b*w + 2*d*w)*modr^2*w^2 -
5044124484*d^2*E^(4*b*w + 2*d*w)*modr^2*w^2 +
2503205768*b^2*E^(2*b*w + 4*d*w)*modr^2*w^2 -
5006411536*b*d*E^(2*b*w + 4*d*w)*modr^2*w^2 +
12591454736*d^2*E^(2*b*w + 4*d*w)*modr^2*w^2 -
1251602884*b^2*E^(2*b*w + 6*d*w)*modr^2*w^2 +
2503205768*b*d*E^(2*b*w + 6*d*w)*modr^2*w^2 -
1251602884*d^2*E^(2*b*w + 6*d*w)*modr^2*w^2 +
2531508168*d^2*E^(6*d*w)*modr*mods*w^2 -
1261013432*b^2*E^(2*b*w + 2*d*w)*modr*mods*w^2 +
2522026864*b*d*E^(2*b*w + 2*d*w)*modr*mods*w^2 -
1261013432*d^2*E^(2*b*w + 2*d*w)*modr*mods*w^2 +
2531508168*d^2*E^(4*b*w + 2*d*w)*modr*mods*w^2 +
2522026864*b^2*E^(2*b*w + 4*d*w)*modr*mods*w^2 +
17597866272*b*d*E^(2*b*w + 4*d*w)*modr*mods*w^2
-
25182909472*d^2*E^(2*b*w + 4*d*w)*modr*mods*w^2
-
1261013432*b^2*E^(2*b*w + 6*d*w)*modr*mods*w^2 +
2522026864*b*d*E^(2*b*w + 6*d*w)*modr*mods*w^2 -
1261013432*d^2*E^(2*b*w + 6*d*w)*modr*mods*w^2 +
2512616316*d^2*E^(6*d*w)*mods^2*w^2 +
2512616316*b^2*E^(2*b*w + 2*d*w)*mods^2*w^2 -
5025232632*b*d*E^(2*b*w + 2*d*w)*mods^2*w^2 +
2512616316*d^2*E^(2*b*w + 2*d*w)*mods^2*w^2 +
2512616316*d^2*E^(4*b*w + 2*d*w)*mods^2*w^2 +
6295727368*b^2*E^(2*b*w + 4*d*w)*mods^2*w^2 -
12591454736*b*d*E^(2*b*w + 4*d*w)*mods^2*w^2 +
12591454736*d^2*E^(2*b*w + 4*d*w)*mods^2*w^2 +
2512616316*b^2*E^(2*b*w + 6*d*w)*mods^2*w^2 -
5025232632*b*d*E^(2*b*w + 6*d*w)*mods^2*w^2 +
2512616316*d^2*E^(2*b*w + 6*d*w)*mods^2*w^2 +
5006411536*b^2*d^2*E^(2*b*w + 4*d*w)*modr^2*w^4
-
10012823072*b*d^3*E^(2*b*w + 4*d*w)*modr^2*w^4 +
5006411536*d^4*E^(2*b*w + 4*d*w)*modr^2*w^4 -
10012823072*b^2*d^2*E^(2*b*w +
4*d*w)*modr*mods*w^4 +
20025646144*b*d^3*E^(2*b*w +
```

```
4*d*w)*modr*mods*w^4 -
        10012823072*d^4*E^(2*b*w + 4*d*w)*modr*mods*w^4
+
        5006411536*b^2*d^2*E^(2*b*w + 4*d*w)*mods^2*w^4
-
        10012823072*b*d^3*E^(2*b*w + 4*d*w)*mods^2*w^4 +
        5006411536*d^4*E^(2*b*w + 4*d*w)*mods^2*w^4));
```

□ *?a2r*

```
a2r = (133*(-9481437*E^(6*d*w)*modr^2*w^35 +
        9481437*E^(8*d*w)*modr^2*w^35 -
        9481437*E^(4*b*w + 2*d*w)*modr^2*w^35 +
        18962874*E^(2*b*w + 4*d*w)*modr^2*w^35 +
        9481437*E^(4*b*w + 4*d*w)*modr^2*w^35 -
        18962874*E^(2*b*w + 6*d*w)*modr^2*w^35 +
        4758474*E^(6*d*w)*modr*mods*w^35 -
        18962874*E^(8*d*w)*modr*mods*w^35 +
        4758474*E^(4*b*w + 2*d*w)*modr*mods*w^35 -
        9516948*E^(2*b*w + 4*d*w)*modr*mods*w^35 +
        23757126*E^(4*b*w + 4*d*w)*modr*mods*w^35 -
        4794252*E^(2*b*w + 6*d*w)*modr*mods*w^35 +
        4722963*E^(6*d*w)*mods^2*w^35 +
        9481437*E^(8*d*w)*mods^2*w^35 +
        4722963*E^(4*b*w + 2*d*w)*mods^2*w^35 +
        11834074*E^(2*b*w + 4*d*w)*mods^2*w^35 +
        9481437*E^(4*b*w + 4*d*w)*mods^2*w^35 +
        23757126*E^(2*b*w + 6*d*w)*mods^2*w^35 +
        18962874*d*E^(6*d*w)*modr^2*w^36 +
        18962874*d*E^(4*b*w + 2*d*w)*modr^2*w^36 -
        37925748*d*E^(2*b*w + 4*d*w)*modr^2*w^36 -
        9516948*d*E^(6*d*w)*modr*mods*w^36 -
        9516948*d*E^(4*b*w + 2*d*w)*modr*mods*w^36 -
        42560000*b*E^(2*b*w + 4*d*w)*modr*mods*w^36 +
        61593896*d*E^(2*b*w + 4*d*w)*modr*mods*w^36 -
        9445926*d*E^(6*d*w)*mods^2*w^36 -
        9445926*d*E^(4*b*w + 2*d*w)*mods^2*w^36 -
        23668148*d*E^(2*b*w + 4*d*w)*mods^2*w^36 +
        9410548*b^2*E^(2*b*w + 4*d*w)*modr^2*w^37 -
        18821096*b*d*E^(2*b*w + 4*d*w)*modr^2*w^37 +
        9410548*d^2*E^(2*b*w + 4*d*w)*modr^2*w^37 -
        9410548*b^2*E^(2*b*w + 6*d*w)*modr^2*w^37 +
        18821096*b*d*E^(2*b*w + 6*d*w)*modr^2*w^37 -
        9410548*d^2*E^(2*b*w + 6*d*w)*modr^2*w^37 -
        18821096*b^2*E^(2*b*w + 4*d*w)*modr*mods*w^37 +
```

```
     37642192*b*d*E^(2*b*w + 4*d*w)*modr*mods*w^37 -
     18821096*d^2*E^(2*b*w + 4*d*w)*modr*mods*w^37 -
     9481304*b^2*E^(2*b*w + 6*d*w)*modr*mods*w^37 +
     18962608*b*d*E^(2*b*w + 6*d*w)*modr*mods*w^37 -
     9481304*d^2*E^(2*b*w + 6*d*w)*modr*mods*w^37 +
     9410548*b^2*E^(2*b*w + 4*d*w)*mods^2*w^37 -
     18821096*b*d*E^(2*b*w + 4*d*w)*mods^2*w^37 +
     9410548*d^2*E^(2*b*w + 4*d*w)*mods^2*w^37 +
     18891852*b^2*E^(2*b*w + 6*d*w)*mods^2*w^37 -
     37783704*b*d*E^(2*b*w + 6*d*w)*mods^2*w^37 +
     18891852*d^2*E^(2*b*w + 6*d*w)*mods^2*w^37 -
     18821096*b^2*d*E^(2*b*w + 4*d*w)*modr^2*w^38 +
     37642192*b*d^2*E^(2*b*w + 4*d*w)*modr^2*w^38 -
     18821096*d^3*E^(2*b*w + 4*d*w)*modr^2*w^38 +
     37642192*b^2*d*E^(2*b*w + 4*d*w)*modr*mods*w^38
-
     75284384*b*d^2*E^(2*b*w + 4*d*w)*modr*mods*w^38
+
     37642192*d^3*E^(2*b*w + 4*d*w)*modr*mods*w^38 -
     18821096*b^2*d*E^(2*b*w + 4*d*w)*mods^2*w^38 +
     37642192*b*d^2*E^(2*b*w + 4*d*w)*mods^2*w^38 -
     18821096*d^3*E^(2*b*w + 4*d*w)*mods^2*w^38))/
(w^36*(1261031121*E^(4*b*w)*modr^2 +
     1261031121*E^(4*d*w)*modr^2 -
     2522062242*E^(6*d*w)*modr^2 +
     1261031121*E^(8*d*w)*modr^2 -
     2522062242*E^(2*b*w + 2*d*w)*modr^2 -
     2522062242*E^(4*b*w + 2*d*w)*modr^2 +
     5044124484*E^(2*b*w + 4*d*w)*modr^2 +
     1261031121*E^(4*b*w + 4*d*w)*modr^2 -
     2522062242*E^(2*b*w + 6*d*w)*modr^2 -
     2522062242*E^(4*b*w)*modr*mods +
     3159697758*E^(4*d*w)*modr*mods -
     637635516*E^(6*d*w)*modr*mods -
     2522062242*E^(8*d*w)*modr*mods -
     637635516*E^(2*b*w + 2*d*w)*modr*mods -
     637635516*E^(4*b*w + 2*d*w)*modr*mods +
     1275271032*E^(2*b*w + 4*d*w)*modr*mods +
     3159697758*E^(4*b*w + 4*d*w)*modr*mods -
     637635516*E^(2*b*w + 6*d*w)*modr*mods +
     1261031121*E^(4*b*w)*mods^2 +
     1261031121*E^(4*d*w)*mods^2 +
     3159697758*E^(6*d*w)*mods^2 +
     1261031121*E^(8*d*w)*mods^2 +
```

```
3159697758*E^(2*b*w + 2*d*w)*mods^2 +
3159697758*E^(4*b*w + 2*d*w)*mods^2 +
7917084484*E^(2*b*w + 4*d*w)*mods^2 +
1261031121*E^(4*b*w + 4*d*w)*mods^2 +
3159697758*E^(2*b*w + 6*d*w)*mods^2 -
5044124484*d^2*E^(6*d*w)*modr^2*w^2 -
1251602884*b^2*E^(2*b*w + 2*d*w)*modr^2*w^2 +
2503205768*b*d*E^(2*b*w + 2*d*w)*modr^2*w^2 -
1251602884*d^2*E^(2*b*w + 2*d*w)*modr^2*w^2 -
5044124484*d^2*E^(4*b*w + 2*d*w)*modr^2*w^2 +
2503205768*b^2*E^(2*b*w + 4*d*w)*modr^2*w^2 -
5006411536*b*d*E^(2*b*w + 4*d*w)*modr^2*w^2 +
12591454736*d^2*E^(2*b*w + 4*d*w)*modr^2*w^2 -
1251602884*b^2*E^(2*b*w + 6*d*w)*modr^2*w^2 +
2503205768*b*d*E^(2*b*w + 6*d*w)*modr^2*w^2 -
1251602884*d^2*E^(2*b*w + 6*d*w)*modr^2*w^2 +
2531508168*d^2*E^(6*d*w)*modr*mods*w^2 -
1261013432*b^2*E^(2*b*w + 2*d*w)*modr*mods*w^2 +
2522026864*b*d*E^(2*b*w + 2*d*w)*modr*mods*w^2 -
1261013432*d^2*E^(2*b*w + 2*d*w)*modr*mods*w^2 +
2531508168*d^2*E^(4*b*w + 2*d*w)*modr*mods*w^2 +
2522026864*b^2*E^(2*b*w + 4*d*w)*modr*mods*w^2 +
17597866272*b*d*E^(2*b*w + 4*d*w)*modr*mods*w^2
-
25182909472*d^2*E^(2*b*w + 4*d*w)*modr*mods*w^2
-
1261013432*b^2*E^(2*b*w + 6*d*w)*modr*mods*w^2 +
2522026864*b*d*E^(2*b*w + 6*d*w)*modr*mods*w^2 -
1261013432*d^2*E^(2*b*w + 6*d*w)*modr*mods*w^2 +
2512616316*d^2*E^(6*d*w)*mods^2*w^2 +
2512616316*b^2*E^(2*b*w + 2*d*w)*mods^2*w^2 -
5025232632*b*d*E^(2*b*w + 2*d*w)*mods^2*w^2 +
2512616316*d^2*E^(2*b*w + 2*d*w)*mods^2*w^2 +
2512616316*d^2*E^(4*b*w + 2*d*w)*mods^2*w^2 +
6295727368*b^2*E^(2*b*w + 4*d*w)*mods^2*w^2 -
12591454736*b*d*E^(2*b*w + 4*d*w)*mods^2*w^2 +
12591454736*d^2*E^(2*b*w + 4*d*w)*mods^2*w^2 +
2512616316*b^2*E^(2*b*w + 6*d*w)*mods^2*w^2 -
5025232632*b*d*E^(2*b*w + 6*d*w)*mods^2*w^2 +
2512616316*d^2*E^(2*b*w + 6*d*w)*mods^2*w^2 +
5006411536*b^2*d^2*E^(2*b*w + 4*d*w)*modr^2*w^4
-
10012823072*b*d^3*E^(2*b*w + 4*d*w)*modr^2*w^4 +
5006411536*d^4*E^(2*b*w + 4*d*w)*modr^2*w^4 -
```

```
        10012823072*b^2*d^2*E^(2*b*w +
4*d*w)*modr*mods*w^4 +
        20025646144*b*d^3*E^(2*b*w +
4*d*w)*modr*mods*w^4 -
        10012823072*d^4*E^(2*b*w + 4*d*w)*modr*mods*w^4
+
        5006411536*b^2*d^2*E^(2*b*w + 4*d*w)*mods^2*w^4
-
        10012823072*b*d^3*E^(2*b*w + 4*d*w)*mods^2*w^4 +
        5006411536*d^4*E^(2*b*w + 4*d*w)*mods^2*w^4));
```

□ *?b2r*

```
b2r = (133*(-9481437*E^(4*b*w)*modr^2 -
        9481437*E^(4*d*w)*modr^2 +
9481437*E^(6*d*w)*modr^2 +
        18962874*E^(2*b*w + 2*d*w)*modr^2 +
        9481437*E^(4*b*w + 2*d*w)*modr^2 -
        18962874*E^(2*b*w + 4*d*w)*modr^2 +
        18962874*E^(4*b*w)*modr*mods -
        23757126*E^(4*d*w)*modr*mods -
        4758474*E^(6*d*w)*modr*mods +
        4794252*E^(2*b*w + 2*d*w)*modr*mods -
        4758474*E^(4*b*w + 2*d*w)*modr*mods +
        9516948*E^(2*b*w + 4*d*w)*modr*mods -
        9481437*E^(4*b*w)*mods^2 -
9481437*E^(4*d*w)*mods^2 -
        4722963*E^(6*d*w)*mods^2 -
        23757126*E^(2*b*w + 2*d*w)*mods^2 -
        4722963*E^(4*b*w + 2*d*w)*mods^2 -
        11834074*E^(2*b*w + 4*d*w)*mods^2 +
        18962874*d*E^(6*d*w)*modr^2*w +
        18962874*d*E^(4*b*w + 2*d*w)*modr^2*w -
        37925748*d*E^(2*b*w + 4*d*w)*modr^2*w -
        9516948*d*E^(6*d*w)*modr*mods*w -
        9516948*d*E^(4*b*w + 2*d*w)*modr*mods*w -
        42560000*b*E^(2*b*w + 4*d*w)*modr*mods*w +
        61593896*d*E^(2*b*w + 4*d*w)*modr*mods*w -
        9445926*d*E^(6*d*w)*mods^2*w -
        9445926*d*E^(4*b*w + 2*d*w)*mods^2*w -
        23668148*d*E^(2*b*w + 4*d*w)*mods^2*w +
        9410548*b^2*E^(2*b*w + 2*d*w)*modr^2*w^2 -
        18821096*b*d*E^(2*b*w + 2*d*w)*modr^2*w^2 +
        9410548*d^2*E^(2*b*w + 2*d*w)*modr^2*w^2 -
        9410548*b^2*E^(2*b*w + 4*d*w)*modr^2*w^2 +
```

```
    -18821096*b*d*E^(2*b*w + 4*d*w)*modr^2*w^2 -
     9410548*d^2*E^(2*b*w + 4*d*w)*modr^2*w^2 +
     9481304*b^2*E^(2*b*w + 2*d*w)*modr*mods*w^2 -
     18962608*b*d*E^(2*b*w + 2*d*w)*modr*mods*w^2 +
     9481304*d^2*E^(2*b*w + 2*d*w)*modr*mods*w^2 +
     18821096*b^2*E^(2*b*w + 4*d*w)*modr*mods*w^2 -
     37642192*b*d*E^(2*b*w + 4*d*w)*modr*mods*w^2 +
     18821096*d^2*E^(2*b*w + 4*d*w)*modr*mods*w^2 -
     18891852*b^2*E^(2*b*w + 2*d*w)*mods^2*w^2 +
     37783704*b*d*E^(2*b*w + 2*d*w)*mods^2*w^2 -
     18891852*d^2*E^(2*b*w + 2*d*w)*mods^2*w^2 -
     9410548*b^2*E^(2*b*w + 4*d*w)*mods^2*w^2 +
     18821096*b*d*E^(2*b*w + 4*d*w)*mods^2*w^2 -
     9410548*d^2*E^(2*b*w + 4*d*w)*mods^2*w^2 -
     18821096*b^2*d*E^(2*b*w + 4*d*w)*modr^2*w^3 +
     37642192*b*d^2*E^(2*b*w + 4*d*w)*modr^2*w^3 -
     18821096*d^3*E^(2*b*w + 4*d*w)*modr^2*w^3 +
     37642192*b^2*d*E^(2*b*w + 4*d*w)*modr*mods*w^3 -
     75284384*b*d^2*E^(2*b*w + 4*d*w)*modr*mods*w^3 +
     37642192*d^3*E^(2*b*w + 4*d*w)*modr*mods*w^3 -
     18821096*b^2*d*E^(2*b*w + 4*d*w)*mods^2*w^3 +
     37642192*b*d^2*E^(2*b*w + 4*d*w)*mods^2*w^3 -
     18821096*d^3*E^(2*b*w + 4*d*w)*mods^2*w^3))/
(w*(1261031121*E^(4*b*w)*modr^2 +
     1261031121*E^(4*d*w)*modr^2 -
     2522062242*E^(6*d*w)*modr^2 +
     1261031121*E^(8*d*w)*modr^2 -
     2522062242*E^(2*b*w + 2*d*w)*modr^2 -
     2522062242*E^(4*b*w + 2*d*w)*modr^2 +
     5044124484*E^(2*b*w + 4*d*w)*modr^2 +
     1261031121*E^(4*b*w + 4*d*w)*modr^2 -
     2522062242*E^(2*b*w + 6*d*w)*modr^2 -
     2522062242*E^(4*b*w)*modr*mods +
     3159697758*E^(4*d*w)*modr*mods -
     637635516*E^(6*d*w)*modr*mods -
     2522062242*E^(8*d*w)*modr*mods -
     637635516*E^(2*b*w + 2*d*w)*modr*mods -
     637635516*E^(4*b*w + 2*d*w)*modr*mods +
     1275271032*E^(2*b*w + 4*d*w)*modr*mods +
     3159697758*E^(4*b*w + 4*d*w)*modr*mods -
     637635516*E^(2*b*w + 6*d*w)*modr*mods +
     1261031121*E^(4*b*w)*mods^2 +
     1261031121*E^(4*d*w)*mods^2 +
     3159697758*E^(6*d*w)*mods^2 +
```

```
1261031121*E^(8*d*w)*mods^2 +
3159697758*E^(2*b*w + 2*d*w)*mods^2 +
3159697758*E^(4*b*w + 2*d*w)*mods^2 +
7917084484*E^(2*b*w + 4*d*w)*mods^2 +
1261031121*E^(4*b*w + 4*d*w)*mods^2 +
3159697758*E^(2*b*w + 6*d*w)*mods^2 -
5044124484*d^2*E^(6*d*w)*modr^2*w^2 -
1251602884*b^2*E^(2*b*w + 2*d*w)*modr^2*w^2 +
2503205768*b*d*E^(2*b*w + 2*d*w)*modr^2*w^2 -
1251602884*d^2*E^(2*b*w + 2*d*w)*modr^2*w^2 -
5044124484*d^2*E^(4*b*w + 2*d*w)*modr^2*w^2 +
2503205768*b^2*E^(2*b*w + 4*d*w)*modr^2*w^2 -
5006411536*b*d*E^(2*b*w + 4*d*w)*modr^2*w^2 +
12591454736*d^2*E^(2*b*w + 4*d*w)*modr^2*w^2 -
1251602884*b^2*E^(2*b*w + 6*d*w)*modr^2*w^2 +
2503205768*b*d*E^(2*b*w + 6*d*w)*modr^2*w^2 -
1251602884*d^2*E^(2*b*w + 6*d*w)*modr^2*w^2 +
2531508168*d^2*E^(6*d*w)*modr*mods*w^2 -
1261013432*b^2*E^(2*b*w + 2*d*w)*modr*mods*w^2 +
2522026864*b*d*E^(2*b*w + 2*d*w)*modr*mods*w^2 -
1261013432*d^2*E^(2*b*w + 2*d*w)*modr*mods*w^2 +
2531508168*d^2*E^(4*b*w + 2*d*w)*modr*mods*w^2 +
2522026864*b^2*E^(2*b*w + 4*d*w)*modr*mods*w^2 +
17597866272*b*d*E^(2*b*w + 4*d*w)*modr*mods*w^2
-
25182909472*d^2*E^(2*b*w + 4*d*w)*modr*mods*w^2
-
1261013432*b^2*E^(2*b*w + 6*d*w)*modr*mods*w^2 +
2522026864*b*d*E^(2*b*w + 6*d*w)*modr*mods*w^2 -
1261013432*d^2*E^(2*b*w + 6*d*w)*modr*mods*w^2 +
2512616316*d^2*E^(6*d*w)*mods^2*w^2 +
2512616316*b^2*E^(2*b*w + 2*d*w)*mods^2*w^2 -
5025232632*b*d*E^(2*b*w + 2*d*w)*mods^2*w^2 +
2512616316*d^2*E^(2*b*w + 2*d*w)*mods^2*w^2 +
2512616316*d^2*E^(4*b*w + 2*d*w)*mods^2*w^2 +
6295727368*b^2*E^(2*b*w + 4*d*w)*mods^2*w^2 -
12591454736*b*d*E^(2*b*w + 4*d*w)*mods^2*w^2 +
12591454736*d^2*E^(2*b*w + 4*d*w)*mods^2*w^2 +
2512616316*b^2*E^(2*b*w + 6*d*w)*mods^2*w^2 -
5025232632*b*d*E^(2*b*w + 6*d*w)*mods^2*w^2 +
2512616316*d^2*E^(2*b*w + 6*d*w)*mods^2*w^2 +
5006411536*b^2*d^2*E^(2*b*w + 4*d*w)*modr^2*w^4
-
10012823072*b*d^3*E^(2*b*w + 4*d*w)*modr^2*w^4 +
```

```
        5006411536*d^4*E^(2*b*w + 4*d*w)*modr^2*w^4 -
        10012823072*b^2*d^2*E^(2*b*w +
4*d*w)*modr*mods*w^4 +
        20025646144*b*d^3*E^(2*b*w +
4*d*w)*modr*mods*w^4 -
        10012823072*d^4*E^(2*b*w + 4*d*w)*modr*mods*w^4
+
        5006411536*b^2*d^2*E^(2*b*w + 4*d*w)*mods^2*w^4
-
        10012823072*b*d^3*E^(2*b*w + 4*d*w)*mods^2*w^4 +
        5006411536*d^4*E^(2*b*w + 4*d*w)*mods^2*w^4));
```

■ *Coefficients after Limit*

```
Clear[nur,lima0r,limb0r,lima2r,limb2r]
nur=33/100
```

$$\frac{33}{100}$$

```
lima0r  =  (2379237*E^(2*d*w)*modr^2  -
       2379237*E^(4*d*w)*modr^2  -
       4758474*E^(2*d*w)*modr*mods  -
       5961526*E^(4*d*w)*modr*mods  +
       2379237*E^(2*d*w)*mods^2  -
       2379237*E^(4*d*w)*mods^2  -
       4758474*d*E^(2*d*w)*modr^2*w  +
       2388148*d*E^(2*d*w)*modr*mods*w  +
       2370326*d*E^(2*d*w)*mods^2*w  -
       9445926*d^2*E^(2*d*w)*modr^2*w^2  +
       4740652*d^2*E^(2*d*w)*modr*mods*w^2  +
       4705274*d^2*E^(2*d*w)*mods^2*w^2)/
    (133*(-35511*modr^2*w^2  +
71022*E^(2*d*w)*modr^2*w^2  -
         35511*E^(4*d*w)*modr^2*w^2  +
71022*modr*mods*w^2  +
         17956*E^(2*d*w)*modr*mods*w^2  -
         88978*E^(4*d*w)*modr*mods*w^2  -
35511*mods^2*w^2  -
         88978*E^(2*d*w)*mods^2*w^2  -
35511*E^(4*d*w)*mods^2*w^2  +
         142044*d^2*E^(2*d*w)*modr^2*w^4  -
         71288*d^2*E^(2*d*w)*modr*mods*w^4  -
         70756*d^2*E^(2*d*w)*mods^2*w^4));

limb0r  =  (17889*modr^2  -  17889*E^(2*d*w)*modr^2
-
       35778*modr*mods  +  35778*E^(2*d*w)*modr*mods
+
       17889*mods^2  -  17889*E^(2*d*w)*mods^2  -
       35778*d*E^(2*d*w)*modr^2*w  +
       17956*d*E^(2*d*w)*modr*mods*w  +
       17822*d*E^(2*d*w)*mods^2*w  +
       71022*d^2*E^(2*d*w)*modr^2*w^2  -
       35644*d^2*E^(2*d*w)*modr*mods*w^2  -
       35378*d^2*E^(2*d*w)*mods^2*w^2)/
    (35511*modr^2*w^2  -
71022*E^(2*d*w)*modr^2*w^2  +
       35511*E^(4*d*w)*modr^2*w^2  -
71022*modr*mods*w^2  -
       17956*E^(2*d*w)*modr*mods*w^2  +
       88978*E^(4*d*w)*modr*mods*w^2  +
35511*mods^2*w^2  +
       88978*E^(2*d*w)*mods^2*w^2  +
35511*E^(4*d*w)*mods^2*w^2  -
```

```
        142044*d^2*E^(2*d*w)*modr^2*w^4  +
        71288*d^2*E^(2*d*w)*modr*mods*w^4  +
        70756*d^2*E^(2*d*w)*mods^2*w^4);

lima2r  =  (35511*E^(2*d*w)*modr^2  -
       35511*E^(4*d*w)*modr^2  -
       17822*E^(2*d*w)*modr*mods  -
       88978*E^(4*d*w)*modr*mods  -
       17689*E^(2*d*w)*mods^2  -
35511*E^(4*d*w)*mods^2  -
       71022*d*E^(2*d*w)*modr^2*w  +
       35644*d*E^(2*d*w)*modr*mods*w  +
       35378*d*E^(2*d*w)*mods^2*w)/
     (w*(-35511*modr^2  +  71022*E^(2*d*w)*modr^2  -
          35511*E^(4*d*w)*modr^2  +  71022*modr*mods
+
          17956*E^(2*d*w)*modr*mods  -
88978*E^(4*d*w)*modr*mods  -
          35511*mods^2  -  88978*E^(2*d*w)*mods^2  -
          35511*E^(4*d*w)*mods^2  +
142044*d^2*E^(2*d*w)*modr^2*w^2  -
          71288*d^2*E^(2*d*w)*modr*mods*w^2  -
          70756*d^2*E^(2*d*w)*mods^2*w^2));

limb2r  =  (133*(-267*modr^2  +
267*E^(2*d*w)*modr^2  +
          534*modr*mods  -  134*E^(2*d*w)*modr*mods  -
          267*mods^2  -  133*E^(2*d*w)*mods^2  +
          534*d*E^(2*d*w)*modr^2*w  -
          268*d*E^(2*d*w)*modr*mods*w  -
          266*d*E^(2*d*w)*mods^2*w))/
     (35511*modr^2*w  -  71022*E^(2*d*w)*modr^2*w  +
       35511*E^(4*d*w)*modr^2*w  -
71022*modr*mods*w  -
       17956*E^(2*d*w)*modr*mods*w  +
88978*E^(4*d*w)*modr*mods*w  +
       35511*mods^2*w  +  88978*E^(2*d*w)*mods^2*w  +
       35511*E^(4*d*w)*mods^2*w  -
142044*d^2*E^(2*d*w)*modr^2*w^3  +
        71288*d^2*E^(2*d*w)*modr*mods*w^3  +
        70756*d^2*E^(2*d*w)*mods^2*w^3);
```

Calibration with Track Modulus (the "unlimited" coefficients must be used for this)

Variable Definitions

```
nur=33/100
```

$$\frac{33}{100}$$

```
ymodr=30000
```

30000

```
modr=ymodr/(2  (1+nur))
```

$$\frac{1500000}{133}$$

```
d=7+5/16
```

$$\frac{117}{16}$$

```
b=100 -d
```

$$\frac{2925}{4}$$

```
fbar=1/Sqrt[2  Pi]
```

$$\frac{1}{\text{Sqrt}[2\ \text{Pi}]}$$

```
x=0
```

0

```
y=-d/2
```

$$-\left(\frac{117}{32}\right)$$

```
Clear [y0,inertia,trakmod]

y0=1/(64 ymodr inertia trakmod^3)^(1/4)

                  1
-----------------------------------
            1/4                 3 1/4
20 Sqrt[2] 3    (inertia trakmod )

inertia=32.58

32.58
```

■ *Iterations*

```
trakmod=10

10

N[y0]

0.00199957

mods=461.5

461.5

NIntegrate[fbar Cos[w x]
intvr[a0r,b0r,a2r,b2r],{w,0,10}]

0.00200494
```

■ *Data Reduction*

```
1+1

2

calib={{0.01124,0.01123},{0.006686,0.006692},{0.
004933,0.004931},{0.003976,0.00398},{0.003363,
0.003364},{0.002933,0.002932},{0.002613,0.002612
},{0.002364,
0.002363},{0.002164,0.002166},{0.002,0.002005}}

{{0.01124, 0.01123}, {0.006685999999999999999,
0.006692},

  {0.004933, 0.004931}, {0.003976, 0.00398}, {0.003363,
0.003364},
```

```
  {0.002933, 0.002932}, {0.002613, 0.002612},
{0.002364, 0.002363},

  {0.002164, 0.002166}, {0.002, 0.002005}}
```

```
data={{0,0},{1,70},{2,123.5},{3,172.5},{4,218},{
5,262},{6,304.5},{7,345.5},{8,385.5},{9,424},{10
,461.5}}
```

```
{{0, 0}, {1, 70}, {2, 123.5}, {3, 172.5}, {4, 218},

  {5, 262}, {6, 304.5}, {7, 345.5}, {8, 385.5}, {9,
424},

  {10, 461.5}}
```

```
Fit[data,{s,s^2,s^3},s]
```

```
67.91952712970414*s - 3.878452668275688*s^2 +

  0.1721194243318149*s^3
```

```
plt1=ListPlot[data,PlotRange->{{0,10},{0,500}}]
```

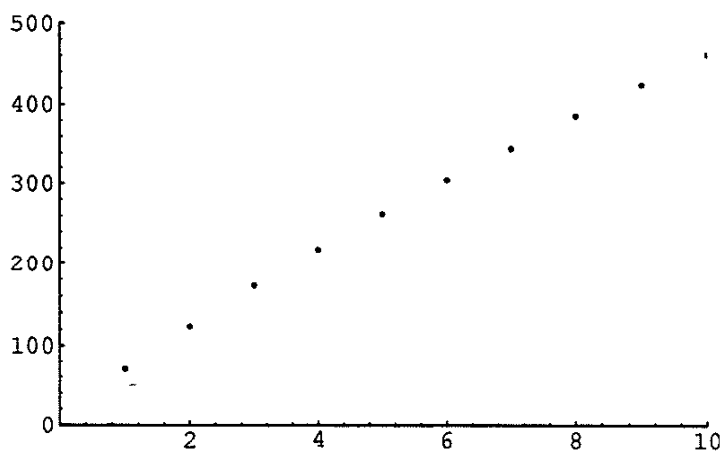


```
-Graphics-
```

```
plt2=Plot[67.92*s  -  3.88*s^2  +
0.1721*s^3,{s,0,10}]
```

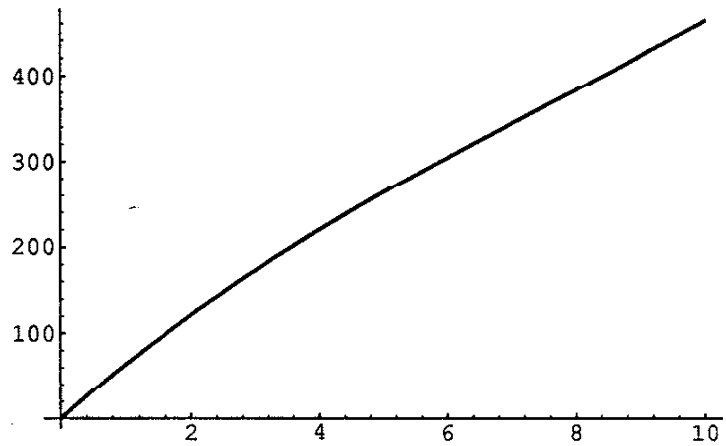

-Graphics-

```
Show[plt1,plt2]
```

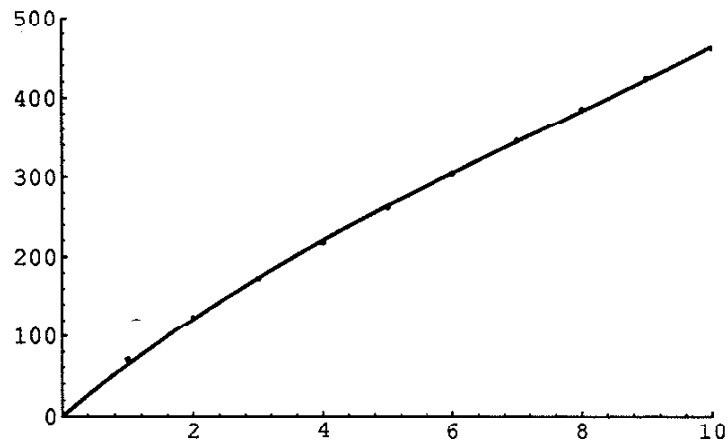

-Graphics-

Obtain Asymptotic Expressions for the Stress Inverse Transform Integrand Coefficient Functions using the "Limited" Coefficients

```
domexpcoeff[expr_,mant_,bigexp_,arbexp_]:=Max[Ca
ses[expr,(mant^(x2_ bigexp arbexp +
y2_)|mant^(x2_ bigexp arbexp))->x2, Infinity]]
```

```
domexp[expr_,mant_,bigexp_,arbexp_]:=Cases[expr,
(mant^(x_ bigexp arbexp + y_)|mant^(x_ bigexp
arbexp)) /; x ==
domexpcoeff[expr,mant,bigexp,arbexp], Infinity]
```

```
collectterms[expr_,formlist_]:=Sum[Coefficient[E
xpand[expr],formlist[[i]]]
formlist[[i]],{i,1,Length[formlist]}]

collectcoeff[expr_,formlist_]:=Sum[Coefficient[E
xpand[expr],formlist[[i]]],{i,1,Length[formlist]
}]

Clear[smxint,smyint,smxyint]

smxint[x_,y_]=Together[intxr[lima0r,limb0r,lima2
r,limb2r]];

smyint[x_,y_]=Together[intyr[lima0r,limb0r,lima2
r,limb2r]];

smxyint[x_,y_]=Together[inttauxyr[lima0r,limb0r,
lima2r,limb2r]];

simpxup=Max[domexpcoeff[Numerator[smxint[x,y]],E
,d,w]];

simpxdown=Max[domexpcoeff[Denominator[smxint[x,y
]],E,d,w]];

simpyup=Max[domexpcoeff[Numerator[smyint[x,y]],E
,d,w]];

simpydown=Max[domexpcoeff[Denominator[smyint[x,y
]],E,d,w]];

simpxyup=Max[domexpcoeff[Numerator[smxyint[x,y]]
,E,d,w]];

simpxydown=Max[domexpcoeff[Denominator[smxyint[x
,y]],E,d,w]];

numlstx=Union[domexp[Expand[Numerator[smxint[x,y
]]],E,d,w]]

numlsty=Union[domexp[Expand[Numerator[smyint[x,y
]]],E,d,w]]

numlstxy=Union[domexp[Expand[Numerator[smxyint[x
,y]]],E,d,w]]

xpndnumx=collectcoeff[Numerator[smxint[x,y]],num
lstx];

xpndnumy=collectcoeff[Numerator[smyint[x,y]],num
lsty];
```

```
xpndnumxy=collectcoeff[Numerator[smxyint[x,y]],n
umlstxy];

denlstx=Union[domexp[Expand[Denominator[smxint[x
,y]]],E,d,w]]

denlsty=Union[domexp[Expand[Denominator[smyint[x
,y]]],E,d,w]]

denlstxy=Union[domexp[Expand[Denominator[smxyint
[x,y]]],E,d,w]]

xpnddenx=collectcoeff[Denominator[smxint[x,y]],d
enlstx];

xpnddeny=collectcoeff[Denominator[smyint[x,y]],d
enlsty];

xpnddenxy=collectcoeff[Denominator[smxyint[x,y]]
,denlstxy];

holdx=Expand[xpndnumx]/Expand[xpnddenx];

holdy=Expand[xpndnumy]/Expand[xpnddeny];

holdxy=Expand[xpndnumxy]/Expand[xpnddenxy];

Clear[bgxint,bgyint,bgxyint]

bgxint[x_,y_]=fbar
Simplify[Together[numlstx[[1]]/denlstx[[1]]
Normal[Series[holdx,{w,Infinity,100}]]]]
```

```
 w y            2
E    fbar Sqrt[--] (1 + w y)
                Pi
```

```
bgyint[x_,y_]=fbar
Simplify[Together[numlsty[[1]]/denlsty[[1]]
Normal[Series[holdy,{w,Infinity,100}]]]]
```

```
 w y            2
E    fbar Sqrt[--] (1 - w y)
                Pi
```

```
bgxyint[x_,y_]=fbar
Simplify[Together[numlstxy[[1]]/denlstxy[[1]]
Normal[Series[holdxy,{w,Infinity,100}]]]]
```

```
 w y            2
E    fbar Sqrt[--] w y
                Pi
```

Obtain Analytic Expressions for the Asymptotic Contribution to the Stresses (integrated over w from wstar to Infinity)

Concentrated Load

```
Clear[asyconcxinthold,asyconcyinthold,asyconcxyi
nthold]
```

```
asyconcxinthold[x_,y_]=PowerExpand[Integrate[Cos
[w  x]  (E^(w*y)*(1  +
w*y))/Pi,{w,wstar,Infinity}]]
```

```
(E^(wstar*y)*(-(y*Cos[wstar*x]) -
wstar*y^2*Cos[wstar*x] +

      y*Cos[wstar*x - 2*ArcTan[x/y]] - x*Sin[wstar*x] -

      wstar*x*y*Sin[wstar*x]))/(Pi*(x^2 + y^2))
```

```
asyconcyinthold[x_,y_]=PowerExpand[Integrate[Cos
[w  x]  (E^(w*y)*(1  -
w*y))/Pi,{w,wstar,Infinity}]]
```

```
(E^(wstar*y)*(-(y*Cos[wstar*x]) +
wstar*y^2*Cos[wstar*x] -

      y*Cos[wstar*x - 2*ArcTan[x/y]] - x*Sin[wstar*x] +

      wstar*x*y*Sin[wstar*x]))/(Pi*(x^2 + y^2))
```

```
asyconcxyinthold[x_,y_]=PowerExpand[Integrate[Si
n[w  x]  (E^(w*y)*w*y)/Pi,{w,wstar,Infinity}]]
```

```
(E^(wstar*y)*y*(wstar*x*Cos[wstar*x] -

      wstar*y*Sin[wstar*x] + Sin[wstar*x -
2*ArcTan[x/y]]))/

  (Pi*(x^2 + y^2))
```

Hertzian Contact Distribution

```
Clear[asydistxinthold,asydistyinthold,asydistxyi
nthold]
```

```
asydistxinthold[x_,y_]=asyconcxinthold[x-t,y]  n0
Sqrt[1  -  t^2/a^2]
```

```
(E^(wstar*y)*n0*(1 - t^2/a^2)^(1/2)*

    (-(y*Cos[wstar*(-t + x)]) -

      wstar*y^2*Cos[wstar*(-t + x)] +

      y*Cos[wstar*(-t + x) - 2*ArcTan[(-t + x)/y]] -

      (-t + x)*Sin[wstar*(-t + x)] -

      wstar*(-t + x)*y*Sin[wstar*(-t + x)]))/

  (Pi*((-t + x)^2 + y^2))
```

```
asydistyinthold[x_,y_]=asyconcyinthold[x-t,y]  n0
Sqrt[1  -  t^2/a^2]
```

```
(E^(wstar*y)*n0*(1 - t^2/a^2)^(1/2)*

    (-(y*Cos[wstar*(-t + x)]) +

      wstar*y^2*Cos[wstar*(-t + x)] -

      y*Cos[wstar*(-t + x) - 2*ArcTan[(-t + x)/y]] -

      (-t + x)*Sin[wstar*(-t + x)] +

      wstar*(-t + x)*y*Sin[wstar*(-t + x)]))/

  (Pi*((-t + x)^2 + y^2))
```

```
asydistxyinthold[x_,y_]=asyconcxyinthold[x-t,y]
n0  Sqrt[1  -  t^2/a^2]
```

```
(E^(wstar*y)*n0*(1 - t^2/a^2)^(1/2)*y*

    (wstar*(-t + x)*Cos[wstar*(-t + x)] -
```

```
    wstar*y*Sin[wstar*(-t + x)] +

    Sin[wstar*(-t + x) - 2*ArcTan[(-t + x)/y]]))/

  (Pi*((-t + x)^2 + y^2))
```

Definitions of the Asymptotic Integrand Coefficient Functions

```
Clear[fbar,ackxx,ackyy,ackxy]

fbar=1/Sqrt[2  Pi]
```

$$\frac{1}{\text{Sqrt}[2\ \text{Pi}]}$$

```
ackxx[y_,w_]=Simplify[E^(w*y)*fbar*(2/Pi)^(1/2)*
(1  +  w*y)]

(E^(w*y)*(1 + w*y))/Pi

ackyy[y_,w_]=Simplify[E^(w*y)*fbar*(2/Pi)^(1/2)*
(1  -  w*y)]

(E^(w*y)*(1 - w*y))/Pi

ackxy[y_,w_]=Simplify[E^(w*y)*fbar*(2/Pi)^(1/2)*
w*y]

(E^(w*y)*w*y)/Pi
```

Definitions of the "Exact" Inverse Transform Integrand Coefficient Functions

Concentrated Load

```
Clear[exconcxint,exconcyint,exconcxyint,fbar]

fbar=N[1/Sqrt[2  Pi]]

exconcxint[x_,y_]=fbar
intxr[lima0r,limb0r,lima2r,limb2r];

exconcyint[x_,y_]=fbar
intyr[lima0r,limb0r,lima2r,limb2r];
```

```
exconcxyint[x_,y_]=fbar
inttauxyr[lima0r,limb0r,lima2r,limb2r];
```

Hertzian Contact Load Distribution

```
Clear[exdistxint,exdistyint,exdistxyint,fbar]
```

```
fbar=N[PowerExpand[((a^(-2))^(1/2)*n0*(Pi/2)^(1/
2)*(a^2*w^2)^(1/2)*BesselJ[1,(a^2*w^2)^(1/2)])/w
^2]]
```

```
1.25331 n0 BesselJ[1., a w]
-------------------------
            w
```

```
exdistxint[x_,y_]=fbar
intxr[lima0r,limb0r,lima2r,limb2r];
```

```
exdistyint[x_,y_]=fbar
intyr[lima0r,limb0r,lima2r,limb2r];
```

```
exdistxyint[x_,y_]=fbar
inttauxyr[lima0r,limb0r,lima2r,limb2r];
```

Definitions of the Asymptotic Stress Functions

Concentrated Load

```
Clear[asyconcxint,asyconcyint,asyconcxyint]
```

```
asyconcxint[x_,y_]=(E^(wstar*y)*(-(y*Cos[wstar*x
]) - wstar*y^2*Cos[wstar*x] + y*Cos[wstar*x -
2*ArcTan[x/y]] - x*Sin[wstar*x] -
wstar*x*y*Sin[wstar*x]))/(Pi*(x^2 + y^2));
```

```
asyconcyint[x_,y_]=(E^(wstar*y)*(-(y*Cos[wstar*x
]) + wstar*y^2*Cos[wstar*x] - y*Cos[wstar*x -
2*ArcTan[x/y]] - x*Sin[wstar*x] +
wstar*x*y*Sin[wstar*x]))/(Pi*(x^2 + y^2));
```

```
asyconcxyint[x_,y_]=(E^(wstar*y)*y*(wstar*x*Cos[
wstar*x] - wstar*y*Sin[wstar*x] + Sin[wstar*x -
2*ArcTan[x/y]]))/(Pi*(x^2 + y^2));
```

Hertzian Contact Distribution

```
Clear[asydistxint,asydistyint,asydistxyint]
```

```
asydistxint[x_,y_]=(E^(wstar*y)*n0*(1 -
t^2/a^2)^(1/2)*(-(y*Cos[wstar*(-t + x)]) -
wstar*y^2*Cos[wstar*(-t + x)] + y*Cos[wstar*(-t
+ x) - 2*ArcTan[(-t + x)/y]] - (-t +
x)*Sin[wstar*(-t + x)] - wstar*(-t +
x)*y*Sin[wstar*(-t + x)]))/(Pi*((-t + x)^2 +
y^2));
```

```
asydistyint[x_,y_]=(E^(wstar*y)*n0*(1 -
t^2/a^2)^(1/2)*(-(y*Cos[wstar*(-t + x)]) +
wstar*y^2*Cos[wstar*(-t + x)] - y*Cos[wstar*(-t
+ x) - 2*ArcTan[(-t + x)/y]] - (-t +
x)*Sin[wstar*(-t + x)] + wstar*(-t +
x)*y*Sin[wstar*(-t + x)]))/(Pi*((-t + x)^2 +
y^2));
```

```
asydistxyint[x_,y_]=(E^(wstar*y)*n0*(1 -
t^2/a^2)^(1/2)*y*(wstar*(-t + x)*Cos[wstar*(-t +
x)] - wstar*y*Sin[wstar*(-t + x)] +
Sin[wstar*(-t + x) - 2*ArcTan[(-t +
x)/y]]))/(Pi*((-t + x)^2 + y^2));
```

Definitions of Stress Components

Close to the Load

```
Clear[sigx,sigy,tauxy,wstar]
```

```
sigx[x_,y_]:=NIntegrate[Cos[w x]
exdistxint[x,y],{w,0,wstar},MaxRecursion->20] +
NIntegrate[asydistxint[x,y],{t,-a,a},MaxRecursio
n->20]
```

```
sigy[x_,y_]:=NIntegrate[Cos[w x]
exdistyint[x,y],{w,0,wstar},MaxRecursion->20] +
NIntegrate[asydistyint[x,y],{t,-a,a},MaxRecursio
n->20]
```

```
tauxy[x_,y_]:=NIntegrate[Sin[w  x]
exdistxyint[x,y],{w,0,wstar},MaxRecursion->20]  +
NIntegrate[asydistxyint[x,y],{t,-a,a},MaxRecursi
on->20]
```

■ *Far from the Load*

```
Clear[sigxfar,sigyfar,tauxyfar,wstar]

sigxfar[x_,y_]:=(NIntegrate[Cos[w  x]
exconcxint[x,y],{w,0,wstar},MaxRecursion->20]  +
N[asyconcxint[x,y]])  wheelload/railthick

sigyfar[x_,y_]:=(NIntegrate[Cos[w  x]
exconcyint[x,y],{w,0,wstar},MaxRecursion->20]  +
N[asyconcyint[x,y]])  wheelload/railthick

tauxyfar[x_,y_]:=(NIntegrate[Sin[w  x]
exconcxyint[x,y],{w,0,wstar},MaxRecursion->20]  +
N[asyconcxyint[x,y]])  wheelload/railthick
```

▩ *Problem Constants (Poisson's Ratio for the rail and support have been given the value 0.33)*

■ *Contact Expressions*

```
Clear[a,wheelload,wheelradius,ymodr,delta,railth
ick,raildepth,railinertia,n0]

delta=4  wheelradius  (1  -  (33  /  100)^2)  /  ymodr;

railthick=N[12  railinertia  /  raildepth^3];

a=N[Simplify[PowerExpand[Sqrt[2  wheelload  delta
/  (railthick  Pi)]]]]
```

$$\frac{0.434853\ \text{raildepth}^{3/2}\ \text{Sqrt[wheelload]}\ \text{Sqrt[wheelradius]}}{\text{Sqrt[railinertia]}\ \text{Sqrt[ymodr]}}$$

```
n0=N[Simplify[PowerExpand[2 wheelload / (Pi a
railthick)]]]
```

$$\frac{0.121999\ \text{raildepth}^{3/2}\ \text{Sqrt[wheelload]}\ \text{Sqrt[ymodr]}}{\text{Sqrt[railinertia]}\ \text{Sqrt[wheelradius]}}$$

■ *User-Defined Constants*

Track Modulus [kips per inch per inch]

```
trackmod=5.
```

5.

Young's Modulus for the Rail [MPa]

```
youngmodrail=206843.
```

206843.

Vertical Wheel Load [MN]

```
wheelload=0.17348
```

0.17348

Radius of the Wheel [m]

```
wheelradius=0.4826
```

0.4826

Depth of the Rail [m]

```
raildepth=0.18574
```

0.18574

Strong-Axis Moment of Inertia for the Rail [m^4]

```
railinertia=0.0000395
```

0.0000395

□ *assignment of constants to notebook variables*

```
Clear[modr,ymodr,mods,d]
```

```
modr=N[youngmodrail/(2  (1+33/100))]
```

77760.5

```
ymodr=N[youngmodrail]
```

206843.

```
mods=6.894757  (67.92*trackmod  -  3.88*trackmod^2
+  0.172*trackmod^3)
```

1820.91

```
d=N[raildepth]
```

0.18574

Check Some Values

```
a
```

0.00352371

```
n0
```

423.709

```
wstar=50.
```

50.

```
x=.001
```

0.001

```
y=-.003
```

-0.003

```
sigx[x,y]
```

109.097

```
sigy[x,y]
```

305.688

```
tauxy[x,y]
```

-43.9917

```
x=.5
```

0.5

```
sigx[x,y]
3.85605
sigy[x,y]
0.00069965
tauxy[x,y]
-0.108467
sigxfar[x,y]
3.85582
sigyfar[x,y]
0.000699642
tauxyfar[x,y]
-0.108465
41/6.9
5.94203
```

Calculation of Stresses

Some Preliminary Issues

Determine wstar

```
Clear[x,y,w,asympnt]
```

```
asympnt[asymp_,exact_,var_,toler_]  :=  Module[
     {relerr,ex,as,step},
     ex  =  Compile[{var},exact];
     as  =  Compile[{var},asymp];
    relerr = 2 toler;
    step = 3.;

    While[
        relerr > toler,
        step = step + 1.;
        relerr = Abs[(as[step] -
ex[step])/ex[step]];
    ];

    step
]
```

```
y=-.0254
```

```
-0.0254
```

```
asympnt[ackxx[y,w],1/Sqrt[2  Pi]
intxr[lima0r,limb0r,lima2r,limb2r],w,.0001]
```

```
49.
```

```
asympnt[ackyy[y,w],1/Sqrt[2  Pi]
intyr[lima0r,limb0r,lima2r,limb2r],w,.0001]
```

```
40.
```

```
asympnt[ackxy[y,w],1/Sqrt[2  Pi]
inttauxyr[lima0r,limb0r,lima2r,limb2r],w,.0001]
```

```
44.
```

```
wstar=50
```

```
50
```

□ *A Couple of Useful Functions*

```
reflecteven[{aa__}]:=Flatten[Append[{aa},
Reverse[{aa}]]]
```

```
reflectodd[{aa__}]:=Flatten[Append[{aa},
Reverse[-{aa}]]]
```

APPENDIX C

Mathematica Notebook for the Tangential Load Solution

1+1

2

Presentation of the Papkovich-Neuber Function

For the Rail

i) Fr = phi0r + x Phi1r + y Phi2r; phi0r, phi1r, and phi2r are harmonic
ii) 2 modr ur = -Dx(Fr) + 4(1 - 1/(1+nur)) phi1r
iii) 2 modr vr = -Dy(Fr) + 4(1 - 1/(1+nur)) phi2r
where Dx( ) and Dy( ) denote differentiation wrt x and y respectively

For the Support

iv) Fs = phi0s + x Phi1s + y Phi2s; phi0s, phi1s, and phi2s are harmonic
v) 2 mods us = -Dx(Fs) + 4(1 - 1/(1+nus)) phi1s
vi) 2 mods vs = -Dy(Fs) + 4(1 - 1/(1+nus)) phi2s
where Dx( ) and Dy( ) denote differentiation wrt x and y respectively

Description of Solution

Using the theorems of infinitesimal elasticity, and the above relationships (i - vi) expressions can be derived for displacements, strains, and stresses in terms of the phi0#, phi1#, and phi2# functions. Using the arbitrariness of one of the functions, phi1# are set to zero. The phi0# and phi2# functions are expressed in the frequency domain as linear combinations of exponential functions with coefficients determined by the boundary conditions. In the present case there are 8 coefficients -- which are functions of the frequency coordinate, w. Therefore, 8 boundary condition equations are required. Once the coefficients are determined as functions of w, the spatial domain stresses can be recovered by evaluating the Inverse Fourier Transform on the stress component expressions in the frequency domain.

Descriptions of Variables

Physical Domain -> an infinitely long elastic strip bonded to an elastic half-space

x -> Horizontal Coordinate (positive to the right) [L]
y -> Vertical Coordinate (positive upward) [L]
w -> Fourier Transform Coordinate [1/L]
d -> Depth of Rail Strip [L]
b -> Depth of Support Strip [L]
modr -> Shear Modulus of the Rail [F/L^2]
nur -> Poisson's Ratio for the Rail
mods -> Shear Modulus of the Support [F/L^2]
nus -> Poisson's Ratio for the Support
t0 -> Peak Value of Hertzian Tangential Traction [F/L^2]
a -> Half-Width of Contact Zone [L]
gbar -> Transformed Tangential Traction Function [F/L]
a0r, b0r, a2r, b2r, a0s, b0s, a2s, b2s -> Harmonic Function Coefficients

Clear the Variables

```
Clear[x,y,w,d,b,modr,nur,mods,nus,t0,a,gbar,a0r,
b0r,a2r,b2r,a0s,b0s,a2s,b2s,wstar]
```

Definitions of Harmonic Functions in the Frequency Domain

```
Clear[fphi0r,fphi2r,fphi0s,fphi2s]

fphi0r[y_]  =  (a0r  Exp[w  y]  +  b0r  Exp[-w  y]);

fphi2r[y_]  =  (a2r  Exp[w  y]  +  b2r  Exp[-w  y]);

fphi0s[y_]  =  (a0s  Exp[w  y]  +  b0s  Exp[-w  y]);

fphi2s[y_]  =  (a2s  Exp[w  y]  +  b2s  Exp[-w  y]);
```

Definitions of Stresses and Displacements in the Frequency Domain

```
Clear[fsigxr,fsigyr,ftauxyr,fur,fvr,fsigxs,fsigy
s,ftauxys,fus,fvs]
```

```
fsigxr[y_] = w^2 fphi0r[y] + y w^2 fphi2r[y] +2
nur/(1+nur) D[fphi2r[y],{y,1}];

fsigyr[y_] = -D[fphi0r[y],{y,2}] - y
D[fphi2r[y],{y,2}]+2/(1+nur) D[fphi2r[y],{y,1}];

ftauxyr[y_] = I w D[fphi0r[y],{y,1}] + I w y
D[fphi2r[y],{y,1}] - I w (1-nur)/(1+nur)
fphi2r[y];

fur[y_]=1/(2 modr) (I w fphi0r[y] + y I w
fphi2r[y]);

fvr[y_]=1/(2 modr) (-D[fphi0r[y],{y,1}]-y
D[fphi2r[y],{y,1}]+(3-nur)/(1+nur) fphi2r[y]);

fsigxs[y_] = w^2 fphi0s[y] + y w^2 fphi2s[y] +2
nus/(1+nus) D[fphi2s[y],{y,1}];

fsigys[y_] = -D[fphi0s[y],{y,2}] - y
D[fphi2s[y],{y,2}]+2/(1+nus) D[fphi2s[y],{y,1}];

ftauxys[y_] = I w D[fphi0s[y],{y,1}] + I w y
D[fphi2s[y],{y,1}] - I w (1-nus)/(1+nus)
fphi2s[y];

fus[y_]=1/(2 mods) (I w fphi0s[y] + y I w
fphi2s[y]);

fvs[y_]=1/(2 mods) (-D[fphi0s[y],{y,1}]-y
D[fphi2s[y],{y,1}]+(3-nus)/(1+nus) fphi2s[y]);
```

■ *Definitions of Inverse Fourier Transform Integrands for the Stress Components (real parts only -- the coefficients a0r, b0r, etc. are pure Imagionary)*

```
Clear[intxr,intyr,inttauxyr,intur,intvr]

intxr[a0r_,b0r_,a2r_,b2r_]=Collect[Expand[Numera
tor[Together[fsigxr[y]]] (-2 I)],
{a0r,a2r,b0r,b2r,Exp[w y],Exp[-w y]}]/(Sqrt[2
Pi] Denominator[Together[fsigxr[y]]]);

intyr[a0r_,b0r_,a2r_,b2r_]=Collect[Expand[Numera
tor[Together[fsigyr[y]]] (-2 I)],
{a0r,a2r,b0r,b2r,Exp[w y],Exp[-w y]}]/(Sqrt[2
Pi] Denominator[Together[fsigyr[y]]]);
```

```
inttauxyr[a0r_,b0r_,a2r_,b2r_]=Collect[Numerator
[Together[ftauxyr[y]]],  {a0r,a2r,b0r,b2r,Exp[w
y],Exp[-w  y]}]  2/(Sqrt[2  Pi]
Denominator[Together[ftauxyr[y]]]);
```

Determine the Unknown Coefficients

Boundary Condition Expansions

```
Clear[nur,nus]
```

```
nur=33/100
```

$$\frac{33}{100}$$

```
nus=33/100
```

$$\frac{33}{100}$$

```
Clear[eq1,eq2,eq3,eq4,eq5,eq6,eq7,eq8]
eq1=Expand[fsigyr[0]];
eq2=Expand[ftauxyr[0]];
eq3=Expand[fsigyr[-d]-fsigys[-d]];
eq4=Expand[ftauxyr[-d]-ftauxys[-d]];
eq5=Expand[fur[-d]-fus[-d]];
eq6=Expand[fvr[-d]-fvs[-d]];
eq7=Expand[fus[-b]];
eq8=Expand[fvs[-b]];
```

Coefficient Matrix Construction and Matrix Equation Solution

```
Clear[mat,coeflist]
```

```
mat = {
{Coefficient[eq1,a0r],Coefficient[eq1,b0r],Coeff
icient[eq1,a2r],Coefficient[eq1,b2r],Coefficient
[eq1,a0s],Coefficient[eq1,b0s],Coefficient[eq1,a
2s],Coefficient[eq1,b2s]},
{Coefficient[eq2,a0r],Coefficient[eq2,b0r],Coeff
icient[eq2,a2r],Coefficient[eq2,b2r],Coefficient
[eq2,a0s],Coefficient[eq2,b0s],Coefficient[eq2,a
2s],Coefficient[eq2,b2s]},
{Coefficient[eq3,a0r],Coefficient[eq3,b0r],Coeff
icient[eq3,a2r],Coefficient[eq3,b2r],Coefficient
[eq3,a0s],Coefficient[eq3,b0s],Coefficient[eq3,a
2s],Coefficient[eq3,b2s]},
{Coefficient[eq4,a0r],Coefficient[eq4,b0r],Coeff
icient[eq4,a2r],Coefficient[eq4,b2r],Coefficient
[eq4,a0s],Coefficient[eq4,b0s],Coefficient[eq4,a
2s],Coefficient[eq4,b2s]},
{Coefficient[eq5,a0r],Coefficient[eq5,b0r],Coeff
icient[eq5,a2r],Coefficient[eq5,b2r],Coefficient
[eq5,a0s],Coefficient[eq5,b0s],Coefficient[eq5,a
2s],Coefficient[eq5,b2s]},
{Coefficient[eq6,a0r],Coefficient[eq6,b0r],Coeff
icient[eq6,a2r],Coefficient[eq6,b2r],Coefficient
[eq6,a0s],Coefficient[eq6,b0s],Coefficient[eq6,a
2s],Coefficient[eq6,b2s]},
{Coefficient[eq7,a0r],Coefficient[eq7,b0r],Coeff
icient[eq7,a2r],Coefficient[eq7,b2r],Coefficient
[eq7,a0s],Coefficient[eq7,b0s],Coefficient[eq7,a
2s],Coefficient[eq7,b2s]},
{Coefficient[eq8,a0r],Coefficient[eq8,b0r],Coeff
icient[eq8,a2r],Coefficient[eq8,b2r],Coefficient
[eq8,a0s],Coefficient[eq8,b0s],Coefficient[eq8,a
2s],Coefficient[eq8,b2s]}};
```

```
coeflist=LinearSolve[mat,{0,1,0,0,0,0,0,0}];
```

■ *Define the Coefficients*

```
Clear[a0r,a2r,b0r,b2r]

a0r=Together[coeflist[[1]]];

b0r=Together[coeflist[[2]]];

a2r=Together[coeflist[[3]]];
```

```
b2r=Together[coeflist[[4]]];
```

Find Limit of Coefficients (b --> Infinity)

```
domexpcoeff[expr_,mant_,bigexp_,arbexp_]:=Max[Ca
ses[expr,(mant^(x2_ bigexp arbexp +
y2_)|mant^(x2_ bigexp arbexp))->x2, Infinity]]
domexp[expr_,mant_,bigexp_,arbexp_]:=Cases[expr,
(mant^(x_ bigexp arbexp + y_)|mant^(x_ bigexp
arbexp)) /; x ==
domexpcoeff[expr,mant,bigexp,arbexp], Infinity]
collectterms[expr_,formlist_]:=Sum[Coefficient[E
xpand[expr],formlist[[i]]]
formlist[[i]],{i,1,Length[formlist]}]
simpa0=Min[domexpcoeff[Numerator[a0r],E,b,w],dom
expcoeff[Denominator[a0r],E,b,w]];
simpb0=Min[domexpcoeff[Numerator[b0r],E,b,w],dom
expcoeff[Denominator[b0r],E,b,w]];
simpa2=Min[domexpcoeff[Numerator[a2r],E,b,w],dom
expcoeff[Denominator[a2r],E,b,w]];
simpb2=Min[domexpcoeff[Numerator[b2r],E,b,w],dom
expcoeff[Denominator[b2r],E,b,w]];
numlsta0=Union[domexp[Numerator[a0r],E,b,w]];
numlstb0=Union[domexp[Numerator[b0r],E,b,w]];
numlsta2=Union[domexp[Numerator[a2r],E,b,w]];
numlstb2=Union[domexp[Numerator[b2r],E,b,w]];
xpndnuma0=collectterms[Numerator[a0r],numlsta0];
xpndnumb0=collectterms[Numerator[b0r],numlstb0];
xpndnuma2=collectterms[Numerator[a2r],numlsta2];
xpndnumb2=collectterms[Numerator[b2r],numlstb2];
denlsta0=Union[domexp[Denominator[a0r],E,b,w]];
denlstb0=Union[domexp[Denominator[b0r],E,b,w]];
denlsta2=Union[domexp[Denominator[a2r],E,b,w]];
```

```
denlstb2=Union[domexp[Denominator[b2r],E,b,w]];
xpnddena0=collectterms[Denominator[a0r],denlsta0
];
xpnddenb0=collectterms[Denominator[b0r],denlstb0
];
xpnddena2=collectterms[Denominator[a2r],denlsta2
];
xpnddenb2=collectterms[Denominator[b2r],denlstb2
];
holda0=Expand[E^(-simpa0  b  w)
xpndnuma0]/Expand[(E^(-simpa0  b  w)  xpnddena0)];
holdb0=Expand[E^(-simpb0  b  w)
xpndnumb0]/Expand[(E^(-simpb0  b  w)  xpnddenb0)];
holda2=Expand[E^(-simpa2  b  w)
xpndnuma2]/Expand[(E^(-simpa2  b  w)  xpnddena2)];
holdb2=Expand[E^(-simpb2  b  w)
xpndnumb2]/Expand[(E^(-simpb2  b  w)  xpnddenb2)];
lima0r=Cancel[Limit[holda0,b->Infinity]];
limb0r=Cancel[Limit[holdb0,b->Infinity]];
lima2r=Cancel[Limit[holda2,b->Infinity]];
limb2r=Cancel[Limit[holdb2,b->Infinity]];
```

Appearance of Coefficients

Coefficients before Limit

?a0r

```
a0r = (-2*I*(-948143700*E^(6*d*w)*modr^2 +
        948143700*E^(8*d*w)*modr^2 -
        948143700*E^(4*b*w + 2*d*w)*modr^2 +
        1896287400*E^(2*b*w + 4*d*w)*modr^2 +
        948143700*E^(4*b*w + 4*d*w)*modr^2 -
        1896287400*E^(2*b*w + 6*d*w)*modr^2 -
        1896287400*E^(8*d*w)*modr*mods +
        2375712600*E^(4*b*w + 4*d*w)*modr*mods -
        479425200*E^(2*b*w + 6*d*w)*modr*mods +
        948143700*E^(6*d*w)*mods^2 + 948143700*E^(8*d*w)*
        948143700*E^(4*b*w + 2*d*w)*mods^2 +
        2375712600*E^(2*b*w + 4*d*w)*mods^2 +
        948143700*E^(4*b*w + 4*d*w)*mods^2 +
        2375712600*E^(2*b*w + 6*d*w)*mods^2 -
        1896287400*d*E^(6*d*w)*modr^2*w -
        1896287400*d*E^(4*b*w + 2*d*w)*modr^2*w +
        3792574800*d*E^(2*b*w + 4*d*w)*modr^2*w +
        951694800*d*E^(6*d*w)*modr*mods*w +
        951694800*d*E^(4*b*w + 2*d*w)*modr*mods*w +
        4256000000*b*E^(2*b*w + 4*d*w)*modr*mods*w -
        6159389600*d*E^(2*b*w + 4*d*w)*modr*mods*w +
        944592600*d*E^(6*d*w)*mods^2*w +
        944592600*d*E^(4*b*w + 2*d*w)*mods^2*w +
        2366814800*d*E^(2*b*w + 4*d*w)*mods^2*w -
        1261031121*d^2*E^(6*d*w)*modr^2*w^2 -
        1261031121*d^2*E^(4*b*w + 2*d*w)*modr^2*w^2 +
        941054800*b^2*E^(2*b*w + 4*d*w)*modr^2*w^2 -
        1882109600*b*d*E^(2*b*w + 4*d*w)*modr^2*w^2 +
        3463117042*d^2*E^(2*b*w + 4*d*w)*modr^2*w^2 -
        941054800*b^2*E^(2*b*w + 6*d*w)*modr^2*w^2 +
        1882109600*b*d*E^(2*b*w + 6*d*w)*modr^2*w^2 -
        941054800*d^2*E^(2*b*w + 6*d*w)*modr^2*w^2 +
        632877042*d^2*E^(6*d*w)*modr*mods*w^2 +
        632877042*d^2*E^(4*b*w + 2*d*w)*modr*mods*w^2 +
        5660480000*b*d*E^(2*b*w + 4*d*w)*modr*mods*w^2 -
        6926234084*d^2*E^(2*b*w + 4*d*w)*modr*mods*w^2 -
```

```
    948130400*b^2*E^(2*b*w + 6*d*w)*modr*mods*w^2 +
    1896260800*b*d*E^(2*b*w + 6*d*w)*modr*mods*w^2 -
    948130400*d^2*E^(2*b*w + 6*d*w)*modr*mods*w^2 +
    628154079*d^2*E^(6*d*w)*mods^2*w^2 +
    628154079*d^2*E^(4*b*w + 2*d*w)*mods^2*w^2 +
    1889185200*b^2*E^(2*b*w + 4*d*w)*mods^2*w^2 -
    3778370400*b*d*E^(2*b*w + 4*d*w)*mods^2*w^2 +
    3463117042*d^2*E^(2*b*w + 4*d*w)*mods^2*w^2 +
    1889185200*b^2*E^(2*b*w + 6*d*w)*mods^2*w^2 -
    3778370400*b*d*E^(2*b*w + 6*d*w)*mods^2*w^2 +
    1889185200*d^2*E^(2*b*w + 6*d*w)*mods^2*w^2 +
    1882109600*b^2*d*E^(2*b*w + 4*d*w)*modr^2*w^3 -
    3764219200*b*d^2*E^(2*b*w + 4*d*w)*modr^2*w^3 +
    1882109600*d^3*E^(2*b*w + 4*d*w)*modr^2*w^3 -
    3764219200*b^2*d*E^(2*b*w + 4*d*w)*modr*mods*w^3
    7528438400*b*d^2*E^(2*b*w + 4*d*w)*modr*mods*w^3
    3764219200*d^3*E^(2*b*w + 4*d*w)*modr*mods*w^3 +
    1882109600*b^2*d*E^(2*b*w + 4*d*w)*mods^2*w^3 -
    3764219200*b*d^2*E^(2*b*w + 4*d*w)*mods^2*w^3 +
    1882109600*d^3*E^(2*b*w + 4*d*w)*mods^2*w^3 +
    1251602884*b^2*d^2*E^(2*b*w + 4*d*w)*modr^2*w^4 -
    2503205768*b*d^3*E^(2*b*w + 4*d*w)*modr^2*w^4 +
    1251602884*d^4*E^(2*b*w + 4*d*w)*modr^2*w^4 -
    2503205768*b^2*d^2*E^(2*b*w + 4*d*w)*modr*mods*w^
    5006411536*b*d^3*E^(2*b*w + 4*d*w)*modr*mods*w^4
    2503205768*d^4*E^(2*b*w + 4*d*w)*modr*mods*w^4 +
    1251602884*b^2*d^2*E^(2*b*w + 4*d*w)*mods^2*w^4 -
    2503205768*b*d^3*E^(2*b*w + 4*d*w)*mods^2*w^4 +
    1251602884*d^4*E^(2*b*w + 4*d*w)*mods^2*w^4))/
(w^2*(1261031121*E^(4*b*w)*modr^2 +
    1261031121*E^(4*d*w)*modr^2 -
    2522062242*E^(6*d*w)*modr^2 +
    1261031121*E^(8*d*w)*modr^2 -
    2522062242*E^(2*b*w + 2*d*w)*modr^2 -
    2522062242*E^(4*b*w + 2*d*w)*modr^2 +
    5044124484*E^(2*b*w + 4*d*w)*modr^2 +
    1261031121*E^(4*b*w + 4*d*w)*modr^2 -
    2522062242*E^(2*b*w + 6*d*w)*modr^2 -
    2522062242*E^(4*b*w)*modr*mods +
    3159697758*E^(4*d*w)*modr*mods -
    637635516*E^(6*d*w)*modr*mods -
    2522062242*E^(8*d*w)*modr*mods -
    637635516*E^(2*b*w + 2*d*w)*modr*mods -
    637635516*E^(4*b*w + 2*d*w)*modr*mods +
```

```
1275271032*E^(2*b*w + 4*d*w)*modr*mods +
3159697758*E^(4*b*w + 4*d*w)*modr*mods -
637635516*E^(2*b*w + 6*d*w)*modr*mods +
1261031121*E^(4*b*w)*mods^2 +
1261031121*E^(4*d*w)*mods^2 +
3159697758*E^(6*d*w)*mods^2 +
1261031121*E^(8*d*w)*mods^2 +
3159697758*E^(2*b*w + 2*d*w)*mods^2 +
3159697758*E^(4*b*w + 2*d*w)*mods^2 +
7917084484*E^(2*b*w + 4*d*w)*mods^2 +
1261031121*E^(4*b*w + 4*d*w)*mods^2 +
3159697758*E^(2*b*w + 6*d*w)*mods^2 -
5044124484*d^2*E^(6*d*w)*modr^2*w^2 -
1251602884*b^2*E^(2*b*w + 2*d*w)*modr^2*w^2 +
2503205768*b*d*E^(2*b*w + 2*d*w)*modr^2*w^2 -
1251602884*d^2*E^(2*b*w + 2*d*w)*modr^2*w^2 -
5044124484*d^2*E^(4*b*w + 2*d*w)*modr^2*w^2 +
2503205768*b^2*E^(2*b*w + 4*d*w)*modr^2*w^2 -
5006411536*b*d*E^(2*b*w + 4*d*w)*modr^2*w^2 +
12591454736*d^2*E^(2*b*w + 4*d*w)*modr^2*w^2 -
1251602884*b^2*E^(2*b*w + 6*d*w)*modr^2*w^2 +
2503205768*b*d*E^(2*b*w + 6*d*w)*modr^2*w^2 -
1251602884*d^2*E^(2*b*w + 6*d*w)*modr^2*w^2 +
2531508168*d^2*E^(6*d*w)*modr*mods*w^2 -
1261013432*b^2*E^(2*b*w + 2*d*w)*modr*mods*w^2 +
2522026864*b*d*E^(2*b*w + 2*d*w)*modr*mods*w^2 -
1261013432*d^2*E^(2*b*w + 2*d*w)*modr*mods*w^2 +
2531508168*d^2*E^(4*b*w + 2*d*w)*modr*mods*w^2 +
2522026864*b^2*E^(2*b*w + 4*d*w)*modr*mods*w^2 +
17597866272*b*d*E^(2*b*w + 4*d*w)*modr*mods*w^2 -
25182909472*d^2*E^(2*b*w + 4*d*w)*modr*mods*w^2 -
1261013432*b^2*E^(2*b*w + 6*d*w)*modr*mods*w^2 +
2522026864*b*d*E^(2*b*w + 6*d*w)*modr*mods*w^2 -
1261013432*d^2*E^(2*b*w + 6*d*w)*modr*mods*w^2 +
2512616316*d^2*E^(6*d*w)*mods^2*w^2 +
2512616316*b^2*E^(2*b*w + 2*d*w)*mods^2*w^2 -
5025232632*b*d*E^(2*b*w + 2*d*w)*mods^2*w^2 +
2512616316*d^2*E^(2*b*w + 2*d*w)*mods^2*w^2 +
2512616316*d^2*E^(4*b*w + 2*d*w)*mods^2*w^2 +
6295727368*b^2*E^(2*b*w + 4*d*w)*mods^2*w^2 -
12591454736*b*d*E^(2*b*w + 4*d*w)*mods^2*w^2 +
12591454736*d^2*E^(2*b*w + 4*d*w)*mods^2*w^2 +
2512616316*b^2*E^(2*b*w + 6*d*w)*mods^2*w^2 -
5025232632*b*d*E^(2*b*w + 6*d*w)*mods^2*w^2 +
```

```
2512616316*d^2*E^(2*b*w + 6*d*w)*mods^2*w^2 +
5006411536*b^2*d^2*E^(2*b*w + 4*d*w)*modr^2*w^4 -
10012823072*b*d^3*E^(2*b*w + 4*d*w)*modr^2*w^4 +
5006411536*d^4*E^(2*b*w + 4*d*w)*modr^2*w^4 -
10012823072*b^2*d^2*E^(2*b*w + 4*d*w)*modr*mods*w
20025646144*b*d^3*E^(2*b*w + 4*d*w)*modr*mods*w^4
10012823072*d^4*E^(2*b*w + 4*d*w)*modr*mods*w^4 +
5006411536*b^2*d^2*E^(2*b*w + 4*d*w)*mods^2*w^4 -
10012823072*b*d^3*E^(2*b*w + 4*d*w)*mods^2*w^4 +
5006411536*d^4*E^(2*b*w + 4*d*w)*mods^2*w^4));
```

□ *?b0r*

```
b0r = (2*I*(948143700*E^(4*b*w)*modr^2 +
948143700*E^(4*d*w)*modr^2 - 948143700*E^(6*d*w)*
1896287400*E^(2*b*w + 2*d*w)*modr^2 -
948143700*E^(4*b*w + 2*d*w)*modr^2 +
1896287400*E^(2*b*w + 4*d*w)*modr^2 -
1896287400*E^(4*b*w)*modr*mods +
2375712600*E^(4*d*w)*modr*mods -
479425200*E^(2*b*w + 2*d*w)*modr*mods +
948143700*E^(4*b*w)*mods^2 + 948143700*E^(4*d*w)*
948143700*E^(6*d*w)*mods^2 +
2375712600*E^(2*b*w + 2*d*w)*mods^2 +
948143700*E^(4*b*w + 2*d*w)*mods^2 +
2375712600*E^(2*b*w + 4*d*w)*mods^2 +
1896287400*d*E^(6*d*w)*modr^2*w +
1896287400*d*E^(4*b*w + 2*d*w)*modr^2*w -
3792574800*d*E^(2*b*w + 4*d*w)*modr^2*w -
951694800*d*E^(6*d*w)*modr*mods*w -
951694800*d*E^(4*b*w + 2*d*w)*modr*mods*w -
4256000000*b*E^(2*b*w + 4*d*w)*modr*mods*w +
6159389600*d*E^(2*b*w + 4*d*w)*modr*mods*w -
944592600*d*E^(6*d*w)*mods^2*w -
944592600*d*E^(4*b*w + 2*d*w)*mods^2*w -
2366814800*d*E^(2*b*w + 4*d*w)*mods^2*w -
1261031121*d^2*E^(6*d*w)*modr^2*w^2 -
941054800*b^2*E^(2*b*w + 2*d*w)*modr^2*w^2 +
1882109600*b*d*E^(2*b*w + 2*d*w)*modr^2*w^2 -
941054800*d^2*E^(2*b*w + 2*d*w)*modr^2*w^2 -
1261031121*d^2*E^(4*b*w + 2*d*w)*modr^2*w^2 +
941054800*b^2*E^(2*b*w + 4*d*w)*modr^2*w^2 -
1882109600*b*d*E^(2*b*w + 4*d*w)*modr^2*w^2 +
3463117042*d^2*E^(2*b*w + 4*d*w)*modr^2*w^2 +
632877042*d^2*E^(6*d*w)*modr*mods*w^2 -
```

```
    948130400*b^2*E^(2*b*w + 2*d*w)*modr*mods*w^2 +
    1896260800*b*d*E^(2*b*w + 2*d*w)*modr*mods*w^2 -
    948130400*d^2*E^(2*b*w + 2*d*w)*modr*mods*w^2 +
    632877042*d^2*E^(4*b*w + 2*d*w)*modr*mods*w^2 +
    5660480000*b*d*E^(2*b*w + 4*d*w)*modr*mods*w^2 -
    6926234084*d^2*E^(2*b*w + 4*d*w)*modr*mods*w^2 +
    628154079*d^2*E^(6*d*w)*mods^2*w^2 +
    1889185200*b^2*E^(2*b*w + 2*d*w)*mods^2*w^2 -
    3778370400*b*d*E^(2*b*w + 2*d*w)*mods^2*w^2 +
    1889185200*d^2*E^(2*b*w + 2*d*w)*mods^2*w^2 +
    628154079*d^2*E^(4*b*w + 2*d*w)*mods^2*w^2 +
    1889185200*b^2*E^(2*b*w + 4*d*w)*mods^2*w^2 -
    3778370400*b*d*E^(2*b*w + 4*d*w)*mods^2*w^2 +
    3463117042*d^2*E^(2*b*w + 4*d*w)*mods^2*w^2 -
    1882109600*b^2*d*E^(2*b*w + 4*d*w)*modr^2*w^3 +
    3764219200*b*d^2*E^(2*b*w + 4*d*w)*modr^2*w^3 -
    1882109600*d^3*E^(2*b*w + 4*d*w)*modr^2*w^3 +
    3764219200*b^2*d*E^(2*b*w + 4*d*w)*modr*mods*w^3
    7528438400*b*d^2*E^(2*b*w + 4*d*w)*modr*mods*w^3
    3764219200*d^3*E^(2*b*w + 4*d*w)*modr*mods*w^3 -
    1882109600*b^2*d*E^(2*b*w + 4*d*w)*mods^2*w^3 +
    3764219200*b*d^2*E^(2*b*w + 4*d*w)*mods^2*w^3 -
    1882109600*d^3*E^(2*b*w + 4*d*w)*mods^2*w^3 +
    1251602884*b^2*d^2*E^(2*b*w + 4*d*w)*modr^2*w^4 -
    2503205768*b*d^3*E^(2*b*w + 4*d*w)*modr^2*w^4 +
    1251602884*d^4*E^(2*b*w + 4*d*w)*modr^2*w^4 -
    2503205768*b^2*d^2*E^(2*b*w + 4*d*w)*modr*mods*w^
    5006411536*b*d^3*E^(2*b*w + 4*d*w)*modr*mods*w^4
    2503205768*d^4*E^(2*b*w + 4*d*w)*modr*mods*w^4 +
    1251602884*b^2*d^2*E^(2*b*w + 4*d*w)*mods^2*w^4 -
    2503205768*b*d^3*E^(2*b*w + 4*d*w)*mods^2*w^4 +
    1251602884*d^4*E^(2*b*w + 4*d*w)*mods^2*w^4))/
(w^2*(1261031121*E^(4*b*w)*modr^2 +
    1261031121*E^(4*d*w)*modr^2 -
    2522062242*E^(6*d*w)*modr^2 +
    1261031121*E^(8*d*w)*modr^2 -
    2522062242*E^(2*b*w + 2*d*w)*modr^2 -
    2522062242*E^(4*b*w + 2*d*w)*modr^2 +
    5044124484*E^(2*b*w + 4*d*w)*modr^2 +
    1261031121*E^(4*b*w + 4*d*w)*modr^2 -
    2522062242*E^(2*b*w + 6*d*w)*modr^2 -
    2522062242*E^(4*b*w)*modr*mods +
    3159697758*E^(4*d*w)*modr*mods -
    637635516*E^(6*d*w)*modr*mods -
```

```
2522062242*E^(8*d*w)*modr*mods -
637635516*E^(2*b*w + 2*d*w)*modr*mods -
637635516*E^(4*b*w + 2*d*w)*modr*mods +
1275271032*E^(2*b*w + 4*d*w)*modr*mods +
3159697758*E^(4*b*w + 4*d*w)*modr*mods -
637635516*E^(2*b*w + 6*d*w)*modr*mods +
1261031121*E^(4*b*w)*mods^2 +
1261031121*E^(4*d*w)*mods^2 +
3159697758*E^(6*d*w)*mods^2 +
1261031121*E^(8*d*w)*mods^2 +
3159697758*E^(2*b*w + 2*d*w)*mods^2 +
3159697758*E^(4*b*w + 2*d*w)*mods^2 +
7917084484*E^(2*b*w + 4*d*w)*mods^2 +
1261031121*E^(4*b*w + 4*d*w)*mods^2 +
3159697758*E^(2*b*w + 6*d*w)*mods^2 -
5044124484*d^2*E^(6*d*w)*modr^2*w^2 -
1251602884*b^2*E^(2*b*w + 2*d*w)*modr^2*w^2 +
2503205768*b*d*E^(2*b*w + 2*d*w)*modr^2*w^2 -
1251602884*d^2*E^(2*b*w + 2*d*w)*modr^2*w^2 -
5044124484*d^2*E^(4*b*w + 2*d*w)*modr^2*w^2 +
2503205768*b^2*E^(2*b*w + 4*d*w)*modr^2*w^2 -
5006411536*b*d*E^(2*b*w + 4*d*w)*modr^2*w^2 +
12591454736*d^2*E^(2*b*w + 4*d*w)*modr^2*w^2 -
1251602884*b^2*E^(2*b*w + 6*d*w)*modr^2*w^2 +
2503205768*b*d*E^(2*b*w + 6*d*w)*modr^2*w^2 -
1251602884*d^2*E^(2*b*w + 6*d*w)*modr^2*w^2 +
2531508168*d^2*E^(6*d*w)*modr*mods*w^2 -
1261013432*b^2*E^(2*b*w + 2*d*w)*modr*mods*w^2 +
2522026864*b*d*E^(2*b*w + 2*d*w)*modr*mods*w^2 -
1261013432*d^2*E^(2*b*w + 2*d*w)*modr*mods*w^2 +
2531508168*d^2*E^(4*b*w + 2*d*w)*modr*mods*w^2 +
2522026864*b^2*E^(2*b*w + 4*d*w)*modr*mods*w^2 +
17597866272*b*d*E^(2*b*w + 4*d*w)*modr*mods*w^2 -
25182909472*d^2*E^(2*b*w + 4*d*w)*modr*mods*w^2 -
1261013432*b^2*E^(2*b*w + 6*d*w)*modr*mods*w^2 +
2522026864*b*d*E^(2*b*w + 6*d*w)*modr*mods*w^2 -
1261013432*d^2*E^(2*b*w + 6*d*w)*modr*mods*w^2 +
2512616316*d^2*E^(6*d*w)*mods^2*w^2 +
2512616316*b^2*E^(2*b*w + 2*d*w)*mods^2*w^2 -
5025232632*b*d*E^(2*b*w + 2*d*w)*mods^2*w^2 +
2512616316*d^2*E^(2*b*w + 2*d*w)*mods^2*w^2 +
2512616316*d^2*E^(4*b*w + 2*d*w)*mods^2*w^2 +
6295727368*b^2*E^(2*b*w + 4*d*w)*mods^2*w^2 -
12591454736*b*d*E^(2*b*w + 4*d*w)*mods^2*w^2 +
```

```
12591454736*d^2*E^(2*b*w + 4*d*w)*mods^2*w^2 +
2512616316*b^2*E^(2*b*w + 6*d*w)*mods^2*w^2 -
5025232632*b*d*E^(2*b*w + 6*d*w)*mods^2*w^2 +
2512616316*d^2*E^(2*b*w + 6*d*w)*mods^2*w^2 +
5006411536*b^2*d^2*E^(2*b*w + 4*d*w)*modr^2*w^4 -
10012823072*b*d^3*E^(2*b*w + 4*d*w)*modr^2*w^4 +
5006411536*d^4*E^(2*b*w + 4*d*w)*modr^2*w^4 -
10012823072*b^2*d^2*E^(2*b*w + 4*d*w)*modr*mods*w
20025646144*b*d^3*E^(2*b*w + 4*d*w)*modr*mods*w^4
10012823072*d^4*E^(2*b*w + 4*d*w)*modr*mods*w^4 +
5006411536*b^2*d^2*E^(2*b*w + 4*d*w)*mods^2*w^4 -
10012823072*b*d^3*E^(2*b*w + 4*d*w)*mods^2*w^4 +
5006411536*d^4*E^(2*b*w + 4*d*w)*mods^2*w^4));
```

□ *?a2r*

```
a2r = (-133*I*(-9481437*E^(6*d*w)*modr^2*w^27 +
9481437*E^(8*d*w)*modr^2*w^27 -
9481437*E^(4*b*w + 2*d*w)*modr^2*w^27 +
18962874*E^(2*b*w + 4*d*w)*modr^2*w^27 +
9481437*E^(4*b*w + 4*d*w)*modr^2*w^27 -
18962874*E^(2*b*w + 6*d*w)*modr^2*w^27 +
4758474*E^(6*d*w)*modr*mods*w^27 -
18962874*E^(8*d*w)*modr*mods*w^27 +
4758474*E^(4*b*w + 2*d*w)*modr*mods*w^27 -
9516948*E^(2*b*w + 4*d*w)*modr*mods*w^27 +
23757126*E^(4*b*w + 4*d*w)*modr*mods*w^27 -
4794252*E^(2*b*w + 6*d*w)*modr*mods*w^27 +
4722963*E^(6*d*w)*mods^2*w^27 +
9481437*E^(8*d*w)*mods^2*w^27 +
4722963*E^(4*b*w + 2*d*w)*mods^2*w^27 +
11834074*E^(2*b*w + 4*d*w)*mods^2*w^27 +
9481437*E^(4*b*w + 4*d*w)*mods^2*w^27 +
23757126*E^(2*b*w + 6*d*w)*mods^2*w^27 -
18962874*d*E^(6*d*w)*modr^2*w^28 -
18962874*d*E^(4*b*w + 2*d*w)*modr^2*w^28 +
37925748*d*E^(2*b*w + 4*d*w)*modr^2*w^28 +
9516948*d*E^(6*d*w)*modr*mods*w^28 +
9516948*d*E^(4*b*w + 2*d*w)*modr*mods*w^28 +
42560000*b*E^(2*b*w + 4*d*w)*modr*mods*w^28 -
61593896*d*E^(2*b*w + 4*d*w)*modr*mods*w^28 +
9445926*d*E^(6*d*w)*mods^2*w^28 +
9445926*d*E^(4*b*w + 2*d*w)*mods^2*w^28 +
23668148*d*E^(2*b*w + 4*d*w)*mods^2*w^28 +
9410548*b^2*E^(2*b*w + 4*d*w)*modr^2*w^29 -
```

```
    18821096*b*d*E^(2*b*w + 4*d*w)*modr^2*w^29 +
    9410548*d^2*E^(2*b*w + 4*d*w)*modr^2*w^29 -
    9410548*b^2*E^(2*b*w + 6*d*w)*modr^2*w^29 +
    18821096*b*d*E^(2*b*w + 6*d*w)*modr^2*w^29 -
    9410548*d^2*E^(2*b*w + 6*d*w)*modr^2*w^29 -
    18821096*b^2*E^(2*b*w + 4*d*w)*modr*mods*w^29 +
    37642192*b*d*E^(2*b*w + 4*d*w)*modr*mods*w^29 -
    18821096*d^2*E^(2*b*w + 4*d*w)*modr*mods*w^29 -
    9481304*b^2*E^(2*b*w + 6*d*w)*modr*mods*w^29 +
    18962608*b*d*E^(2*b*w + 6*d*w)*modr*mods*w^29 -
    9481304*d^2*E^(2*b*w + 6*d*w)*modr*mods*w^29 +
    9410548*b^2*E^(2*b*w + 4*d*w)*mods^2*w^29 -
    18821096*b*d*E^(2*b*w + 4*d*w)*mods^2*w^29 +
    9410548*d^2*E^(2*b*w + 4*d*w)*mods^2*w^29 +
    18891852*b^2*E^(2*b*w + 6*d*w)*mods^2*w^29 -
    37783704*b*d*E^(2*b*w + 6*d*w)*mods^2*w^29 +
    18891852*d^2*E^(2*b*w + 6*d*w)*mods^2*w^29 +
    18821096*b^2*d*E^(2*b*w + 4*d*w)*modr^2*w^30 -
    37642192*b*d^2*E^(2*b*w + 4*d*w)*modr^2*w^30 +
    18821096*d^3*E^(2*b*w + 4*d*w)*modr^2*w^30 -
    37642192*b^2*d*E^(2*b*w + 4*d*w)*modr*mods*w^30 +
    75284384*b*d^2*E^(2*b*w + 4*d*w)*modr*mods*w^30 -
    37642192*d^3*E^(2*b*w + 4*d*w)*modr*mods*w^30 +
    18821096*b^2*d*E^(2*b*w + 4*d*w)*mods^2*w^30 -
    37642192*b*d^2*E^(2*b*w + 4*d*w)*mods^2*w^30 +
    18821096*d^3*E^(2*b*w + 4*d*w)*mods^2*w^30))/
(w^28*(1261031121*E^(4*b*w)*modr^2 +
    1261031121*E^(4*d*w)*modr^2 -
    2522062242*E^(6*d*w)*modr^2 +
    1261031121*E^(8*d*w)*modr^2 -
    2522062242*E^(2*b*w + 2*d*w)*modr^2 -
    2522062242*E^(4*b*w + 2*d*w)*modr^2 +
    5044124484*E^(2*b*w + 4*d*w)*modr^2 +
    1261031121*E^(4*b*w + 4*d*w)*modr^2 -
    2522062242*E^(2*b*w + 6*d*w)*modr^2 -
    2522062242*E^(4*b*w)*modr*mods +
    3159697758*E^(4*d*w)*modr*mods -
    637635516*E^(6*d*w)*modr*mods -
    2522062242*E^(8*d*w)*modr*mods -
    637635516*E^(2*b*w + 2*d*w)*modr*mods -
    637635516*E^(4*b*w + 2*d*w)*modr*mods +
    1275271032*E^(2*b*w + 4*d*w)*modr*mods +
    3159697758*E^(4*b*w + 4*d*w)*modr*mods -
    637635516*E^(2*b*w + 6*d*w)*modr*mods +
```

```
1261031121*E^(4*b*w)*mods^2 +
1261031121*E^(4*d*w)*mods^2 +
3159697758*E^(6*d*w)*mods^2 +
1261031121*E^(8*d*w)*mods^2 +
3159697758*E^(2*b*w + 2*d*w)*mods^2 +
3159697758*E^(4*b*w + 2*d*w)*mods^2 +
7917084484*E^(2*b*w + 4*d*w)*mods^2 +
1261031121*E^(4*b*w + 4*d*w)*mods^2 +
3159697758*E^(2*b*w + 6*d*w)*mods^2 -
5044124484*d^2*E^(6*d*w)*modr^2*w^2 -
1251602884*b^2*E^(2*b*w + 2*d*w)*modr^2*w^2 +
2503205768*b*d*E^(2*b*w + 2*d*w)*modr^2*w^2 -
1251602884*d^2*E^(2*b*w + 2*d*w)*modr^2*w^2 -
5044124484*d^2*E^(4*b*w + 2*d*w)*modr^2*w^2 +
2503205768*b^2*E^(2*b*w + 4*d*w)*modr^2*w^2 -
5006411536*b*d*E^(2*b*w + 4*d*w)*modr^2*w^2 +
12591454736*d^2*E^(2*b*w + 4*d*w)*modr^2*w^2 -
1251602884*b^2*E^(2*b*w + 6*d*w)*modr^2*w^2 +
2503205768*b*d*E^(2*b*w + 6*d*w)*modr^2*w^2 -
1251602884*d^2*E^(2*b*w + 6*d*w)*modr^2*w^2 +
2531508168*d^2*E^(6*d*w)*modr*mods*w^2 -
1261013432*b^2*E^(2*b*w + 2*d*w)*modr*mods*w^2 +
2522026864*b*d*E^(2*b*w + 2*d*w)*modr*mods*w^2 -
1261013432*d^2*E^(2*b*w + 2*d*w)*modr*mods*w^2 +
2531508168*d^2*E^(4*b*w + 2*d*w)*modr*mods*w^2 +
2522026864*b^2*E^(2*b*w + 4*d*w)*modr*mods*w^2 +
17597866272*b*d*E^(2*b*w + 4*d*w)*modr*mods*w^2 -
25182909472*d^2*E^(2*b*w + 4*d*w)*modr*mods*w^2 -
1261013432*b^2*E^(2*b*w + 6*d*w)*modr*mods*w^2 +
2522026864*b*d*E^(2*b*w + 6*d*w)*modr*mods*w^2 -
1261013432*d^2*E^(2*b*w + 6*d*w)*modr*mods*w^2 +
2512616316*d^2*E^(6*d*w)*mods^2*w^2 +
2512616316*b^2*E^(2*b*w + 2*d*w)*mods^2*w^2 -
5025232632*b*d*E^(2*b*w + 2*d*w)*mods^2*w^2 +
2512616316*d^2*E^(2*b*w + 2*d*w)*mods^2*w^2 +
2512616316*d^2*E^(4*b*w + 2*d*w)*mods^2*w^2 +
6295727368*b^2*E^(2*b*w + 4*d*w)*mods^2*w^2 -
12591454736*b*d*E^(2*b*w + 4*d*w)*mods^2*w^2 +
12591454736*d^2*E^(2*b*w + 4*d*w)*mods^2*w^2 +
2512616316*b^2*E^(2*b*w + 6*d*w)*mods^2*w^2 -
5025232632*b*d*E^(2*b*w + 6*d*w)*mods^2*w^2 +
2512616316*d^2*E^(2*b*w + 6*d*w)*mods^2*w^2 +
5006411536*b^2*d^2*E^(2*b*w + 4*d*w)*modr^2*w^4 -
10012823072*b*d^3*E^(2*b*w + 4*d*w)*modr^2*w^4 +
```

```
5006411536*d^4*E^(2*b*w + 4*d*w)*modr^2*w^4 -
10012823072*b^2*d^2*E^(2*b*w + 4*d*w)*modr*mods*w
20025646144*b*d^3*E^(2*b*w + 4*d*w)*modr*mods*w^4
10012823072*d^4*E^(2*b*w + 4*d*w)*modr*mods*w^4 +
5006411536*b^2*d^2*E^(2*b*w + 4*d*w)*mods^2*w^4 -
10012823072*b*d^3*E^(2*b*w + 4*d*w)*mods^2*w^4 +
5006411536*d^4*E^(2*b*w + 4*d*w)*mods^2*w^4));
```

□ *?b2r*

```
b2r = (133*I*(-9481437*E^(4*b*w)*modr^2 -
9481437*E^(4*d*w)*modr^2 + 9481437*E^(6*d*w)*modr
18962874*E^(2*b*w + 2*d*w)*modr^2 +
9481437*E^(4*b*w + 2*d*w)*modr^2 -
18962874*E^(2*b*w + 4*d*w)*modr^2 +
18962874*E^(4*b*w)*modr*mods -
23757126*E^(4*d*w)*modr*mods -
4758474*E^(6*d*w)*modr*mods +
4794252*E^(2*b*w + 2*d*w)*modr*mods -
4758474*E^(4*b*w + 2*d*w)*modr*mods +
9516948*E^(2*b*w + 4*d*w)*modr*mods -
9481437*E^(4*b*w)*mods^2 - 9481437*E^(4*d*w)*mods
4722963*E^(6*d*w)*mods^2 -
23757126*E^(2*b*w + 2*d*w)*mods^2 -
4722963*E^(4*b*w + 2*d*w)*mods^2 -
11834074*E^(2*b*w + 4*d*w)*mods^2 -
18962874*d*E^(6*d*w)*modr^2*w -
18962874*d*E^(4*b*w + 2*d*w)*modr^2*w +
37925748*d*E^(2*b*w + 4*d*w)*modr^2*w +
9516948*d*E^(6*d*w)*modr*mods*w +
9516948*d*E^(4*b*w + 2*d*w)*modr*mods*w +
42560000*b*E^(2*b*w + 4*d*w)*modr*mods*w -
61593896*d*E^(2*b*w + 4*d*w)*modr*mods*w +
9445926*d*E^(6*d*w)*mods^2*w +
9445926*d*E^(4*b*w + 2*d*w)*mods^2*w +
23668148*d*E^(2*b*w + 4*d*w)*mods^2*w +
9410548*b^2*E^(2*b*w + 2*d*w)*modr^2*w^2 -
18821096*b*d*E^(2*b*w + 2*d*w)*modr^2*w^2 +
9410548*d^2*E^(2*b*w + 2*d*w)*modr^2*w^2 -
9410548*b^2*E^(2*b*w + 4*d*w)*modr^2*w^2 +
18821096*b*d*E^(2*b*w + 4*d*w)*modr^2*w^2 -
9410548*d^2*E^(2*b*w + 4*d*w)*modr^2*w^2 +
9481304*b^2*E^(2*b*w + 2*d*w)*modr*mods*w^2 -
18962608*b*d*E^(2*b*w + 2*d*w)*modr*mods*w^2 +
9481304*d^2*E^(2*b*w + 2*d*w)*modr*mods*w^2 +
```

```
    18821096*b^2*E^(2*b*w + 4*d*w)*modr*mods*w^2 -
    37642192*b*d*E^(2*b*w + 4*d*w)*modr*mods*w^2 +
    18821096*d^2*E^(2*b*w + 4*d*w)*modr*mods*w^2 -
    18891852*b^2*E^(2*b*w + 2*d*w)*mods^2*w^2 +
    37783704*b*d*E^(2*b*w + 2*d*w)*mods^2*w^2 -
    18891852*d^2*E^(2*b*w + 2*d*w)*mods^2*w^2 -
    9410548*b^2*E^(2*b*w + 4*d*w)*mods^2*w^2 +
    18821096*b*d*E^(2*b*w + 4*d*w)*mods^2*w^2 -
    9410548*d^2*E^(2*b*w + 4*d*w)*mods^2*w^2 +
    18821096*b^2*d*E^(2*b*w + 4*d*w)*modr^2*w^3 -
    37642192*b*d^2*E^(2*b*w + 4*d*w)*modr^2*w^3 +
    18821096*d^3*E^(2*b*w + 4*d*w)*modr^2*w^3 -
    37642192*b^2*d*E^(2*b*w + 4*d*w)*modr*mods*w^3 +
    75284384*b*d^2*E^(2*b*w + 4*d*w)*modr*mods*w^3 -
    37642192*d^3*E^(2*b*w + 4*d*w)*modr*mods*w^3 +
    18821096*b^2*d*E^(2*b*w + 4*d*w)*mods^2*w^3 -
    37642192*b*d^2*E^(2*b*w + 4*d*w)*mods^2*w^3 +
    18821096*d^3*E^(2*b*w + 4*d*w)*mods^2*w^3))/
(w*(1261031121*E^(4*b*w)*modr^2 +
    1261031121*E^(4*d*w)*modr^2 -
    2522062242*E^(6*d*w)*modr^2 +
    1261031121*E^(8*d*w)*modr^2 -
    2522062242*E^(2*b*w + 2*d*w)*modr^2 -
    2522062242*E^(4*b*w + 2*d*w)*modr^2 +
    5044124484*E^(2*b*w + 4*d*w)*modr^2 +
    1261031121*E^(4*b*w + 4*d*w)*modr^2 -
    2522062242*E^(2*b*w + 6*d*w)*modr^2 -
    2522062242*E^(4*b*w)*modr*mods +
    3159697758*E^(4*d*w)*modr*mods -
    637635516*E^(6*d*w)*modr*mods -
    2522062242*E^(8*d*w)*modr*mods -
    637635516*E^(2*b*w + 2*d*w)*modr*mods -
    637635516*E^(4*b*w + 2*d*w)*modr*mods +
    1275271032*E^(2*b*w + 4*d*w)*modr*mods +
    3159697758*E^(4*b*w + 4*d*w)*modr*mods -
    637635516*E^(2*b*w + 6*d*w)*modr*mods +
    1261031121*E^(4*b*w)*mods^2 +
    1261031121*E^(4*d*w)*mods^2 +
    3159697758*E^(6*d*w)*mods^2 +
    1261031121*E^(8*d*w)*mods^2 +
    3159697758*E^(2*b*w + 2*d*w)*mods^2 +
    3159697758*E^(4*b*w + 2*d*w)*mods^2 +
    7917084484*E^(2*b*w + 4*d*w)*mods^2 +
    1261031121*E^(4*b*w + 4*d*w)*mods^2 +
```

```
3159697758*E^(2*b*w + 6*d*w)*mods^2 -
5044124484*d^2*E^(6*d*w)*modr^2*w^2 -
1251602884*b^2*E^(2*b*w + 2*d*w)*modr^2*w^2 +
2503205768*b*d*E^(2*b*w + 2*d*w)*modr^2*w^2 -
1251602884*d^2*E^(2*b*w + 2*d*w)*modr^2*w^2 -
5044124484*d^2*E^(4*b*w + 2*d*w)*modr^2*w^2 +
2503205768*b^2*E^(2*b*w + 4*d*w)*modr^2*w^2 -
5006411536*b*d*E^(2*b*w + 4*d*w)*modr^2*w^2 +
12591454736*d^2*E^(2*b*w + 4*d*w)*modr^2*w^2 -
1251602884*b^2*E^(2*b*w + 6*d*w)*modr^2*w^2 +
2503205768*b*d*E^(2*b*w + 6*d*w)*modr^2*w^2 -
1251602884*d^2*E^(2*b*w + 6*d*w)*modr^2*w^2 +
2531508168*d^2*E^(6*d*w)*modr*mods*w^2 -
1261013432*b^2*E^(2*b*w + 2*d*w)*modr*mods*w^2 +
2522026864*b*d*E^(2*b*w + 2*d*w)*modr*mods*w^2 -
1261013432*d^2*E^(2*b*w + 2*d*w)*modr*mods*w^2 +
2531508168*d^2*E^(4*b*w + 2*d*w)*modr*mods*w^2 +
2522026864*b^2*E^(2*b*w + 4*d*w)*modr*mods*w^2 +
17597866272*b*d*E^(2*b*w + 4*d*w)*modr*mods*w^2 -
25182909472*d^2*E^(2*b*w + 4*d*w)*modr*mods*w^2 -
1261013432*b^2*E^(2*b*w + 6*d*w)*modr*mods*w^2 +
2522026864*b*d*E^(2*b*w + 6*d*w)*modr*mods*w^2 -
1261013432*d^2*E^(2*b*w + 6*d*w)*modr*mods*w^2 +
2512616316*d^2*E^(6*d*w)*mods^2*w^2 +
2512616316*b^2*E^(2*b*w + 2*d*w)*mods^2*w^2 -
5025232632*b*d*E^(2*b*w + 2*d*w)*mods^2*w^2 +
2512616316*d^2*E^(2*b*w + 2*d*w)*mods^2*w^2 +
2512616316*d^2*E^(4*b*w + 2*d*w)*mods^2*w^2 +
6295727368*b^2*E^(2*b*w + 4*d*w)*mods^2*w^2 -
12591454736*b*d*E^(2*b*w + 4*d*w)*mods^2*w^2 +
12591454736*d^2*E^(2*b*w + 4*d*w)*mods^2*w^2 +
2512616316*b^2*E^(2*b*w + 6*d*w)*mods^2*w^2 -
5025232632*b*d*E^(2*b*w + 6*d*w)*mods^2*w^2 +
2512616316*d^2*E^(2*b*w + 6*d*w)*mods^2*w^2 +
5006411536*b^2*d^2*E^(2*b*w + 4*d*w)*modr^2*w^4 -
10012823072*b*d^3*E^(2*b*w + 4*d*w)*modr^2*w^4 +
5006411536*d^4*E^(2*b*w + 4*d*w)*modr^2*w^4 -
10012823072*b^2*d^2*E^(2*b*w + 4*d*w)*modr*mods*w
20025646144*b*d^3*E^(2*b*w + 4*d*w)*modr*mods*w^4
10012823072*d^4*E^(2*b*w + 4*d*w)*modr*mods*w^4 +
5006411536*b^2*d^2*E^(2*b*w + 4*d*w)*mods^2*w^4 -
10012823072*b*d^3*E^(2*b*w + 4*d*w)*mods^2*w^4 +
5006411536*d^4*E^(2*b*w + 4*d*w)*mods^2*w^4));
```

■ *Coefficients after Limit*

```
Clear[nur,lima0r,limb0r,lima2r,limb2r]

nur=33/100

33
---
100

lima0r  =  ((-2*I)/133*(3551100*E^(2*d*w)*modr^2  -
          3551100*E^(4*d*w)*modr^2  -
          8897800*E^(4*d*w)*modr*mods  -
          3551100*E^(2*d*w)*mods^2  -
          3551100*E^(4*d*w)*mods^2  +
          7102200*d*E^(2*d*w)*modr^2*w  -
          3564400*d*E^(2*d*w)*modr*mods*w  -
          3537800*d*E^(2*d*w)*mods^2*w  +
          4722963*d^2*E^(2*d*w)*modr^2*w^2  -
          2370326*d^2*E^(2*d*w)*modr*mods*w^2  -
          2352637*d^2*E^(2*d*w)*mods^2*w^2))/
     (-35511*modr^2*w^2  +
71022*E^(2*d*w)*modr^2*w^2  -
       35511*E^(4*d*w)*modr^2*w^2  +
71022*modr*mods*w^2  +
       17956*E^(2*d*w)*modr*mods*w^2  -
       88978*E^(4*d*w)*modr*mods*w^2  -
35511*mods^2*w^2  -
       88978*E^(2*d*w)*mods^2*w^2  -
35511*E^(4*d*w)*mods^2*w^2  +
       142044*d^2*E^(2*d*w)*modr^2*w^4  -
       71288*d^2*E^(2*d*w)*modr*mods*w^4  -
        70756*d^2*E^(2*d*w)*mods^2*w^4);
```

```
limb0r  =  (-2*I*(-26700*modr^2  +
          26700*E^(2*d*w)*modr^2  +  53400*modr*mods
-
          26700*mods^2  -  26700*E^(2*d*w)*mods^2  -
          53400*d*E^(2*d*w)*modr^2*w  +
          26800*d*E^(2*d*w)*modr*mods*w  +
          26600*d*E^(2*d*w)*mods^2*w  +
          35511*d^2*E^(2*d*w)*modr^2*w^2  -
          17822*d^2*E^(2*d*w)*modr*mods*w^2  -
          17689*d^2*E^(2*d*w)*mods^2*w^2))/
     (35511*modr^2*w^2  -
71022*E^(2*d*w)*modr^2*w^2  +
        35511*E^(4*d*w)*modr^2*w^2  -
71022*modr*mods*w^2  -
        17956*E^(2*d*w)*modr*mods*w^2  +
        88978*E^(4*d*w)*modr*mods*w^2  +
35511*mods^2*w^2  +
        88978*E^(2*d*w)*mods^2*w^2  +
35511*E^(4*d*w)*mods^2*w^2  -
        142044*d^2*E^(2*d*w)*modr^2*w^4  +
        71288*d^2*E^(2*d*w)*modr*mods*w^4  +
        70756*d^2*E^(2*d*w)*mods^2*w^4);
```

```
lima2r  =  (-I*(35511*E^(2*d*w)*modr^2  -
          35511*E^(4*d*w)*modr^2  -
          17822*E^(2*d*w)*modr*mods  -
          88978*E^(4*d*w)*modr*mods  -
          17689*E^(2*d*w)*mods^2  -
          35511*E^(4*d*w)*mods^2  +
          71022*d*E^(2*d*w)*modr^2*w  -
          35644*d*E^(2*d*w)*modr*mods*w  -
          35378*d*E^(2*d*w)*mods^2*w))/
     (w*(-35511*modr^2  +  71022*E^(2*d*w)*modr^2  -
          35511*E^(4*d*w)*modr^2  +  71022*modr*mods
+
          17956*E^(2*d*w)*modr*mods  -
88978*E^(4*d*w)*modr*mods  -
          35511*mods^2  -  88978*E^(2*d*w)*mods^2  -
          35511*E^(4*d*w)*mods^2  +
142044*d^2*E^(2*d*w)*modr^2*w^2  -
          71288*d^2*E^(2*d*w)*modr*mods*w^2  -
          70756*d^2*E^(2*d*w)*mods^2*w^2));
```

```
limb2r = (-133*I*(267*modr^2 -
267*E^(2*d*w)*modr^2 -
          534*modr*mods + 134*E^(2*d*w)*modr*mods +
          267*mods^2 + 133*E^(2*d*w)*mods^2 +
          534*d*E^(2*d*w)*modr^2*w -
          268*d*E^(2*d*w)*modr*mods*w -
          266*d*E^(2*d*w)*mods^2*w))/
     (35511*modr^2*w - 71022*E^(2*d*w)*modr^2*w +
       35511*E^(4*d*w)*modr^2*w -
71022*modr*mods*w -
       17956*E^(2*d*w)*modr*mods*w +
88978*E^(4*d*w)*modr*mods*w +
       35511*mods^2*w + 88978*E^(2*d*w)*mods^2*w +
       35511*E^(4*d*w)*mods^2*w -
142044*d^2*E^(2*d*w)*modr^2*w^3 +
       71288*d^2*E^(2*d*w)*modr*mods*w^3 +
      - 70756*d^2*E^(2*d*w)*mods^2*w^3);
```

Obtain Asymptotic Expressions for the Stress Inverse Transform Integrand Coefficient Functions using the "Limited" Coefficients

```
domexpcoeff[expr_,mant_,bigexp_,arbexp_]:=Max[Ca
ses[expr,(mant^(x2_ bigexp arbexp +
y2_)|mant^(x2_ bigexp arbexp))->x2, Infinity]]
```

```
domexp[expr_,mant_,bigexp_,arbexp_]:=Cases[expr,
(mant^(x_ bigexp arbexp + y_)|mant^(x_ bigexp
arbexp)) /; x ==
domexpcoeff[expr,mant,bigexp,arbexp], Infinity]
```

```
collectterms[expr_,formlist_]:=Sum[Coefficient[E
xpand[expr],formlist[[i]]]
formlist[[i]],{i,1,Length[formlist]}]
```

```
collectcoeff[expr_,formlist_]:=Sum[Coefficient[E
xpand[expr],formlist[[i]]],{i,1,Length[formlist]
}]
```

```
Clear[smxint,smyint,smxyint]
```

```
smxint[x_,y_]=Together[intxr[lima0r,limb0r,lima2
r,limb2r]];
```

```
smyint[x_,y_]=Together[intyr[lima0r,limb0r,lima2
r,limb2r]];
```

```
smxyint[x_,y_]=Together[inttauxyr[lima0r,limb0r,
lima2r,limb2r]];

simpxup=Max[domexpcoeff[Numerator[smxint[x,y]],E
,d,w]];

simpxdown=Max[domexpcoeff[Denominator[smxint[x,y
]],E,d,w]];

simpyup=Max[domexpcoeff[Numerator[smyint[x,y]],E
,d,w]];

simpydown=Max[domexpcoeff[Denominator[smyint[x,y
]],E,d,w]];

simpxyup=Max[domexpcoeff[Numerator[smxyint[x,y]]
,E,d,w]];

simpxydown=Max[domexpcoeff[Denominator[smxyint[x
,y]],E,d,w]];

numlstx=Union[domexp[Expand[Numerator[smxint[x,y
]]],E,d,w]]

  4 d w + 2 w y
{E             }

numlsty=Union[domexp[Expand[Numerator[smyint[x,y
]]],E,d,w]]

  4 d w + 2 w y
{E             }

numlstxy=Union[domexp[Expand[Numerator[smxyint[x
,y]]],E,d,w]]

  4 d w + 2 w y
{E             }

xpndnumx=collectcoeff[Numerator[smxint[x,y]],num
lstx];

xpndnumy=collectcoeff[Numerator[smyint[x,y]],num
lsty];

xpndnumxy=collectcoeff[Numerator[smxyint[x,y]],n
umlstxy];

denlstx=Union[domexp[Expand[Denominator[smxint[x
,y]]],E,d,w]]
```

```
  4 d w + w y
{E           }

denlsty=Union[domexp[Expand[Denominator[smyint[x
,y]]],E,d,w]]

  4 d w + w y
{E           }

denlstxy=Union[domexp[Expand[Denominator[smxyint
[x,y]]],E,d,w]]

  4 d w + w y
{E           }

xpnddenx=collectcoeff[Denominator[smxint[x,y]],d
enlstx];

xpnddeny=collectcoeff[Denominator[smyint[x,y]],d
enlsty];

xpnddenxy=collectcoeff[Denominator[smxyint[x,y]]
,denlstxy];

holdx=Expand[xpndnumx]/Expand[xpnddenx];

holdy=Expand[xpndnumy]/Expand[xpnddeny];

holdxy=Expand[xpndnumxy]/Expand[xpnddenxy];

Clear[bgxint,bgyint,bgxyint]

bgxint[x_,y_]=gbar
Simplify[Together[numlstx[[1]]/denlstx[[1]]
Normal[Series[holdx,{w,Infinity,100}]]]]

   w y            2
-(E    gbar Sqrt[--] (2 + w y))
                 Pi

bgyint[x_,y_]=gbar
Simplify[Together[numlsty[[1]]/denlsty[[1]]
Normal[Series[holdy,{w,Infinity,100}]]]]

 w y            2
E    gbar Sqrt[--] w y
                Pi

bgxyint[x_,y_]=gbar
Simplify[Together[numlstxy[[1]]/denlstxy[[1]]
Normal[Series[holdxy,{w,Infinity,100}]]]]
```

```
 w y            2
E    gbar Sqrt[—] (1 + w y)
                Pi
```

Obtain Analytic Expressions for the Asymptotic Contribution to the Stresses (integrated over w from wstar to Infinity)

Concentrated Load

```
Clear[asyconcxinthold,asyconcyinthold,asyconcxyi
nthold]
```

```
asyconcxinthold[x_,y_]=PowerExpand[Integrate[Sin
[w  x]  (-((E^(w*y)*(2  +
w*y))/Pi)),{w,wstar,Infinity}]]
```

```
(E^(wstar*y)*(-2*x*Cos[wstar*x] -

      wstar*x*y*Cos[wstar*x] + 2*y*Sin[wstar*x] +

      wstar*y^2*Sin[wstar*x] -

      y*Sin[wstar*x - 2*ArcTan[x/y]]))/(Pi*(x^2 + y^2))
```

```
asyconcyinthold[x_,y_]=PowerExpand[Integrate[Sin
[w  x]  (E^(w*y)*w*y)/Pi,{w,wstar,Infinity}]]
```

```
(E^(wstar*y)*y*(wstar*x*Cos[wstar*x] -

      wstar*y*Sin[wstar*x] + Sin[wstar*x -
2*ArcTan[x/y]]))

   /(Pi*(x^2 + y^2))
```

```
asyconcxyinthold[x_,y_]=PowerExpand[Integrate[Co
s[w  x]  (E^(w*y)*(1  +
w*y))/Pi,{w,wstar,Infinity}]]
```

```
(E^(wstar*y)*(-(y*Cos[wstar*x]) -
wstar*y^2*Cos[wstar*x] +

      y*Cos[wstar*x - 2*ArcTan[x/y]] - x*Sin[wstar*x] -

      wstar*x*y*Sin[wstar*x]))/(Pi*(x^2 + y^2))
```

Hertzian Contact Distribution

```
Clear[asydistxinthold,asydistyinthold,asydistxyi
nthold]
```

```
asydistxinthold[x_,y_]=asyconcxint[x-t,y]  t0
Sqrt[1  -  t^2/a^2]
```

```
(E^(wstar*y)*(1 - t^2/a^2)^(1/2)*t0*

    (-2*(-t + x)*Cos[wstar*(-t + x)] -

      wstar*(-t + x)*y*Cos[wstar*(-t + x)] +

      2*y*Sin[wstar*(-t + x)] +

      wstar*y^2*Sin[wstar*(-t + x)] -

      y*Sin[wstar*(-t + x) - 2*ArcTan[(-t + x)/y]]))/

  (Pi*((-t + x)^2 + y^2))
```

```
asydistyinthold[x_,y_]=asyconcyint[x-t,y]  t0
Sqrt[1  -  t^2/a^2]
```

```
(E^(wstar*y)*(1 - t^2/a^2)^(1/2)*t0*y*

    (wstar*(-t + x)*Cos[wstar*(-t + x)] -

      wstar*y*Sin[wstar*(-t + x)] +

      Sin[wstar*(-t + x) - 2*ArcTan[(-t + x)/y]]))/

  (Pi*((-t + x)^2 + y^2))
```

```
asydistxyinthold[x_,y_]=asyconcxyint[x-t,y]  t0
Sqrt[1  -  t^2/a^2]
```

```
(E^(wstar*y)*(1 - t^2/a^2)^(1/2)*t0*

    (-(y*Cos[wstar*(-t + x)]) -

      wstar*y^2*Cos[wstar*(-t + x)] +

      y*Cos[wstar*(-t + x) - 2*ArcTan[(-t + x)/y]] -
```

```
      (-t + x)*Sin[wstar*(-t + x)] -

      wstar*(-t + x)*y*Sin[wstar*(-t + x)]))/

   (Pi*((-t + x)^2 + y^2))
```

Definitions of Asymptotic Integrand Coefficients

```
Clear[gbar,ackxxn,ackyyn,ackxyn]

gbar=1/Sqrt[2  Pi]

    1
-----------
Sqrt[2 Pi]

ackxx[y_,w_]=Simplify[-(E^(w*y)*gbar*(2/Pi)^(1/2
)*(2  +  w*y))]

-((E^(w*y)*(2 + w*y))/Pi)

ackyy[y_,w_]=Simplify[E^(w*y)*gbar*(2/Pi)^(1/2)*
w*y]

(E^(w*y)*w*y)/Pi

ackxy[y_,w_]=Simplify[E^(w*y)*gbar*(2/Pi)^(1/2)*
(1  +  w*y)]

(E^(w*y)*(1 + w*y))/Pi
```

Definitions of the "Exact" Inverse Transform Integrand Coefficient Functions

Concentrated Load

```
Clear[exconcxint,exconcyint,exconcxyint,gbar]

gbar=N[1/Sqrt[2  Pi]]

0.398942

exconcxint[x_,y_]=gbar
intxr[lima0r,limb0r,lima2r,limb2r];

exconcyint[x_,y_]=gbar
intyr[lima0r,limb0r,lima2r,limb2r];
```

```
exconcxyint[x_,y_]=gbar
inttauxyr[lima0r,limb0r,lima2r,limb2r];
```

Hertzian Contact Load Distribution

```
Clear[exdistxint,exdistyint,exdistxyint,gbar]
gbar=N[PowerExpand[((a^(-2))^(1/2)*t0*(Pi/2)^(1/
2)*(a^2*w^2)^(1/2)*BesselJ[1,(a^2*w^2)^(1/2)])/w
^2]]
```

$$\frac{1.25331\ t0\ \mathrm{BesselJ}[1.,\ a\ w]}{w}$$

```
exdistxint[x_,y_]=gbar
intxr[lima0r,limb0r,lima2r,limb2r];
exdistyint[x_,y_]=gbar
intyr[lima0r,limb0r,lima2r,limb2r];
exdistxyint[x_,y_]=gbar
inttauxyr[lima0r,limb0r,lima2r,limb2r];
```

Definitions of the Asymptotic Stress Functions

Concentrated Load

```
Clear[asyconcxint,asyconcyint,asyconcxyint]
asyconcxint[x_,y_]=(E^(wstar*y)*(-2*x*Cos[wstar*
x] - wstar*x*y*Cos[wstar*x] + 2*y*Sin[wstar*x] +
wstar*y^2*Sin[wstar*x] - y*Sin[wstar*x -
2*ArcTan[x/y]]))/(Pi*(x^2 + y^2));
asyconcyint[x_,y_]=(E^(wstar*y)*y*(wstar*x*Cos[w
star*x] - wstar*y*Sin[wstar*x] + Sin[wstar*x -
2*ArcTan[x/y]]))/(Pi*(x^2 + y^2));
asyconcxyint[x_,y_]=(E^(wstar*y)*(-(y*Cos[wstar*
x]) - wstar*y^2*Cos[wstar*x] + y*Cos[wstar*x -
2*ArcTan[x/y]] - x*Sin[wstar*x] -
wstar*x*y*Sin[wstar*x]))/(Pi*(x^2 + y^2));
```

Hertzian Contact Distribution

```
Clear[asydistxint,asydistyint,asydistxyint]
```

```
asydistxint[x_,y_]=(E^(wstar*y)*(1 -
t^2/a^2)^(1/2)*t0*(-2*(-t + x)*Cos[wstar*(-t +
x)] - wstar*(-t + x)*y*Cos[wstar*(-t + x)] +
2*y*Sin[wstar*(-t + x)] +
wstar*y^2*Sin[wstar*(-t + x)] - y*Sin[wstar*(-t
+ x) - 2*ArcTan[(-t + x)/y]]))/(Pi*((-t + x)^2 +
y^2));
```

```
asydistyint[x_,y_]=(E^(wstar*y)*(1 -
t^2/a^2)^(1/2)*t0*y*(wstar*(-t +
x)*Cos[wstar*(-t + x)] - wstar*y*Sin[wstar*(-t +
x)] + Sin[wstar*(-t + x) - 2*ArcTan[(-t +
x)/y]]))/(Pi*((-t + x)^2 + y^2));
```

```
asydistxyint[x_,y_]=(E^(wstar*y)*(1 -
t^2/a^2)^(1/2)*t0*(-(y*Cos[wstar*(-t + x)]) -
wstar*y^2*Cos[wstar*(-t + x)] + y*Cos[wstar*(-t
+ x) - 2*ArcTan[(-t + x)/y]] - (-t +
x)*Sin[wstar*(-t + x)] - wstar*(-t +
x)*y*Sin[wstar*(-t + x)]))/(Pi*((-t + x)^2 +
y^2));
```

Definitions of Stress Components

Close to the Load

```
Clear[sigx,sigy,tauxy,wstar]
```

```
sigx[x_,y_]:=NIntegrate[Sin[w x]
exdistxint[x,y],{w,0,wstar},MaxRecursion->20] +
NIntegrate[asydistxint[x,y],{t,-a,a},MaxRecursio
n->20]
```

```
sigy[x_,y_]:=NIntegrate[Sin[w x]
exdistyint[x,y],{w,0,wstar},MaxRecursion->20] +
NIntegrate[asydistyint[x,y],{t,-a,a},MaxRecursio
n->20]
```

```
tauxy[x_,y_]:=NIntegrate[Cos[w  x]
exdistxyint[x,y],{w,0,wstar},MaxRecursion->20]  +
NIntegrate[asydistxyint[x,y],{t,-a,a},MaxRecursi
on->20]
```

■ *Far from the Load*

```
Clear[sigxfar,sigyfar,tauxyfar,wstar]

sigxfar[x_,y_]:=(NIntegrate[Sin[w  x]
exconcxint[x,y],{w,0,wstar},MaxRecursion->20]  +
N[asyconcxint[x,y]])  frictionfact
wheelload/railthick

sigyfar[x_,y_]:=(NIntegrate[Sin[w  x]
exconcyint[x,y],{w,0,wstar},MaxRecursion->20]  +
N[asyconcyint[x,y]])  frictionfact
wheelload/railthick

tauxyfar[x_,y_]:=(NIntegrate[Cos[w  x]
exconcxyint[x,y],{w,0,wstar},MaxRecursion->20]  +
N[asyconcxyint[x,y]])  frictionfact
wheelload/railthick
```

■ *Problem Constants (Poisson's Ratio for the rail and support have been given the value 0.33)*

■ *Contact Expressions*

```
Clear[a,wheelload,wheelradius,ymodr,delta,railth
ick,raildepth,railinertia,n0]

delta=4  wheelradius  (1  -  (33  /  100)^2)  /  ymodr;

railthick=N[12  railinertia  /  raildepth^3];

a=N[Simplify[PowerExpand[Sqrt[2  wheelload  delta
/  (railthick  Pi)]]]]
```

$$\frac{0.434853\ \text{raildepth}^{3/2}\ \text{Sqrt[wheelload]}\ \text{Sqrt[wheelradius]}}{\text{Sqrt[railinertia]}\ \text{Sqrt[ymodr]}}$$

```
n0=N[Simplify[PowerExpand[2 wheelload / (Pi a
railthick)]]]
```

$$\frac{0.121999\ \text{raildepth}^{3/2}\ \text{Sqrt[wheelload]}\ \text{Sqrt[ymodr]}}{\text{Sqrt[railinertia]}\ \text{Sqrt[wheelradius]}}$$

```
t0=frictionfact*n0
```

$$(0.121999\ \text{frictionfact raildepth}^{3/2}\ \text{Sqrt[wheelload]}\ \text{Sqrt[ymodr]})\ /\ (\text{Sqrt[railinertia]}\ \text{Sqrt[wheelradius]})$$

■ *User-Defined Constants*

Track Modulus [kips per inch per inch]

```
trackmod=5.
```

5.

Young's Modulus for the Rail [MPa]

```
youngmodrail=206843.
```

206843.

Vertical Wheel Load [MN]

```
wheelload=0.17348
```

0.17348

Radius of the Wheel [m]

```
wheelradius=0.4826
```

0.4826

Depth of the Rail [m]

```
raildepth=0.18574
```

0.18574

Strong-Axis Moment of Inertia for the Rail [m^4]

```
railinertia=0.0000395
```

0.0000395

Tangential Load Factor (will multiply n0)

```
frictionfact=1.
```

1.

□ *assignment of constants to notebook variables*

```
Clear[modr,ymodr,mods,d]
modr=N[youngmodrail/(2  (1+33/100))]
```

77760.5

```
ymodr=N[youngmodrail]
```

206843.

```
mods=6.894757  (67.92*trackmod  -  3.88*trackmod^2
+  0.172*trackmod^3)
```

1820.91

```
d=N[raildepth]
```

0.18574

■ *Check Some Values*

```
a
```

0.00352371

```
n0
```

423.709

```
t0
```

423.709

```
wstar=50.
```

50.

```
x=.001
```

0.001

```
y=-.003
-0.003
sigx[x,y]
-38.5685
sigy[x,y]
-43.9883
tauxy[x,y]
70.6767
x=.5
0.5
sigx[x,y]
-9.7009
sigy[x,y]
-0.000198212
tauxy[x,y]
0.0473503
sigxfar[x,y]
-9.70083
sigyfar[x,y]
-0.000198212
tauxyfar[x,y]
0.0473499
```

Calculation of Stresses

Some Preliminary Issues

Determine wstar

```
Clear[x,y,w,asympnt]
```

```
asympnt[asymp_,exact_,var_,toler_]  :=  Module[
     {relerr,ex,as,step},
     ex  =  Compile[{var},exact];
     as  =  Compile[{var},asymp];
    relerr  =  2  toler;
    step  =  3.;

    While[
        relerr > toler,
        step  =  step  +  1.;
        relerr  =  Abs[(as[step]  -
ex[step])/ex[step]];
    ];

    step
]
```

```
y=-.0254
```

```
-0.0254
```

```
asympnt[ackxx[y,w],1/Sqrt[2  Pi]
intxr[lima0r,limb0r,lima2r,limb2r],w,.0001]
```

```
43.
```

```
asympnt[ackyy[y,w],1/Sqrt[2  Pi]
intyr[lima0r,limb0r,lima2r,limb2r],w,.0001]
```

```
42.
```

```
asympnt[ackxy[y,w],1/Sqrt[2  Pi]
inttauxyr[lima0r,limb0r,lima2r,limb2r],w,.0001]
```

```
49.
```

```
wstar=50
```

```
50
```

□ *A Couple of Useful Functions*

```
reflecteven[{aa__}]:=Flatten[Append[{aa},
Reverse[{aa}]]]
```

```
reflectodd[{aa__}]:=Flatten[Append[{aa},
Reverse[-{aa}]]]
```

```
reflecteven[{9,8,7,6,5,4,3,2,1,0}]
{9, 8, 7, 6, 5, 4, 3, 2, 1, 0, 0, 1, 2, 3, 4, 5, 6, 7,
  8, 9}
reflectodd[{9,8,7,6,5,4,3,2,1,0}]
{9, 8, 7, 6, 5, 4, 3, 2, 1, 0, 0, -1, -2, -3, -4, -5,
  -6, -7, -8, -9}
```

APPENDIX D

Mathematica Notebook for the Discontinuity Analysis and Fatigue Evaluation

```
1 + 1
```

```
2
```

Integral Definitions for the Ellipsoidal Inclusion

Initialize the Parameters used in the Integral Difinitions

```
Clear[q,r,ia,ib,ic,iaa,iab,iac,ibb,ibc,icc,f,g,h
,j,s]
```

Define the Elliptic Integrals (Eshelby 1957, 384-385)

```
q[j ]=3/(8  Pi  (1-j));
r[j ]=(1-2  j)/(8  Pi  (1-j));
ia[f_,g_,h_]=(4  Pi  f  g  h)/((f^2-g^2)
Sqrt[f^2-h^2])(EllipticF[ArcSin[Sqrt[1-h^2/f^2]]
,(f^2-g^2)/(f^2-h^2)]-EllipticE[ArcSin[Sqrt[1-h^
2/f^2]],(f^2-g^2)/(f^2-h^2)]);
ic[f_,g_,h_]=(4  Pi  f  g  h)/((g^2-h^2)
Sqrt[f^2-h^2])((g  Sqrt[f^2-h^2])/(f
h)-EllipticE[ArcSin[Sqrt[1-h^2/f^2]],(f^2-g^2)/(
f^2-h^2)]);
ib[f ,g ,h ]=4  Pi  -  ia[f,g,h]  -  ic[f,g,h];
iab[f_,g_,h_]=(ib[f,g,h]-ia[f,g,h])/(3
(f^2-g^2));
iac[f_,g_,h_]=(ic[f,g,h]-ia[f,g,h])/(3
(f^2-h^2));
ibc[f_,g_,h_]=(ic[f,g,h]-ib[f,g,h])/(3
(g^2-h^2));
iaa[f_,g_,h_]=4  Pi/(3
f^2)-iab[f,g,h]-iac[f,g,h];
ibb[f_,g_,h_]=4  Pi/(3
g^2)-iab[f,g,h]-ibc[f,g,h];
icc[f_,g_,h_]=4  Pi/(3
h^2)-iac[f,g,h]-ibc[f,g,h];
```

Define the Components of the Tensor which Relates the Equivalent Transformarion Strain to the Constrained Strain (Eshelby 1957, 384)

```
s[1,1,1,1][f_,g_,h_,j_]=q[j]  f^2  iaa[f,g,h]+r[j]
ia[f,g,h];

s[1,1,2,2][f_,g_,h_,j_]=q[j]  g^2  iab[f,g,h]-r[j]
ia[f,g,h];

s[1,1,3,3][f_,g_,h_,j_]=q[j]  h^2  iac[f,g,h]-r[j]
ia[f,g,h];

s[2,2,1,1][f_,g_,h_,j_]=q[j]  f^2  iab[f,g,h]-r[j]
ib[f,g,h];

s[2,2,2,2][f_,g_,h_,j_]=q[j]  g^2  ibb[f,g,h]+r[j]
ib[f,g,h];

s[2,2,3,3][f_,g_,h_,j_]=q[j]  h^2  ibc[f,g,h]-r[j]
ib[f,g,h];

s[3,3,1,1][f_,g_,h_,j_]=q[j]  f^2  iac[f,g,h]-r[j]
ic[f,g,h];

s[3,3,2,2][f_,g_,h_,j_]=q[j]  g^2  ibc[f,g,h]-r[j]
ic[f,g,h];

s[3,3,3,3][f_,g_,h_,j_]=q[j]  h^2  icc[f,g,h]+r[j]
ic[f,g,h];

s[1,2,1,2][f_,g_,h_,j_]=q[j]/2  (f^2+g^2)
iab[f,g,h]+r[j]/2  (ia[f,g,h]+ib[f,g,h]);

s[1,3,1,3][f_,g_,h_,j_]=q[j]/2  (f^2+h^2)
iac[f,g,h]+r[j]/2  (ia[f,g,h]+ic[f,g,h]);

s[2,3,2,3][f_,g_,h_,j_]=q[j]/2  (g^2+h^2)
ibc[f,g,h]+r[j]/2  (ib[f,g,h]+ic[f,g,h]);
```

Definitions of the Problem Parameters

Elastic Property Assignments

The ellipsoidal inhomogeneity can model the behavior of a pore or an elastic bonded discontinuity depending upon the definitions of its elastic properties. All units should be compatible with the remote tractions.

```
Clear[youngmatrix, younginhomog, poissonmatrix,
poissoninhomog]
youngmatrix=30000.;
poissonmatrix=0.3;
younginhomog=0.;
poissoninhomog=0.25;
```

Definition of the Inhomogeneous Inclusion's Free-Transformation Strain Tensor

```
Clear[epsp]
epsp[1,1]=0.;
epsp[1,2]=0.;
epsp[1,3]=0.;
epsp[2,2]=0.;
epsp[2,3]=0.;
epsp[3,3]=0.;
```

Definition of Ellipsoid's Shape

The local coordinate axes have been selected so that the equation of the ellipsoid is

x^2 / a^2 + y^2 / b^2 + z^2 /c^2 = d.

(The problem was solved taking "d" as unity and specifying the strict inequality a>b>c.)

```
Clear[a,b,c]
a=1.;
b=.99999;
c=.99998;
```

Simultaneous Equations for Determination of the Equivalent Inclusion Strains

Equivalent Extension Strains

```
Clear[epsa,epst,lambda1,lambda,mu1,mu,sigma]

sigma=poissonmatrix;

lambda1=(younginhomog
poissoninhomog)/((1+poissoninhomog)  (1-2
poissoninhomog));

mu1=younginhomog/(2  (1+poissoninhomog));

lambda=(youngmatrix
poissonmatrix)/((1+poissonmatrix)  (1-2
poissonmatrix));

mu=youngmatrix/(2  (1+poissonmatrix));

eq1=Expand[(lambda1-lambda)Sum[s[m,m,p,p][a,b,c,
sigma]  epst[p,p],{p,1,3},{m,1,3}]+
2(mu1-mu)  Sum[s[1,1,m,m][a,b,c,sigma]
epst[m,m],{m,1,3}]+lambda
Sum[epst[m,m],{m,1,3}]+2  mu  epst[1,1]];

eq2=Expand[(lambda1-lambda)Sum[s[m,m,p,p][a,b,c,
sigma]  epst[p,p],{p,1,3},{m,1,3}]+
2(mu1-mu)  Sum[s[2,2,m,m][a,b,c,sigma]
epst[m,m],{m,1,3}]+lambda
Sum[epst[m,m],{m,1,3}]+2  mu  epst[2,2]];

eq3=Expand[(lambda1-lambda)Sum[s[m,m,p,p][a,b,c,
sigma]  epst[p,p],{p,1,3},{m,1,3}]+
2(mu1-mu)  Sum[s[3,3,m,m][a,b,c,sigma]
epst[m,m],{m,1,3}]+lambda
Sum[epst[m,m],{m,1,3}]+2  mu  epst[3,3]];

rhs1=(lambda-lambda1)Sum[s[m,m,p,p][a,b,c,sigma]
epsp[p,p],{p,1,3},{m,1,3}]+
2(mu-mu1)  Sum[s[1,1,m,m][a,b,c,sigma]
epsp[m,m],{m,1,3}]+
(lambda1-lambda)  Sum[epsp[m,m],{m,1,3}]+2
(mu1-mu)  epsp[1,1]+(lambda-lambda1)
Sum[epsa[i,i],{i,1,3}]+2(mu-mu1)epsa[1,1];
```

```
rhs2=(lambda-lambda1)Sum[s[m,m,p,p][a,b,c,sigma]
epsp[p,p],{p,1,3},{m,1,3}]+
2(mu-mu1)  Sum[s[2,2,m,m][a,b,c,sigma]
epsp[m,m],{m,1,3}]+
(lambda1-lambda)  Sum[epsp[m,m],{m,1,3}]+2
(mu1-mu)  epsp[2,2]+(lambda-lambda1)
Sum[epsa[i,i],{i,1,3}]+2(mu-mu1)epsa[2,2];

rhs3=(lambda-lambda1)Sum[s[m,m,p,p][a,b,c,sigma]
epsp[p,p],{p,1,3},{m,1,3}]+
2(mu-mu1)  Sum[s[3,3,m,m][a,b,c,sigma]
epsp[m,m],{m,1,3}]+
(lambda1-lambda)  Sum[epsp[m,m],{m,1,3}]+2
(mu1-mu)  epsp[3,3]+(lambda-lambda1)
Sum[epsa[i,i],{i,1,3}]+2(mu-mu1)epsa[3,3];

mat={{Coefficient[eq1,epst[1,1]],Coefficient[eq1
,epst[2,2]],Coefficient[eq1,epst[3,3]]},
{Coefficient[eq2,epst[1,1]],Coefficient[eq2,epst
[2,2]],Coefficient[eq2,epst[3,3]]},
{Coefficient[eq3,epst[1,1]],Coefficient[eq3,epst
[2,2]],Coefficient[eq3,epst[3,3]]}};

extensions=LinearSolve[mat,{rhs1,rhs2,rhs3}];

epst[1,1]=Simplify[extensions[[1]]];

epst[2,2]=Simplify[extensions[[2]]];

epst[3,3]=Simplify[extensions[[3]]];
```

■ Equivalent Shear Strains

```
epst[1,2]=Simplify[(mu-mu1)/(2  (mu1-mu)
s[1,2,1,2][a,b,c,sigma]  +mu)  ((2
s[1,2,1,2][a,b,c,sigma]-1)
epsp[1,2]+epsa[1,2])];

epst[1,3]=Simplify[(mu-mu1)/(2  (mu1-mu)
s[1,3,1,3][a,b,c,sigma]  +mu)  ((2
s[1,3,1,3][a,b,c,sigma]-1)
epsp[1,3]+epsa[1,3])];

epst[2,3]=Simplify[(mu-mu1)/(2  (mu1-mu)
s[2,3,2,3][a,b,c,sigma]  +mu)  ((2
s[2,3,2,3][a,b,c,sigma]-1)
epsp[2,3]+epsa[2,3])];
```

Solution for the General Ellipsoid

The shape is defined above using "a," "b," and "c"

Definitions of Applied Strain Components (Hooke's Law)

```
Clear[pappl,n,epsa]

epsa[1,1]=1/youngmatrix
(pappl[1,1]-poissonmatrix(pappl[2,2]+pappl[3,3])
);

epsa[2,2]=1/youngmatrix
(pappl[2,2]-poissonmatrix(pappl[1,1]+pappl[3,3])
);

epsa[3,3]=1/youngmatrix
(pappl[3,3]-poissonmatrix(pappl[2,2]+pappl[1,1])
);

epsa[1,2]=pappl[1,2]/(2  mu);

epsa[1,3]=pappl[1,3]/(2  mu);

epsa[2,3]=pappl[2,3]/(2  mu);
```

Definitions of Scalar and Deviatoric Strain Components

```
Clear[m,n,tra,deva,trc,devc,trep,devep,trt,devt]
;

tra=epsa[1,1]+epsa[2,2]+epsa[3,3];

deva[1,1]=2/3  epsa[1,1]-1/3
(epsa[2,2]+epsa[3,3]);

deva[1,2]=epsa[1,2];

deva[1,3]=epsa[1,3];

deva[2,2]=2/3  epsa[2,2]-1/3
(epsa[1,1]+epsa[3,3]);

deva[2,3]=epsa[2,3];

deva[3,3]=2/3  epsa[3,3]-1/3
(epsa[1,1]+epsa[2,2]);

deva[2,1]=deva[1,2];

deva[3,2]=deva[2,3];
```

```
deva[3,1]=deva[1,3];

trep=epsp[1,1]+epsp[2,2]+epsp[3,3];

devep[1,1]=2/3  epsp[1,1]-1/3
(epsp[2,2]+epsp[3,3]);

devep[1,2]=epsp[1,2];

devep[1,3]=epsp[1,3];

devep[2,2]=2/3  epsp[2,2]-1/3
(epsp[1,1]+epsp[3,3]);

devep[2,3]=epsp[2,3];

devep[3,3]=2/3  epsp[3,3]-1/3
(epsp[1,1]+epsp[2,2]);

devep[2,1]=devep[1,2];

devep[3,2]=devep[2,3];

devep[3,1]=devep[1,3];

trc=Sum[s[m,m,n,n][a,b,c,sigma]
epst[n,n],{n,1,3},{m,1,3}]+Sum[s[m,m,n,n][a,b,c,
sigma]  epsp[n,n],{n,1,3},{m,1,3}];

devc[1,1]=2/3  (s[1,1,1,1][a,b,c,sigma]
epst[1,1]+s[1,1,2,2][a,b,c,sigma]
epst[2,2]+s[1,1,3,3][a,b,c,sigma]  epst[3,3])-
1/3  (s[2,2,1,1][a,b,c,sigma]
epst[1,1]+s[2,2,2,2][a,b,c,sigma]
epst[2,2]+s[2,2,3,3][a,b,c,sigma]  epst[3,3]+
s[3,3,1,1][a,b,c,sigma]
epst[1,1]+s[3,3,2,2][a,b,c,sigma]
epst[2,2]+s[3,3,3,3][a,b,c,sigma]  epst[3,3])+2/3
(s[1,1,1,1][a,b,c,sigma]
epsp[1,1]+s[1,1,2,2][a,b,c,sigma]
epsp[2,2]+s[1,1,3,3][a,b,c,sigma]  epsp[3,3])-
1/3  (s[2,2,1,1][a,b,c,sigma]
epsp[1,1]+s[2,2,2,2][a,b,c,sigma]
epsp[2,2]+s[2,2,3,3][a,b,c,sigma]  epsp[3,3]+
s[3,3,1,1][a,b,c,sigma]
epsp[1,1]+s[3,3,2,2][a,b,c,sigma]
epsp[2,2]+s[3,3,3,3][a,b,c,sigma]  epsp[3,3]);

devc[1,2]=2  s[1,2,1,2][a,b,c,sigma]  epst[1,2]+2
s[1,2,1,2][a,b,c,sigma]  epsp[1,2];

devc[1,3]=2  s[1,3,1,3][a,b,c,sigma]  epst[1,3]+2
s[1,3,1,3][a,b,c,sigma]  epsp[1,3];
```

```
devc[2,2]=2/3  (s[2,2,1,1][a,b,c,sigma]
epst[1,1]+s[2,2,2,2][a,b,c,sigma]
epst[2,2]+s[2,2,3,3][a,b,c,sigma]  epst[3,3])-
1/3  (s[1,1,1,1][a,b,c,sigma]
epst[1,1]+s[1,1,2,2][a,b,c,sigma]
epst[2,2]+s[1,1,3,3][a,b,c,sigma]  epst[3,3]+
s[3,3,1,1][a,b,c,sigma]
epst[1,1]+s[3,3,2,2][a,b,c,sigma]
epst[2,2]+s[3,3,3,3][a,b,c,sigma]  epst[3,3])+2/3
(s[2,2,1,1][a,b,c,sigma]
epsp[1,1]+s[2,2,2,2][a,b,c,sigma]
epsp[2,2]+s[2,2,3,3][a,b,c,sigma]  epsp[3,3])-
1/3  (s[1,1,1,1][a,b,c,sigma]
epsp[1,1]+s[1,1,2,2][a,b,c,sigma]
epsp[2,2]+s[1,1,3,3][a,b,c,sigma]  epsp[3,3]+
s[3,3,1,1][a,b,c,sigma]
epsp[1,1]+s[3,3,2,2][a,b,c,sigma]
epsp[2,2]+s[3,3,3,3][a,b,c,sigma]  epsp[3,3]);

devc[2,3]=2  s[2,3,2,3][a,b,c,sigma]  epst[2,3]+2
s[2,3,2,3][a,b,c,sigma]  epsp[2,3];

devc[3,3]=2/3  (s[3,3,1,1][a,b,c,sigma]
epst[1,1]+s[3,3,2,2][a,b,c,sigma]
epst[2,2]+s[3,3,3,3][a,b,c,sigma]  epst[3,3])-
1/3  (s[2,2,1,1][a,b,c,sigma]
epst[1,1]+s[2,2,2,2][a,b,c,sigma]
epst[2,2]+s[2,2,3,3][a,b,c,sigma]  epst[3,3]+
s[1,1,1,1][a,b,c,sigma]
epst[1,1]+s[1,1,2,2][a,b,c,sigma]
epst[2,2]+s[1,1,3,3][a,b,c,sigma]  epst[3,3])+2/3
(s[3,3,1,1][a,b,c,sigma]
epsp[1,1]+s[3,3,2,2][a,b,c,sigma]
epsp[2,2]+s[3,3,3,3][a,b,c,sigma]  epsp[3,3])-
1/3  (s[2,2,1,1][a,b,c,sigma]
epsp[1,1]+s[2,2,2,2][a,b,c,sigma]
epsp[2,2]+s[2,2,3,3][a,b,c,sigma]  epsp[3,3]+
s[1,1,1,1][a,b,c,sigma]
epsp[1,1]+s[1,1,2,2][a,b,c,sigma]
epsp[2,2]+s[1,1,3,3][a,b,c,sigma]  epsp[3,3]);

devc[2,1]=devc[1,2];

devc[3,2]=devc[2,3];

devc[3,1]=devc[1,3];

trt=epst[1,1]+epst[2,2]+epst[3,3];

devt[1,1]=2/3  epst[1,1]-1/3
(epst[2,2]+epst[3,3]);

devt[1,2]=epst[1,2];
```

```
devt[1,3]=epst[1,3];

devt[2,2]=2/3  epst[2,2]-1/3
(epst[1,1]+epst[3,3]);

devt[2,3]=epst[2,3];

devt[3,3]=2/3  epst[3,3]-1/3
(epst[1,1]+epst[2,2]);

devt[2,1]=devt[1,2];

devt[3,2]=devt[2,3];

devt[3,1]=devt[1,3];
```

■ Definitions of the Stress Components at the Inhomogeneity's Surface in the Matrix (Eshelby 1957, 380)

```
Clear[i,l,j2,k,u,v,n,delt,trp,devp,p]

delt[1,1]=1;

delt[2,2]=1;

delt[3,3]=1;

delt[1,2]=0;

delt[1,3]=0;

delt[2,3]=0;

delt[2,1]=0;

delt[3,1]=0;

delt[3,2]=0;

trp=(3  lambda+2  mu)  (trc+tra-1/3  (trt+trep)
(1+sigma)/(1-sigma)-
(1-2  sigma)/(1-sigma)  Sum[(devt[u,v]+devep[u,v])
n[u]  n[v],{u,1,3},{v,1,3}]);

devp[i_,l_]=2  mu
(devc[i,l]+deva[i,l]+1/(1-sigma)
Sum[(devt[j2,k]+devep[j2,k])  n[j2]  n[k]  n[i]
n[l],{j2,1,3},{k,1,3}]-
Sum[(devt[i,k]+devep[i,k])  n[k]
n[l],{k,1,3}]-Sum[(devt[l,k]+devep[l,k])  n[k]
n[i],{k,1,3}]+
(1-2  sigma)/(3  (1-sigma))
Sum[(devt[j2,k]+devep[j2,k])  n[j2]
n[k],{j2,1,3},{k,1,3}]  delt[i,l]-
1/3  (1+sigma)/(1-sigma)  (trt+trep)  (n[i]
n[l]-1/3  delt[i,l]));
```

■ **This is the stress tensor for an unspecified point on the surface of the inhomogeneity for an unspecified remote-traction system. A point is specified by its unit normal vector, `n[i]`. A remote traction system is specified by its independent components through `pappl[i,j]`.**

```
p[i ,l ]=devp[i,l]+1/3  trp  delt[i,l];
```

□ **An Example for a Spherical Pore in a Steel Matrix**

```
n[1]=0.
0.
n[2]=1.
1.
n[3]=0.
0.
pappl[1,1]=0.
0.
pappl[1,2]=0.
0.
pappl[1,3]=0.
0.
pappl[2,2]=0.
0.
pappl[2,3]=0.
0.
pappl[3,3]=1.
1.
{{p[1,1],p[1,2],p[1,3]},{p[2,1],p[2,2],p[2,3]},{
p[3,1],p[3,2],p[3,3]}}  //  MatrixForm
```

0.136368	0.	0.
0.	$1.11022\ 10^{-16}$	0.
0.	0.	2.04547

Below is an application of the solution to fatigue. The "critical" fatigue plane is determined using Findley's Parameter at a selection of material points that lie in the matrix at the surface of the ellipsoidal inhomogeneity.

Residual Stresses (Steele and Joerms 1993, 4-6,44)

longitudinal

```
datlong={{0,-22},{-.15,-13},{-.3,-3},{-.45,7},{-
.6,16},{-.75,19},{-.9,14},{-1.05,8},{-1.2,1}}
```

```
{{0, -22}, {-0.15, -13}, {-0.3, -3}, {-0.45, 7}, {-0.6,
16},
  {-0.75, 19}, {-0.9, 14}, {-1.05, 8}, {-1.2, 1}}
```

```
Fit[datlong,{1,dep,dep^2,dep^3,dep^4,dep^5},dep]
```

```
-21.93473193473193472 - 54.2517482517482515*dep +

  9.42760942760942916 7*dep^2 -
158.7239920573253869*dep^3 -

  346.4847909292353696*dep^4 -
156.1675635749709809*dep^5
```

```
longplt=ListPlot[datlong]
```

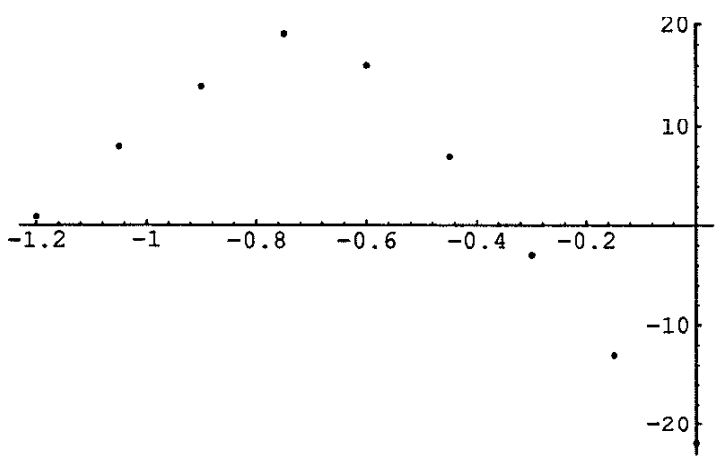


```
-Graphics-
```

```
longpltfit=Plot[-21.6184926184926185 -
24.77121643788310444*dep +

  216.7400500733834072*dep^2 +
331.2517386591460672*dep^3 +

  122.0178997956775738*dep^4,{dep,-1.2,0}]
```

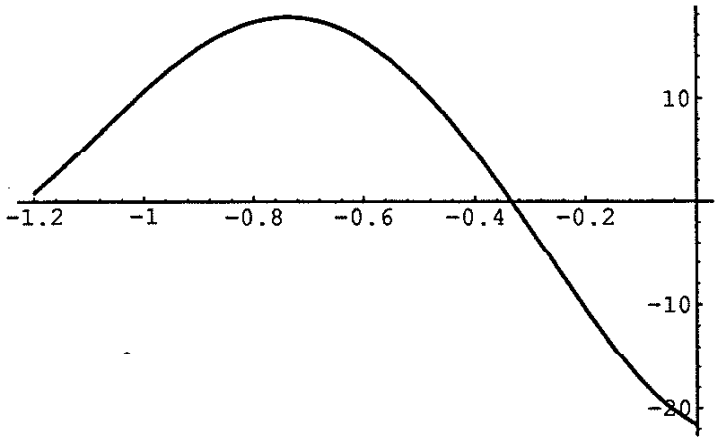


```
-Graphics-
```

□ **transverse**

```
dattran={{0,-27},{-.15,-10},{-.3,2},{-.45,24},{-
.6,36},{-.75,36},{-.9,30},{-1.05,3},{-1.2,-20}}

{{0, -27}, {-0.15, -10}, {-0.3, 2}, {-0.45, 24}, {-0.6,
36},
  {-0.75, 36}, {-0.9, 30}, {-1.05, 3}, {-1.2, -20}}

Fit[dattran,{1,dep,dep^2,dep^3,dep^4},dep]

-25.8787878787878788 - 35.89225589225589223*dep +

  381.9865319865319866*dep^2 +
564.9083426861204639*dep^3 +

  187.0557426112981669*dep^4
```

```
tranplt=ListPlot[dattran]
```

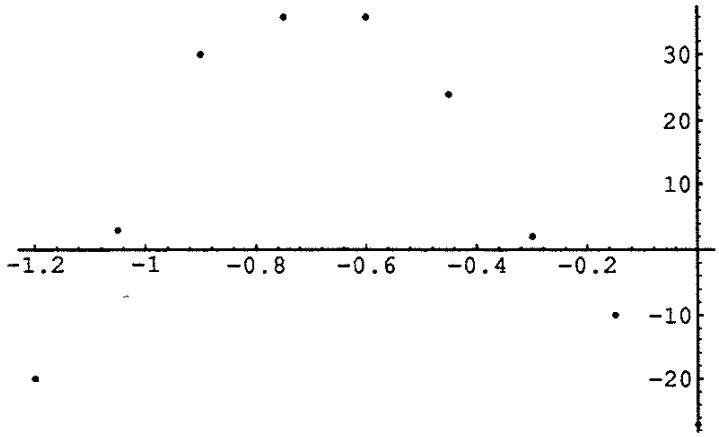


```
-Graphics-
```

```
tranpltfit=Plot[-25.8787878787878788 -
35.89225589225589223*dep +

  381.9865319865319866*dep^2 +
564.9083426861204639*dep^3 +

  187.0557426112981669*dep^4,{dep,-1.2,0}]
```

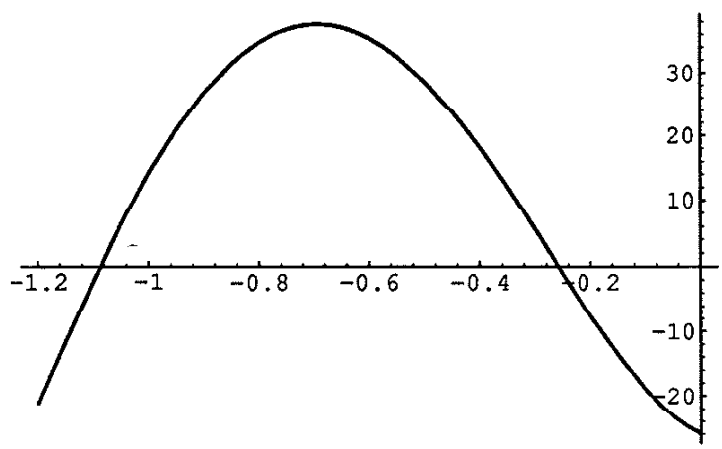


```
-Graphics-
```

◻ vertical

```
datvert={{0,0},{-.15,-30},{-.3,-10},{-.45,3},{-.
6,7},{-.75,6},{-.9,5},{-1.05,0},{-1.2,-7}}
```

```
{{0, 0}, {-0.15, -30}, {-0.3, -10}, {-0.45, 3}, {-0.6,
7},
  {-0.75, 6}, {-0.9, 5}, {-1.05, 0}, {-1.2, -7}}
```

```
Fit[datvert,{1,dep,dep^2,dep^3,dep^4,dep^5,dep^6
},dep]
```

```
-0.02828282828282761931 + 627.4718466718467091*dep +

  4194.044778267000808*dep^2 +
10732.25992114881108*dep^3 +

  13405.43772642538234*dep^4 +
8196.405332207802498*dep^5 +

  1959.050957679215881*dep^6
```

```
vertplt=ListPlot[datvert]
```

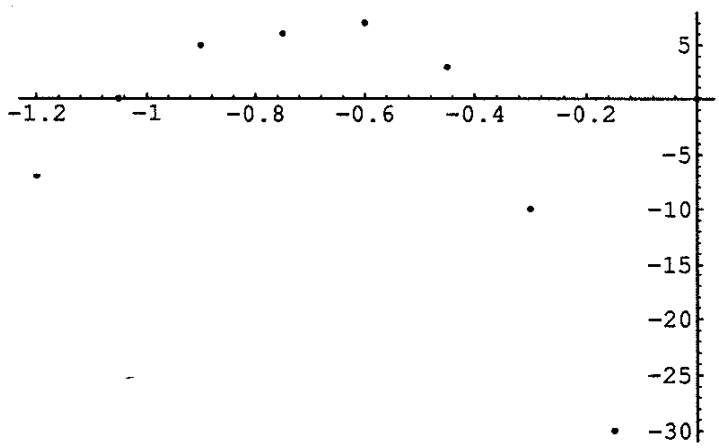


```
-Graphics-
```

```
vertpltfit=Plot[-0.02828282828282761931 +
627.4718466718467091*dep +

  4194.044778267000808*dep^2 +
10732.25992114881108*dep^3 +

  13405.43772642538234*dep^4 +
8196.405332207802498*dep^5 +

  1959.050957679215881*dep^6,{dep,-1.2,0}]
```

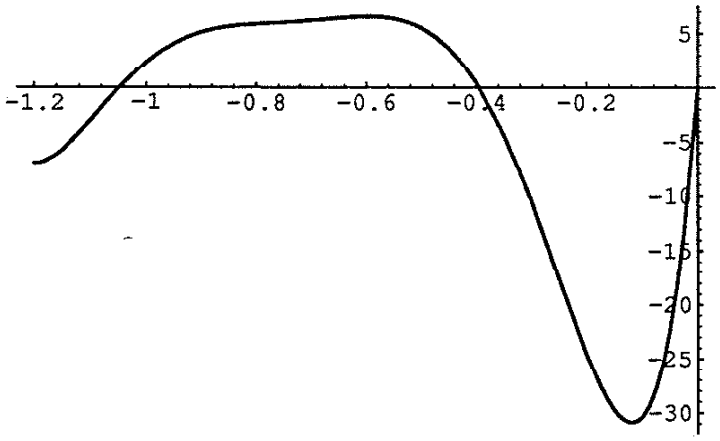

-Graphics-

□ **polynomial fit results**

```
Show[longplt,longpltfit]
```

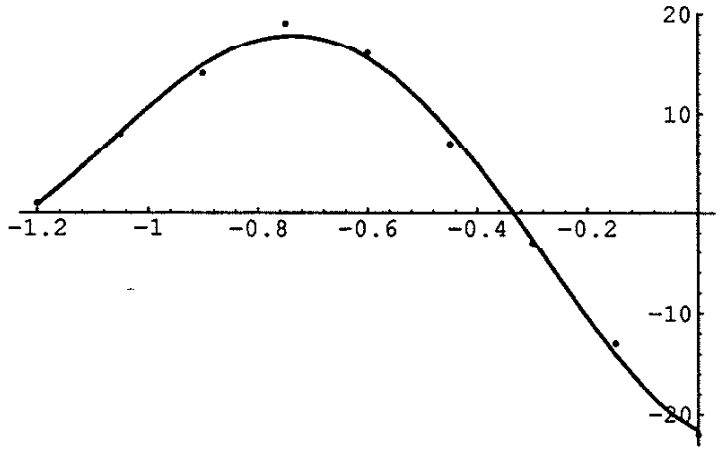

-Graphics-

```
Show[tranplt,tranpltfit]
```

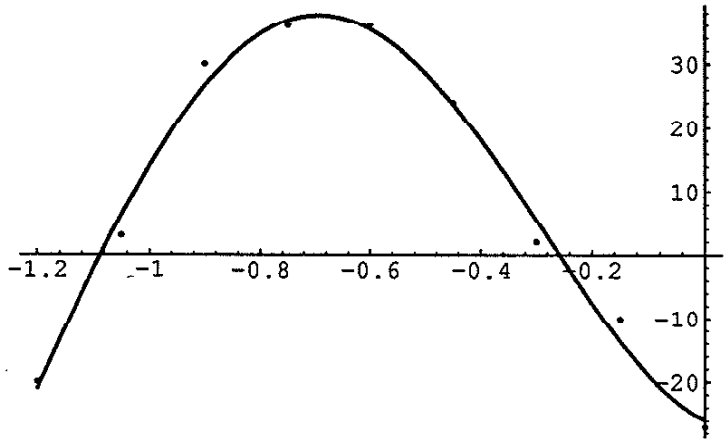

-Graphics-

```
Show[vertplt,vertpltfit]
```

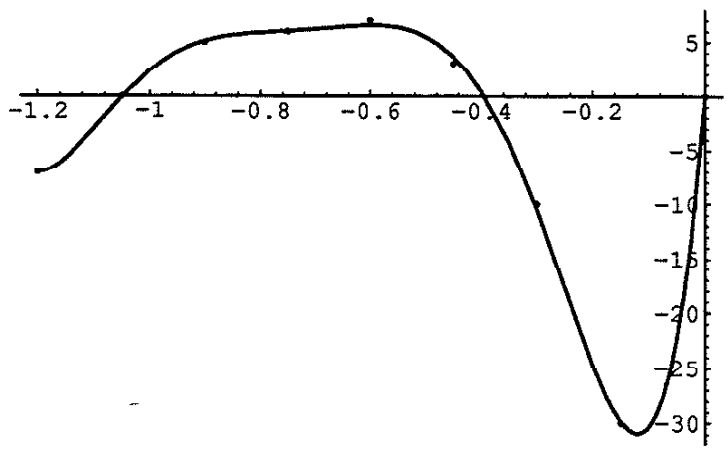

-Graphics-

```
longres[dep_]:=-21.93473193473193472  -
54.2517482517482515*dep  +
9.427609427609429167*dep^2  -
158.7239920573253869*dep^3  -
346.4847909292353696*dep^4  -
156.1675635749709809*dep^5

tranres[dep_]:=-25.8787878787878788  -
35.89225589225589223*dep  +
381.9865319865319866*dep^2  +
564.9083426861204639*dep^3  +
187.0557426112981669*dep^4
```

```
vertres[dep_]:=-0.02828282828282761931  +
627.4718466718467091*dep  +
4194.044778267000808*dep^2  +
10732.25992114881108*dep^3  +
13405.43772642538234*dep^4  +
8196.405332207802498*dep^5  +
1959.050957679215881*dep^6
```

■ Orientation of Ellipsoid's Local Coordinate System wrt the Component's Global Coordinate System

□ Descriptions of the angles

The semiaxis of length "a" lies on the local "x-axis."
The semiaxis of length "b" lies on the local "y-axis."
The semiaxis of length "c" lies on the local "z-axis."

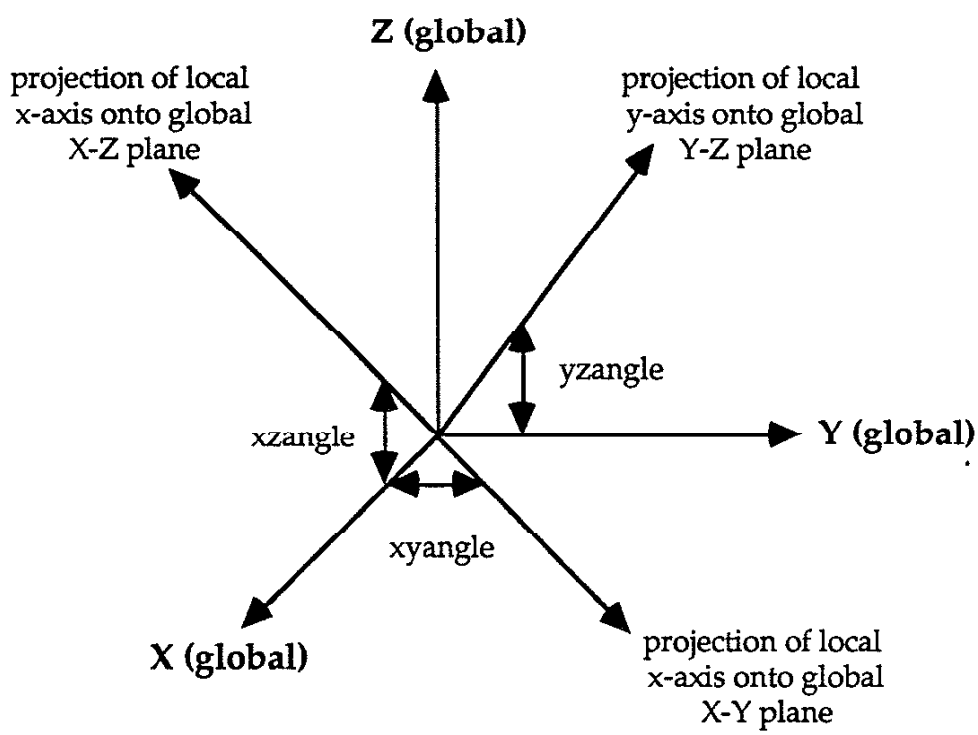

Each angle is shown in its positive sense.
All angles are assumed to be measured in degrees.

"xyangle" --> acute angle ($-90^\circ \leq$ xyangle $\leq 90^\circ$) measured from the global X-axis to the projection of the local x-axis in the global X-Y plane, taken positive toward the positive ray of the global Y-axis and negative toward the negative ray of the global Y-axis.

"xzangle" --> acute angle ($-90^\circ \leq$ xzangle $\leq 90^\circ$) measured from the global X-axis to the projection of the local x-axis in the global X-Z plane, taken positive toward the positive ray of the global Z-axis and negative toward the negative ray of the global Z-axis.

"yzangle" --> acute angle ($-90^\circ \leq$ yzangle $\leq 90^\circ$) measured from the global Y-axis to the projection of the local y-axis in the global Y-Z plane, taken positive toward the positive ray of the global Z-axis and negative toward the negative ray of the global Z-axis.

□ Definitions of Direction Cosines

```
dircos[1,1]:=(1  +  Tan[(Pi*xyangle)/180]^2  +
Tan[(Pi*xzangle)/180]^2)^(-1/2)
dircos[1,2]:=Tan[(Pi*xyangle)/180]/(1  +
Tan[(Pi*xyangle)/180]^2  +
Tan[(Pi*xzangle)/180]^2)^(1/2)
dircos[1,3]:=Tan[(Pi*xzangle)/180]/(1  +
Tan[(Pi*xyangle)/180]^2  +
Tan[(Pi*xzangle)/180]^2)^(1/2)
dircos[2,1]:=(-Tan[(Pi*xyangle)/180]  -
Tan[(Pi*xzangle)/180]*Tan[(Pi*yzangle)/180])/(1
+  Tan[(Pi*xyangle)/180]^2  +
2*Tan[(Pi*xyangle)/180]*Tan[(Pi*xzangle)/180]*Ta
n[(Pi*yzangle)/180]  +  Tan[(Pi*yzangle)/180]^2  +
Tan[(Pi*xzangle)/180]^2*Tan[(Pi*yzangle)/180]^2)
^(1/2)
dircos[2,2]:=(1  +  Tan[(Pi*xyangle)/180]^2  +
2*Tan[(Pi*xyangle)/180]*Tan[(Pi*xzangle)/180]*Ta
n[(Pi*yzangle)/180]  +  Tan[(Pi*yzangle)/180]^2  +
Tan[(Pi*xzangle)/180]^2*Tan[(Pi*yzangle)/180]^2)
^(-1/2)
```

```
dircos[2,3]:=Tan[(Pi*yzangle)/180]/(1  +
Tan[(Pi*xyangle)/180]^2  +
2*Tan[(Pi*xyangle)/180]*Tan[(Pi*xzangle)/180]*Ta
n[(Pi*yzangle)/180]  +  Tan[(Pi*yzangle)/180]^2  +
Tan[(Pi*xzangle)/180]^2*Tan[(Pi*yzangle)/180]^2)
^(1/2)

e1:={dircos[1,1],dircos[1,2],dircos[1,3]}

e2:={dircos[2,1],dircos[2,2],dircos[2,3]}

e3:={
dircos[1,2]  dircos[2,3]-dircos[1,3]  dircos[2,2],
dircos[1,3]  dircos[2,1]-dircos[1,1]  dircos[2,3],
dircos[1,1]  dircos[2,2]-dircos[1,2]  dircos[2,1]
}
```

□ **Definitions of the projected angles**

```
xyangle=0.

0.

xzangle=0.

0.

yzangle=0.

0.
```

□ **Definition of transformation matrix**

```
tranmat=N[{e1,e2,e3},15]

{{1., 0., 0.}, {0., 1., 0.}, {0., 0., 1.}}
```

■ **The lists of components for the stress history at a single macroscopic material point must be provided. These components are rotated to accomodate the orientation of the microscopic inhomogeneity within the macroscopic component. Using the rotated global components a nested list of stress histories at the sample points on the surface of the inhomogeneity is constructed (denoted "historylist").**

```
MemoryInUse[]
Unprotect[Out]
Clear[Out]
Protect[Out]
MemoryInUse[]
```

```
70611192

{Out}

{Out}

14580232
```

□ **Paste the lists of the individual global stress component histories here (plane-stress conditions were used in this study)**

```
sigx=(-.14504)  {0.,3.943203011971619,
8.14201479287347,  14.27872560899256,

   22.72657818818669,  32.69640850120272,

   39.32341891802103,  40.55551844238693,
42.129479981147,

   44.23370998054366,  47.18614613250045,

   51.53477224103473,  58.1925740158729,
68.24152199848196,

   79.37386117918456,  70.2250614916962,
67.04995866485303,

   63.59629740146622,  59.98858783868465,

   56.37659581521361,  52.92639099266272,
49.8087945142907,

   47.18653707957832,  45.20160024403481,

   43.96408593508735,  43.54364024321792,
43.96408593508735,

   45.20160024403481,  47.18653707957832,
49.8087945142907,

   52.92639099266272,  56.37659581521361,

   59.98858783868465,  63.59629740146622,

   67.04995866485303,  70.2250614916962,
79.37386117918456,

   68.24152199848196,  58.1925740158729,
51.53477224103473,

   47.18614613250045,  44.23370998054366,
42.129479981147,

   40.55551844238693,  39.32341891802103,

   32.69640850120272,  22.72657818818669,

   14.27872560899256,  8.14201479287347,
3.943203011971619,0.};
```

```
sigy=(-.14504)  {0.,0.004889628261591721,
0.006580580949547345,

   0.00818075812020629,  0.005151352128488828,

   -0.00820687908761792,  0.0885019592681608,

   0.1474869094196389,  0.2498590641393612,

   0.4385862821975906,  0.814600782113885,

   1.642896339914252,  3.721594594083101,
9.87021663204468,

   31.310005484359,  100.1510031200371,
110.1183997725787,

   120.186066501562,  130.0972201454044,
139.5614504257503,

   148.2697321371692,  155.9129944426833,

   162.2023700315379,  166.8890132657605,

   169.7815209861665,  170.7593985479832,
169.7815209861665,

   166.8890132657605,  162.2023700315379,

   155.9129944426833,  148.2697321371692,

   139.5614504257503,  130.0972201454044,
120.186066501562,

   110.1183997725787,  100.1510031200371,
31.310005484359,

   9.87021663204468,  3.721594594083101,
1.642896339914252,

   0.814600782113885,  0.4385862821975906,

   0.2498590641393612,  0.1474869094196389,

   0.0885019592681608,  -0.00820687908761792,

   0.005151352128488828,  0.00818075812020629,

   0.006580580949547345,
0.004889628261591721,0.};
```

```
tauxy=-.14504  {0.,0.282612067302559,
0.4232220287824469,

   0.6069627618999142,  0.7919960450180345,

   0.7767242344731918,  1.135627554955773,

   1.361167624552131,  1.724753597975228,

   2.330619166364958,  3.388683952406627,

   5.355637085824869,  9.30865194946052,
17.90912143678587,

   36.3891298453481,  54.74643320637684,
53.81459371398822,

   51.87159164018225,  48.82966651224157,

   44.64448958053468,  39.32470851246572,

   32.93749789870718,  25.60916049291126,

   17.52058277872066,  8.89799806591314,  0.,

   -8.89799806591314,  -17.52058277872066,

   -25.60916049291126,  -32.93749789870718,

   -39.32470851246572,  -44.64448958053468,

   -48.82966651224157,  -51.87159164018225,

   -53.81459371398822,  -54.74643320637684,

   -36.3891298453481,  -17.90912143678587,

   -9.30865194946052,  -5.355637085824869,

   -3.388683952406627,  -2.330619166364958,

   -1.724753597975228,  -1.361167624552131,

   -1.135627554955773,  -0.7767242344731918,

   -0.7919960450180345,  -0.6069627618999142,

   -0.4232220287824469,  -0.282612067302559,0.};
```

```
sigz=Table[0,{p,1,51}]
```

```
{0, 0, 0, 0, 0, 0, 0, 0, 0, 0, 0, 0, 0, 0, 0, 0, 0,
  0, 0, 0, 0, 0, 0, 0, 0, 0, 0, 0, 0, 0, 0, 0, 0,
  0, 0, 0, 0, 0, 0, 0, 0, 0, 0, 0, 0, 0, 0, 0, 0,
  0, 0}
```

■ **The components are now combined (into "stresslist") to form the list of global stress tensor histories that are transformed into the ellipsoid's coordinate system. The application presented in this study uses two-dimensional plane-stress components (with superposed orthogonal residual stresses). Obvious modification is required for a more general case.**

□ **Construction of stresslist**

```
Do[tensor[m]={{sigx[[m]],tauxy[[m]],0.},
{tauxy[[m]],sigy[[m]],0.},
{0.,0.,sigz[[m]]}},{m,1,Length[sigx]}]
```

```
stresslist=Table[Transpose[tranmat] . tensor[m]
. tranmat, {m,Length[sigx]}];
```

```
Length[stresslist]
```

```
51
```

```
Length[sigx]
```

```
51
```

```
Length[sigy]
```

```
51
```

```
Length[tauxy]
```

```
51
```

```
Length[sigz]
```

```
51
```

■ Construction of historylist

"pointlist" contains the list of unit normal vectors to the points of interest on the discontinuity's surface.

```
pointlist={{1.,0.,0.},{0.,1.,0.},{0.,0.,1.}}
```

```
{{1., 0., 0.}, {0., 1., 0.}, {0., 0., 1.}}
```

```
Clear[historylist, spaceinc, timeinc, matpnt,
pappl, n]

Do[

  pappl[1,1]=stresslist[[timeinc,1,1]];
  pappl[1,2]=stresslist[[timeinc,1,2]];
  pappl[1,3]=stresslist[[timeinc,1,3]];
  pappl[2,2]=stresslist[[timeinc,2,2]];
  pappl[2,3]=stresslist[[timeinc,2,3]];
  pappl[3,3]=stresslist[[timeinc,3,3]];

  n[1]=pointlist[[spaceinc,1]];
  n[2]=pointlist[[spaceinc,2]];
  n[3]=pointlist[[spaceinc,3]];

   matpnt[spaceinc,timeinc]=
   {{p[1,1],p[1,2],p[1,3]},
   {p[1,2],p[2,2],p[2,3]},
   {p[1,3],p[2,3],p[3,3]}}
  ,

{spaceinc,Length[pointlist]},
{timeinc,Length[stresslist]}

];

historylist=Table[
matpnt[spaceinc,timeinc],
{spaceinc,Length[pointlist]},
{timeinc,Length[stresslist]}
];

Clear[n,pappl]
```

The following algorithms were produced for the application contained in this thesis. Some tailoring will probably be desirable for a different application.

Check for Yielding at Points of Interest

```
Clear[yield]
```

```
yield=N[Table[1/Sqrt[2]
Sqrt[(historylist[[point,time,1,1]]  -
historylist[[point,time,2,2]])^2  +
(historylist[[point,time,2,2]]  -
historylist[[point,time,3,3]])^2  +
(historylist[[point,time,3,3]]  -
historylist[[point,time,1,1]])^2  +  6  (
historylist[[point,time,1,2]]^2  +
historylist[[point,time,1,3]]^2  +
historylist[[point,time,2,3]]^2)],
{point,1,Length[pointlist]},
{time,1,Length[stresslist]}],6];
```

```
Max[yield[[1]]]
```

```
46.8248
```

```
Max[yield[[2]]]
```

```
21.256
```

```
Max[yield[[3]]]
```

```
45.6111
```

■ Description of Direction Cosine Generation

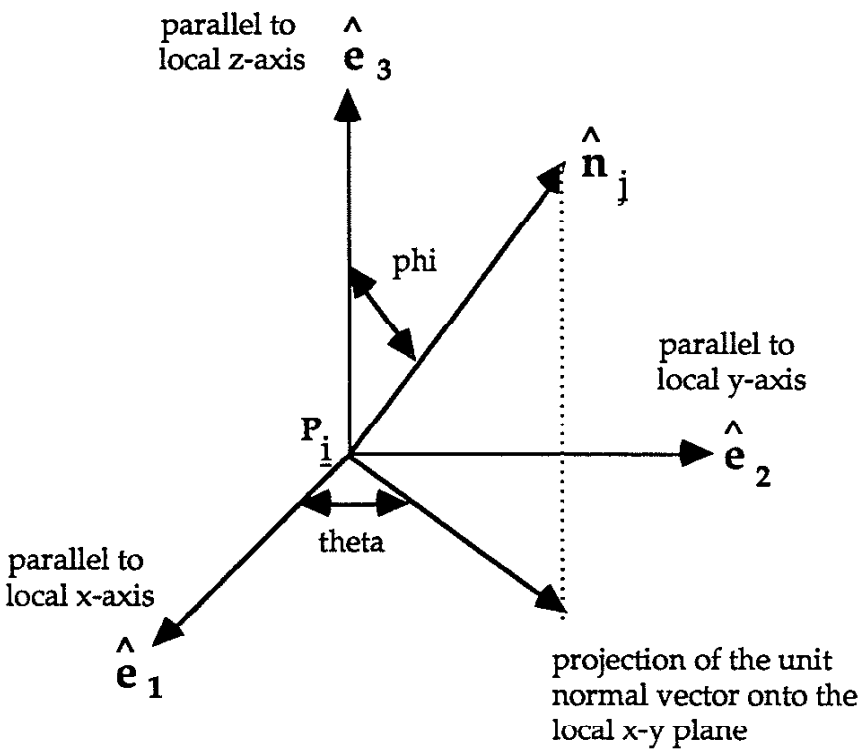

Specify the amount, in degrees, to increment the spherical coordinates when generating the list of planes that will be examined at each point. "phi" is the angle from the local z-axis to the plane's unit normal vector. "theta" is the angle from the local x-axis to the projection of the plane's unit normal vector in the local x-y plane. Small numbers for "incphi" and/or "inctheta" will result in a large number of sample planes. "incphi" and inctheta" need not be equal or integer-valued.

◻ Construct the list of direction cosines for the normal to the sample planes through each point, P_i

```
incphi=20
```

```
20
```

```
inctheta=20
```

```
20
```

```
splist=Prepend[Flatten[Table[{phi,theta},{phi,in
cphi,180,incphi},{theta,0,180,inctheta}],1],{0,0
}];
```

```
njlist=N[Table[{Sin[splist[[m,1]]  Pi/180]
Cos[splist[[m,2]]  Pi/180],Sin[splist[[m,1]]
Pi/180]  Sin[splist[[m,2]]
Pi/180],Cos[splist[[m,1]]
Pi/180]},{m,Length[splist]}]];
```

```
Length[njlist]
```

```
91
```

■ Define the traction vectors, incremented through time, for each of the planes through each of the points

```
Clear[traclist,normlist,shearlist]
```

```
traclist=Table[historylist[[pnt,tme]]
njlist[[plane]],  {pnt,Length[pointlist]},
{plane,Length[njlist]},
{tme,Length[stresslist]}];
```

```
normlist=Table[(traclist[[pnt,plane,tme]]  .
njlist[[plane]])  njlist[[plane]],
{pnt,Length[pointlist]},  {plane,Length[njlist]},
{tme,Length[stresslist]}];
```

```
maxnormlist=Table[traclist[[pnt,plane,tme]]  .
njlist[[plane]],{pnt,Length[pointlist]},
{plane,Length[njlist]},
{tme,Length[stresslist]}];

shearlist=Table[traclist[[pnt,plane,tme]]  -
(traclist[[pnt,plane,tme]]  .  njlist[[plane]])
njlist[[plane]],  {pnt,Length[pointlist]},
{plane,Length[njlist]},
{tme,Length[stresslist]}];
```

■ Fatigue Analysis Calculations for Findley's Parameter

```
Clear[ediagonals,maxlength]

ediagonals[eveclist_]:=
Flatten[Table[eveclist[[i]]  -  eveclist[[i+j]]  ,
{i,1,Length[eveclist]-1},
{j,1,Length[eveclist]-i}],1]

maxlength[eveclist_]:=Max[Table[Sqrt[eveclist[[i
]]  .  eveclist[[i]]],  {i,1,Length[eveclist]}]]

meanfact=.3
```

0.3

◻ Findley Calculations (for first ellipsoid point in historylist)

```
shearrangevect=Table[ediagonals[shearlist[[1,
plane]]],{plane,1,Length[njlist]}];

Table[maxlength[shearrangevect[[plane]]]  /  2  +
meanfact  Max[maxnormlist[[1,plane]]],
{plane,1,Length[njlist]}];

Max[%]
```

13.4189

```
njlist[[Position[%%,Max[%%]][[1,1]]]].tranmat
```

{0.604023, 0.719846, 0.34202}

```
splist[[Position[%%%,Max[%%%]][[1,1]]]]
```

{70, 50}

```
Position[%%%%,Max[%%%%]]
```

{{58}}

Correlation of Rotating-Steel-Beam Fatigue Data with Findley's Parameter (Liu 1994)

```
par=.3
```

```
0.3
```

```
rawdata={{60,302000},{53,429000},{50,682000},{48
,821000},{46,3039000}}
```

```
{{60, 302000}, {53, 429000}, {50, 682000},
  {48, 821000}, {46, 3039000}}
```

```
reddata=Table[{Sqrt[(rawdata[[i,1]]/2)^2+par^2
(rawdata[[i,1]]/2)^2]  +  par
rawdata[[i,1]]/2,rawdata[[i,2]]},{i,Length[rawda
ta]}]
```

```
{{40.3209, 302000}, {35.6168, 429000},
  {33.6008, 682000}, {32.2567, 821000},
  {30.9127, 3039000}}
```

```
life[find ,lga ,pwr ]:=10^lga  find^(pwr)
```

```
Fit[Log[10,reddata],{1,f},f]
```

```
17.318 - 7.45178 f
```

```
lga=17.318
```

```
17.318
```

```
pwr=-7.45178
```

```
-7.45178
```

```
life[25,lga,pwr]  39/1000000
```

```
310.401
```

LIST OF REFERENCES

AAR. 1990. "1990 Heavy Haul Workshop and FAST/HAL Program Description of Experiments." In *Proceedings: Workshop on Heavy Axle Loads*, 6.0-6.10. Pueblo, CO: Association of American Railroads.

Abbott, R. A., and A. M. Zarembski. 1980. "User's Manual for Rail Fatigue Life Program." (Association of American Railroads Technical Center, Chicago) Report Number R-336.

Andrews, K. W. and D. Brooksbank. 1972. "Stresses Associated with Inclusions in Steel: A Photoelastic Analogue and the Effects of Inclusions in Proximity." *Journal of The Iron and Steel Institute,* (October): 765-776

Bannantine, Julie A., Jess J. Comer, and James L. Handrock. 1990. "Multiaxial Fatigue." Chap. 7 in *Fundamentals of Metal Fatigue Analysis.* Englewood Cliffs, NJ: Prentice Hall

Bowles C. Q., and J. Schijve. 1973. "The Role of Inclusions in Fatigue Crack Initiation in an Aluminum Alloy." *International Journal of Fracture,* vol. 9, no. 2 (June): 171-179.

Brave, Glenn. 1990. "FAST/HAL Rail Weld Performance." In *Proceedings: Workshop on Heavy Axle Loads*, 11.0-11.11. Pueblo, CO: Association of American Railroads.

Brooksbank, D. and K. W. Andrews. 1972. "Stress Fields around Inclusions and Their Relation to Mechanical Properties." *Journal of The Iron and Steel Institute,* (April): 246-255.

Carpenter, G. F., R. K. Steele, and M. J. Markase. 1993. "Effect of Inclusion Content on Fatigue Performance and Fracture Toughness of Rail Steels." (Association of American Railroads Technical Center, Chicago) Report Number R-856.

Carrier, George F., and Carl E. Pearson. 1988. "More on Transforms." Chap. 15 in *Partial Differential Equations: Theory and Technique.* 2d ed. Boston: Academic Press, Inc.

Chipperfield, C. G., and A. S. Blicblau. 1984. "Modelling Rolling Contact Fatigue in Rails." *Rail International,* (January): 25-31.

Chiu, Y. P., T. E. Tallian, and J. I. McCool. 1971. "An Engineering Model of Spalling Fatigue Failure in Rolling Contact: I. The Subsurface Model." *Wear,* vol. 17, no. 516 (May/June): 433-446.

Eshelby, J. D. 1957. "The Determination of the Elastic Field of an Ellipsoidal Inclusion, and Related Problems." *Proceedings of the Royal Society* (London), ser. A, vol. 241: 376-396.

Farris, T. N., L. M. Keer, and R. K. Steele. 1987. "The Effect of Service Loading on Shell Growth in Rails." *J. Mech. Phys. Solids,* vol. 35 no. 6: 677-700.

Farris, T. N., L. M. Keer, and R. K. Steele. 1990. "Life Prediction for Unstable Shell Growth in Rails." *Journal of Engineering for Industry,* vol. 112 (May): 175-180.

Findley, W. N. 1959. "A Theory for the Effect of Mean Stress on Fatigue of Metals Under Combined Torsion and Axial Load or Bending." *Journal of Engineering for Industry,* ser. B, vol. 81, no. 4 (November): 301-306.

Fowler, G. J., and A. S. Tetelman. 1978. "Stress Concentration Effect of Nonmetallic Inclusions and Its Effect on Fatigue Crack Initiation in Rail Steel." American Railway Engineering Association, vol. 79, Bulletin 668:447-471.

Fry, Gary T. 1992. "A Modified Thermite Rail Welding Procedure." Master's thesis, University of Illinois, Urbana, IL.

Gibert, F. 1988. "Thermit-Welding of Rails: Old Recipe for Modern Track." *Rail International,* vol. 19, no. 5 (May): 8-11.

Hauser, Daniel. 1978. "Welding of Railroad Rails: A Literature and Industry Survey." In *Rail Steels - Developments, Processing, and Use,* ASTM STP 644, edited by D. H. Stone, and G. G. Knupp, 118-141. Philadelphia: American Society for Testing and Materials.

Hay, William W. 1982. "Track Analysis." Chap 15 in *Railroad Engineering.* 2d ed. New York: John Wiley & Sons.

Hyzak, J. M., and I. M. Bernstein. 1982a. "The Effect of Defects on the Fatigue Crack Initiation Process in Two P/M Superalloys: Part I. Fatigue Origins." *Metallurgical Transactions,* ser. A, vol. 13 (January): 33-43.

Hyzak, J. M., and I. M. Bernstein. 1982b. "The Effect of Defects on the Fatigue Crack Initiation Process in Two P/M Superalloys: Part II. Surface-Subsurface Transition." *Metallurgical Transactions,* ser. A, vol. 13 (January): 45-52.

Jha, Bijendra. 1989. "Thermite Welding of Rail Steel." Ph.D. diss., Illinois Institute of Technology, Chicago, IL.

Jiang, Yanyao Roger, and Huseyin Sehitoglu. 1992. "Fatigue and Stress Analysis of Rolling Contact." Materials Engineering-Mechanical Behavior (College of Engineering, University of Illinois at Urbana-Champaign) Report No. 161 (February), UILU-ENG 92-3602.

Jiang, Yanyao. 1993. "Cyclic Plasticity with an Emphasis on Ratchetting." Ph.D. diss., University of Illinois, Urbana, IL.

Kannel, J. W., and J. L. Tevaarwerk. 1984. "Subsurface Stress Evaluations under Rolling/Sliding Contacts." *Journal of Tribology,* vol. 106, no. 1 (January): 96-103.

Lankford, J. and F. N. Kusenberger. 1973. "Initiation of Fatigue Cracks in 4340 Steel." *Metallurgical Transactions,* vol. 4 (February): 553-559.

Liu, Wei. 1994. "Microstructures and Mechanical Properties of Standard and Modified Thermite-Welded Railroad Rails." Master's thesis, University of Illinois, Urbana, IL.

Martin, G. C. and W. W. Hay. 1970. "The Influence of Wheel-Rail Contact Forces on the Formation of Rail Shells." Civil Engineering Studies, Transportation Series No. 5 (College of Engineering, University of Illinois at Urbana-Champaign) (December), UILU-ENG 70-102.

McEvily, A. J., and K. Minakawa. 1981. "Metallurgical Evaluation of Fast [Rail] Steels." Final report to the U.S. DOT: Contract No. DOT-TSC-1551. Photocopy.

Miller, G. R., and L. M. Keer. 1983. "Interaction Between a Rigid Indenter and a Near-Surface Void or Inclusion." Paper presented at the winter annual meeting of The American Society of Mechanical Engineers, Boston, MA, November.

Murakami, Yukitaka. 1989. "Effects of Small Defects and Nonmetallic Inclusions on the Fatigue Strength of Metals." *JSME International Journal,* ser. I, vol. 32, no. 2: 167-180.

Oderio, Jill A. 1992. "A Metallurgical Study of the Detail Fracture in Thermite-Welded Railroad Rails." Master's thesis, University of Illinois, Urbana, IL.

O'Toole, B. J. and M. H. Santare. 1990. "Photoelastic Investigation of Crack-Inclusion Interaction." *Experimental Mechanics,* (September): 253-257.

Puskar, Anton, and Stanislav A. Golovin. 1985. *Fatigue in Materials: Cumulative Damage Processes.* New York: Elsevier.

Reiff, Richard P. 1990. "Introduction to the FAST/HAL Program." In *Proceedings: Workshop on Heavy Axle Loads*, 5.0-5.14. Pueblo, CO: Association of American Railroads.

Sampath, S. G., T. G. Johns, P. M. McGuire, and K. B. Davies. 1978. "Stresses Around Transverse Fissure Flaws in Rails Due to Service Loads." In *Rail Steels - Developments, Processing, and Use,* ASTM STP 644, edited by D. H. Stone, and G. G. Knupp, 330-341. Philadelphia: American Society for Testing and Materials.

Schroeder, L. C., and D. R. Poirier. 1985. "Thermite Rail Welds; The Process, Mechanical and Metallurgical Properties, and Possible Improvements." In *Railroad Rail Welding,* 21-59. Northfield,NJ: Railway Systems & Management Association.

Smith, J. O., and Chang Keng Liu. 1953. "Stresses Due to Tangential and Normal Loads on an Elastic Solid with Application to Some Contact Problems." *Journal of Applied Mechanics* vol. 20 (June): 157-166.

Sokolnikoff, I. S. 1983. *Mathematical Theory of Elasticity.* Reprint ed. Malabar, FL: Robert R. Krieger Publishing Company.

Sperry Rail Service. 1989. *Rail Defect Manual.* Danbury, CT: Sperry Rail Service.

Steele, R. K. 1985. "Field Welding of Rails." (Association of American Railroads Technical Center, Chicago) Report Number R-618.

Steele, R. K. Conversation with author, 1 September 1994.

Steele, R. K., and M. W. Joerms. 1993. "Users Guide to PHOENIX 7L3: A Three Dimensional Rail Fatigue Model." (Association of American Railroads Technical Center, Chicago) Report Number R-728.

Suresh, S. 1991. *Fatigue of Materials.* Cambridge: Cambridge University Press.

Tallian, T. E. 1971. "An Engineering Model of Spalling Fatigue Failure in Rolling Contact: III. Engineering Discussion and Illustrative Examples." *Wear,* vol. 17, no. 516 (May/June): 463-480.

Tallian, T. E. and J. I. McCool. 1971. "An Engineering Model of Spalling Fatigue Failure in Rolling Contact: II. The Surface Model." *Wear,* vol. 17, no. 516 (May/June): 447-461.

Tanaka, K., and T. Mura. 1982. "A Theory of Fatigue Crack Initiation at Inclusions." *Metallurgical Transactions,* ser. A, vol. 13 (January): 117-123.

Ting, Chih-Hsien, and F. V. Lawrence. 1991. "A Model for the Long-Life Fatigue Behavior of Small Notches." Materials Engineering-Mechanical Behavior (College of Engineering, University of Illinois at Urbana-Champaign) Report No. 156 (November), UILU-ENG 91-3602.

Tinnon, John B. 1938. "Thermit Welding." In *Welding Handbook.* edited by W. Spraragen, 251-279. New York: American Welding Society.

Uflyand, Ya S. 1965. *Survey of Articles on the Applications of Integral Transforms in the Theory of Elasticity.* Translated from the Russian by W. J. A. Whyte, and edited by Ian N. Sneddon. Raleigh: North Carolina State University.

Wolfram Research, Inc. 1993. *Mathematica.* Version 2.2. Champaign, IL: Wolfram Research, Inc.

Yu, Maria Min-Hui, and L. M. Keer. 1989. "Growth of the Shell/Transverse Defect in Rails." *Journal of Tribology,* vol. 111 (October): 648-654.

Yu, Maria Min-Hui. 1992. "Elastic-Plastic Analyses of Cyclic Rolling Contacts." Ph.D. diss., Northwestern University, Evanston, IL.